PLASMA MODIFIED STEEL PROCESSING BY-PRODUCT FOR REMOVING HEAVY METALS AND ANTIBIOTICS FROM WATER

By

Van Son Tran

A dissertation

Submitted in fulfillment for the degree of

DOCTOR OF PHILOSOPHY

In

Environmental Engineering

University of Technology Sydney

New South Wales, Australia

June, 2017

CERTIFICATE OF ORIGINAL AUTHORSHIP

I certify that the work in this thesis has not previously been submitted for a degree nor has it been submitted as part of requirements for a degree except as part of the collaborative doctoral degree and/or fully acknowledged within the text.

I also certify that the thesis has been written by me. Any help that I have received in my research work and the preparation of the thesis itself has been acknowledged. In addition, I certify that all information sources and literature used are indicated in the thesis.

SIGNATURE OF STUDENT:

Van Son Tran

Date: 30 June 2017

ACKNOWLEDGMENT

First of all, I owe my deepest gratitude to my principal supervisor, Prof. Huu Hao Ngo for his continuous supports, guidance, time, patience and inspiration. I have learnt a lot from his ideas, critical review of my study plans and papers, knowledge and motivation which encouraged me to overcome many difficulties in the research as well as other aspects of life to achieve this milestone. I also would like to thank my supervisory committee, Dr. Wenshan Guo and Assoc. Prof. Cuong Ton-that for their mentor supports, papers revising and useful comments on this dissertation.

I gratefully acknowledge the Australian government for awarding me the Australia Awards Scholarship. The financial support from Centre for Technology in Water and Wastewater, and the research collaboration between UTS and Shanghai Advanced Research Institute/Tianjin Polytechnic University are also grateful.

The technical supports and guidance from Dr. Johir, the environmental engineering laboratories, UTS are greatly appreciated. Also, I would like to thank Dr. Andrzej from Water Reclamation and Management Scheme, Sydney Olympic Park Authority for his supports and valuable advices. Many thanks go to Katie and other staffs at Microstructure Analysis Unit, UTS and Dr. Alfonso, University of Macquarie for guiding me to characterize the materials surface. I would like to express my appreciation to Christian and Boshir for their technical assistances and useful discussion. I am thankful to Jean, Ronald, Phuong, Hang, Van, Tram, Lam, Chung, Lijuan for their supports and contributions.

Finally, I am hugely indebted to all my family, colleagues and friends for their emotional supports, unconditional love and guidance.

DEDICATION

This thesis is deeply dedicated to the following people:

To my respective parents, Xuan Hoa Tran & Thi Theu Nguyen
For their sacrifices, endless love, hard work and inspiration

To my wonderful wife, Thi Thuan Tran
For her constant love, supports and caring

To my lovely daughter and son, Ha Linh & Huy Phong
For bringing joy and hope

TABLE OF CONTENTS

NOMENCLATURES

Symbol	Description	Unit
Å	Angstrom	
Ar	Argon	
As	Arsenic	
C_{ad}	The different in the adsorbate concentration at the initial time and time t caused by adsorption	mg/L
C_b	Adsorbate concentration at breakthrough time	mg/L or µg/L
Cd^{2+}	Cadmium	
C_e	Concentration at equilibrium	mg/L
C_o	Initial concentration	mg/L
C_b	Desired effluent concentration of BDST model	mg/L or µg/L
Cr^{3+}	Chromium	
C_t	Concentration of adsorbate at time (t)	mg/L or µg/L
Cu^{2+}	Copper	mg/L
CH_3COOH	Acetic acid	
cm^3/g	Cubic centimeter per gram	
CP	Chloramphenicol	
F	Linear velocity	cm/min
Fe_2O_3	Iron (III) oxide	
g/L	Gram per liter	
H_2	Hydrogen	
HCL	Hydrochloric acid	
HNO_3	Nitric acid	
HRT	Hydraulic retention time	
H_2SO_4	Sulfuric acid	
k_{1p}	Equilibrium rate constant of PFO	1/min
k_{2p}	Equilibrium rate constant of PSO	1/min
k_{AB}	Adams-Bohart kinetic constant	
k_b	Rate constant of BDST model	L/(mg.h)
k_F	Freundlich isotherm constant	

k_i	Equilibrium rate constant of IDM	mg/g.min or µg/g.min
k_L	Langmuir isotherm constant	
k_{Th}	Thomas rate constant	
k_{YN}	Yoon-Nelson rate velocity constant	
L/h	Liter per hour	
M	The amount of M_3-plN_2 packed in the column	g
mg/L	Milligram per liter	
min	Minute	
mL/min	Milliliter per minute	
m^2/g	Square meter per gram	
m^3/day	Cubic meter per day	
mmol/g	milimol per gram	
n	Freundlich constant	
N_o	Saturation adsorbate concentration	
N_2	Nitrogen	
NaOH	Sodium hydroxide	
Ni	Nikel	
O_2	Oxygen	
Pb^{2+}	Lead	
ppm	Part per million	
Q	Volumetric flow rate	mL/min
q_o	Column adsorption capacity	mg/g or µg/g
q_b	Amount of adsorbate adsorbed per unit of dry weight of adsorbent at breakthrough time	mg/g or µg/g
q_e	Adsorption capacity at equilibrium	mg/g or µg/g
$q_{exp.}$	Experimental adsorption capacity	mg/g or µg/g
q_{max}	Langmuir maximum adsorption capacity of the adsorbent	mg/g or µg/g
q_s	Amount of adsorbate adsorbed per unit of dry weight of adsorbent at saturation/exhaustion time	mg/g or µg/g

q_t	Amount of adsorbate adsorbed per unit of dry weight of adsorbent at time t	mg/g or µg/g
r^2	Correlation constant	
R_b	Removal percentage of adsorbate at breakthrough time	%
R_s	Removal percentage of adsorbate at saturation/exhaustion time	%
RF	Radio frequency	
rpm	Revolutions per minute	
SCCM	Standard cubic centimeters per minute	
SMT	Sulfamethazine	
t	Service time of column	
TC	Tetracycline	
V	Volume	
V_b	Volume of water treated at breakthrough time	L
Z	Bed height	cm
Zn^{2+}	Zinc	
ΔG	Change in Gibbs free energy	J/mol
ΔH	Change in enthalpy	J/mol
ΔS	Change in entropy	J/mol/K
µm	Micro meter	
τ	The time required for 50% adsorbate breakthrough	min

ABBREVIATIONS

Symbol	Description
HMs	Heavy metals
ABs	Antibiotics
StS	Steel shavings
BDST	Bed depth service time
M_1, M_2, M_3, M_x-plN_2, M_x-plAr, $M_x$plO_2, $M_x$plH_2	Steel shavings with particles sizes 0-75; 75-150 and 150-425µm; modified steel shavings with plasma in N_2, Ar, O_2 and H_2 gases
RO	Reverse osmosis
SEM-EDS	Scanning electron microscopy - energy-dispersive X-ray spectroscopy
SEM- SUPRA 55VP	Scanning electron microscopy SUPRA 55V
XRD	Powder X-ray diffraction
XPS	X-ray photoelectron spectroscopy
BET	Brunauer emmett teller
FTIR	Fourier transform infrared spectroscopy
MP-AES	Microwave plasma-atomic emission spectrometry
HPLC	High-performance liquid chromatography

LIST OF TABLES

LIST OF FIGURES

LIST OF RESEARCH OUTCOMES

Peer-riewed journal papers

1. **Tran, V.S.**, Ngo, H.H., Guo, W., Zhang, J., Liang, S., Ton-That, C., Zhang, X., 2015. Typical low cost biosorbents for adsorptive removal of specific organic pollutants from water. Bioresource technology, 182, pp.353-363.
2. **Tran, V.S.**, Ngo, H.H., Guo, W., Ton-That, C., Li, J., Li, J., Liu, Y., 2017. Removal of antibiotics (sulfamethazine, tetracycline and chloramphenicol) from aqueous solution by raw and nitrogen plasma modified steel shavings. Science of The Total Environment, 601, pp.845-856.
3. **Tran, V.S.**, Guo W.S., Ngo, H.H., Li, J., Liu, Y., Li, J., Ton-That, C., 2017. Enhancement of steel shavings' heavy metal adsorption capacity by a novel plasma modification method. Journal of Industrial and Engineering Chemistry (Submitted and under reviewing).

Contribution to scientific forums

1. **Tran, V.S.**, Ngo, H.H., Guo, W.S., Ton-that, C., 2017. Single and competive adsorption of antibiotics (sulfamethazine, tetracycline and chloramphenicol) onto nitrogen plasma modified steel shavings (oral presentation). The Inaugural International Conference on Green Technologies for Sustainable Water (GTSW). Hanoi, Vietnam, 13-16 October, 2017 (accepted).

Awards

1. 2015 HDR Students publication Award from Faculty of Engineering and Information Technology (FEIT), University of Technology Sydney (UTS) for publishing in high quality Journals.
2. 2014 one-off scholarship from Centre for Technology in Water and Wastewater (CTWW), University of Technology Sydney (UTS).

PhD DISSERTATION ABSTRACT

Author: Van Son Tran

Date: 23 June 2017

Thesis title: Plasma modified steel processing by-product for removing heavy metals and antibiotics from water

School: Civil and Environmental Engineering

Supervisors: Prof. Dr. Huu Hao Ngo (Principal supervisor)

Dr. Wenshan Guo (Alternative supervisor)

Assoc. Prof. Dr. Cuong Ton-that (Co-supervisor)

Abstract:

The presence of heavy metals (HMs) and antibiotics (ABs) in the aquatic environment causes critical problems to human health and the environment. The adsorptive removal of HMs and ABs onto cost-effective adsorbents has a high potential. In this study, adsorbents were prepared from steel shavings (StS), a by-product generated from the steel processing industries. Among adsorbents, nitrogen plasma modified StS (M_3-plN_2) has highest adsorption capacities of HMs and ABs. Adsorption and co-precipitation were the mechanisms for HMs removal by the adsorbents, while main driving forces for ABs adsorption were hydrogen bonding, electrostatic and non-electrostatic interactions, and redox reaction. Thermodynamic data demonstrated that both adsorption processes of HMs and ABs onto the adsorbents were feasible, spontaneous and endothermic. Solution pH, particle size, adsorbent dose and contact time exerted great influences on the adsorption process. Optimal conditions for the adsorptive removal of HMs were pH 5, adsorbent dose

5g/L, at 25^{o}C. The best removal of sulfamethazine (SMT) and chloramphenicol (CP) was observed at pH 3, while tetracycline (TC) was ultimately removed at pH 5 (with the same adsorbent dose of 2 g/L and at 25^{o}C). The Pseudo-first-order kinetic and Pseudo-second-order kinetic models described the adsorptive kinetics of HMs and ABs very well. The Langmuir maximum single adsorption capacities of Pb^{2+}, Cu^{2+}, Cd^{2+}, Cr^{3+} and Zn^{2+} onto M_3-plN_2 were: 27.04, 20.64, 16.87, 14.89 and 18.47 mg/g, respectively. In competitive adsorption of multi-metals solutions, each competitive solute adsorption capacities were approximately 2-fold less than the single adsorption capacities. However, the total of competitive adsorption capacities was higher than those of single solute sorption. Single Langmuir adsorption capacities of SMT, TC and CP onto M_3-plN_2 were 2702.55, 2158.36 and 2920.11 µg/g, respectively. Adsorption capacities of mixed-ABs onto the adsorbents were nearly 2-fold less than individual adsorption capacities. Furthermore, the metals-loaded M_3-plN_2 was well regenerated using sulphuric acid 0.1N after 5 cycles of adsorption-desorption, while the most effective reagent to regenerate ABs-loaded M_3-plN_2 was methanol 0.1N solution after 2-3 adsorption-desorption cycles. The semi-pilot scale experiments confirmed that fixed-bed column using M_3-plN_2 could efficient abate both HMs and ABs from water with the highest removal efficiencies at a flow rate of 3.47 L/min and bed height of 35 cm. The column adsorption data was well described by The Thomas, Yoon-Nelson and BDST models. Overall, the application of M_3-plN_2 for removing HMs and ABs from aqueous solution can provide tremendous benefits in treating water and reducing solid wastes.

Key words: Heavy metals, Antibiotics, Removal, Adsorption, Mechanism, Desorption, regeneration, Industrial waste/by-product, Steel shavings (StS), Gas plasma, Nitrogen plasma modified steel shavings (M_3-plN_2), Characterization.

Graphical Abstract

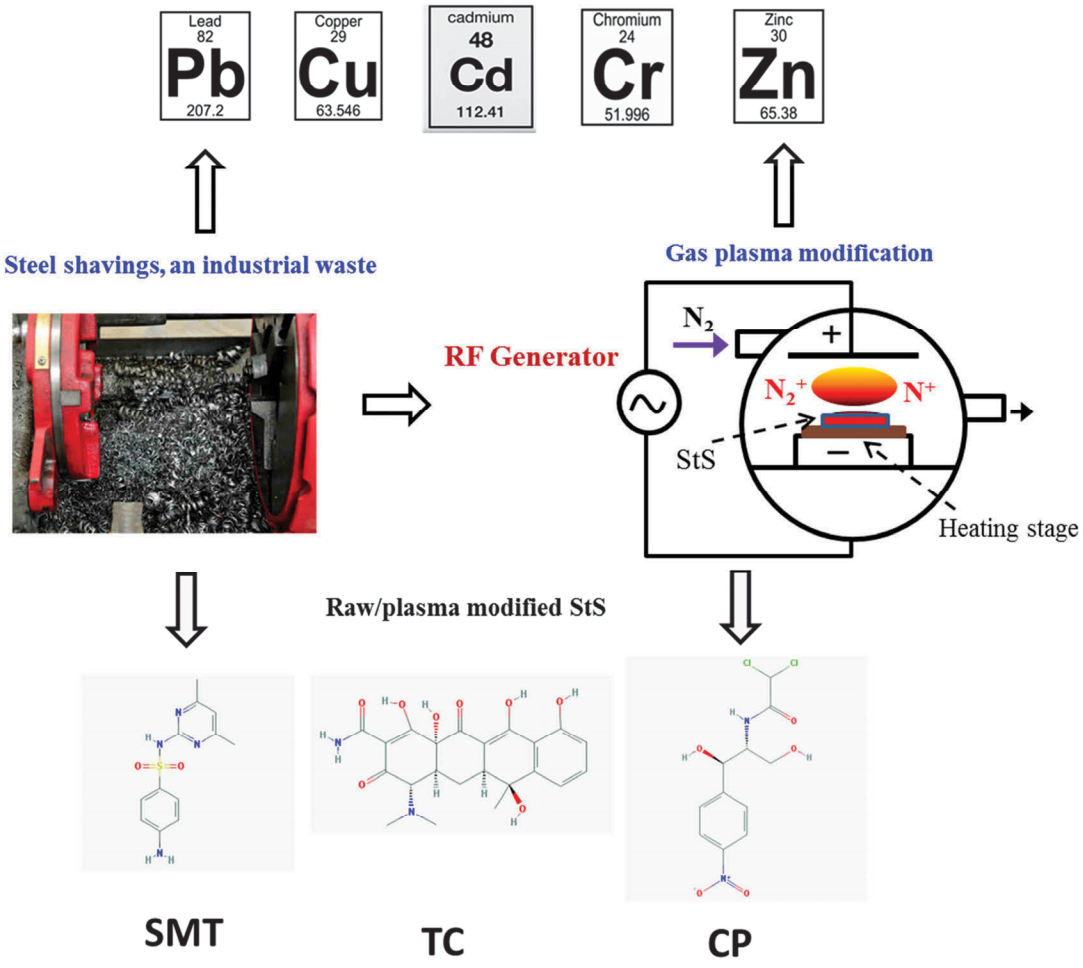

Faculty of Engineering and Information Technology

CHAPTER 1

INTRODUCTION

1.1. Problem statement

1.1.1. Heavy metals and antibiotics pollution in water and health risk

Typical heavy metals (HMs) in wastewater such as lead, copper, cadmium, chromium and zinc can endanger public health and the natural environment due to their toxicity, persistence and steady accumulation (Ali et al., 2013). Exposure to HMs can cause damage to internal organs and many diseases, even at very low dosages (Fu and Wang, 2011). The United States Environmental Protection Agency (USEPA) has established maximum contamination levels for some typical HMs in surface or groundwater to be used in supplying water for drinking (Nguyen et al., 2013). For instance, the safe levels for lead, copper, cadmium, chromium and zinc are 0.006, 0.25, 0.01, 0.05 and 0.80 mg/L, respectively.

Water pollution caused by antibiotics has also become a widespread environmental problem (Rajapaksha et al., 2015). The chemicals are widely used in human and veterinary medicine for inhibiting illness (Lu et al., 2016). Recent studies have shown that a number of antibiotics are detected in surface and groundwater (Adams et al., 2002). Most antibiotics access the environment, particularly in the aquatic matrix, through discharge or disposal from medical, municipal, and agricultural sources (Adams et al., 2002, Pouran et al., 2014). Even at low concentrations in water, pharmaceuticals can pose serious problems to the ecosystem such as potential risks of environmental toxicity and promotion of microbial resistance (Chen et al., 2011; Qiang et al., 2013; Fan et al., 2010; Lu et al., 2016).

Some typical antibiotics are selected in this study including sulfamethazine (SMT), tetracycline (TC) and chloramphenicol (CP). Sulfamethazine (SMT) is a compound belonging to the sulphonamide group. SMT is usually used in veterinary

medicine or livestock feeds for cattle and swine which can be detected at high concentration in aqueous solution due to poor adsorption ability on soil (Rajapaksha et al., 2015). Tetracycline (TC) belonging to the tetracyclines group of antibiotics, is also applied to livestock as an additive to combat diseases (Chen et al., 2011). Chloramphenicol (CP) is an antibiotic commonly utilized in veterinary clinics. The appearance of the compounds in water results in several side effects such as aplastic anemia (Nie et al., 2015). While being banned from applying to food-producing for animals in developed countries, these chemicals are still used in many developing nations due to their low cost, effectiveness and availability (Nie et al., 2015).

Thus, the developing efficient and cost-effective techniques for the removal of such compounds (HMs and ABs) from water are critically important (Chen et al., 2011; Nguyen et al., 2013).

1.1.2. Removal technologies of heavy metals and antibiotics from water

Current literature shows that several common methods have been used for the removal of HMs from aqueous solution such as chemical precipitation, ion exchange, adsorption, membrane filtration, coagulation-flocculation, flotation, electrochemical, electrodialysis and photocatalysis (Fu et al., 2011; Nguyen et al., 2013; Wang and Chen, 2009; Cundy et al., 2008). Adsorption has distinct advantages over other methods for removing HMs at low concentration due to its environmental friendly, economical and highly efficient (Tran et al. 2015). Hence, the adsorption technique has become a forefront among the major processes for removing heavy metal from water (Hua et al., 2012).

Recently, a variety of methods to remove antibiotics and other pharmaceuticals from aquatic matrix such as advanced oxidation processes,

combined chemical/biological treatment, aerobic digestion integrated with activated carbon, ion exchange, coagulation, flocculation, sedimentation, ultraviolet irradiation, have been attempted by a number of reseachers (Adams et al., 2002; Homem and Santos, 2011; Qiang et al., 2013; Nie et al., 2015). However, Qiang et al. (2013) reported that these conventional methods are moderately ineffective in removing antibiotics from aquatic media. The authors suggested that adsorption using cost-effective adsorbents is considered as an effective process to remove antibiotics from aqueous solution.

1.1.3. Adsorption of heavy metals and antibiotics by steel shavings

There are many kinds of adsorbents, however, studies on iron (in the zero valent (Fe^0) and oxides state) as an adsorbent has garnered significant interest because of its adsorption ability, abundance and its known role in the environment as a cycler of heavy metal contaminants (Cundy et al., 2008). Moreover, some types of iron-based adsorbents are magnetic and offer advantages in the separation process from aqueous solutions under a magnetic field for recycling or regeneration (Hua et al., 2012).

Several types of magnetic materials have been employed in HMs abatement, for instance, magnetic iron, nanoparticles, magnetite, iron coated sand, blast furnace slag, green rust and iron oxides (Bhatnagar and Mika, 2010; Haider, 2011; Üzüm et al., 2008; Sikder et al., 2014; Gheju and Balcu, 2011).

Similarly, a number of iron-based adsorbents have been used for the removal of antibiotics from aqueous solution (Xia et al., 2014; Chen et al., 2011; Qiang et al., 2013; Ghauch et al., 2009; Fang et al., 2011).

Using adsorbents from wastes or by-products of agricultural, municipal and industrial sectors can reduce the quantity of solid waste, coupling with an increase in the value of the materials. Steel shavings (StS), a magnetic waste generated in very large amounts from steel processing industry. The materials contain large amounts of zero-valent iron and iron oxides (Tran et al., 2017). Hence, studies on the utilization of steel shavings to abate metal ions and antibiotics from aqueous solution are urgently required.

The application of a novel modification technique to produce a superior adsorbent is certainly valuable for water treatment. In recent years, one of the most promising modification methods for iron-based adsorbents is plasma cleaning (Tran et al., 2017). Gas plasma treatment causes to potential effects on chemical or physical surface changes. When exposing the iron to a plasma generated in a vacuum, the surface of the adsorbent is bombarded. It leads to adventitious hydrocarbons being removed from the iron surface, enhancing the iron surface available for adsorption of pollutants. Selecting employed gas to produce the plasma is very important (Deiries et al., 2005). Some common gases have been used for the process such as oxygen, hydrogen, argon, nitrogen and helium (Plasma etch, 2017). Oxygen, the most commonly gas in plasma cleaning, is effective in removing hydrocarbons both physically and chemically on the surfaces of oxidation-resistant metals such as aluminum and stainless steel (Deiries et al., 2005). Nevertheless, when using a material prone to oxidation as iron, inert gasses, for instance argon and nitrogen, can serve to generate the plasma with the purpose of achieving the same result without further oxidizing the sample (Tran et al., 2017).

This research "Plasma modified steel processing by-product for removing heavy metals and antibiotics from water" aims to use steel shavings, a low-cost adsorbent, for removing HMs and ABs from water. In this study, gas plasma method was employed to improve the efficiency of HMs and ABs removal from aqueous solution by the adsorbents.

1.2. Research hypotheses

The principal hypothesis for this research is the removal of HMs and ABs from water using nitrogen plasma modified steel shavings.

The subsequent hypothesis is steel shavings will be an efficient, affordable and sustainable adsorbent for the removal of HMs and ABs from water. With the regeneration of adsorbent and applicability of plasma modified steel shavings in synthesized wastewater at semi-pilot scale treatment will be economically achievable.

1.3. Objectives

The overall objective of this research is to explore novel, economical and approachable materials to abate toxicants such as heavy metals and antibiotics from water.

To achieve this overall objective, this study has set out a number of specific targets as follows:

- Reviewing current studies in the literature on water pollution by heavy metals and antibiotics, together with technologies for removing them from aqueous solution;
- Exploring novel low-cost materials for heavy metals and antibiotics removal from water, based on findings in the literature review and conducting experimental studies;

- Determining optimal conditions such as particle size, employed gas in plasma modification to develop adsorbents for the removal of pollutants;
- Characterizing the developed materials in the pre and post adsorption states;
- Conducting parametric studies to determine the factors influencing adsorption process such as pH, adsorbent dose, temperature;
- Discovering adsorption isotherm and kinetic models of single and competitive solutes of toxicants on the material;
- Proposing adsorption mechanisms of metal ions and antibiotics onto the adsorbent based on literature review and experimental data;
- Evaluating the regeneration of the adsorbents after adsorption of metal ions and antibiotics from aqueous solution;
- Designing treatment units at semi-pilot scales for synthesized wastewater treatment by using the adsorbent;
- Examining the factors affecting the removal efficiencies of heavy metals and antibiotics to achieve the optimal treatment design for the applicability of the materials in wastewater treatment;
- Assessing column adsorption data by the use of dynamic breakthrough curves models.

1.4. Research significance

The use of steel shavings not only can reduce large quantity of solid waste but also produce a good adsorbent for removing pollutants from water and wastewater. The amount of steel shavings as a by-product from steel processing industry is very large. Applicability of the adsorbent to wastewater treatment depends on the adsorption capacity, regeneration ability and treatment design.

1.5. Thesis outline

This thesis consists of 8 chapters with the following structure:

Chapter 1 presents a context for this study and identifies the research problem, together with the research objectives and its significance. In addition, the main tasks to achieve the objectives and scope of this research are also emphasized in details. Chapter 1 finishes with the layout of the thesis.

Chapter 2 offers a research background for this study. This chapter starts with the introduction of literature review. Then, the water pollution caused by HMs and ABs (definition, sources, adverse effects and regulations) are discussed. Subsequently, the chapter introduces technologies for removing HMs and ABs from water, especially adsorption method using low-cost adsorbents. The use of iron-based adsorbents focuses on the removal mechanisms, adsorption capacities and applications. The plasma technique for adsorbent modification is also introduced in this chapter. Chapter 2 concludes with key findings from literature review and determines the proper research direction.

Chapter 3 provides the materials and methodologies utilized in this study. This chapter describes in details all experiments conducted in the present study such as chemical preparation, experimental set up and experimental procedures. Furthermore, instruments for material characterization, analytical methods and equipment for analyzing HMs and ABs concentrations are presented.

Chapter 4 refers to the development of adsorbents from steel shavings for removing HMs and ABs from water. A comparative study on different kinds of adsorbents is carried out to determine the most effective adsorbent. Characterization of the selected adsorbent is then implemented using Scanning electron microscope

(SEM-EDS), Powder X-ray diffraction (XRD), Brunauer-Emmett-Teller (BET), Fourier transform infrared spectroscopy (FTIR), X-ray photoelectron spectroscopy (XPS) and Zeta-potential methods.

Chapter 5 explores the performance of raw and modified steel shavings in batch experiments for removing HMs. The influential factors of the adsorption process including pH, adsorbent dose and temperature are studied. Adsorption kinetics and isotherms in single and competitive solutes of metal ions are critically analyzed. In addition, the proposed mechanism of HMs sorption on the adsorbents is proposed and discussed. In the final part of this chapter, regeneration of adsorbents and adsorption-desorption cycles are also carried out.

Chapter 6 focuses on the antibiotics removal by raw and modified steel shavings in batch experiments. A frame work of experimental study is set up in this chapter for the removal of ABs to appraise the affecting factors such as pH, adsorbent dose and temperature to adsorption process. The isotherms and kinetics models are used to analyze the experimental data of single and competitive adsorptive removal of ABs from water. Additionally, desorption ability of the adsorbents is determined. Finally, uptake pathways for abatement of ABs from water by raw and modified steel shavings are suggested using XPS and FTIR spectra analyzing.

Chapter 7 reports the performance of nitrogen plasma modified steel shavings for removing HMs and ABs in semi-pilot scales. Removal efficiencies of pollutants using the adsorbent in different semi-pilot scale treatment designs are discussed in details. From experimental results, the optimal semi-pilot treatment design is chosen and analyzed. Influences of solution pH, flow rate and bed height of

the column design are implemented. The chapter also presents the evaluation of experimental adsorption data by dynamic breakthrough curves models including Adams–Bohart, Thomas, Yoon–Nelson and BDST.

Chapter 8 summarizes major findings of this work for HMs and ABs removal from water and recommendations for future research.

Faculty of Engineering and Information Technology

CHAPTER 2

LITERATURE REVIEW

2.1. Introduction

This chapter investigates heavy metal and antibiotics pollution in water such as definition, characteristics of the pollutants, sources and occurrence in the environment, negative effects on human health and natural ecosystems, and relevant regulations for those contaminants. Subsequently, the techniques for removing the pollutants from aqueous solution, focusing on adsorption method using low-cost adsorbents are also mentioned and discussed. Additionally, the use of iron-based adsorbents (emphasizing on adsorption mechanism and application) in the removal of metal ions and antibiotics is analyzed. The use of steel shavings as a novel adsorbent is mentioned. This chapter discusses the utilization of gas plasma technique for improving surface properties of steel shavings for abating metal ions and antibiotics from aqueous solution. Finally, chapter 2 summarizes major findings and research gaps, which guide the thesis research.

2.2. Heavy metal and antibiotics pollution in water

2.2.1. Heavy metals pollution in water

A. Definition, characteristics

Definition of heavy metals

Heavy metals (HMs) are usually defined as metals with moderately high densities, atomic weights, or atomic numbers. Typical heavy metals in wastewater selected in this study including lead, copper, cadmium, chromium and zinc can endanger public health and the natural environment due to their toxicity, persistence and steady accumulation (Barakat and Kumar, 2015).

Characteristics of these typical heavy metals

According to USEPA (2002), lead occurs in several oxidation states: 0, +1, +2 and +4, in which Pb^{2+} is the most stable ionic species in natural environments. On the other hand, copper exists in four oxidation states: 0, +1, +2 and +3. Since most copper ions exist in Cu^{1+} (cuprous) and Cu^{2+} (cupric), Cu^{1+} is not stable and often oxidized to Cu^{2+} (Hossain, 2013). Cadmium is present in +2 oxidation state in nature, and can form complexes with hydroxide, carbonate, chloride, sulfate and humic material (Arain et al., 2008; USEPA, 2002). Chromium occurs in two oxidation forms including primarily in the trivalent state (+3) and hexavalent state (+6). Among the two forms, Cr^{3+} is the primary and most stable state of chromium (Barceloux and Barceloux, 1999). The chemical nature of zinc is quite similar to that of cadmium. Zn^{2+} is the oxidation state in aqueous solution (Hossain, 2013).

B. Sources and occurrence of HMs in the environment

Heavy metals are naturally present in the environment and enter aquatic environments via various geochemical processes (Sapkota et al., 2008). The pollutants may go into the aquatic environment due to anthropogenic sources such as discharge from households, agriculture and industries (Nagajyoti et al., 2010). There is also an increasing awareness that urban runoff causes a serious metal problem (Raskin et al., 1997). Street dust (from the air), dirt, and various solids, together with various applied chemicals (e.g., pest control), have contributed significantly to the problem (Nagajyoti et al., 2010). Another domestic source of heavy metal contaminants is landfill which is an engineered measure for solid waste storage. Each year the amounts of lead, copper and zinc generated are 332,350; 35,370; 131,880 tons into the atmosphere, 138,000; 112,000; 226,000 tons into the aquatic

environment and 796,000; 954,000; 1,372,000 tons into the soil, respectively (Hossain, 2013).

The concern about negative effects of HMs on human health and aquatic ecosystems has been rising since the early 1970s (Karvelas et al., 2003). Generally, HMs pollution was mostly associated with areas of intensive industries (Hossain, 2013; Karvelas et al., 2003). Nowadays, heavy metal pollution is a problem in both industrial and developing countries. The concentrations of HMs in various environmental matrices are in the ppb range to less than 10 ppm (Tchounwou et al., 2012).

C. Adverse effects of the HMs pollution

Metals can be classified into two groups including those that are vital for survival, such as iron and calcium, and those that are unnecessary or toxic, such as cadmium and lead (Hossain, 2013). Exposure to HMs can cause neurotoxic and carcinogenic effects, damage to internal organs and many diseases, even at significant low dosages (Rahimi et al., 2015; Sapkota et al., 2008). Lead can cause several adverse effects to human health such as encephalopathy, seizures and mental retardation, kidney damage, disruption of the nervous system, and reducing hemoglobin production (Igwe and Abia, 2007; Hossain, 2013). Correspondingly, the intake of copper can lead to health problems, e.g. gastrointestinal disturbance, liver and kidney failure, Wilson's disease and insomnia to human (Hossain, 2013). Negative effects of cadmium include birth defects, kidney damage, renal disorder, Itai-Itai disease, hepatic damage, cancer, and hypertension (Han et al., 2009; Igwe and Abia, 2007; Kurniawan et al., 2006). Moreover, chromium can result in liver and kidney necrosis (Dayan and Paine, 2001). Zinc could create some severe effects to

human health such as depression, lethargy, neurologic signs (seizures and ataxia, and increased thirst) (Kurniawan et al., 2006).

Correspondingly, the higher accumulation of HMs in the surface and groundwater systems prevents the growth of aqueous organisms and ends the beneficial usages of the water bodies. The metal ions could accumulate in fishes and other aquatic organisms, and lastly could reach the human body through food chains (Hu et al., 2005). Moreover, the heavy metals can leach into the groundwater and drinking water (Hossain, 2013).

D. HMs relevant regulations

Because of HMs toxicity and bioaccumulation, many countries have set up legislation and regulations for disposal of waste containing heavy metal (European Commission, 2002; Karvelas et al., 2003). The United States Environmental Protection Agency (USEPA) has established maximum contamination levels of some typical HMs for surface or groundwater to be used in the drinking water supply. For instance, the safe levels of lead, copper, cadmium, chromium and zinc are 0.006, 0.25, 0.01, 0.05 and 0.80 mg/L, respectively (Nguyen et al, 2013).

2.2.2. Antibiotics pollution in water

A. Definition, characteristics

Definition of antibiotics

Antibiotics (ABs) are traditionally defined as a group of compounds that eradicate microorganisms or inhibit their growth (Sapkota et al., 2008; Marzo and Bo, 1998). Nevertheless, the term “antibiotic” has been extended for antibacterial, antiviral, antifungal and antitumor substances. Most of these chemicals are natural from microbial origin, however possibly semi-synthetic or totally synthetic (Sapkota

et al., 2008; Homem and Santos, 2011). The chemicals are widely used in large quantities to treat bacterial diseases in both humans and animals (Nie et al., 2015).

Characteristics of antibiotics

There are several classes of ABs depending on the spectrum, the mechanism of action or the chemical structure. There are about 3000 different compounds which are used as constituents of medicinal products in human and veterinary medicine (Ghauch et al., 2009). The physicochemical properties of antibiotics will affect their distribution in the environment as reported by Kemper (2008). Some typical antibiotics are selected in the present study including sulfamethazine (SMT), tetracycline (TC) and chloramphenicol (CP). Sulfamethazine (SMT) is a compound belonging to the sulphonamide group. SMT is usually used in veterinary medicine or livestock feeds for cattle and swine, and can be detected at high concentration in aqueous solution due to soil's poor ability to adsorb it (Rajapaksha et al., 2015). Tetracycline (TC), which belongs to the tetracyclines group of antibiotics, is also applied to livestock as additives to combat diseases (Chen et al., 2011). Chloramphenicol (CP) is an antibiotic commonly utilized in veterinary clinics and effective against Gram-positive and Gram-negative cocci and bacilli (Liu et al. 2009). The characteristics of SMT, TC and CP such as molecular formular, weight, core structure and treatment methods are shown in Table 2.1.

B. Sources and occurrence of ABs in the environment

ABs are widely used in veterinary and human medicine with annual consumption was 100000-200000 tons (Xu et al., 2007; Lu et al., 2016). While being banned from application to food-producing animals in developed countries, these chemicals are still used in many developing nations due to their low cost,

effectiveness, availability and limited or no regulatory guidelines in place (Nie et al., 2015; Sapkota et al., 2008). Human and veterinary antibiotics have been detected in different matrices, as observed by Homem and Santos (2011). Recent studies have shown that several ABs are detected in surface and groundwater (Adams et al., 2002).

Most antibiotics enter the environment, notably in the aquatic matrix, through discharge or disposal from medical, municipal, and agricultural sources (Adams et al., 2002, Pouran et al., 2014). Figure 2.1 illustrates the pathway of antibiotics going into the natural environment through a diversity of sources. The chemicals can contaminate soil, surface and groundwater via runoff or leaching by using manure of livestock, aquaculture, poultry, pets as fertilizer for agriculture production (Homem and Santos, 2011). In the same way, disposal and excretion of households, industry, hospitals and services introduce human antibiotics into the environment (Homem and Santos, 2011). According to Xu et al. (2007), most of wastewater treatment plants (WWTPs) and drinking water treatment plants (DWTPs) are not prepared to eradicate high polar micropollutants such as antibiotics. Thus, antibiotics can enter the surface water, groundwater and drinking water.

Table 2.1 Chemical structure and properties of the study antibiotics (Ahmed et al., 2015; Adams et al., 2002; Homem and Santos, 2011; Xia et al., 2014; Pubchem, 2017)

Compound, CAS number	**Molecular formular, weight**	**Logkow, pKa, Solubility**	**Analysis wave length**	**Possible structure**	**Core structure**	**Treatment methods**
Sulfamethazine 57-68-1	$C_{12}H_{14}N_4O_2S$ 278.34	0.14/0.28 2.65/7.65 4.3(10^2)	275	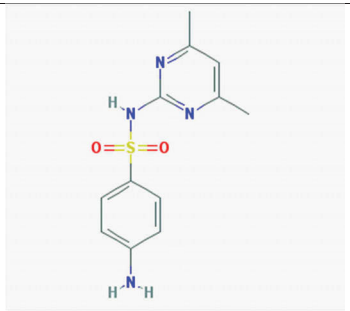	It is characterized by sulfonyl group connected to an amine group	Coagulation, flocculation, sedimentation, excess lime, soda ash, softening, powdered activated carbon sorption, chlorination, ozonation, direct photolysis, ion exchange, reverse osmosis, nanofiltration, semiconductor photocatalysis, photo-fenton
Tetracycline 60-54-8	$C_{22}H_{24}N_2O_8 \cdot HCl$ 444.43	−1.37 3.3 8.3	260	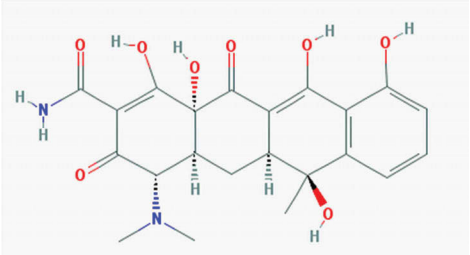	This antibiotic contains an octrahydronaphtacene ring skeleton, consisting of 4 fused rings	Ion exchange, nanofiltration, coagulation, adsorption with activated carbon, adsorption with aluminum oxide, semiconductor photocatalysis, photo-fenton, direct photolysis

Compound, CAS number	**Molecular formular, weight**	**Logkow, pKa, Solubility**	**Analysis wave length**	**Possible structure**	**Core structure**	**Treatment methods**
Chloramphenicol 56-75-7	$C_{12}H_{12}Cl_2N_2O_5$ 323.13	1.14 - 5.5[2]	272/278	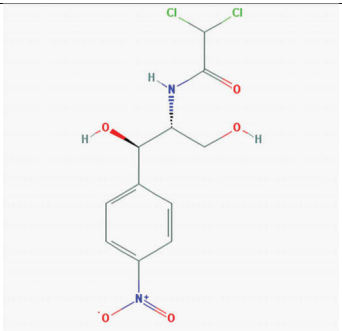	It contains a nitrobenzene moiety connected to a propanol group as well as an amino group binding a derivative of dichloroacetic acid	Semiconductor photocatalysis, nano zero-valent iron, adsorption, advanced oxidation

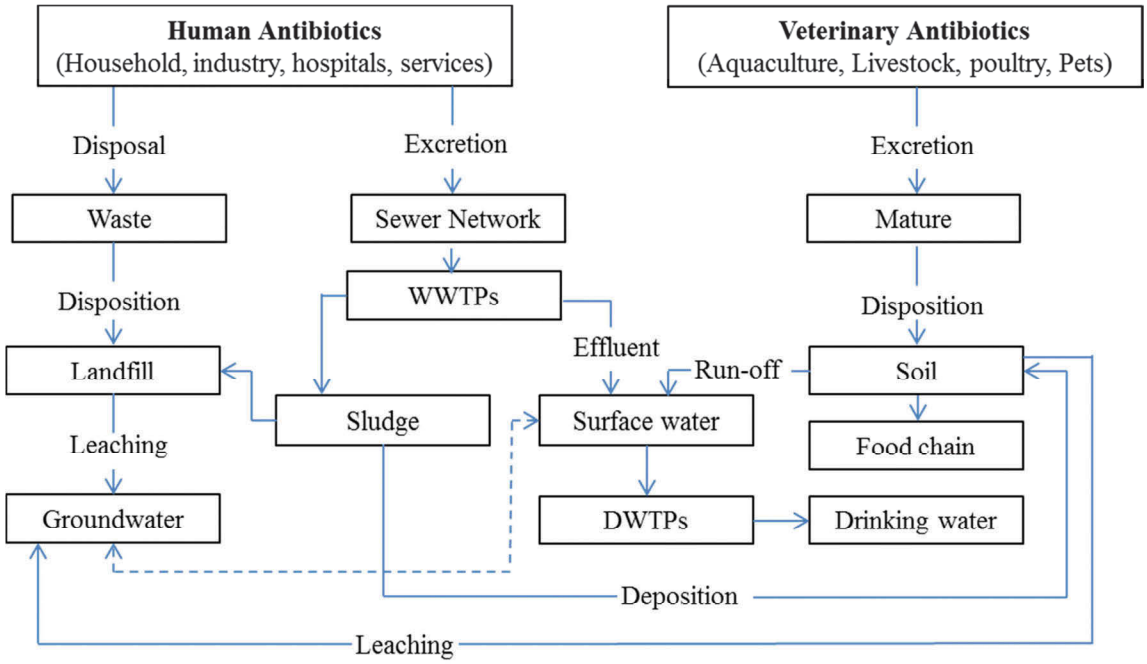

Figure 2.1 Sources of antibiotics in the environment (Adapted from Homem and Santos, 2011)

First reports regarding appearance of ABs in water were seen around 40 years ago (WHO, 2011). According to Homem and Santos (2011), the presence of ABs in environmental matrices has been investigated. Antibiotics have been detected in several environmental matrices including surface water, groundwater, seawater, drinking water, wastewater treatment plants effluent, hospital wastewater and biosolids (Adams et al., 2002; Ghauch et al., 2009). Typically, the concentrations of ABs are in the higher mg/L range in hospital effluents, and lower mg/L range in municipal wastewater and ng/L in surface, sea and groundwater (Adams et al., 2002; Homem and Santos, 2011).

According to WHO (2011), concentrations of pharmaceuticals in surface water, groundwater and partially treated water are usually less than 0.1 µg/L and concentrations in treated water are generally below 0.05 µg/L. For instance,

concentrations of chloramphenicol (CP) in municipal sewage, the Nanming River and the sediment of Nanming River of Guiyang City, China were reported at 47.4 µg/L; 19.0 µg/L and 1138 µg/kg, respectively (Liu et al., 2009). The chemical was also revealed in sewage treatment plant effluents and river water at concentrations up to 0.56 and 0.06 µg/L, respectively (Liu et al., 2009).

Furthermore, sediments from rivers that are influenced by agricultural activities have higher ABs levels than sediments from other areas (Kümmerer, 2009). Due to the use of manure or sludge as fertilizers, appearance of ABs in soil is also more prevalent. Thus, the findings of these compounds in vegetables and cereals were also reported by Homem and Santos (2011). Current literature shows detection of TCs at up to 0.15 µg/L in groundwater and surface water, 86–199 µg/kg in soil, 4.0 mg/kg in liquid manure, and 3 µg/L in farm lagoons (Chen et al., 2011). The ABs are very stable in the environment due to their highly polarity and non-volatile nature (Hernando et al., 2006).

C. Adverse effects of the ABs pollution

Even low concentrations of pharmaceuticals in water can pose serious problems to the ecosystem such as their potential risks of environmental toxicity and promotion of microbial resistance (Chen et al., 2011; Qiang et al., 2013; Fan et al., 2010; Lu et al., 2016). The appearance of the compounds in water results in several side effects such as aplastic anemia. Aplastic anemia is a condition that occurs when the human body stops producing enough new blood cells, causing fatigue and a higher risk of infections and uncontrolled bleeding (Figure 2.2). While being banned from application to food-producing animals in developed countries, these chemicals are still used in many developing nations due to their low cost, effectiveness and

availability (Nie et al., 2015). Antibiotics cannot be effectively removed by conventional wastewater treatment methods. Thus, they can accumulate causing a serious problem for aquatic organism and the ecosystem (Xi et al., 2014; Nie et al., 2015; Rajapaksha et al., 2015). Different negative effects of CP were discovered, e.g., fatal bone marrow depression and aplastic anemia as reported by Liu et al. (2009).

Additionally, ABs are responsible for the production of resistant microorganisms, resulting in serious problems of public health such as difficulties in treating pathologies and imbalance of microbial ecosystems (Homem and Santos, 2011).

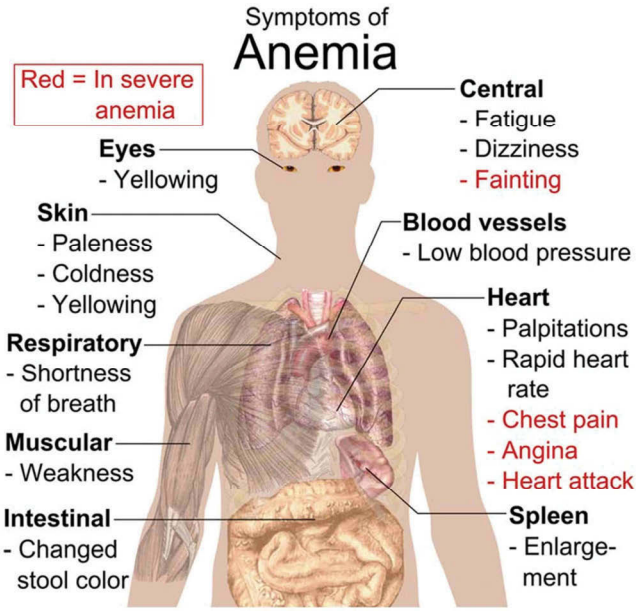

Figure 2.2 symptom of aplastic anemia (Pinterest, 2017)

D. ABs relevant regulations

Pharmaceuticals in general, and specifically antibiotics are normally controlled by stringent regulatory processes and necessarily rigorous preclinical and clinical studies to evaluate their efficacy and safety prior to commercialization

(WHO, 2011). Thus, ABs are generally better characterized than other environmental pollutants. The European Union (1990) has set up several legal limits for ABs in food such as 4-1500 µg/kg for milk and 25-6000 µg/kg for other food products from animal origin. However, there is no legislation applied to environmental matrices (Homem and Santos, 2011).

2.3. Technologies for the removal of heavy metals and antibiotics from water

Due to negative effects of water pollution caused by HMs and ABs, developments in efficient and cost-effective techniques for the removal of such compounds from water are necessary (Chen et al., 2011). There are different methods for removing HMs and ABs from water.

2.3.1. Heavy metals removal technologies

Numerous methods have been employed for the removal of heavy metals from water and wastewater. Table 2.2 shows the advantages and disadvantages of each method for removing metals from wastewater.

Table 2.2 Common methods for HMs removal from aqueous solution (Rahimi et al., 2015; Nguyen et al., 2013; Atta et al., 2015; Simate and Ndlovu, 2015)

Method	**Advantages**	**Disadvantages**
Chemical precipitation	Inexpensive Simple process	Ineffective at low contaminant concentration High consumption of reagents Large amounts of sludge
Ion exchange	High treatment capacity Energy efficient Metal selective High regeneration of materials	High cost Less number of metal ions removed Ion-exchange resins must be regenerated by chemical reagents
Adsorption	Most of metals can be removed Effectively removes low concentration of heavy metals (>99%) Regeneration by desorption	Cost of adsorbent Limited by ability of adsorbent

Method	Advantages	Disadvantages
Membrane filtration	High efficiency Treat large volumes Small space requirement, high separation selectivity	High cost due to membrane fouling Process complexity
Coagulation-flocculation	Good recoverability properties	High chemical consumption High cost
Flotation	High contaminant selectivity Low operating cost	High initial capital cost
Electrochemical	Metal selective Pure metals can be achieved Rapid and highly controlled removal No additional reagents required	Initial solution pH and current density High consumption of electricity Production of sludge
Electrodialysis	High separation selectivity	High operational cost due to membrane fouling and energy consumption
Photocatalysis	Removal of metals and organic pollutant simultaneously, less harmful by-products	Long duration time, limited applications

A. Chemical precipitation

Due to some metal salts being insoluble in water and can be precipitated, some necessary anions are added to remove heavy metals from aqueous solution (Hossain, 2013). This method is usually utilized for the removal of HMs up to parts per million (ppm) from wastewater. The sludge is often produced during the treatment process, leading to a significant problem (Gray and Schrefler, 2001). Precipitation is also ineffective in the removal of HMs at low concentrations and consumes a lot of reagents (Srivastava and Majumder, 2008; Hossain, 2013).

B. Ion exchange

The ion exchange process uses electrostatic forces on the exchange resin for exchanging metal ions from water (Kurniawan et al., 2006). The treatment method is

not suggested for any wastewater containing over 2500 mg/L of dissolved solids (Dabrowski et al., 2004). This technique uses an ion exchanger, commonly synthetic organic resins, to exchange either cations or anions and it can clean up water at ppb levels.

However, this removal technology requires high investment and operational cost as well as partial uptake of certain ions (Hossain, 2013). Other disadvantages of ion exchange include ineffectiveness with concentrated metal ions and highly sensitive to pH of the solution (Dabrowski et al., 2004). Furthermore, the ion exchange needs chemical reagents to regenerate (Hossain, 2013).

C. Adsorption

Adsorption has distinct advantages over other methods for removing HMs at low concentration because it is environmental friendly, economical and highly efficient (Tran et al., 2015; Wang and Chen, 2009). The removal process is flexible in design and operation and frequently produces high-quality treated effluent. In addition, adsorbents can be regenerated by suitable desorption reagents (Fu and Wang, 2011). Hence, the adsorption technique has become at the forefront among the major processes for removing heavy metals from water. Nevertheless, the efficiency of this method is limited depending on the capability of the adsorbent.

D. Membrane filtration

Membrane technology has been used in many industries for the removal of metal ions from water (Hossain, 2013). The treatment method can be used to abate oil and metal ions. This removal technique is highly efficient, treating large volumes, requiring a small space and has high separation selectivity. Membrane practices regularly consist of microfiltration, ultrafiltration, nanofiltration and reverse osmosis.

Most of membrane technologies require high quality of feed solution, hence they are often utilized as the last process in wastewater treatment. Conversely, the high cost of membranes and instability with certain kinds of chemicals and pH of solution are disadvantages of this method. Additionally, the membrane must be cleaned and washed, high cost due to membrane fouling and complexity of operation (Nguyen et al., 2013; Radjenovic' et al., 2008).

E. Coagulation-flocculation

Coagulation-flocculation is a treatment process for removing suspended solids, colloidal particles and heavy metals. This technique is used in the final stage of liquid-solid separation and followed by sedimentation and filtration (Fu and Wang, 2011). Coagulation is the destabilization of colloids through the forces that keep them apart. Various coagulants were applied in the conventional treatment processes such as aluminium, ferrous sulfate, ferric chloride and polyaluminium chloride (PAC) (El Samrani et al., 2008). Flocculation is the agglomeration of polymers to form bridges between the flocs and bind the particles into large agglomerates or clumps, which then can be settled (Fu and Wang, 2011; Hossain, 2013). While the coagulation-flocculation has a good recoverability of HMs, the technique requires high chemical consumption, high cost and it cannot completely remove the HMs from wastewater (Nguyen et al., 2013).

F. Flotation

Flotation is a technique that was used in mineral and environmental technologies. The process is often applied following a biological treatment stage in a wastewater treatment plant for removing metal-loaded biomass. Several kinds of flotation have been utilized such as foam or bubble fractionation, foam separation or

froth flotation to remove HMs from water (Hossain, 2013). The flotation technology has a high contaminant selectivity and low operating cost. However, it requires high initial capital investment (Nguyen et al., 2013).

G. Electrochemical

Electrochemical technique uses a cathode and anode system with electricity to remove HMs from water. In this method, the metal ions are attached to the cathode surface and can recover metals in the elemental metal state (Fu and Wang, 2011). Advantages of the process are metal selectivity, pure metals achievement, rapid and highly controlled removal and no additional reagents requirement (Wang et al., 2007). However, the wastewater treatment by electrochemical technology involves high capital investment and electricity supply cost. Moreover, the process also produces a large amount of sludge (Nguyen et al., 2013; Tran et al., 2015).

H. Electrodialysis

Electrodialysis is a membrane separation technique for removing HMs using an ion exchange membrane by applying an electric potential (Barakat, 2011). This method separates ionic species (heavy metals) of a solution by the use of semipermeable ion-selective membranes (Hossain, 2013). The advantages of this process are high separation selectivity and maintaining a low metal ions concentration. The method's drawbacks are energy consumption, high capital cost and the formation of metal hydroxides which clog the membrane resulting in high operational cost (Tran et al., 2015; Hossain, 2013). As a membrane process, electrodialysis requires clean feed, careful operation, periodic maintenance to inhibit any damages (Barakat, 2011).

K. Photocatalysis

Photocatalytic process is a technique that converts solar energy for useful purposes such as HMs removal. Many semiconductors have been used for this technique including TiO_2, ZnO, CeO_2, CdS, ZnS, etc (Barakat, 2011). Among those, titanium dioxide has achieved the best performance in removing contaminants from aqueous solution. The technology can remove metals and organic pollutants simultaneously and creates less harmful by-products. The destruction of environmental pollutants by a photocatalytic process is rapid and efficient. However, this treatment process involves a long duration time and has limited applications.

2.3.2. Antibiotics removal technologies

So far, no studies on the removal of pharmaceuticals via conventional drinking water treatment processes have been reported (Adams et al., 2002). On the other hand, a variety of methods to remove antibiotics and other pharmaceuticals from aquatic matrix such as advanced oxidation processes, combined chemical/biological treatment, aerobic digestion integrated with activated carbon, ion exchange, coagulation, flocculation, sedimentation, ultraviolet irradiation, have been attempted (Adams et al., 2002; Homem and Santos, 2011; Qiang et al., 2013; Nie et al., 2015). However, it was reported that these conventional methods were moderately ineffective in removing antibiotics from aquatic media (Qiang et al., 2013). Adsorption using cost-effective adsorbents is considered an effective process that removes antibiotics from aqueous solution (Qiang et al., 2013). Table 2.3 summarizes several conventional methods for the removal of ABs from water.

Table 2.3 Common methods for removing ABs from aqueous solution (Homem and Santos, 2011)

Method	Advantages	Disadvantages
Conventional methods		
Biological process, filtration, coagulation, flocculation, sedimentation	Can treat large effluent flow rate	Cannot apply for high concentration of pollutants, creates new waste, low efficiency
Oxidation and advanced oxidation		
Chlorination	High efficiency	Uses chemicals, high operating cost
Ozonation	Fast speed, working well with fluctuating flow rate and composition of influent	High cost of equipment and maintenance, chemicals, energy supply, highly affected by operating conditions
Fenton and photo-Fenton	Energy saving, low-cost reagents, environmental safe	Dependent on operating conditions and target pollutants concentration
Photolysis	Appropriate removal of wastewater containing photo-sensitive contaminants	Low removal efficiency Dependent on the chemical structure of the ABs, COD level
Semiconductor photocatalysis	High efficiency and energy saving	Dependent on catalyst concentration, and operating conditions
Electrochemical processes	Effective, versatile, cost-effective, ease and clean technology; can treat high levels of ABs and COD	Can treat small flow rates only; high operating cost; dependences of electrode material and experimental conditions
Adsorption	High efficiency Not producing toxic metabolites	Not able to destroy ABs but adsorb them on adsorbents' surface High cost of conventional adsorbent (activated carbon)
Membrane		
Reverse osmosis, nano and ultrafiltration	Simple and high energy efficiency	High maintenance cost Slow speed for ABs removal Sensitive to temperature
Ion exchange	Reversible process	Requiring backwashing and regeneration regularly; fouling problem
Combined chemical and biological processes	Maximize removal efficiency	Need careful set up and operation

A. Conventional methods

The conventional wastewater treatment plants frequently used techniques such as biological processes, filtration and coagulation/flocculation/sedimentation (Adams et al., 2002; Homem and Santos, 2011; Arikan, 2008). The biological process degraded organic compounds in activated sludge tanks and treating large effluent flow rates. However, this technique cannot be applied for treatment of high toxic pollutants due to their being toxic to microorganisms (Homem and Santos, 2011). The filtration removes the solid particles by passing the wastewater via a filtration media such as sand, coal, diatomaceous earth, granular activated carbon. The disadvantage of filtration is it cannot degrade pollutants, but accumulate it in the solid phase, creating a new waste (Eckenfelder, 2006). Coagulation/flocculation/sedimentation utilizes chemicals to increase the solids sedimentation, pollutants precipitation and colloids formation and is easy to settle down. Nevertheless, the methods achieve low efficiency for removing ABs and need a following treatment to remove the pollutants from water (Homem and Santos, 2011).

B. Oxidation and advanced oxidation processes

One of the alternative treatment methods for removing antibiotics from aqueous solution is oxidation and advanced oxidation processes. The methods use oxidation reagent or oxidants to oxidize the pollutants to less toxic compounds. Oxidants were used such as chlorine and molecular ozone. Advanced oxidation processes are oxidative methods based on the generation of intermediate radicals, the hydroxyl radicals (.OH), which are extremely reactive and less selective than chlorine or molecular ozone. The advanced oxidation processes are very effective to

treat many organic pollutants (Bautitz and Nogueira, 2007). Homem and Santos (2011) indicated several types of oxidants were used in advanced oxidation processes including ozonation, Fenton, photo-Fenton, photolysis, semiconductor photocatalysis and electrochemical processes.

Chlorination

Chlorine gas or hypochlorite has been often used for disinfecting the drinking water in the post-treatment stage because of its low cost and high efficiency (Acero et al., 2010). Recently, chlorinated species such as chlorine, chlorine dioxide, hypochlorous acid were also utilized for treating wastewater containing pharmaceuticals. Due to its oxidizing power, chlorine oxidizes them to readily biodegradable and less toxic compounds (Deborde and von Gunten, 2008).

Ozonation

Ozone is a strong direct or indirect oxidant. Due to its selective reaction with nucleophilic molecules, molecular ozone can oxidize organic compounds which have carbon-carbon double bonds, aromatic bonds or nitrogen, phosphorous, oxygen or sulphur atoms (Ikehata et al., 2006). On the other hand, molecular ozone will be decomposed in water to form hydroxyl radicals. The .OH groups react with ABs, and then remove the pollutants from water. This is a fast process and can work well with fluctuating flow rate and composition of wastewater. In contrast, disadvantages of this technique are high cost of equipment and maintenance, mass transfer limitations requiring large amount of oxidant as well as energy supply (Homem and Santos, 2011). Furthermore, antibiotics removal from water by ozonation treatment was influenced by the presence of organic matter, suspended solids, carbonate, bicarbonate and chlorine ions, pH and temperature (Homem and Santos, 2011).

Fenton and photo-Fenton

Fenton's reagent is a mixture of hydrogen peroxide and ferrous ions in acidic medium that has a strong oxidizing ability (Gan et al., 2009). The mixture produces hydroxyl radicals which react with antibiotics from aqueous solution (Homem and Santos, 2011). Generally, the application of UV light in the Fenton process (photo-Fenton) improves the treatment performance. The benefits of this technology are energy saving as solar radiation is used, using low-cost reagents, environmentally safe. The dependencies on pH, temperature, catalyst, hydrogen peroxide and target-compound concentration of the ABs removal are the drawbacks of Fenton and photo-Fenton. For high turbidity wastewater, the photo-Fenton is unsuitable since the turbidity prevents the penetration of UV light.

Photolysis

Photolysis uses the natural or artificial light to decompose or dissociate chemical compounds. Typically, photolysis can work in two ways: direct and indirect. In direct photolysis, organic pollutants absorb UV light and react with the constituents of the water matrix or suffer self-decomposition (Trovó et al., 2009). On the other hand, indirect photolysis degrades the contaminants by photosensitizers like oxygen and hydroxyl or peroxyl radicals (Arslan-Alaton and Dogruel, 2004). The efficiency of photolysis is affected by the absorption spectrum of the target-compound, radiation intensity and frequency, reagent concentration, and very long reaction times (Kümmerer, 2009). This technology is ineffective to remove antibiotics from water compared to other methods and only appropriate to wastewater containing photo-sensitive contaminants with low chemical oxygen

demand (COD) concentrations (Homem and Santos, 2011). Moreover, this process depends on the chemical structure of the antibiotics.

Semiconductor photocatalysis

Semiconductor photocatalysis is the technique which uses artificial or sunlight to activate a semiconductor (commonly TiO_2 due to its high stability, good performance and low cost) for degrading pollutants. The removal mechanism of this technology includes both hydroxyl radicals and other radical species derived from oxygen (Homem and Santos, 2011). Removal efficiency of ABs by **s**emiconductor photocatalysis depends on catalyst concentration, wavelength, radiation intensity, pH and water matrix. The technique can use solar energy and achieves high efficiency, thus it is energy saving. In contrast, it is difficult to apply widely as it depends on the penetration of light through aqueous solution (Homem and Santos, 2011). It can be time consuming and costly.

Electrochemical processes

The electrochemical process has also been used to remove toxic organic compounds. In this technique, pollutants are oxidized in anodes (graphite, TiO_2, Ti-based alloys, Ru or Ir oxides, boron-doped diamond) in the presence of an electrolyte. Antibiotics can be destroyed by direct anodic oxidation or indirectly in the liquid bulk with mediation of electroactive species (Panizza and Cerisola, 2009).

Advantages of this technique are effective, versatile, cost-effective, easy and clean technology (Panizza and Cerisola, 2009). The technology can also treat wastewater containing high concentrations of both antibiotics and COD (Homem and Santos, 2011). However, the applicability of this technology is limited to small flow rates and the high operating cost is also a disadvantage. The process performance

depends on the nature and structure of the electrode material, experimental conditions (pH, temperature) and electrolyte composition (Jara et al., 2007).

C. Adsorption processes

The adsorptive removal of organic pollutants from water has been widely applied. The most common adsorbents are solid materials. Remediation of antibiotic-contaminated water has been studied by sorption on various sorbents such as natural sorbents, clays, chitosan derivative, activated carbon, and more (Rajapaksha et al., 2015). There are two different kinds of adsorption regarding the nature of forces involved including chemical and physical adsorption. In physical adsorption, van der Waals interactions are mainly forces which are moderately weak. On the other hand, chemical adsorption relates to the electron transfer and chemical bonds formation between antibiotics and the solid surface. The interactions in chemical adsorption are strong and limited to the monolayer coverage (Ruthven, 2006). The advantage of adsorption is removing ABs instead of producing potentially more dangerous metabolites (Putra et al., 2009). Conversely, the technology did not destroyed the antibiotics but concentrated them on adsorbents' surface. The conventional and most used adsorbent is activated carbons. However, their high cost means wide application of this adsorbent is difficult. Thus, adsorption using cost-effective adsorbents is considered an effective process that removes antibiotics from aqueous solution (Qiang et al., 2013).

D. Membrane processes

The application of membrane technology for removing antibiotics from aqueous solution has been increased. The process is unable to degrade the toxicants

but transfers them into concentrated form. There are several kinds of membrane to abate ABs such as reverse osmosis, nanofiltration, ultrafiltration and ion exchange.

Reverse osmosis, nano and ultrafiltration

Reverse osmosis is a kind of membrane techniques (Radjenović et al., 2008). This process is often used to immobilize large molecules and ions of pollutants. The flow occurs against the concentration gradient in reverse osmosis. This technique can efficiently remove dissolved salts but not effectively abate organic compounds. Moreover, reverse osmosis is simple and has high energy efficiency. Nevertheless, the membranes are very quickly fouled or damaged. In comparison with other techniques, reverse osmosis is a slow process for removing ABs from wastewater (Homem and Santos, 2011). Other membrane processes are nanofiltration and ultrafiltration (Radjenović et al., 2008). The technologies are cross-flow filtrations and usually charged (carboxylic groups, sulfonic groups). Hence, ion repulsion is the main factor in this treatment and it can remove smaller molecules such as antibiotics. Furthermore, these membrane processes are sensitive to temperature.

Ion exchange

The water treatment by ion exchange is the use of ion exchange resin (anion or cation exchangers) to exchange with cations or anions in a liquid medium (Choi et al., 2007). The most used materials for iron exchange resin is polymeric (styrenic and acrylic) due to their stability and great selectivity (Dickert, 2000). Ion exchange is also a reversible process which allows a prolonged using time of the resin. On the other hand, the technique requires backwashing and regeneration regularly and fouling is also a problem (Üstün et al., 2007).

E. Combined processes

Combination of different technologies in one water treatment system is necessary to maximize the cleaning performance. However, the combination of techniques as different stages for water treatment needs a careful study to avoid negative influences. For instance, most microorganisms in a biodegradation tank are sensitive to the toxic pollutants or chemicals from previous treatment stages. Thus, advanced oxidize processes or adsorption has been used as a pre-treatment step to oxidize the pollutants, making them less toxic and biodegradable before treating with microorganisms (Tekin et al., 2006).

2.3.3. Adsorption of HMs and ABs using typical low cost materials

Several typical low-cost materials have been applied for removing HMs and ABs from aqueous solution such as natural minerals, agricultural waste/by-products and industrial waste/by-products. Table 2.4 specifies the cost of some typical low-cost adsorbents and commercial activated carbon.

Table 2.4 Prices of low-cost adsorbents (Bailey et al., 1999; Bhattacharyya and Gupta, 2008; Rafatullah et al., 2010; Olivella et al., 2012; Tran et al., 2015)

Types of adsorbent	**Price (US.kg^{-1})**	**Source**
Coconut shell charcoal	0.34	Bhattacharyya and Gupta, 2008
Rice husk	0.025	Rafatullah et al., 2010
Lignin	0.06	Bhattacharyya and Gupta, 2008
Chitosan	2.2-15.43	Bailey et al., 1999; Rafatullah et al., 2010
Clay	0.04 – 0.12	Rafatullah et al., 2010
Zeolite	0.03 – 0.12	Rafatullah et al., 2010
Clinoptilolite	0.03 – 0.12	Bhattacharyya and Gupta, 2008
Spheroidal cellulose	1.07	Bhattacharyya and Gupta, 2008
Peat	0.023	Bhattacharyya and Gupta, 2008
Commercial activated carbon	20 – 22.00	Rafatullah et al., 2010
Cork waste	0.48	Olivella et al., 2012

A. Natural minerals

Natural minerals have been used as sorbents for toxicants removal from wastewater. Typical kinds of these adsorbents such as zeolite, peat, and clays were used for removing HMs and ABs from aqueous solution. The three materials have high adsorption capacity, are locally available and inexpensive. Hence, they are also considered as low-cost adsorbents.

Zeolite

Zeolites are naturally occurring hydrated aluminosilicate minerals, belonging to the class of "tectosilicates" mineral (Erdem et al., 2004). Erdem et al. (2004) presented the molecular structure of zeolites consists of three-dimensional frameworks of SiO_4 and AlO_4 tetrahedra with composition (% by weight): SiO_2 69.31, Al_2O_3 13.11, Fe_2O_3 1.31, CaO 2.07, MgO 1.13, Na_2O 0.52, K_2O 2.83, SO_3 0.10, H_2O 6.88 and Si/Al 4.66. The authors argued that the aluminum ion is small enough to occupy the position in the center of the tetrahedron of four oxygen atoms, the excess oxygen in the alumina molecules gives the framework of a negative charge which can be balanced by trapping positively-charged ions (sodium, potassium, or calcium). These cations are exchangeable with metal ions in solutions such as lead, cadmium, zinc, and manganese. Perić et al. (2004) reported that the sorption mechanism of heavy metals on zeolites is a complex procedure due to their porous structure, inner and outer charged surfaces, mineralogical heterogeneity, existence of crystal edges, broken bonds, and other imperfections on the surface. Furthermore, surfactant modified zeolite can also remove organic compounds and oxyanions from water (Kuleyin, 2007). The sorption of oxyanions by surfactant modified zeolite was recognized as being due to anion exchange on the positively

charged surfactant bilayer, whereas the sorption of hydrophobic organic contaminants was due to partitioning of the organics into the organic phase created by the surfactant tail groups (Li et al., 2000).

Brazilian natural scolecite, a kind of natural zeolites which has the molecular formula $Na_{0,26}Ca_{0,95}Al_{2,07}Si_{3,00}O_{10}.3H_2O$, was used as an adsorbent for toxic metal removal by Dal Bosco et al. (2005). The study revealed that the sorption capacity of scolecite for metals at 298 K followed the series Cr > Mn > Cd > Ni and the adsorption process was best described by a Freundlich isotherm. With the same conditions, conversely, adsorption capacity of metal ions on natural zeolite is different, depending on characteristics of the ion. In their study, Zamzow et al. (1990) claimed that the selectivity series of clinoptilolite in the sodium form is: Pb^{2+} > Cd^{2+} > Cs^{+} > Cu^{2+} > Co^{2+} > Cr^{3+} > Zn^{2+} > Ni^{2+} > Hg^{2+}. Maximum adsorption capacities of toxicants on zeolites (mg/g) following the Langmuir isotherm were also reported by many authors: Cu^{2+} 9.0, Co^{2+} 14.4, Zn^{2+} 8.8, Mn^{2+} 4.2 (Erdem et al., 2004); Cr^{3+} 106.4, Ni^{2+} 122.0, Cd^{2+} 100.0, Mn^{2+} 109.9 (Dal Bosco et al., 2005); Zn^{2+} 41.8, Cu^{2+} 44.2, Cd^{2+} 45.2, Pb^{2+} 56.8 (Baker et al., 2009).

The removal of ABs by natural and synthesized zeolites has been reported by some authors (Fukahori et al., 2012; Fukahori et al., 2011; Ötker and Akmehmet-Balcıoğlu, 2005; Blasioli et al., 2014; Fukahori and Fujiwara, 2014; Liu et al., 2013). Adsorption and degradation of enrofloxacin on natural zeolite achieved maximum adsorption capacities of 19.3 to 22.6 (mg/g) (Ötker and Akmehmet-Balcıoğlu, 2005). Fukahori et al. (2012) used the high-silica zeolite HSZ-385 to remove seven sulfonamide antibiotics from livestock urine. The adsorbed amounts of sulfathiazole, sulfamerazine, sulfamethizole, sulfadimidine and sulfamethoxazole on high-silica

zeolite HSZ-385 were 75.0, 87.9, 93.2, 91.7, and 94.5 mg/g, respectively. A study by Martucci et al. (2012) reported the use of synthetic organophilic zeolites for adsorptive removal of pharmaceuticals such as erythromycin, carbamazepine and levofloxacin from aqueous solutions. Other studies researched the removal of sulfamethoxazole by high silica zeolites; sulfonamide antibiotic removal by TiO2/high-silica zeolite HSZ-385 composite; tetracycline antibiotics removal by MCM-41 has been modified by impregnation with zeolite (Blasioli et al., 2014; Fukahori and Fujiwara, 2014; Liu et al., 2013).

Peat

Peat moss is a complex matter with lignin and cellulose as primary constituents. These constituents, especially lignin and humic acid, bear polar functional groups, such as alcohols, aldehydes, ketones, carboxylic acids, phenolic hydroxides and ethers that can be involved in chemical bonding (Coupal and Lalancette, 1976). Brown et al. (2000) claimed that due to the polar character of peat, it has a quite high adsorption capacity for dissolved solids, such as metals and polar organic molecules. The authors stated that the mechanism of metal ions binding to peat remains a controversial area with ion-exchange, complexation, and surface adsorption being the prevalent theories. It is frequently believed that ion exchange is the most predominant process. The humification of peat produces humic and fulvic acids and thus can capture heavy metals. Metals react with the carboxylic and phenolic acid groups of the acids to release protons or, at sufficiently high pH, with their anion sites to displace an existing metal (Brown et al., 2000). In a study, Couillard (1994) noted that the mechanism of sorption process on peat might be explained as a chemical reaction between functional groups of peat with heavy metal

ions to form metals organic complexes or a cation exchange reaction. According to this study's results, there are many probable interactions between toxicants and peat: (1) cation exchange with H ions found in the -COOH, phenolic hydroxyl and heterocyclic groups; (2) the interaction of metallic cations to form chelate complexes; (3) the formation of hydrogen bonds between polyvalent cations and the hydroxyl, lignin, cellulose and hemicellulose groups within the porous structure; and (4) the formation of anion-cation bonds. These interactions depend on the characteristics of the peat and the contaminants.

The maximum adsorption capacities of HMs onto two kinds of peat following the Langmuir model which have been reported by Gosset et al. (1986) were: HCl modified eutrophic peat: Cu^{2+} 12.1, Cd^{2+} 20.2, Zn^{2+} 11.1, Ni^{2+} 11.2 mg/g; and HCl modified oligotrophic peat Cu^{2+} 12.1, Cd^{2+} 22.5, Zn^{2+} 13.1, Ni^{2+} 11.7 mg/g.

So far, there is no study on directly using peat for the abatement of ABs from wastewater. Only some studies have used activated carbon from peat to remove ABs from water (Carabineiro et al., 2011; Aroguz, 2006; Mohammad-Khah and Ansari, 2009). Adsorption capacities of ciprofloxacin on activated carbons prepared from peat ranged from 60 to 300 mg/g (Carabineiro et al., 2011). Langmuir adsorption capacity of azinphosmethyl on pyrolyzed (at 600°C) ocean peat moss was 4.54 mg/g (Aroguz, 2006).

Clays

The last natural mineral which will be discussed is clay, which has been used since a very early time for ceramic and building purposes. Clays have a net negative charge in their structures, hence lead to the adsorption capacity of the minerals. The adsorption ability of clays usually depends on their chemical nature and pore

structure (Lin and Juang, 2002). Due to the properties of clays such as the large specific surface area, chemical and mechanical stability, layered structure, and high cation exchange capacity (CEC), they are excellent adsorbent materials (Bhattacharyya and Gupta, 2008). The edges and the faces of clay particles can adsorb anions, cations, non-ionic and polar contaminants from water (Bhattacharyya and Gupta, 2008). Clays may be classified into three main classes including kaolinite, micas (such as illite), and smectites (for instance montmorillonite) (Bailey et al., 1999). Montmorillonite is a three layer mineral that has a basic unit consisting of one aluminate layer sandwiched between two silicate layers, while the basic unit of kaolinite is a double layer consisting of one silicate and one aluminate layer (Srivastava et al., 1989). Kaolinite has the theoretical composition (%) of SiO_2 46.54, Al_2O_3 39.50 and H_2O 13.96 expressed in terms of the oxides (Bhattacharyya and Gupta, 2008). Montmorillonite demonstrates it has the highest cation exchange capacity among other kinds of clays (Bailey et al., 1999). Its theoretical composition (%) without the interlayer material was SiO_2 66.7, Al_2O_3 28.3, H_2O 5.0.

Some elements have been used to improve clays adsorption capacity including acid, bases, pillar ions, organic compounds. Maximum adsorption capacities on sodium dodecylsulfate modified montmorillonite following Langmuir isotherm were (mg/g): Cu^{2+} 16.1, Zn^{2+} 13.3 (Lin and Juang, 2002). According to a study of Gupta and Bhattacharyya (2006), adsorption capacities of Cd^{2+} on materials from clays were (mg/g): kaolinite 6.8, montmorillonite 30.7; polyhydroxo zirconium modified kaolinite 5.3; tetrabutylammonium bromide modified kaolinite 6.3; and tetrabutylammonium bromide montmorillonite 43.5. Akar et al. (2009) reported in their study that adsorption capacities of Cr^{6+} on Turkish montmorillonite clay are

(mg/g): HDTMA modified clay 10.2; natural clay 3.6; heat-activated clay (at 100^{o}C) 4.2; and acid-activated 4.5. In another study which was conducted by Ijagbemi et al. (2009) it was noted that adsorption capacities of metal ions on analytical grade of montmorillonite are (mg/g): Cu^{2+} 7.6 and Ni^{2+} 12.9. A material from clays, which was prepared by Wu et al. (2009), was Fe pillared montmorillonite clay and had adsorption capacity of Cd^{2+} is 25.7 mg/g.

Bentonite (its main content is montmorillonite) has also been used for removing ABs from water by several studies (Ahmed et al., 2015; Zhang et al., 2013a). A study using bentonite, AC, zeolite and pumice for removing ciprofloxacin was investigated (Genç and Dogan, 2015). Genç et al. (2013) concluded that adsorptive removal efficiency of ciprofloxacin from aqueous solution on bentonite was 99% with a contact time of 30 min at pH 4.5. The study indicated that adsorption of ciprofloxacin following Langmuir model on bentonite was 147.1 mg/g. Another study showed maximum adsorption capacities of amoxicillin onto bentonite following Langmuir isotherm were from 47.3715 to 53.9315 (mg/g) (Putra et al., 2009).

B. Agricultural waste and by-products

Tons of cheap biosorbents belonging to some principal categories (including lignocellulose, algae, chitin/chitosan, activated sludge, bacteria biomass, fungal biomass) can be employed for HMs and ABs removal (Abdolali et al., 2014, Ahmad et al., 2009; Liu et al., 2012). Among these categories, lignocellulose and chitin/chitosan are very highly applicable groups because of their representativeness, high adsorption capacity and availability. Maximum adsorption capacities of heavy metals and ABs onto the low-cost biosorbents are presented in Table 2.5 and 2.6.

Lignocellulose

Lignocellulose is plant dry matter, which is often referred to as biomass or lignocellulosic biomass. As the primary building block of plant cell walls, lignocellulose contains cellulose, hemicellulose, lignin, as well as a small amount of pectin, protein, extractives and ash (Jorgensen et al., 2007). Figure 2.3 expresses the chemical composition of several representative examples of lignocellulose.

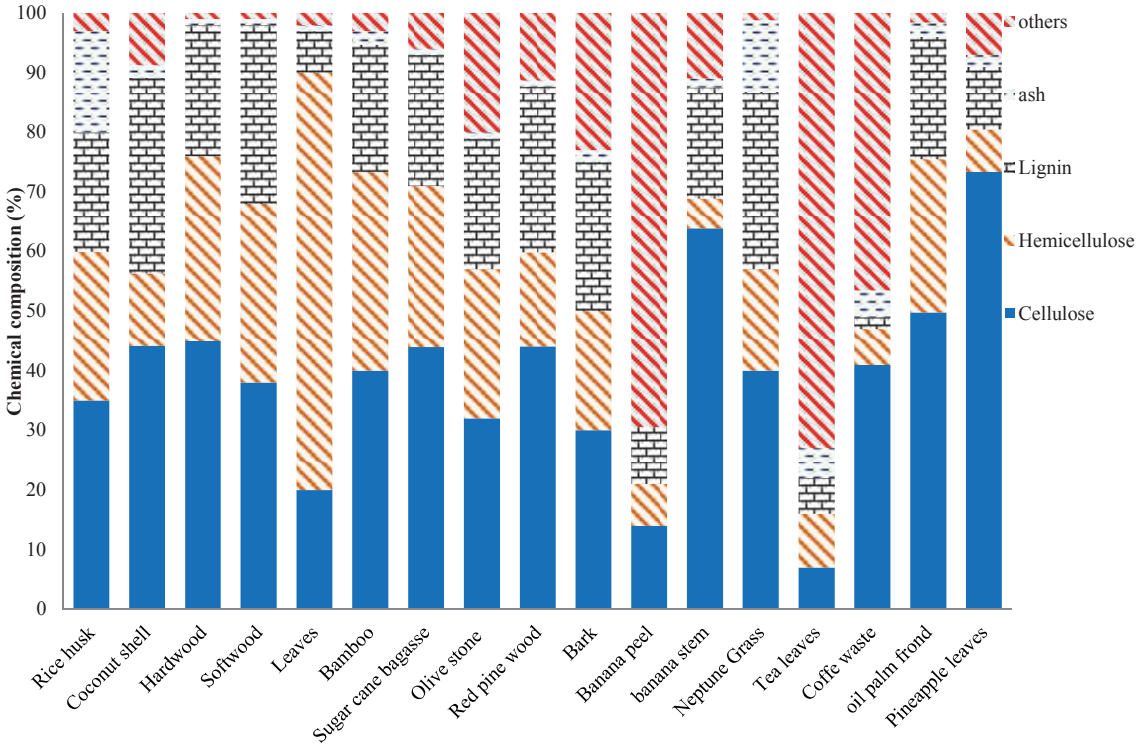

Figure 2.3 Average chemical composition of some typical lignocellulose (% dry weight) (Tran et al., 2015)

Lignocellulosic agricultural wastes have a high potential for sorption of heavy metals because of their inexpensive price and high adsorption properties (Krishnani et al., 2008). Many investigators studied the removal of metal ions by the Lignocellulosic waste and by-products and the Langmuir maximum adsorption capacities of HMs onto the adsorbents are indicated in Table 2.5. Several adsorbents

have highest adsorption capacities of HMs such as Pb^{2+}: natural seaweed 369.6 mg/g (Ahmady-Asbchin et al., 2009), rice husk (tartaric acid) 108 mg/g (Wong et al., 2003); Zn^{2+}: carrot residues (HCl) 29.6 mg/g (Nasernejad et al., 2005), natural seaweed 46.3 mg/g (Ahmady-Asbchin et al., 2009); Cd^{2+}: green coconut shell 285.7 mg/g (Pino et al., 2006); Cu^{2+}: seaweed (2-propanolits) 143.3 mg/g (Basha et al., 2009), sawdust (formaldehyde) 37.2 mg/g (Ahmad et al., 2009); Cr^{6+}: macro algae Gracilaria verrucosa (modified) 377.6 mg/g (Ata et al., 2012).

In other research works, adsorbents from lignocellulosic precursors are also used for the removal of ABs from water. The lignocellulose adsorbents have frequently been modified before use for water containing ABs treatment. Some authors have utilized activated carbon obtained from lignicellulose to uptake antibiotics from aqueous solution. Ilhan et al. (2012) used woodchip for removing antibiotics from water and concluded that 65% of the sorbed atrazine, 70% of sulfamethazine, 90% of enrofloxacin, and 80% of monensin A were reserved in wood chips. In a study, removal of antibiotics by coagulation and granular activated carbon filtration was conducted (Choi et al., 2008). While removal efficiencies of oxytetracycline-HCl, democlocycline-HCl and tetracycline were more than 90%, less than 70% of minocycline-HCl and meclocycline-sulfosalicylate were removed. Torres-Pérez et al. (2012) has used activated carbons from agricultural residues to abate antibiotics from water and the removal efficiencies reduced in the order: commercial granular activated carbon GAC2 (817 mg/g) > beet pulp BP-H_2O (288 mg/g) > commercial granular activated carbon GAC1 (133 mg/g) > peanut hulls PH-H_2O (28 mg/g). In another study, penicillin G uptake capacity was determined as

330.0 mg/g for activated sludge, 459.0 mg/g for *R. arrhizus* and 375.0 mg/g for activated carbon at the experimental conditions (Aksu and Tunç, 2005).

Modification biomass for removing ABs from water has been studied by several investigators. Yu et al. (2017) researched on levofloxacin removal from water using zirconium (IV) loaded corn bracts. The adsorbent exhibited a strong adsorption capacity (Q_{max} = 73 mg/g) and it can also regenerated with desorption rate up to 89% with pH 11. In another study, removal efficiencies of fluoroquinolones antibiotics by microporous activated carbon from lignocellulosic biomass by microwave pyrolysis were 96.12% of ciprofloxacin and 98.13% of norfloxacin, respectively (Ahmed and Theydan, 2014). Maximum Langmuir adsorption capacities of 131.14 and 166.99 mg/g for ciprofloxacin and norfloxacin on the adsorbent were achieved, respectively. Balarak and Mostafapour (2016) have treated canola residues with temperature at 105℃ and 0.5M H_2SO_4 for using as an adsorbent to remove metronidazole antibiotic. The theoretical maximum of adsorption capacity following Langmuir model was 21.42 mg/g and equilibrium status was achieved within 90 min of contact time.

Chitin/chitosan

Chitin is a naturally mucopolysaccharide and its structure is shown in Figure 2.4. This biopolymer is created by a vast number of living creatures, and was seen as the most natural polymer after cellulose in terms of abundance (Rinaudo, 2006). The compound is highly hydrophobic and is insoluble in water and most organic solvents (Ravi Kumar, 2000). It consists of 2-acetamido-2-deoxy-β-D-glucose through a β (1 - 4) linkage and can be degraded by chitinase (Ravi Kumar, 2000). Chitin is a component in the exoskeletons of crabs and other arthropods and in the cell walls of

some fungi (Bailey et al., 1999). Chitin production is associated with sea food processing such as shrimp or crab canning. A very important derivative of chitin is chitosan or glucosamine. It can be produced from chitin and is a component of fungal cell walls (Tran et al., 2015).

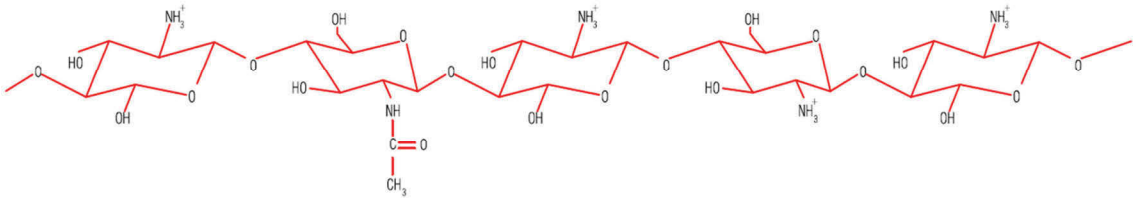

Figure 2.4 Molecular structure of chitosan (adapted from Celis et al., 2012)

Table 2.5 shows several studies using chitin/chitosan for removing HMs from water. The metal ions, its adsorption capacities, isotherm models are showed (Table 2.5). A study used chitosan-coated biosorbent (dip-coating the oxalic acid-treated activated alumina with chitosan gel) for removing arsenic from aqueous solution and Langmuir maximum adsorption capacities were As^{3+} 56.50 and As^{5+} 96.46 mg/g (Boddu et al., 2008). An et al. (2001) utilized crab shell (containing chitin) to remove HMs. The maximum adsorption capacities of HMs onto the material following Langmuir isotherm were Pb^{2+} 198.9, Cd^{2+} 154.0, Cu^{2+} 55.9 and Cr^{3+} 49.4 mg/g (An et al., 2001).

There are only a few studies which have used direct chitin/chitosan to uptake ABs from aqueous solution. Some investigators modified chitin/chitosan with other materials to treat water containing antibiotic pollutants. The removal of penicillin G by chitin/chitosan in fungal biomass was researched (Aksu and Tunç, 2005). Maximum loading capacities of penicillin G at 35°C were 591.8 mg/g for dried *R. arrhizus,* 434.8 mg g^{-1} for dried activated sludge and 463.0 mg g^{-1} for activated

carbon. In another study, Bhowmik and Bajpai (2012) used chitin for removing gatifloxacin from synthetic wastewater and removal capacities reached 97.11 ± 2.35, 100.0 ± 3.23 and 181.82 ± 5.58 mg/g at 18, 28 and 37°C.

Amino-acid-modified-chitosan was used to remove antibiotics and the achieved removal efficiencies were norfloxacin (50%), sulfadiazine or tylosin (60%) from water (Jia et al., 2016). In a study conducted by Ou et al. (2015), maximum adsorption capacity of erythromycin by magnetic imprinted polymers synthesized from chitosan-stabilized Pickering emulsion was from 15.51 to 52.32 μmol/g. In their studies, Priya et al. (2016a,b) used chitosan and other materials to create photocatalytic reagents to mineralizing and degrading oxytetracycline and ampicillin antibiotics from water.

Table 2.5 Heavy metals of adsorption capacity (mg/g) of biosorbents

HMs	Sorbents (modifying agent)	Isotherms	Q_{max} (mg/g)	Source
Pb	Rice husk (alkali and heat)	Langmuir	58	Krishnani et al., 2008
	Rice husk (tartaric acid)	Langmuir	108	Wong et al., 2003
	Sawdust (formaldehyde)	Langmuir	37.0	Ahmad et al., 2009
	Sawdust (formaldehyde and sulphuric acids)	Langmuir	22.2	Taty-Costodes et al., 2003
	Lignin from black liquor	Langmuir	89.5	Guo et al., 2008
	Modified lignin from alkali glycerol delignication	Langmuir	8.2 - 9.0	Demirbas, 2004
	Natural seaweed	Langmuir	369.6	Ahmady-Asbchin et al., 2009
	Crab shell	Langmuir	198.9	An et al., 2001
	Activated carbon prepared from hazelnut husks	Langmuir	13.1	Imamoglu and Tekir, 2008
	Neem leaves (boiling)	Langmuir	91.34	Zafar et al., 2013
	Neem leaves (acetic acid)	Langmuir	89.75	Zafar et al., 2013
	Neem leaves (autoclave)	Langmuir	84.70	Zafar et al., 2013
Zn	Rice husk (alkali and heat)	Langmuir	8.1	Krishnani et al., 2008
	Sawdust (formaldehyde and NaOH)	Langmuir	9.4	Šćiban et al., 2006
	Sawdust (NaOH and H_2SO_4)	Langmuir	14.1	Naiya et al., 2009

HMs	Sorbents (modifying agent)	Isotherms	Q_{max} (mg/g)	Source
Cd	Lignin from black liquor	Langmuir	11.2	Guo et al., 2008
	Carrot residues (HCl)	Langmuir	29.6	Nasernejad et al., 2005
	Natural seaweed	Langmuir	46.3	Ahmady-Asbchin et al., 2009
	Rice husk (alkali and heat)	Langmuir	16.7	Krishnani et al., 2008
	Sawdust (NaOH)	Langmuir	73.6	Memon et al., 2007
	Sawdust (formaldehyde and sulphuric acids)	Langmuir	19.1	Taty-Costodes et al., 2003
	Sawdust (NaOH and H_2SO_4)	Langmuir	26.7	Naiya et al., 2009
	Lignin from black liquor	Langmuir	25.4	Guo et al., 2008
	Green coconut shell powder	Langmuir	285.7	Pino et al., 2006
	Natural seaweed	Langmuir	95.8	Ahmady-Asbchin et al., 2009
	Crab shell	Langmuir	154.0	An et al., 2001
	Activated carbon from coconut coirpith	Langmuir	93.4	Kadirvelu and Namasivayam, 2003
Cu	Rice husk (alkali and heat)	Langmuir	10.9	Krishnani et al., 2008
	Rice husk (tartaric acid)	Langmuir	29	Wong et al., 2003
	Sawdust (raw)	Langmuir	10.6	Larous et al., 2005
	Sawdust (formaldehyde)	Langmuir	37.2	Ahmad et al., 2009
	Sawdust (formaldehyde and NaOH)	Langmuir	12.4	Šćiban et al., 2006
	Sawdust (H_2SO_4)	Langmuir	13.5	Acar and Eren, 2006
	Lignin from black liquor	Langmuir	22.9	Guo et al., 2008
	Modified lignin from alkali glycerol delignication	Langmuir	6.7 - 7.5	Demirbas, 2004
	Carrot residues (HCl)	Langmuir	32.7	Nasernejad et al., 2005
	Seaweed (2-propanolits)	Langmuir	143.3	Basha et al., 2009
	Natural seaweed	Langmuir	109.9	Ahmady-Asbchin et al., 2009
	Crab shell	Langmuir	55.9	An et al., 2001
	Activated carbon prepared from hazelnut husks	Langmuir	6.6	Imamoglu and Tekir, 2008
	Sugar beet pulp	Langmuir	21.2	Huguenot et al., 2010
Ni	Rice husk (alkali and heat)	Langmuir	5.5	Krishnani et al., 2008
	Lignin from black liquor	Langmuir	6.0	Guo et al., 2008
	Seaweed (2-propanolits)	Langmuir	131.6	Basha et al., 2009

HMs	Sorbents (modifying agent)	Isotherms	Q_{max} (mg/g)	Source
	Natural seaweed	Langmuir	55.5	Ahmady-Asbchin et al., 2009
As	Chitosan-coated biosorbent (dip-coating the oxalic acid-treated activated alumina with chitosan gel)	Langmuir	As^{3+} 56.50; As^{5+} 96.46	Boddu et al., 2008
	shelled Moringa oleifera Lamarck seed powder	Langmuir	As^{3+} 1.59; As^{5+} 2.16	Kumari et al., 2006
	Rice polish	Langmuir	As^{3+} 138.88; As^{5+} 147.05	Ranjan et al., 2009
	Fruit rinds of G. cambogia (fresh)	Langmuir	As^{3+} 128.10	Kamala et al., 2005
	Fruit rinds of G. cambogia (immobilized)	Langmuir	As^{3+} 704.11	Kamala et al., 2005
	Sawdust of Picea abies (ferric oxyhydroxides)	Langmuir	As^{5+} 9.259	Urik et al., 2009
Hg	Rice husk (alkali and heat)	Langmuir	36.1	Krishnani et al., 2008
	Almond shell (raw)	Langmuir	135.13	Khaloo et al., 2012
	Sugarcane bagasse (raw)	-	35.71	Abdolali et al., 2014
	Carica papaya wood	Langmuir	185.62	Basha et al., 2011
	Rice straw (raw)	Langmuir	103.10	Song et al., 2013
	Rice straw (modified by grafting method)	Langmuir	161.30	Song et al., 2013
	Coconut fiber (Pristine/raw)	Langmuir	166.670	Johari et al., 2014
	Coconut fiber (NaOH)	Langmuir	142.860	Johari et al., 2014
	Aquatic weed water hyacinth roots	Langmuir	5.53	Padmapriya and Murugesan, 2013
	Aquatic weed water hyacinth shoots	Langmuir	3.92	Padmapriya and Murugesan, 2013
	Leaves of Rambai Tree	Langmuir	121.95	Sen et al., 2010
	Lignin (mercapto-functionalized alkali)	Langmuir	101.2	Zhou et al., 2014
	Sugarcane bagasse	Langmuir	35.71	Khoramzadeh et al., 2013
Cr	Sawdust (raw)	Langmuir	41.5	Gupta and babu, 2009
	Sawdust (formaldehyde)	Langmuir	9.6	Baral et al., 2006
	Sawdust (polyacrylamide)	Freundlich	12.4	Raji and Anirudhan, 1998
	Sawdust (polypyrrole coated)	Langmuir	3.4	Ansari and Fahim, 2007

HMs	Sorbents (modifying agent)	Isotherms	Q_{max} (mg/g)	Source
	Lignin (purified)	Langmuir	6.6	Wiltowski et al., 2000
	Carrot residues (HCl)	Langmuir	45.1	Nasernejad et al., 2005
	Crab shell	Langmuir	49.4	An et al., 2001
	Commercial activated carbon	Langmuir	39.6	Mohan et al., 2006
	Activated carbon derived from acid treated coconut shells	Langmuir	12.2	Mohan et al., 2006
	Activated carbon prepared from coconut tree sawdust	Langmuir	3.5	Selvi et al., 2001
	Hazelnut shell activated carbon	Langmuir	170.0	Kobya, 2004
	Macro algae Gracilaria verrucosa (raw)	Langmuir	343.1	Ata et al., 2012
	Macro algae Gracilaria verrucosa (modified)	Langmuir	377.6	Ata et al., 2012
	Macro algae Gracilaria verrucosa (raw)	Khan	21.17	Ata et al., 2012
	Macro algae Gracilaria verrucosa (modified)	Khan	36.91	Ata et al., 2012
	Macro algae Gracilaria verrucosa (raw)	Sips	134.70	Ata et al., 2012
	Macro algae Gracilaria verrucosa (modified)	Sips	163.00	Ata et al., 2012
	Macro algae Gracilaria verrucosa (raw)	Toth	111.60	Ata et al., 2012
	Macro algae Gracilaria verrucosa (modified)	Toth	136.30	Ata et al., 2012

Table 2.6 ABs adsorption capacities of raw/modified biosorbents

ABs	Adsorbents	Isotherms	Q_{max} (mg/g)	Source
Tetracycline	bio-char derived from fast pyrolysis of biomass	Langmuir	58.8	Liu et al., 2012
Tetracycline	Activated carbon from beet pulp	Langmuir	288	Torres-Pérez et al., 2012
Tetracycline	Activated carbon from peanut hulls	Langmuir	28	Torres-Pérez et al., 2012
Penicillin G	R. arrhizus	Langmuir	459	Aksu and Tunç, 2005
Levofloxacin	Zirconium (IV) loaded corn	Langmuir	73	Yu et al., 2017

ABs	Adsorbents	Isotherms	Q_{max} (mg/g)	Source
	bracts			
Ciprofloxacin	Microporous activated carbon from lignocellulosic biomass by microwave pyrolysis	Langmuir	131.14	Ahmed and Theydan, 2014
Norfloxacin	Microporous activated carbon from lignocellulosic biomass by microwave pyrolysis	Langmuir	166.99	Ahmed and Theydan, 2014
Metronidazole	Acid and thermal modified canola residues	Langmuir	21.42	
Penicillin G	Chitin/chitosan in fungal biomass	Langmuir	591.8	Aksu and Tunç, 2005
Penicillin G	Activated sludge	Langmuir	434.8	Aksu and Tunç, 2005
Penicillin G	Activated carbon	Langmuir	463.0	Aksu and Tunç, 2005
Gatifloxacin	Gatifloxacin	Langmuir	181.82 ± 5.58	Bhowmik and Bajpai, 2012
Erythromycin	Magnetic imprinted polymers synthesized from chitosan-stabilized Pickering emulsion	Langmuir	15.51 to 52.32 μmol/g	Ou et al., 2015

C. Industrial waste and by-products

Using industrial waste and by-products as adsorbents for HMs and ABs removal has also been researched by numerous investigators. This section focuses on two typical kinds of industrial wastes and by-products: fly ash and red muds.

Fly ash

Fly ash or coal fly ash is a by-product and it is generated from the combustion of pulverized coal and collected from the cyclones or electrostatic precipitator systems at power thermal plants (Querol et al., 2002). In the USA and EU, by-products of coal combustion are approximately 115 million tons annually. A large portion of these by-products are coal fly ash (Querol et al., 2002). Fly ash continues to be used in many fields such as construction, agriculture, metal recovery and water

treatment (Ayala et al., 1998). A study conducted by Ayala et al. (1998) indicated that the main components (%) of fly ash in Asturias were SiO_2 (49-53), Al_2O_3 (24-28), Fe_2O_3 (6.3-8.3), CaO (4.3-5.3), MgO (1.6-2.0), Na_2O (0.6), K_2O (3.6-3.7) and TiO_2 (1.0-1.1). As its major contents are alumina, silica, ferric oxide and calcium oxide, fly ash is alkaline and may consequently neutralize wastewater and adsorb metal ions (Ayala et al., 1998). According to Mohan and Gandhimathi (2009), the surface of silica (SiO_2) in fly ash has a high possibility for attracting metal ions. It has been stated that fly ash has a potential for heavy metals as well as organic pollutants removal from wastewater (Mohan and Gandhimathi, 2009).

Results from a study conducted by Panday et al. (1985) showed that maximum adsorption capacity of Cu^{2+} on fly ash was 1.5 mg/g. Another study reported adsorption capacities of HMs onto fly ash were Cd^{2+} (3.77 - 6.36 mg/g), Cu^{2+} (10.18 - 12.78 mg/g), Ni^{2+} (1.25-1.66 mg/g) (Visa et al., 2010). In their study, Nascimento et al. (2009) modified fly ash by hydrothermal method for removing HMs from water. The Langmuir maximum adsorption capacities of Cu^{2+}, Zn^{2+}, Pb^{2+} and Mn^{2+} onto the adsorbent were 76.9, 59.2, 194.7 and 60.4 mg/g, respectively (Nascimento et al., 2009). Gupta and Ali (2004) have experimented using bagasse fly ash as an adsorbent for heavy metals such as lead and chromium. In this study, bagasse fly ash was modified with hydrogen peroxide. The adsorption process of lead and chromium by bagasse fly ash took place through a particle diffusion mechanism, maximum metal ions binding capacities of bagasse fly ash following Langmuir isotherm were Pb^{2+} 2.5 and Cr^{3+} 4.4 mg/g.

ABs abatement by fly ash was conducted by some investigators such as ciprofloxacin hydrochloride removal by adsorption on coal fly ash and activated

alumina; antibiotics by TiO_2/fly-ash cenospheres (Maheshwari et al., 2013; Huo et al., 2012). In another study, Lu et al. (2013) utilized fly-ash cenospheres for selective photodegradation of single and ternary antibiotics solution and removal efficiency was up to 77% in 90 min under visible light irradiation.

Red muds

Red muds are obtained as alkaline leaching wastes of bauxite mineral in the Bayer process of alumina production. Its chemical composition (% by weight) is as follows: Fe_2O_3 37.3, $A1_2O_3$ 17.6, SiO_2 16.9, TiO_2 5.6, Na_2O 8.3, CaO 4.4, loss on ignition 7.2 (Apak et al., 1998). Red muds are composed of sodium aluminosilicates, kaolinite, chamosite, iron oxides (hematite) and hydroxides. Fundamentally, Fe is in the form of hematite, Ti is in the form of Fe-Ti oxides and AI is in the form of ahiminosilicates (Apak et al., 1998). The main components of red muds are Cancrinite and hematite that adsorb heavy metals (Santona et al., 2006). Cancrinite has an open porous structure and can be considered as a material with zeolitic-like properties (Santona et al., 2006). After acid treatment, the proportion of hematite in the material increases (Santona et al., 2006). Cancrinite has a negative charge density in its lattice, thus can attract metal ions to neutralize them (Santona et al., 2006). Adsorption of heavy metals on hematite was through the formation of specific inner-sphere bonds (Santona et al., 2006).

There is extensive research on using red muds for toxicants elimination from aquatic environment such as arsenic (Altundoğan et al., 2000; Genç-Fuhrman et al, 2005; Bertocchi et al., 2006), copper (López et al., 1998; Güçlü and Apak, 2000; Han et al., 2002; Bertocchi et al., 2006; Nadaroglu et al., 2010), Cadmium (López et al., 1998; Güçlü and Apak, 2000; Han et al., 2002; Gupta and Sharma, 2002; Santona et

al., 2006; Bertocchi et al., 2006), lead (Güçlü and Apak, 2000; Gupta et al., 2001; Han et al., 2002; Santona et al., 2006; Bertocchi et al., 2006), Chromium (Pradhan et al., 1999; Gupta et al., 2001), zinc (López et al., 1998; Gupta and Sharma, 2002; Bertocchi et al., 2006; Santona et al., 2006), and nickel (López et al., 1998). Maximum toxicants adsorption capacities following the Langmuir isotherm of materials from red muds were (mg/g): unmodified red muds: Pb^{2+} 389.5, Cd^{2+} 151.8, Zn^{2+} 161.5 (Santona et al., 2006); neutralized red muds or bauxsol: As^{3+} 4.31, As^{5+} 5.07 (Altundoğan et al., 2000), As^{5+} 1.08 (Genç-Fuhrman et al., 2005), Cu^{2+} 5.35 (Nadaroglu et al., 2010); Cu^{2+} 19.7, Ni^{2+} 11.0, Cd^{2+} 10.6, Zn^{2+} 12.6 (López et al., 1998); HCl modified red muds: Pb^{2+} 159.5, Cd^{2+} 102.3 and Zn^{2+} 104 (Santona et al., 2006), Cr^{6+} 8.3 (Pradhan et al., 1999), As^{5+} 3.0 (Genç-Fuhrman et al., 2005); and H_2O_2 and thermal modified red muds: Pb^{2+} 64.8, Cr^{3+} 35.7 (Gupta et al., 2001).

So far, there is no study on ABs adsorptive removal by red muds.

2.4. Adsorption of HMs and ABs using magnetic materials (iron-based adsorbents)

2.4.1. Introduction

Water pollution with toxicants such as heavy metals, antibiotics have caused a lot of concern in recent decades. These kinds of pollutants have high toxicity, low biodegradability and accumulate in the food chain. High concentration of the toxicants can cause negative effects to human health and the aquatic environment. A great deal of studies recently has been motivated by the requirement to lower the concentration of these toxicants in drinking and surface water. Among the methods to address this problem, adsorption on a solid adsorbent is the prominent one (Tran et al., 2015).

Of the different kinds of adsorbents, magnetic materials have demonstrated their high adsorption capacity for pollutants and offer advantages in the separation process from aqueous solutions under a magnetic field for recycling or regeneration (Hua et al., 2012; Oliveira et al. 2004a). Due to its magnetic property, a magnetic adsorbent acts not only as an adsorbent for removing pollutants from solution, but also as a magnetically energizable element for attracting and retaining paramagnetic particles, which can be taken out from solution (Figure 2.5). Magnetic separation replacing the common filtration and centrifuge separation technologies, there are less complex technical requirements and operating cost in the regenerating process may make the adsorption process more economical (Kaminski et al., 1997). The advantage of this separation technology is that the harmful ingredients together with the magnetic particles can be eliminated from the polluted system by a simple magnetic field (Raven et al., 1998). These adsorbents are also suitable for oil spill control or toxicants removal from solid-liquid phase (Oliveira et al., 2004b). After magnetic separation in the external magnetic field, the harmful components can often be removed from the magnetic particles, and the magnetic particles can be used again. Easier operation and lower cost in regenerating process render the adsorption process more economical (Hu, 2005).

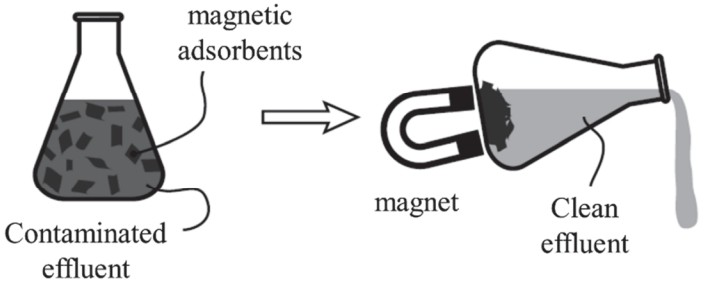

Figure 2.5 Schematic representation of the magnetic adsorbents separation (Adapted from Oliveira et al., 2004b)

Several types of iron based adsorbents for adsorptive removal of heavy metals and antibiotics have been reported such as mineral iron oxides/hydrated oxides, synthesized iron coated-materials, iron nanoparticles and industrial iron containing waste or by-products. The use of relative inexpensive adsorbents obtained from waste or by-products have become very attractive to researcher as they are efficient and reduce the huge volume of solid waste. This section continues with reviewing the practice of cost-effective iron based adsorbents in application for removing toxicants such as metal ions and antibiotics from aqueous solution.

2.4.2. Uptake mechanism of HMs and ABs from water by iron-based adsorbents

A. Removal pathway of HMs

O'Carroll et al. (2013) have proposed 4 mechanisms for heavy metals removal by iron adsorbent including: reduction, adsorption, oxidation/re-oxidation and co-precipitation for specific metal ions (Table 2.7). In another study, three mechanisms were proposed for the adsorption of lead on oxides of iron and manganese include strong specific adsorption, a special affinity for oxides of iron/manganese with the possibility of oxidation of the HMs, and the formation of some specific HMs-iron/manganese minerals (McKenzie, 1980).

Table 2.7 Removal mechanisms of metal ions with Fe^0 (O'Carroll et al., 2013)

Removal process	**Metal**
Reduction	Cr, As, Cu, U, Pb, Ni, Se, Co, Pd, Pt, Hg, Ag
Adsorption	Cr, As, U, Pb, Ni, Se, Co, Cd, Zn, Ba
Oxidation/re-oxidation	As, U, Se, Pb
Co-precipitation	Cr, As, Ni, Se
Precipitation	Cu, Pb, Cd, Co, Zn

B. ABs abatement mechanism

Qiang et al. (2013) proposed three kinds of hydrogen bonding between the nitrogen of the aniline, sulfinol or pyrimidine group of SMT and the surface hydroxyl group of FeM48 being the major driving force for adsorption. Additionally, the л-л electron-donor acceptor interaction between SMT (л-electroneacceptor) and the adsorbent (л-electronedonor) also promoted adsorption (Qiang et al., 2013). Chen et al. (2011) confirmed that the adsorption pathway of TC on PVP-nano zero-valent iron included electrostatic interactions and Fe-TC complexation reactions. Meanwhile the removal of CP as reported by Nie et al. (2015) and Xia et al. (2014) was a redox reaction.

2.4.3. Application of iron adsorbents for removing heavy metals from aqueous solution

Many studies have been conducted to use iron adsorbents for the removal of metal ions from water (Table 2.8).

Hematite (Fe_2O_3) obtained from an Indian iron ore was employed (passed through 200 mesh size) for removing Cd^{2+} from water (Singh et al., 1998). The highest removal efficiency (98%) was reached at 2h and 40 g/L dose of hematite. Maximum adsorption capacity of Cd^{2+} onto the adsorbent was 0.244 mg/g. Guo et al. (2007) also used natural hematite to abate As^{5+} from aqueous solution and the achieved adsorption capacity was 202 µg/g.

Another kind of iron adsorbent which was studied by many researchers for the abatement of HMs was magnetite (Fe_3O_4) (Table 2.8). In their study, Dong et al. (2010) synthesized hydroxyapatire/magnetite for purifying water containing Pb^{2+}. The adsorbent has very large surface area (109 m^2/g) which demonstrated its very high adsorption capacity (598.8 mg/g). In a study, magnetite was synthesized by coprecipitation and coated on natural zeolite for removing Cu^{2+} and Cd^{2+} (Feng et al.,

2000). Removal efficiencies of Cu^{2+} and Cd^{2+} by the adsorbent were 99.33 and 94.29 %, respectively at pH 7-8, 30 min contact time, dose of 2 g/L and 20^0C. A study conducted by Boparai et al. (2011) used nano zerovalent iron (synthesized following "bottom-up" method) to purify Cd^{2+} from water. Maximum adsorption capacity of the adsorbent following Langmuir isotherm was 769.2 mg/g.

A very interesting iron material source which has been used for abating HMs is the waste and by-products from the industrial sector (Rangsivek and Jekel, 2005; Gheju and Balcu, 2011; Lee et al., 2003). In their research, Rangsivek and Jekel (2005) have utilized scrap iron obtained from steel cylinders to remove Cu^{2+} and Zn^{2+} from water. Langmuir adsorption capacities could reach 100 mg/g for both Cu^{2+} and Zn^{2+} at the optimal conditions: pH5, 48h of contact time, dose of 0.5 g/L and at 20^0C. In another study, scrap iron was collected from a steel processing laboratory to abate Cr^{6+} through a packed column (containing 360g of scrap ion) (Gheju and Balcu, 2011). Achieved removal efficiency of Cr^{6+} by the material was 98.5% at pH 9.1. Lee et al. (2003) also used waste iron particles from an iron and steel processing company for the uptake of Cr^{6+}. The removal efficiency could reach 100% within 8 hours when the initial concentration was less than 30mg/L and within 200h when Cr^{6+} initial concentration was 80 mg/L.

2.4.4. Application of iron adsorbents for removing antibiotics from aqueous solution

Table 2.9 summarizes some studies that have been conducted for removing ABs from water by iron adsorbents.

Some iron-based adsorbents have been used for removing antibiotics from water (Xia et al., 2014; Chen et al., 2011; Qiang et al., 2013; Ghauch et al., 2009; Fang et al., 2011). A study conducted by Xia et al. (2014) utilized nanoscale zero-valent iron for degradation of chloramphenicol from water. BET surface area and BJH adsorption average pore diameter of the adsorbent are 32.02 m^2/g and 8.04 nm,

respectively. The removal efficiency of CP by the material increased with an increase of dose and a decrease of initial pH. The CP in the solution (100 mg/L) was fully removed within 5 min in the conditions adsorbent dose of 1.06 g/L, pH 6.8 and at room temperature (Xia et al., 2014). Another study also used nanoscale zero-valent iron to remove metronidazole from aqueous solution (Fang et al., 2011). The adsorbent was synthesized by the same technique as utilized by Xia et al. (2014) (Liquid phase reduction). The material has a very high BET surface area (35 m^2/g). At solution pH of 5.6, initial metronidazole concentration of 80 mg/L and adsorbent dose of 0.1 g/L, the nanoscale zero-valent iron can remove 100% of the antibiotic within 5 min. In the same conditions, removal efficiency of metronidazole by commercial zero-valent iron powder (purchased) only reached 20 % after 12 hours (Fang et al., 2011).

Similarly, Chen et al. (2011) also used liquid phase reduction to prepare polyvinylpyrrolidone modified nanoscale zero valent iron for the uptake of TC. The adsorbent has a BET surface area of 36.9 m^2/g and it has a core-shell structure. After 4 hour of contact time, the material can adsorb both TC and its degradation products from water. Percentage of removed TC reached 98.4% at the conditions: initial concentrations from 50-300 mg/L; initial pH 6.5; 6 hours of contact time; adsorbent dose of 0.1 g/L and at 25^0C (Chen et al., 2011).

The adsorptive removal of SMT by magnetic mesoporous nanocomposite was tested by Qiang et al. (2013). The authors prepared magnetic (Fe_3O_4) nanoparticles by a sonochemical process and then synthesized the magnetic mesoporous nanocomposite by self-assembly technology. Adsorption of SMT onto the adsorbent followed Pseudo-second-order. At pH 6.3, SMT initial concentration of 100 mg/L, contact time of 24 hours, dose of 1 g/L at 25^0C, the adsorbent removed 92.3% of the antibiotic.

Table 2.8 Synthesis/preparation and characterization of iron adsorbents and HMs adsorption isotherms, kinetics, experimental conditions

HMs	**Adsorbents**	**Synthesis/ preparation method**	**Surface area** (m^2/g)	**HMs conc.** (mg/L)	**Experimental condition** (pH, time, dose, temperature)	**Isotherm** (Langmuir: Q_{max}, mg/g; Freundlich K_F $(mg/g/mg)^{-n}$) removal efficiency	**Kinetics** (Best fitted model)	**References**
Pb^{2+}	Hydroxyapatite/ Magnetite	Coprecipitation and precipitation	109	10-500	pH5; 24 h; 0.5 g/L; 25^0C	Q_{max} 598.8	Pseudo-second-order	Dong et al., 2010
Pb^{2+}	Magnetite	Coprecipitation and coating on natural zeolite	-	40	pH 7-8; 30 min; 0.5g/L; 20^0C	100%	-	Feng et al., 2000
Pb^{2+}	Chitosan magnetite	Coprecipitation and hydrothermal	-	-	pH 6; 120 min; 0.1 g/L; room temperature	Q_{max} 63.33	-	Wan Ngah et al., 2011; Tran et al. 2010
Cu^{2+}	Scrap iron	Obtained from steel cylinder, sawing	0.384	1	pH 5, 48 h; 0.5 g/L; 20^0C	Q_{max} 100	-	Rangsivek and Jekel, 2005
Cu^{2+}	Goethite nano-photocatalysts	Coprecipitation	71.49	0.54 - 47.43	pH5.2; 9 h; 0.3g/L; room temperature	Q_{max} 149.25 K_F 72.4	Pseudo-second-order	Chen and Li, 2010
Cu^{2+}	Hematite nano-photocatalysts	Coprecipitation	24.82	0.54 - 47.43	pH5.2; 9 h; 0.3g/L; room temperature	Q_{max} 84.46 K_F 24.46	Pseudo-second-order	Chen and Li, 2010
Cu^{2+}	Magnetite	Coprecipitation and coating on natural zeolite	-	20	pH 7-8; 30 min; 2 g/L; 20^0C	99.33%	-	Feng et al., 2000
Cd^{2+}	Hematite	Mineral from Indian iron ore	4.4	8	pH 9.2; 120 min; 40 g/L; 20^0C	Q_{max} 0.244	-	Singh et al., 1998
Cd^{2+}	Magnetite	Coprecipitation and coating on natural zeolite	-	20	pH 7-8; 30 min; 2 g/L; 20^0C	94.29%	-	Feng et al., 2000

HMs	**Adsorbents**	**Synthesis/ preparation method**	**Surface area** (m^2/g)	**HMs conc.** (mg/L)	**Experimental condition** (pH, time, dose, temperature)	**Isotherm** (Langmuir: Q_{max}, mg/g; Freundlich K_F $(mg/g/mg)^{-n}$) removal efficiency	**Kinetics** (Best fitted model)	**References**
Cd^{2+}	Nano zerovalent iron	Synthesized via "bottom-up" method	26.3	25-450	pH ; 72 h; 0.5 g/L; 25^0C	Q_{max} 769.2 K_F 91	Pseudo-second-order	Boparai et al., 2011
Cr^{6+}	Scrap iron	Scrap iron collected from steel processing laboratory	-	25	pH 9.1; 360 g of adsorbent was packed in a column	98.5%	-	Gheju and Balcu, 2011
Cr^{6+}	Maghemite nanoparticles	Sol-gel	178	5-200	pH 2.5; 15 min; 5 g/L; 25^0C	K_F 19.2	-	Hu et al., 2005
Cr^{6+}	Waste iron particles	Iron particles obtained from iron and steel processing company	1.2	10-100	No pH adjustment; 8 h; 66 g/L; room temperature	100%	-	Lee et al., 2003
Zn^{2+}	Scrap iron	Obtained from steel cylinder, sawing	0.384	5	pH 5, 48 h; 0.5 g/L; 20^0C	Q_{max} 50-100	-	Rangsivek and Jekel, 2005
As^{+5}	Hematite	Mineral hematite	-	1	-; 1440 min; 10-40 g/L; 20^0C	Q_{max} $202x10^{-3}$	-	Guo et al., 2007
Hg^{2+}	Silica coated magnetite	Coprecipitation and coating	9.4-13.2	$50x10^{-3}$	Natural pH; 48 h; - ; 21^0C	74%	-	Girginova et al., 2010
Ni^{2+}	Chitosan magnetite	Coprecipitation and hydrothermal	-	-	pH 6; 120 min; 0.1 g/L; room temperature	Q_{max} 52.55	-	Wan Ngah et al., 2011; Tran et al. 2010

-: no information

Table 2.9 Synthesis/preparation and characterization of iron adsorbents and ABs adsorption isotherms, kinetics, experimental conditions

ABs	**Adsorbents**	**Synthesis/ preparation method**	**Surface area** (m^2/g)	**ABs conc.** (mg/L)	**Experimental condition** (pH, time, dose, temperature)	**Removal efficiency**	**Kinetics** (Best fitted model)	**References**
CP	Nanoscale zero-valent iron	Liquid phase reduction	32.02	100	pH 6.8; 5 min; 1.06 g/L; room temperature	100%	-	Xia et al., 2014
TC	Polyvinylpyrrolidone modified nanoscale zero valent iron	Liquid phase reduction	36.9	50-300	pH 6.5; 6 h; 0.1 g/L; 25^0C	98.4%	-	Chen et al., 2011
SMT	Magnetic mesoporous nanocomposite	Sonochemical; self-assembly technology	-	1-100	pH 6.3; 24 h; 1 g/L; 25^0C	92.3%	Pseudo-second-order	Qiang et al., 2013
Amoxicillin	Microscale and nanoscale ion	Synthesized	-	20	pH 6.6; 0-180 min; -; -	100%	Pseudo-first-order	Ghauch et al., 2009
Ampicillin	Microscale and nanoscale ion	Synthesized	-	20	pH 6.6; 0-180 min; -; -	100%	Pseudo-first-order	Ghauch et al., 2009
Metronidazole	Zero-valent iron powder	purchased	3	80	pH 5.6; 12 h; 0.1 g/L;-	20%	-	Fang et al., 2011
Metronidazole	Nanoscale zero-valent iron	Liquid phase reduction	35	80	pH 5.6; 5min; 0.1 g/L;-	100%	-	Fang et al., 2011

-: no information

2.4.5. Steel shavings as a novel adsorbent

From the above results, iron, particularly in the zero valent (Fe^0) and oxide forms, has been demonstrated to be a good candidate for removing HMs and ABs from water due to its adsorption ability and abundance (Cundy et al. 2008; Tran et al., 2017). In addition, iron-based adsorbents often have a magnetic characteristic. Thus, they offer advantages in solid-liquid separation processes under a magnetic field (Hua et al. 2012). Using adsorbents from wastes or by-products can reduce the quantity of solid waste, coupling with an increase in the value of the materials (Tran et al, 2015).

Steel shavings (StS) are a magnetic waste generated from the steel processing industry with very large volumes (Segura et al., 2013; Tran et al., 2017). The material contains a high content of zero valent iron and iron oxides (Tran et al., 2017). Hence, studying the utilization of steel shavings to abate antibiotics from aqueous solution is needed. Figure 2.6 shows the generation of the steel shavings from a steel processing machine (Dreamstime, 2017).

Figure 2.6 The generation of steel shavings from a steel processing machine (Dreamstime, 2017)

2.5. Gas plasma for modifying iron materials

2.5.1. Introduction

From the literature review, the use of iron materials for abating HMs and ABs from aqueous solution has the research potential. Applying a novel modification technique to produce a superior adsorbent is undoubtedly useful for wastewater treatment. One of the most promising modification methods for material surface treatment is plasma (Tran et al., 2017; Belkind and Gershman, 2008). Plasma is a partly or completely ionized gas containing electrons, free radicals, ions and neutrals (Jiang et al., 2014). In materials field, plasma technique is applied for some purposes such as cleaning the surface of materials (remove contaminants), modifying surfaces, crosslinking polymer surfaces, grafting functional polymers on surfaces, changing surface properties (without affecting the bulk material), promoting adhesion and bonding (Plasma electronic, 2017). Plasma cleaning can remove contaminants from the surface of adsorbents by the use of an ionized gas called plasma in a vacuum chamber at low pressure (Electronic diener, 2017; Belkind and Gershman, 2008). The impurities that form surface layers on top of the adsorbents can be removed by this technique (Belkind and Gershman, 2008). According to Belkind and Gershman (2008), several steps occur during plasma cleaning process comprising of active species generation, their transport to the surface, reactions on the surface, and ultimate removal of the reaction products from the surface (Figure 2.7). Gas plasma cleaning/modification has many advantages such as no hazardous chemicals usage, quickness, safeness, energy savings and simple installation/operation (Xiao et al., 2014; Harrick plasma, 2017).

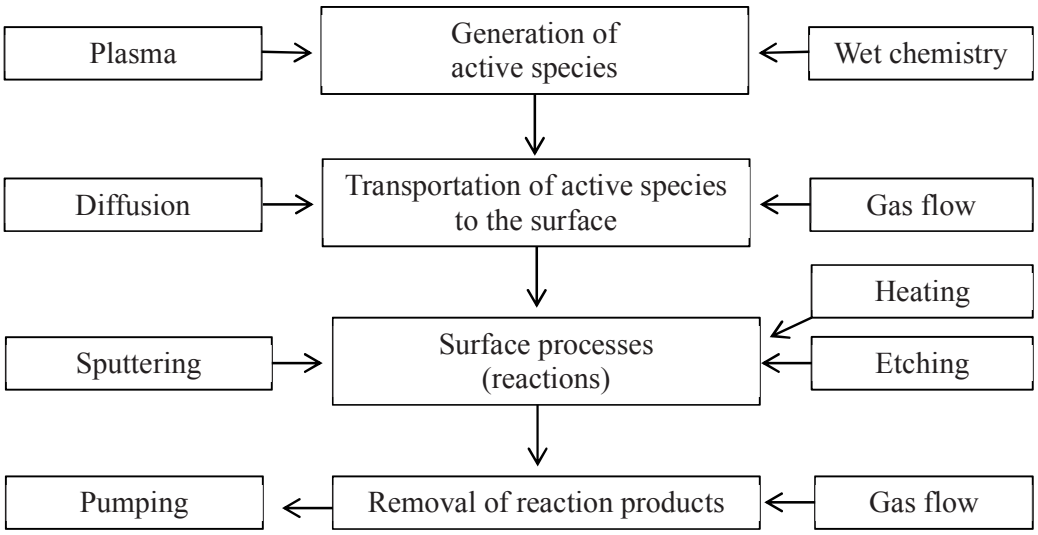

Figure 2.7 diagram of multi-step process in plasma surface cleaning (Belkind and Gershman, 2008)

When exposing the iron-adsorbent to a plasma generated in a vacuum, the surface of the adsorbent is bombarded (Tran et al., 2017). It leads to adventitious hydrocarbons being removed from the iron surface and enhances the iron surface available for adsorption processes (Tran et al., 2017). Figure 2.8 shows the scheme of plasma cleaning with oxygen gas.

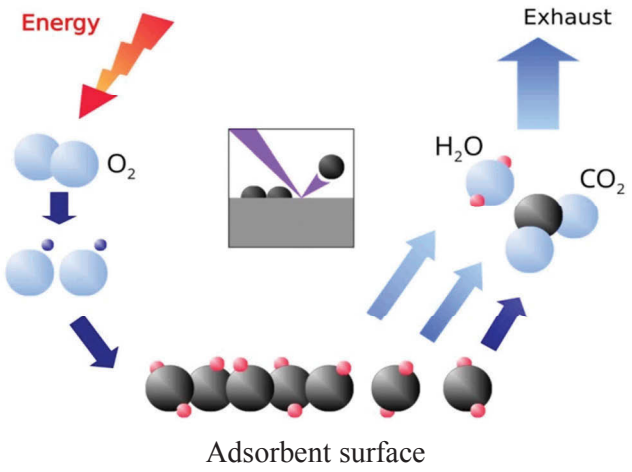

Figure 2.8 Scheme of plasma cleaning with oxygen (Plasma electronic, 2017)

2.5.2. Employed gas in plasma modification

The selection of gas used to produce the plasma is important to produce a good adsorbent (Deiries et al., 2005). Some kinds of gases have been chosen for using in plasma to modify the materials such as oxygen, hydrogen, argon, nitrogen, helium (Plasma etch, 2017). Hydrogen plasma is very effective at eliminating oxide from glass or metal products (Plasma etch, 2017). Oxygen is effective in removing hydrocarbons both physically and chemically on the surfaces of oxidation-resistant metals such as aluminum and stainless steel (Deiries et al., 2005). However, when using a material prone to oxidation such as iron, inert gases, for instance argon and nitrogen, can serve to generate the plasma with the purpose of achieving the same result without further oxidizing the sample (Tran et al., 2017).

2.5.3. The usage of gas plasma for adsorbent modification

Several studies have applied gas plasma for cleaning and modifying the adsorbent's surface to remove pollutants from water (Shao et al., 2010; Xiao et al., 2014; Zhang et al., 2013b; Maldonado et al., 2016; Wu et al., 2012; Shang et al., 2013).

A study used cold oxygen plasma oxidized carbons (obtained from pecan nut shells and peach stones) for removal of lead (Maldonado et al., 2016). Maximum adsorption capacity of Pb^{2+} of the adsorbent was 63 mg/g. Wu et al. (2012) applied oxygen plasma irradiated bamboo activated carbon for adsorption of aniline. The authors suggested the improvements of π–π dispersive interaction and hydrogen bonding are responsible the enhancement of adsorption capacities. In another study, Shang et al. (2013) modified CeO_2/Mg-Fe hydroxides by non-thermal plasma for

abating fluoride from water. After plasma modification the removal capacities by the adsorbent were considerably enhanced.

In their study, Şahin et al. (2015) modified bentonite clay by plasma modification for removing methylene blue. The study concluded that cold plasma enlarged the adsorption capacity of the clay (303 mg/g). In contrast, maximum adsorption capacities of Cu^{2+} on Cameroonian clay decreased from 242.72 mg/g to 202.43 mg/g after 30 min treated with non-thermal plasma (Fouodjouo et al., 2017).

Grafting plasma was also utilized in some studies. Xiao et al., 2014 utilized a low-temperature plasma technique to graft montmorillonite/iron oxide composite for the treatment of water containing uranium (VI). The plasma grafting significantly improved removal efficiency of uranium (VI) from aqueous solution by the material (Q_{max} = 2.79x10^{-4} mol/g). Chen et al. (2012) grafted polyacrylic acid with carbon nanotubes by plasma for removing Co^{2+} from water. Li et al. (2013) synthesized Fe_3O_4@β-cyclodextrim by plasma-induced grafting technique for the removal of 1-naphthylamine and Cu^{2+} from water. Adsorption capacities were observed for Cu^{2+} 9.04 mg/g and for 1-naphthylamine 144.74 mg/g. In another study, Shao et al. (2010) used plasma-induced graft technique for modifying carbon nanotube magnetic composite to remove aniline and phenol from water.

2.6. Conclusion and research gap

2.6.1. Main findings from literature review

Recently, the removal of heavy metal and antibiotics from aqueous solution has gained a lot of interest. From the literature review, a number of chief findings are summarized as below:

- Metal ions are naturally (geochemical processes) and anthropogenic (households, agriculture and industries) present in the aquatic environments. Heavy metals (HMs) such as lead, copper, cadmium, chromium and zinc can endanger public health and the natural environment due to their toxicity, persistence and steady accumulation. Exposure to HMs can cause neurotoxic and carcinogenic effects, damage to internal organs and many diseases, even at very low dosages. Currently, the pollution caused by heavy metals is a problem in both industrial and developing countries. The levels of HMs in various environmental matrices are in the ppb range to less than 10 ppm.
- Antibiotics (ABs) are a group of compounds that eradicate microorganisms or inhibit their growth. The mainstream of these substances are natural from microbial origin, however possibly semi-synthetic or totally synthetic. Antibiotics are widely used in large amounts for treating bacterial diseases in both humans and animals. The compounds can pollute soil, surface and groundwater via runoff or leaching from manure of livestock, aquaculture, poultry and pets as fertilizer for agriculture production. ABs in water can pose serious problems to the ecosystem and has several side effects, e.g. aplastic anemia."A variety of techniques were employed for removing toxic metals from water and wastewater such as adsorption, chemical precipitation, ion exchange, coagulation, reverse osmosis, electrolysis and membrane processes. In addition, numerous methods to eliminate antibiotics from the aquatic environment, e.g. advanced oxidation processes, combined chemical/biological treatment, aerobic digestion integrated with activated carbon, ion exchange, coagulation, flocculation, sedimentation, ultraviolet

irradiation, have been researched. Among these techniques, the most efficient, economic and environmentally friendly method for the removal of HMs and ABs from water is adsorption using cost-effective adsorbents. Many typical low-cost adsorbents obtained from natural minerals, agricultural waste/by-products and industrial waste/by-products have been applied for removing HMs and ABs from aqueous solution.

- Mentioning low-cost adsorbents, iron, particularly in its zero-valent (Fe^0) and oxide forms, is a good candidate due to its adsorption capacity and large quantity. A number of iron adsorbents are magnetic in character, therefore leading to good outcomes in the solid-liquid separation process under a magnetic field. It is documented that varieties of magnetic materials have been used for removing HMs and ABs from aquatic matrices, e.g. scrap iron, iron nanoparticles, magnetite, magnetic montmorillonite, iron oxides, microscale zero-valent iron, nanoscale zero-valent iron.
- To date, adsorption and co-precipitation are proposed as the adsorptive removal mechanisms of HMs such as Pb^{2+}, Cu^{2+}, Cd^{2+}, Cr^{3+} and Zn^{2+} from water by iron adsorbents. The major driving force for adsorption of ABs onto zerovalent iron and iron oxides are hydrogen bonding, л-л electron-donor acceptor, electrostatic and non-electrostatic, complexation and redox interactions.
- As a magnetic waste which is generated from steel processing industries in very large quantities, steel shavings have been examined to abate HMs and ABs. Researching on a novel modification technique to improve adsorption capacity of steel shavings is certainly useful for wastewater treatment. One of

the most capable modification approaches for Fe^0 and iron oxides is plasma cleaning. The technique can eradicate contaminants from the iron surface via an ionized gas called plasma in a vacuum chamber at low pressure. Plasma cleaning has brought many benefits, e.g. no hazardous chemicals usage, quickness, safeness, energy savings and simple installation/operation.

2.6.2. Research gaps

Even though much work has been conducted for removing metal ions and antibiotics from water using iron adsorbents, a number of important research gaps still exist as follows:

- There is a lack of studies on using steel shavings for treating water containing heavy metals as well as antibiotics. Subsequently, more research is needed to understand more and confirm whether the application of steel shavings in removing HMs and ABs from water is warranted and advantageous.
- Application of gas plasma as a novel modification process of adsorbents in water treatment is very interesting. However, the amount of research in this field has been limited. Further studies need to be conducted to choose optimal conditions for the use of this technique to produce the best adsorbent.
- Current studies have only confirmed adsorption mechanisms of HMs and ABs on other iron adsorbents; there is little research focusing on the driving forces for the pollutants removal by steel shavings. Thus, there is a real need for research to provide an understanding of the uptake pathways of metal ions and antibiotics adsorption onto raw and modified steel shavings.
- Most of the studies on using iron adsorbents for the abatement of HMs and ABs from aqueous solution are in batch. In order to apply the adsorbent in

water treatment industries, more studies in dynamic systems or on semi-pilot scales need to be implemented.

Faculty of Engineering and Information Technology

CHAPTER 3

MATERIALS AND METHODS

3.1. Materials

3.1.1. Steel shavings

In this study, steel shavings (StS) samples were collected at the steel processing laboratory at the University of Technology Sydney (UTS), Australia (Figure 3.1). This material, generated from cutting, sawing and other steel processing techniques, can easily be collected in large amounts in Australia.

Figure 3.1 Steel shavings at the steel processing laboratory, UTS

3.1.2. Solutions of heavy metals

Stock solutions of Pb^{2+}, Cu^{2+}, Cd^{2+}, Cr^{3+} and Zn^{2+} (1000 mg/L) were prepared by dissolving required weights of 1,598.46 mg lead(II) nitrate ($Pb(NO_3)_2$); 3,801.97 mg copper nitrate trihydrate ($Cu(NO_3)_2.3H_2O$); 2,744.05 mg cadmium nitrate tetrahydrate salt ($Cd(NO_3)_2.4H_2O$); 7,695.8 mg chromium(III) nitrate nonahydrate ($Cr(NO_3)_3.9H_2O$); and 4,549.9 mg zinc nitrate hexahydrate ($Zn(NO_3)_2.6H_2O$), respectively in a mixture of 1000 mL of distilled water and 10mL of concentrated nitric acid. Working solution was prepared by diluting stock solution with distilled water.

3.1.3. Solutions of antibiotics

A stock solution of 100 mg/L was prepared from chemicals, specifically sulfamethazine (>= 99%), tetracycline (>= 98%), and chloramphenicol (>= 98%). Working solutions were diluted from the stock solutions.

All chemicals used were of analytical reagent grade and purchased from CHEMSUPPLY (Australia).

3.2. Methods

3.2.1. Preparation of adsorbents

Figure 3.2 presents the diagram of adsorbents preparation from steel shavings. The locations and purpose of preparing steps are summarized in Table 3.1.

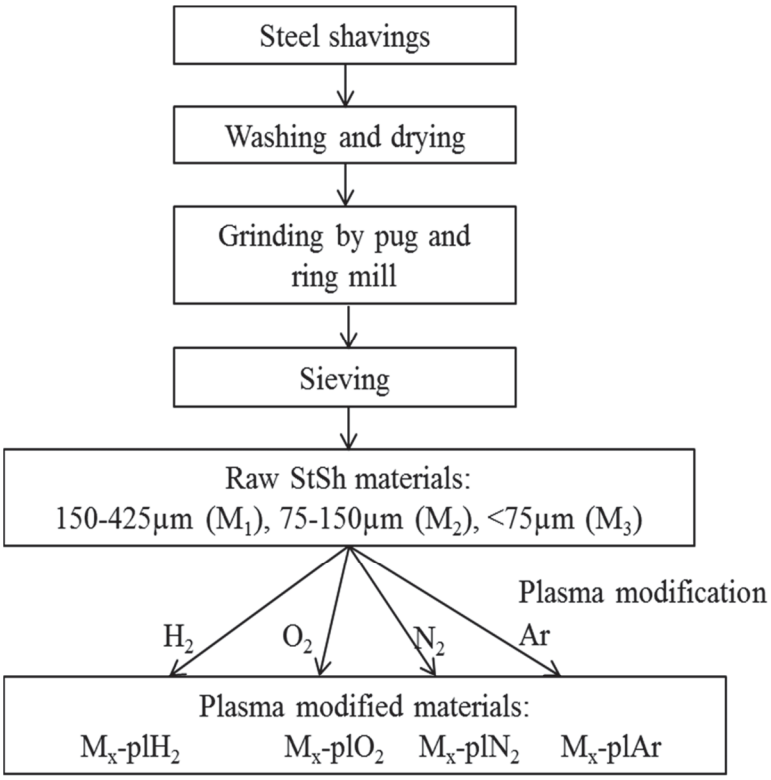

Figure 3.2 Flowchart for the preparation of adsorbents from StS

A. Raw steel shavings

The raw material was washed three times with distilled water, dried at 50^0C and ground in a pug and ring mill (in 3 min). Figure 3.3 shows the images of raw steel shavings after washing and drying, and after grinding. The ground samples were subsequently sieved and divided into three fractions: M_1 with particle sizes in the range 150-425 µm, M_2 75-150 µm and M_3 0-75 µm; the particles were stored in closed bottles prior to experiments.

Table 3.1 Summary of adsorbents preparation steps

Preparation technique	**Location**	**Purpose**
Washing and drying	Laboratories at School of Civil and Environmental Engineering, Faculty of Engineering and Information Technology, UTS	Remove all the dust and unwanted contents in the steel shavings
Pug and ring crusher	Chemistry laboratory, Faculty of Sciences, UTS	To grind the steel shavings into powder
Sieving	Laboratories at School of Civil and Environmental Engineering, Faculty of Engineering and Information Technology, UTS	Classify particle sizes of steel shavings
Plasma modification	Laboratories, School of Physics and Advanced Materials, Faculty of Sciences, UTS	Clean and modify surface structure of the materials

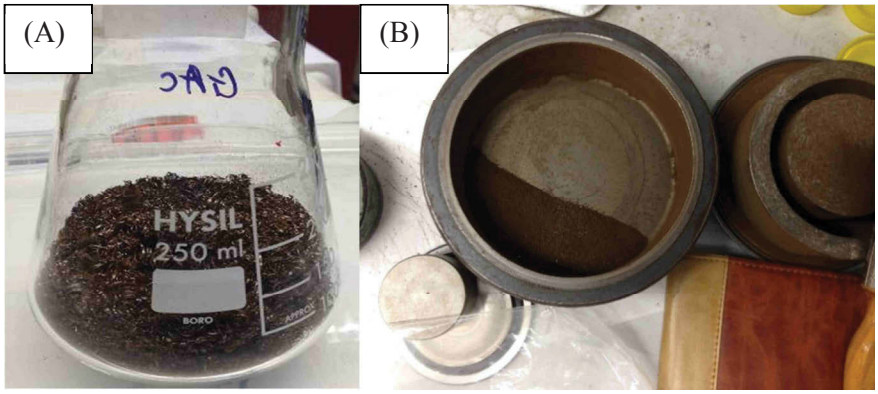

Figure 3.3 Images of steel shavings: (A) after washing and drying; (B) after grinding by a pug and ring crusher

B. Plasma modified material

Gas plasma is a technique to modify unique surface properties of materials, without affecting the bulk properties (see in 2.5, Chapter 2). Figure 3.4 describes the chamber window of the gas plasma equipment before and in action. The gas plasma cleans impurities on the StS surface as well as embedding gas species in the near-surface region of the particles. The cleaning process took place through the use of energetic plasma created from gaseous species. Hence, the effect of plasma on a material is determined by the chemistry of the reactions between the surface and the reactive species present in the process gas employed. Each gas produces a unique plasma composition resulting in different surface properties. In this research four kinds of gases were employed in the plasma treatment including hydrogen (H_2), oxygen (O_2), nitrogen (N_2) and argon (Ar), which produced the following modified adsorbents: M_x-plH_2, M_x-plO_2, M_x-plN_2, and M_x-plAr, respectively.

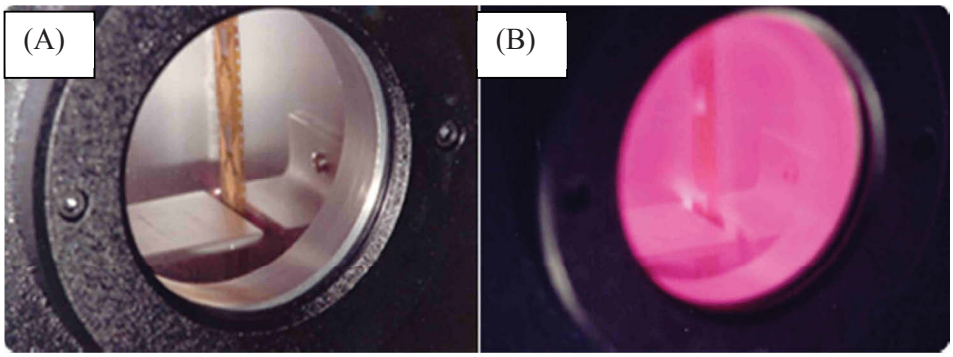

Figure 3.4 Chamber window of plasma equipment: (A) before; (B) in action

Figure 3.5 illustrates the surface modification process of materials by nitrogen plasma. With applied gas flow rate in this study of 20 Standard Cubic Centimetres per Minute (SCCM), visible surfaces of particles would be clean in the

first 15 min. Because of time consuming and the adventitious carbon could be reapplied in 1 hour, the conducting time chosen was 15 min.

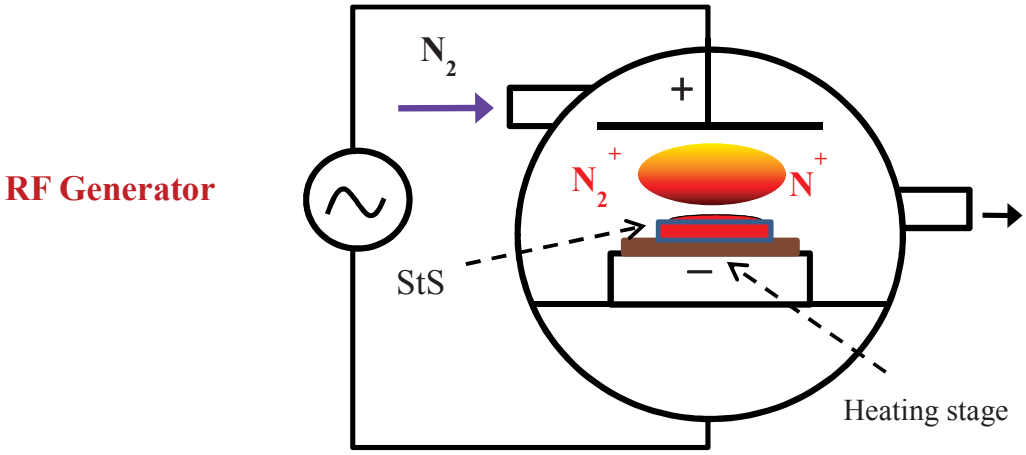

Figure 3.5 Radio frequency (RF) plasma configuration with nitrogen for the surface treatment of StS

Twenty grams of raw steel shavings, after being pre-treated, was evenly distributed into a clean 6 cm diameter glass petri dish. Following that, it was placed in the centre of the chamber of a Harrick plasma cleaner/sterilizer PDC-32G with an attached Adixen ACP 15 vacuum pump set at a pumping speed of 14m^3/h. The PDC-32G was then vacuumed to an ultimate total pressure of 0.3 mbar before the employed gas (H_2, O_2, N_2 or Ar) was injected into the chamber at a flow rate of 20 SCCM. The unit was then powered at the high setting (RF power of 18 W at 12 Mhz, cathode voltage = 300 V) for 15 min before the adsorbent was recovered.

C. Comparison with a commercial iron material

In this study, analytical iron (III) oxide (Fe_2O_3) (purity level 98%) was also used in a control experiment for comparison of removal efficiencies with the studied adsorbents. The commercial iron (III) oxide (Fe_2O_3) was purchased from sigma-Aldrich Pty. Ltd. 12 Anella Avenue, Castle Hill, NSW 2154, Australia.

3.2.2. Characterization methods

The studied adsorbents were characterized by Zeiss Evo SEM, SEM-Supra 55VP, Siemens D5000 X-ray Diffractometer (XRD), Brunauer-Emmett-Teller (BET), X-ray photoelectron spectroscopy (XPS), Zeta potential and sizer, and Fourier transform infrared spectroscopy (FTIR) to obtain the surface morphology, elemental composition, mineral species, surface area, surface charge, and functional groups (Table 3.2).

Table 3.2 Summary of adsorbents characterization studies

Characterization experiment	**Test location**	**Purpose**
Scanning Electron Microscopy and EDS (SEM-Zeiss Evo)	Microstructural Analysis Unit (MAU), Faculty of Sciences, UTS	Determine surface morphology and analyse the elementary composition of the materials
Scanning Electron Microscopy (SEM-55EV)	Microstructural Analysis Unit (MAU), Faculty of Sciences, UTS	Determine surface morphology and structure of steel shavings
Powder X-ray Diffraction (XRD)	Microstructural Analysis Unit (MAU), Faculty of Sciences, UTS	Determine mineral species present in the adsorbents
X-ray photoelectron spectroscopy (XPS)	The Rramaciotti Centre for Gene Function Analysis, University of New South Wales	Determine the chemical stages of elements in the adsorbents
Brunauer–Emmett–Teller (BET)	Centre for Nanoscale BioPhotonics, Dept. of Chemistry and Biomolecular Science, Macquarie University	Determine surface area and porosity of the adsorbents
Zeta potential and Sizer	Environmental Engineering laboratories, Faculty of Engineering and Information Technology, UTS	Determine zeta potential of the surface and particle size of the materials
Fourier transform infrared spectroscopy (FTIR)	Environmental Engineering laboratories, Faculty of Engineering and Information Technology, UTS	Determine functional groups on the surface of the adsorbents

A. SEM-EDS

Surface morphology and elementary composition of the material samples were analysed by Zeiss Evo SEM with attached EDS at 15kV (Figure 3.6). For each particle, images were collected at different magnifications. For some particle samples, high magnification was not possible or images were not sufficiently clear due to excessive charging. Thus, SEM-Supra 55VP also was used for imaging those samples.

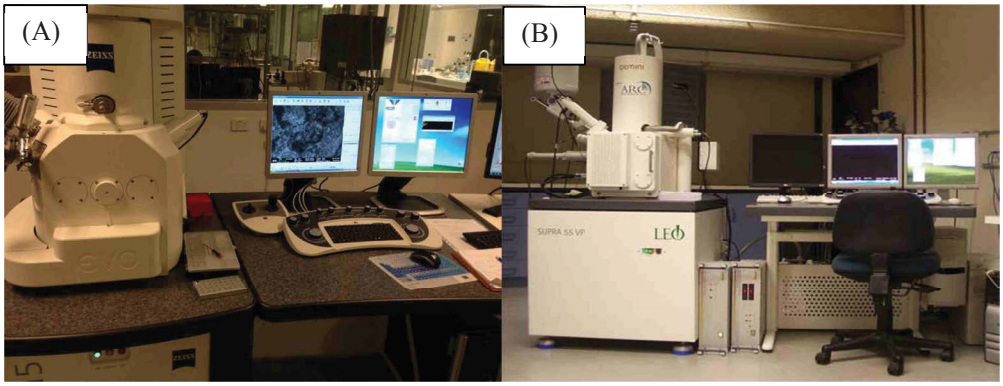

Figure 3.6 SEM-EDS instruments: (A) Zeiss Evo SEM and (B) Supra 55VP SEM

B. XRD

Powder X-ray diffraction (XRD) was used to identify the mineral species present in the steel shavings. The sample was pulverized to powdered form and smeared on a metal holder at room temperature. The X-ray diffractograms were recorded at a rate of 5^{o} per min and a 2θ range of 15^{o} to 80^{o}. XRD analysis was carried out by Seimens D5000 X-ray Diffractometer (Figure 3.7A).

C. XPS

XPS is a surface sensitive technique which is able to determine the binding energy of elements in the top 10 nm of a sample. The measurements were conducted

on a Thermo Scientific ESCALAB 250Xi system fitted with a mono-chromated Al K alpha X-ray source (1486.68 eV) (Figure 3.7B). XPS was implemented in the below conditions: a background vacuum of better than 2E-9 mbar, a power of 150 W (14 kV x 12 mA), a spot size of 500 μm, a photoelectron take-off angle of 90° (electron optics respect to the surface plane), a C 1s = 284.8 eV binding energy reference for adventitious hydrocarbon, a pass energy of 100 eV for survey scans and 20 eV for region scans.

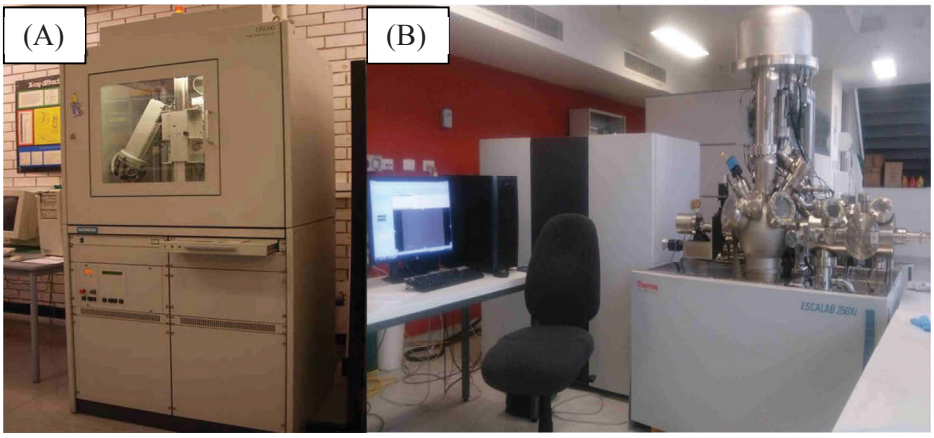

Figure 3.7 XRD and XPS instruments: (A) Seimens D5000 X-ray Diffractometer and (B)Thermo Scientific ESCALAB 250Xi

D. BET

BET characterization was applied to the raw and modified adsorbents. The particles were degassed using the Micrometrics VacPrep 061 Sample Degas System at 60 °C for 24 hours. BET analysis was then performed by the micrometrics tristar III system (Figure 3.8).

E. Zeta potential and particle size distribution

To analyze the surface relating zeta potential of the adsorbents, Malvern Zeta potential and Sizer was utilized. Mixtures of adsorbents with Mili-Q water were

adjusted at different solution pH values, and then shaken at 150 rpm for 24 hours. Subsequently, zeta potential values of the samples were measured by Nano-ZS Zeta-sizer (Malvern, Model: ZEN3600) (Figure 3.9A).

The particle size of M_3 was also measured by this instrument. As this method can only measure particle distribution in the solution, an amount (1 gram) of the particles M_3 was mixed with Mili-Q water and then shaken at 150 rpm for 24 hours. Subsequently, the liquid phase was measured by Nano-ZS Zeta-sizer (Malvern, Model: ZEN3600) and the solid phase was dried and weighted.

F. FTIR

The functional groups on the surface of pre and post adsorption materials were analyzed by Fourier transform infrared spectroscopy (FTIR) on the instrument: MIRacle 10, Shimazhu (Figure 3.9B). FTIR spectra were measured the absorbance from 400 to 4000 cm^{-1}, at 4 cm^{-1} resolution using a combined 40 scans.

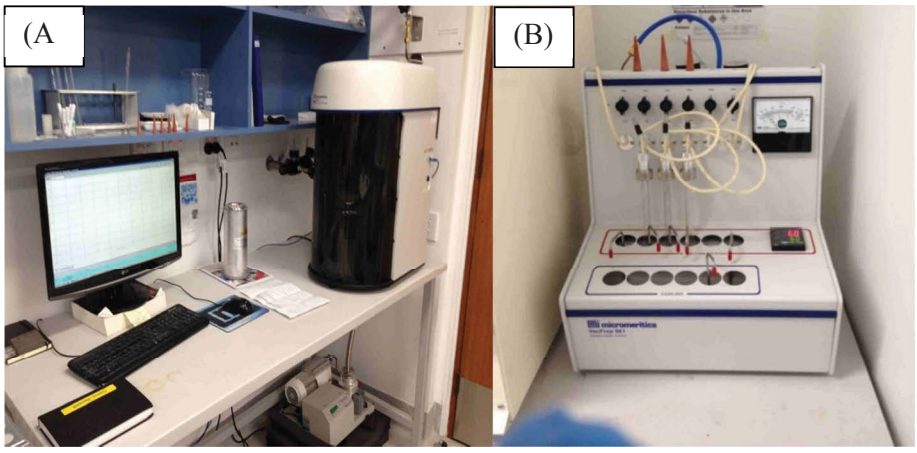

Figure 3.8 BET system instruments: (A) micrometrics tristar III system, and (B) Micrometrics VacPrep 061 Sample Degas

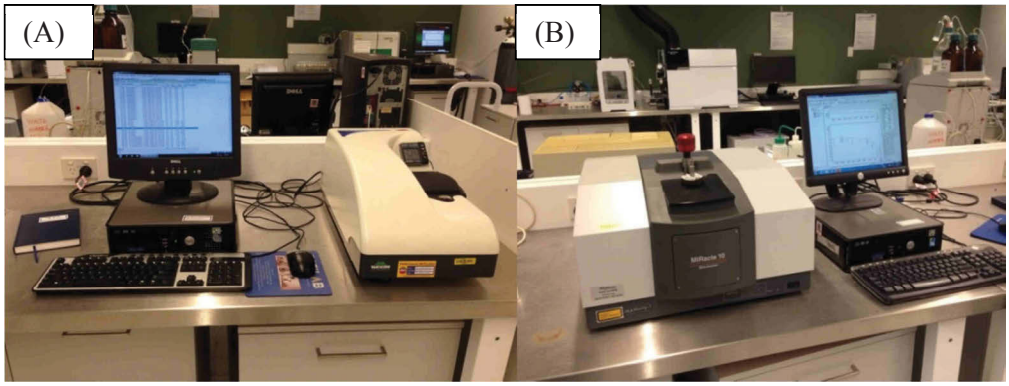

Figure 3.9 Zeta potential and FTIR instruments: (A) Nano-ZS Zeta-sizer (Malvern, Model: ZEN3600) and (B) MIRacle 10, Shimazhu

3.2.3. Development of adsorbents from steel shavings

Adsorption capacity of adsorbents which have different sizes, employed gas in plasma modification and commercial iron (III) oxide are compared to find the most effective adsorbent.

A. Particle size

For studying the effects of particle size onto adsorption ability, different particle sieve sizes of raw and modified StS including 0-75; 75-150 and 150-425 μm are tested.

B. Employed gas in plasma modification

Removal efficiencies of HMs and ABs onto different kinds of adsorbents which were obtained from plasma modification with various applying gases (H_2, O_2, N_2 and Ar) were examined to understand the effects of employed gases.

3.2.4. Batch adsorption experimental set-up for removing HMs

A. Affecting factors on HMs adsorption from aqueous solutions

The effects of solution pH, adsorbent dose and temperature to adsorption of HMs were examined in this research with single metal ion solutions including Pb^{2+}, Cu^{2+}, Cd^{2+}, Cr^{3+} and Zn^{2+} separately.

- In order to study the effects of pH on adsorption, 100 mL of 100 mg/L single metal ion solution were added into a 250 mL flask. The pH value was adjusted from 2-8 with HCL 0.1M and NaOH 0.1M. Then, 0.5 g of adsorbent was put into the solution. The mixture was shaken in a shaking table at 130 rpm at room temperature for 24 hours.
- Effects of adsorbent dosage (0.1, 0.2, 0.5, 1, 2, 5, 10 and 20 g/L) on adsorption efficiency of HMs on raw and modified steel shavings were examined. Different amounts of the adsorbents which were 0.01, 0.02, 0.05, 0.1, 0.2, 0.5, 1 and 2 gram were added to 100 mL solution of the HMs at 100 mg/L. The subsequent steps were carried out in the same procedure as with the pH influence tests.
- Effects of temperature on the adsorption process of HMs onto the adsorbents were observed at 20, 25 and 30^0C. The volume of 100 mL of different metal ion concentrations (0, 5, 10, 20, 40, 60, 100, 200 and 500 mg/L) were added into 250 mL flasks, then pH of the solution was adjusted. The optimal amounts of adsorbent were added, and then shaken at 130 rpm in a thermostatic shaker for 24 hours.

A magnet was used to separate liquid and solid phases after the adsorption process. Subsequently, the metal ions concentration in the effluent was measured by Microwave Plasma - Atomic Emission Spectrophotometer (MP-AES) after passing through a 1.2 μm filter paper. The adsorption isotherm experiments were conducted at room temperature. Adsorbed adsorbents were then used for the desorption examination.

The percentage removal of heavy metals (%) was calculated by the equation:

$$\%\ \text{removal} = \frac{(Co-Ce)x100}{Co} \qquad (3.2.4.1)$$

The sorption capacity q_e (mg/g) was calculated using the following equation:

$$q_e = \frac{(Co-Ce)xV}{m} \qquad (3.2.4.2)$$

where C_o and C_e are the initial and equilibrium concentration respectively (mg/L), m is the mass of adsorbent (g), V is the volume of the HMs solution (L).

B. Isotherms and kinetics models of HMs adsorption

Adsorption kinetics and isotherms models were utilized for describing adsorptive removal of HMs onto the adsorbents including Langmuir and Freundlich isotherm models, Pseudo-first-order kinetic (PFO), Pseudo-second-order kinetic (PSO) and Intra-particle diffusion model (IDM). Table 3.3 describes and summarizes the equations of kinetic and isotherms of HMs adsorption on the adsorbents.

Table 3.3 Kinetic and isotherm models of HMs adsorption on StS

Models	Equation	Linearized form
Langmuir	$q_e = \frac{q_{\max} k_L C_e}{1 + k_L C_e}$	$\frac{C_e}{q_e} = \frac{C_e}{q_{\max}} + \frac{1}{k_L q_{\max}}$
Freundlich	$q_e = k_F C_e^{1/n}$	$\ln q_e = \ln k_F + \frac{1}{n} \ln C_e$
	where: C_e is the equilibrium metal ion concentration (mg/L). q_e is adsorption capacity of StS at equilibrium (mg/g). q_{max} is maximum HMs uptake of the adsorbent (mg/g); k_L is Langmuir constant related to binding energy of adsorption (L/mg); k_F and n are Freundlich constants indicative of the adsorption capacity and adsorption intensity of the adsorbent, respectively.	
PFO	$\frac{dq_t}{d_t} = k_{1p}(q_e - q_t)$	$\ln(q_e - q_t) = \ln q_e - k_1 t$
PSO	$\frac{dq_t}{d_t} = k_{2p}(q_e - q_t)^2$	$\frac{1}{q_t} = \frac{1}{k_2 q_e^2} + \frac{1}{q_e}$
IDM	$q_t = k_i t^{0.5}$	
	where: qe = amount of HMs adsorbed at equilibrium (mg/g); qt = amount of HMs adsorbed at time t (min) (mg/g); k_{1p} = equilibrium rate constant of PFO (1/ min); k_{2p} = equilibrium rate constant of PSO (1/min) and ki (mg/g.min) = the rate constants of IDM, respectively.	

The experiments were performed for Pb^{2+}, Cu^{2+}, Cd^{2+}, Cr^{3+} and Zn^{2+} separately according to the following procedures:

- For investigation of the adsorption isotherms, the solutions of the HMs at different concentrations - 0, 5, 10, 20, 40, 60, 100, 200 and 500 mg/L - were prepared in 250 mL flasks. Optimal amounts of adsorbents were added. The solution pH was adjusted to the optimum value as obtained from the pH effects experiments. The mixtures of adsorbents and HMs solutions were shaken at 130 rpm at a fixed temperature (25^0C) for 24 hours.
- In kinetic experiments, the optimal amount of adsorbent which was obtained from the effect of adsorbent dose tests was mixed with 100 mL of 100 mg/L single metal ion solution. The mixtures were shaken at 130 rpm and room temperature. The samples were taken at 5, 10, 15, 30, 45, 60, 120, 240, 480, 1440 and 2880 min.

Next steps for analysis of HMs concentrations in the effluents were carried out following the same procedure as experiments on the effects of pH and dose of adsorbent.

C. Competitive adsorption of HMs on raw and modified StS

- For calculation of adsorption isotherm of HMs on the adsorbents, 100 mL multi-metals solutions were prepared at different concentrations with total competitive solutes concentrations including 0, 5, 10, 20, 40, 60, 100, 200 and 500 mg/L (each metal solute concentration of 0, 1.67, 3.33, 6.67, 13.33, 20, 33.33, 66.67 and 166.67 mg/L). Optimal adsorbent dosage was used. The mixtures were shaken at 130 rpm for 24 hours at 25^oC.

- In order to study competitive kinetics, 100 mL of mixed solution of Pb^{2+}, Cu^{2+}, Cd^{2+}, Cr^{3+} and Zn^{2+} (100mg/L of total initial solution concentration, and each solute concentration is 20 mg/L) were prepared into 250 mL flasks. The competitive adsorption kinetics was carried out using the optimal solution pH and adsorbent dosage. The mixture was shaken at 130 rpm in shaking tables. The samples were taken at 5, 10, 15, 30, 45, 60, 120, 240, 480, 1440 and 2880 min.

Next steps for analysis of HMs concentrations in the effluents were carried out following the same procedure as above.

The overall competitive adsorption capacities are calculated using summarized Langmuir and Freundlich Equations (Anwar, 2014). The combined Freundlich model for 5 metal ions:

$$Q_{total} = K_{F1}{C_{e1}}^{1/n} + K_{F2}{C_{e2}}^{1/n} + K_{F3}{C_{e3}}^{1/n} + K_{F4}{C_{e4}}^{1/n} + K_{F5}{C_{e5}}^{1/n} \quad (3.2.4.3)$$

$$K_{F(total)} = K_{F1} + K_{F2} + K_{F3} + K_{F4} + K_{F5} \quad (3.2.4.4)$$

The combined Langmuir model for 5 metal ions:

$$Q_{total} = \frac{Q_{max1}K_{L1}C_{e1}}{1+K_{L1}C_{e1}} + \frac{Q_{max2}K_{L2}C_{e2}}{1+K_{L2}C_{e2}} + \frac{Q_{max3}K_{L3}C_{e3}}{1+K_{L3}C_{e3}} + \frac{Q_{max4}K_{L4}C_{e4}}{1+K_{L4}C_{e4}} + \frac{Q_{max5}K_{L5}C_{e5}}{1+K_{L5}C_{e5}} \quad (3.2.4.5)$$

$$Q_{max.(total)} = Q_{max1} + Q_{max2} + Q_{max3} + Q_{max4} + Q_{max5} \quad (3.2.4.6)$$

where K_{F1}, K_{F2}, K_{F3}, K_{F4} and K_{F5} are the Freundlich constant for first competitive solute, second competitive solute and third competitive solute, respectively. Q_{max1}, Q_{max2}, Q_{max3}, Q_{max4} and Q_{max5} are the maximum Langmuir sorption capacity respectively for the first, second, third, fourth, fifth competitive solute.

D. Desorption and regeneration

From the experimental results, the most effective adsorbent in the batch study for removing HMs was chosen for regeneration experiments. Several reagents were utilized for desorbing of metal ions from treated materials including tap water, HCl 0.1N, H_2SO_4 0.1N, HNO_3 0.1N, CH_3COOH 0.1N and NaOH 0.1N. Adsorbed materials and 100 mL of regeneration reagents were added into 250 mL flasks at room temperature, shaken at 130 rpm for 24 hours and filtered through 1.2 μm filter paper. The concentrations of HMs in the solutions were analyzed following the same procedure as above.

After that, the materials were collected and used for the next circles. The adsorption-desorption cycles of HMs on the adsorbent were carried out in 5 continuous cycles.

3.2.5. Batch adsorption experimental set-up for removing antibiotics

A. Affecting factors on antibiotics adsorption from aqueous solutions

In order to select optimal conditions for the removal process, the effects of pH, adsorbent dose and temperature were studied. The efficiency in removing antibiotics from the aqueous solution was calculated as follows:

$$\% \text{ removal} = \frac{(Co-Ce)x100}{Co} \qquad (3.2.5.1)$$

The adsorption capacity was calculated using equation below:

$$q_e = \frac{(Co-Ce)xV}{m} \qquad (3.2.5.2)$$

where C_o and C_e are the initial and equilibrium antibiotics concentrations (μg/L), m is the mass of adsorbent (g) and V (L) is the volume of the antibiotics solutions.

The experiments were undertaken for 3 antibiotics (SMT, TC and CP) separately as per the following procedure:

- For investigation of the pH influence on the adsorption, 50 mL of the antibiotic solution 1000 µg/L were prepared into 250 mL flasks. The pH of the solutions were adjusted from 2-10 using 0.1M HCL and 0.1M NaOH solutions; then 0.5 gram adsorbent was added. The mixture was shaken in a shaking table at 130 rpm for 24 hours. The effluent was filtered through a 0.2 µm filter paper. The concentrations of the compounds were then analyzed using HPLC-UV.
- Effects of adsorbent dosage (0.1, 0.2, 0.5, 1, 2, 5, 10 and 20 g/L) on adsorption efficiency of antibiotics on steel shavings were examined. Different amounts of adsorbent which were 0.005, 0.01, 0.025, 0.05, 0.1, 0.25, 0.5 and 1 gram were added to 50 mL solution of the antibiotic at 1000 µg/L. The subsequent steps were carried out following the same procedure as for the pH influence tests.
- Effects of temperature on the adsorption process of antibiotics onto the adsorbents were carried out at 20, 25 and 30^0C. The volume of 50 mL of SMT, TC and CP concentrations (100, 200, 500, 1000, 2000, 5000, 10000 and 20000 µg/L) were added into 250 mL flasks, and then optimal pH of the solution was adjusted. The optimal amounts of adsorbents were added, and subsequently shaken at 130 rpm in a thermostatic shaker for 24 hours. The subsequent steps for analyzing ABs concentration were carried out following the same procedure as with the pH influence tests.

B. Isotherms and kinetics models of antibiotics adsorption

The Langmuir, Freundlich isotherm models; and Pseudo-first-order kinetic (PFO), Pseudo-second-order kinetic (PSO) and Intra-particle diffusion model (IDM) were used to describe the isotherms and kinetics of the adsorptive removal. The equation and linearized forms of the models are illustrated and summarized in Table 3.4.

Table 3.4 Kinetic and isotherm models of antibiotics adsorption on StS

Models	Equation	Linearized form
Langmuir	$q_e = \frac{q_{\max} k_L C_e}{1 + k_L C_e}$	$\frac{C_e}{q_e} = \frac{C_e}{q_{\max}} + \frac{1}{k_L q_{\max}}$
Freundlich	$q_e = k_F C_e^{1/n}$	$\ln q_e = \ln k_F + \frac{1}{n} \ln C_e$
	where: C_e is the equilibrium concentration (μg/L) of the adsorbate. q_e is adsorption capacity of StS at equilibrium (μg/g). q_{max} is maximum antibiotics uptake of the adsorbent (μg/g); k_L is Langmuir constant related to binding energy of adsorption (L/μg); k_F and n are Freundlich constants indicative of the adsorption capacity and adsorption intensity of the adsorbent, respectively.	
PFO	$\frac{dq_t}{d_t} = k_{1p}(q_e - q_t)$	$\ln(q_e - q_t) = \ln q_e - k_1 t$
PSO	$\frac{dq_t}{d_t} = k_{2p}(q_e - q_t)^2$	$\frac{1}{q_t} = \frac{1}{k_2 q_e^2} + \frac{1}{q_e}$
IDM	$q_t = k_i t^{0.5}$	
	where: qe = amount of antibiotics adsorbed at equilibrium (μg/g); qt = amount of antibiotics adsorbed at time t (min) (μg/g); k_{1p} = equilibrium rate constant of PFO (1/ min); k_{2p} = equilibrium rate constant of PSO (1/min) and ki (μg/g.min) = the rate constants of IDM, respectively.	

The experiments were performed for 3 antibiotics (SMT, TC and CP) separately according to the following procedures:

- For examination of the isotherms, the solutions of the antibiotic at different concentrations - 10, 50, 100, 500, 1000, 2000, 5000, 10000 and 20000 μg/L - were prepared in 250 mL flasks. The pH was adjusted to the optimum values

as obtained from the pH effects experiments. Then the optimal amount of adsorbent which was derived from the adsorbent dose tests was added, and shaken at 130 rpm at a fixed temperature (25^0C) for 24 hours.

- In kinetic experiments, the optimal amount of adsorbent which was obtained from the effect of adsorbent dose tests was mixed with 50 mL the antibiotic solution of 1000 µg/L, and then shaken at 130 rpm at room temperature. The samples were taken at different times: 5, 10, 20, 30, 45, 60, 120, 240, 480 and 1440 min.

The subsequent steps for analyzing ABs concentration were carried out following the same procedure as above.

C. Competitive adsorption of ABs on raw and modified StS

- For investigation of competitive adsorption isotherm of ABs on the adsorbents, 50mL with different concentrations of multi-antibiotics solutions at total multi-antibiotics solutions from 0, 100, 200, 500, 1000, 2000, 5000, 10000 and 20000 µg/L (each solute concentration of antibiotic at 0, 33.33, 66.67, 166.67, 333.33, 666.67, 1666.67, 3333.33 and 6666.67 µg/L) were used. The optimal pH and adsorbent dose were adjusted. The mixtures were shaken at 130 rpm for 24 hours at 25^oC.
- Kinetics: 50 mL of a mixed solution of 3 antibiotics SMT, TC and CP (1000 µg/L of total initial solution concentration, and each solute concentration is 333.33 µg/L) was prepared into 250 mL flasks to study competitive adsorption on adsorbents. Optimal amounts of adsorbent were added. The mixture was shaken at 130 rpm in shaking tables. The samples were taken at different times: 5, 10, 20, 30, 45, 60, 120, 240, 480 and 1440 min.

Next steps for analysis of SMT, TC and CP concentrations in the effluents were carried out following the same procedure as above.

The experimental data regarding competitive adsorption of ABs were calculated using combined Freundlich and combined Langmuir models (Ahmed et al., 2017).

The combined Freundlich model for 3 antibiotics:

$$Q_{total} = K_{F1}{C_{e1}}^{1/n} + K_{F2}{C_{e2}}^{1/n} + K_{F3}{C_{e3}}^{1/n} \quad (3.2.5.3)$$

$$K_{F(total)} = K_{F1} + K_{F2} + K_{F3} \quad (3.2.5.4)$$

The combined Langmuir model for 3 antibiotics:

$$Q_{total} = \frac{Q_{max1}K_{L1}C_{e1}}{1+K_{L1}C_{e1}} + \frac{Q_{max2}K_{L2}C_{e2}}{1+K_{L2}C_{e2}} + \frac{Q_{max3}K_{L3}C_{e3}}{1+K_{L3}C_{e3}} \quad (3.2.5.5)$$

$$Q_{max.(total)} = Q_{max1} + Q_{max2} + Q_{max3} \quad (3.2.5.6)$$

where K_{F1}, K_{F2}, K_{F3} are the Freundlich constants for first competitive solute, second competitive solute and third competitive solute respectively. Q_{max1}, Q_{max2} and Q_{max3} are the maximum Langmuir sorption capacity respectively for the first, second and third competitive solute.

D. Desorption and regeneration

Several reagents were chosen to desorb the ABs loaded adsorbents including tap water, H_2SO_4 0.1N; NaOH 0.1N, Methanol 0.1N and Ethanol 0.1N. Adsorbed materials and 100 mL of regeneration reagents were added into 250 mL flasks at room temperature, shaken at 130 rpm. Concentrations of ABs in the effluents were obtained following the same procedure as above.

After that, five continuous cycles of adsorption-desorption were studied using the optimal reagent that was identified from the above experiments for desorbing the ABs loaded adsorbents.

3.2.6. Semi-pilot scale experimental set up for removing HMs and ABs from synthesized wastewater

In the previous batch study, nitrogen plasma modified steel shavings (M_3-plN_2) have been shown to be successful remove HMs and ABs from water. As the next step, adsorption research using M_3-plN_2 is conducted at semi-pilot scales for removing HMs and ABs from synthesized wastewater. This study aims to design an novel and effective wastewater treatment unit at semi-pilot scale (up to $5m^3$/day) for HMs and ABs removal. The synthesized wastewater containing HMs was prepared by mixing stock solutions of Pb^{2+}, Cu^{2+}, Cd^{2+}, Cr^{3+} and Zn^{2+} with tap water (HMs concentrations: Pb^{2+} 5.94, Cu^{2+} 4.74, Cd^{2+} 6.48, Cr^{3+} 6.44 and Zn^{2+} 5.18 mg/L). Similarly, a mixture of three antibiotics SMT, TC and CP stock solutions was diluted with tap water to synthesize wastewater containing ABs (SMT 100.1, TC 97.3 and CP 99.5 μg/L).

A. Selecting the treatment designs for HMs and ABs removal

For selecting of the most effective design for HMs treatment from water using the M_3-plN_2, three different designs (design 1, 2 and 3 are illustrated in the Figures 3.10, 3.11 and 3.12, respectively) have been assessed. The semi-pilot experiments were conducted with synthesized wastewater following the three treatment designs: two reaction tanks (design 1 and 2) and a fixed-bed column (design 3).

The volume of the reaction tank (design 1 and 2) can be calculated as below:

Hydraulic retention time (HRT) = volume of tank (V) /influent flowrate (f)

→ V = f*HRT

f=5 m^3/day =~0.21 m^3/h = 210 liters/h = 3.5 liters/min=~58.3 ml/s

From the batch adsorption study, the adsorption of HMs and ABs onto M_3-plN_2 increased dramatically and mostly occurred in the first 4 hours (more than 95% of adsorbates were removed). Moreover, 60 min was the contact time to reach equilibrium status.

So, the required HRT = 4 hour → V = 840 liters. Thus reaction tank designs (design 1 and design 2) need to meet the requirement of 4 hour HRT, their functional volumes are larger than 840 liters.

Design 1 description

It includes a tank with 6 panels inside the tank with weirs on the top of 3 panels and at the bottoms of the other three. Panels with weir on top and at the bottom are put next to each other, so water goes through a zigzag route as in Figure 3.10. Bags are made of cotton fiber with the size of 8x5 cm, it is then easy to open and close the lid. The bags containing M_3-plN_2 are hung on the panels (the total weight of M_3-plN_2: 15 kg). Dimensions of the tank: length 150 cm, width 80 cm and height 80 cm. The tank has two pipes at the bottom on two sides for water in (connected to a pump and feed tank) and out.

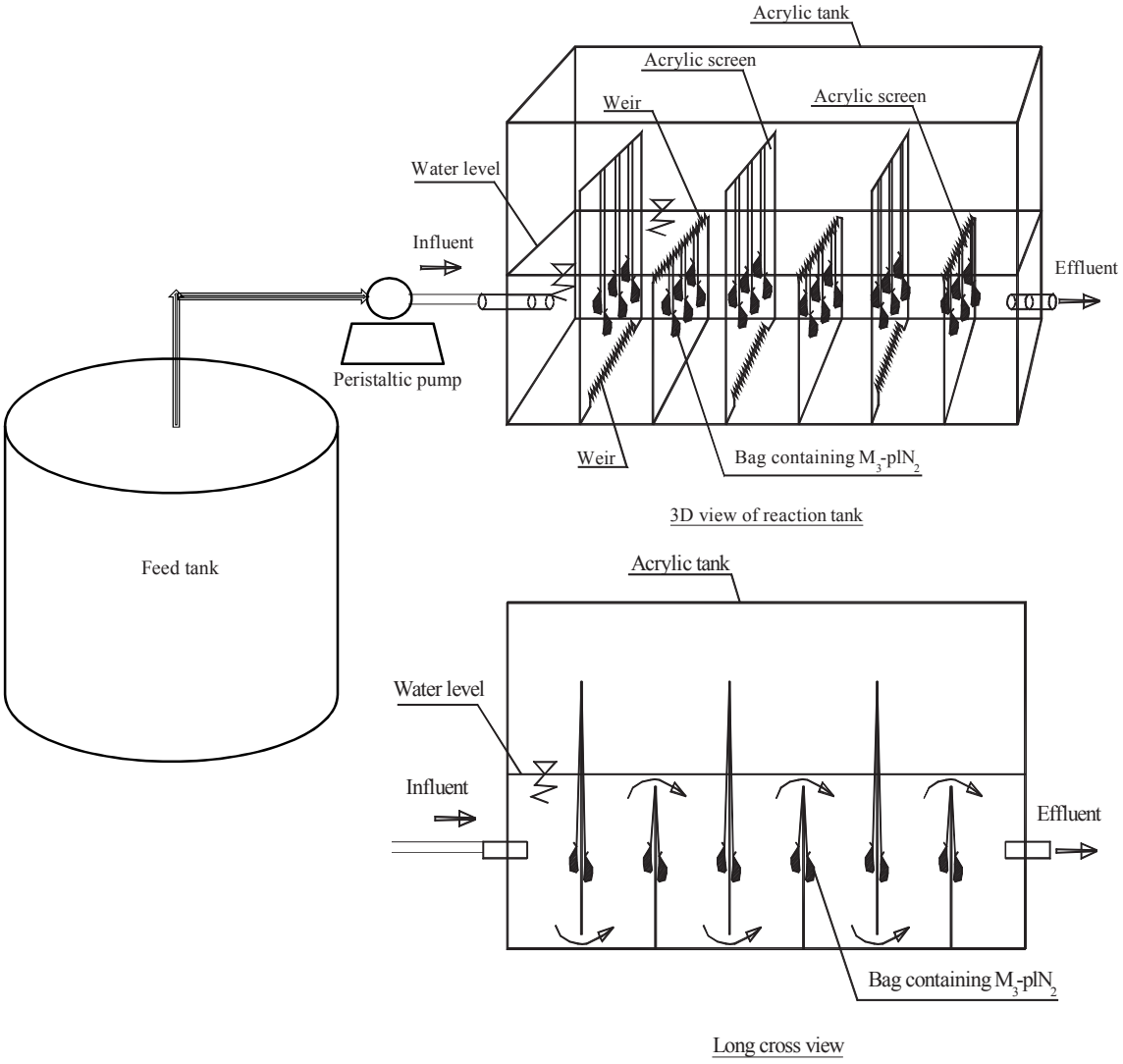

Figure 3.10 Schematic diagram of treatment system using nitrogen plasma modified steel shavings design 1

Design 2 description

A cylindrical tank is used for removing pollutants by M_3-plN_2. The design has 5 hanging bars on top using plastic pipes; the bags containing M_3-plN_2 are hung on the bars with fiber wires (Figure 3.11). A water pump (flow rate of 1000 liters/hour) is used to mix the water and make the water go through the bags (the

total weight of M_3-plN_2: 15 kg). The reaction tank has a radius of 50 cm and a height of 120 cm. The reaction tank is connected to a peristaltic pump and feed tank.

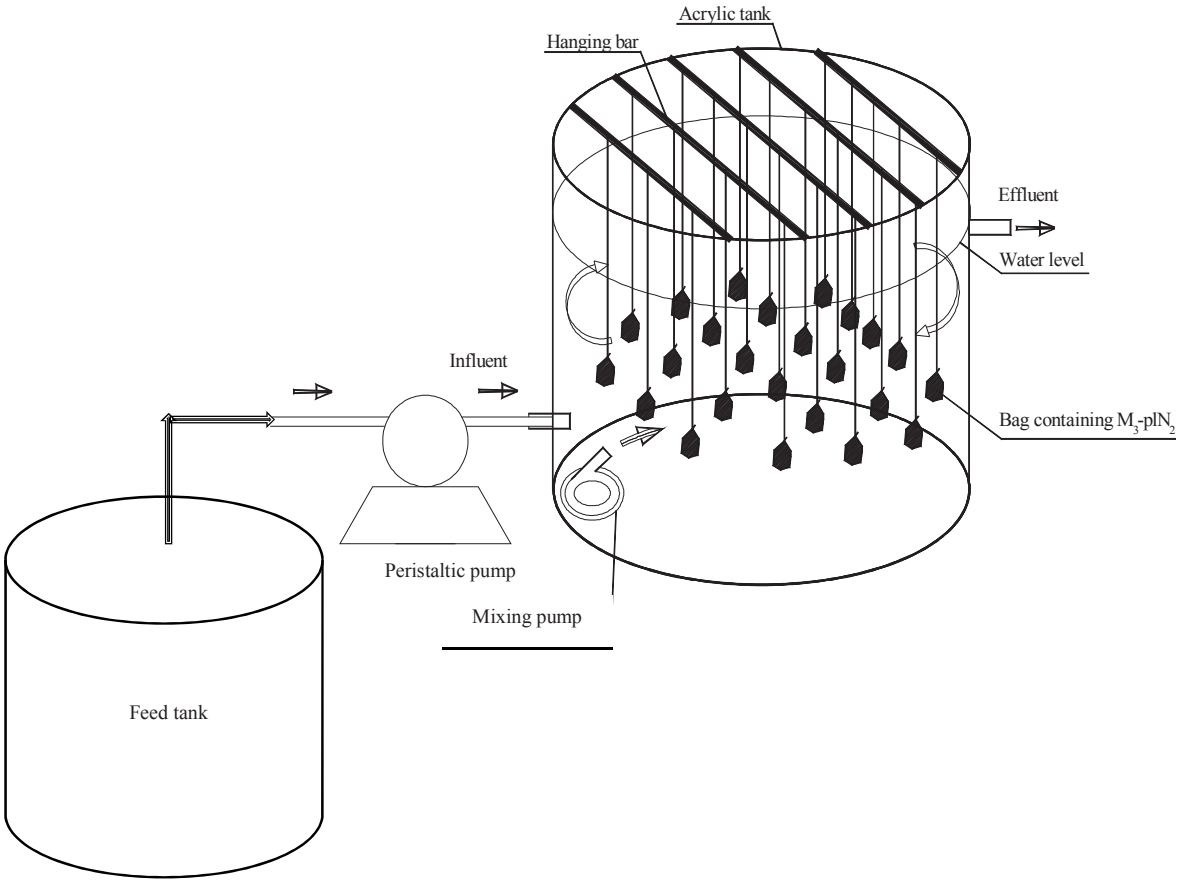

Figure 3.11 Schematic diagram of treatment system using nitrogen plasma modified StS design 2

Design 3 description

In this design, an up-flow packed column is utilized to remove HMs and ABs using M_3-plN_2 (Figure 3.12). The design is developed following a fixed-bed column. However, the adsorbents are stored inside numerous small cotton-fiber bags (bags with the same design as mentioned above were used) to prevent M_3-plN_2 from going with the water flow or column clogging. The dimensions of the column are inner diameter of 20 cm and height of 100 cm. The sides near the bottom and top of the column have pipes for influent and effluents. The column was packed with glass beads and the bags containing M_3-plN_2 (the total weight of M_3-plN_2 is 15 kg,

equivalent with 50cm of bed height) as in Figure 3.12. The bags were filled (about 50% of its volume) with M_3-plN_2. The bags containing M_3-plN_2 were initially mixed with DI water in a container until no air bubbles was observed. This step is quite similar to "slurry method" which was developed by Zach-Maor et al. (2011). A layer of glass beads (5 cm) was put into the column. Subsequently, the wet bags were carefully organized in the column (layer by layer) to minimize spaces inside the bed. Finally, another layer of glass beads (5 cm) was placed on top of the M_3-plN_2 bed. The influent is pumped through the column with an adjustable flow-rate valve.

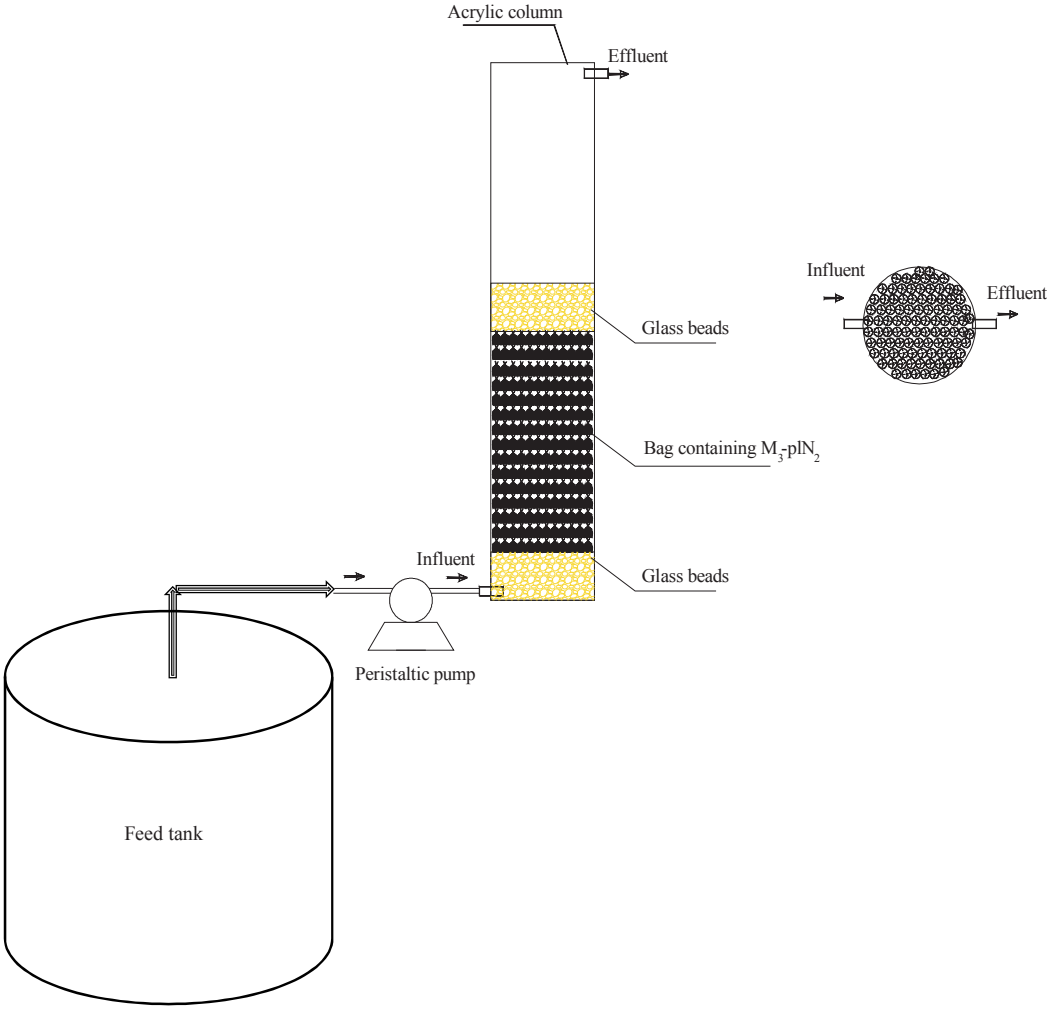

Figure 3.12 Schematic diagram of treatment system using nitrogen plasma modified StS design 3

B. A column design for HMs removal by nitrogen plasma modified steel shavings

After the best design for removing HMs was chosen, affecting factors to adsorption process in the treatment design (fixed-bed column) including flow rate and bed height were studied.

Effects of column design parameters

- For examination of the effect of flow rate on HMs removal by StS in the system, experiments were carried out at fixed bed height of 35 cm, room temperature (25^0C), non-adjusted pH value and at different flow rates of the influent including 2500; 5000; 7500; 10000 L/day (equivalent to 1.74, 3.47, 5.21 and 6.94 L/min). The samples were collected at pre-determined intervals, then the mixtures were filtrated using 1.2 µm filtration paper and finally the metal ions in the remaining solution were analyzed by MP-AES.
- Effects of bed height were evaluated by experiments with different bed height including 20, 35 and 50 cm (by packed with certain amounts of M_3-plN_2: 6, 10.5 and 15 kg) and optimal flow rate which was obtained from the above experiments. The samples were collected at pre-determined intervals and the metal concentrations were defined as in the previous procedure.

Calculation of breakthrough curve parameters

For evaluation of the adsorption performance of a column, it is necessary to analyze the break-through curve by calculating breakthrough curve parameters. The breakthrough time (t_b) and treated volume at break-through time (V_b) are determined as the time and volume when the outlet pollutant concentration (C_t) reached 10% of the inlet concentration (C_t/C_o = 0.1). Likewise, the exhaustion time (t_s) and treated

volume at exhaustion time (V_s) are identified as the time and volume when the outlet concentration (C_t) reached 90% of the inlet concentration (C_t/C_o =0.9).

The total amount of pollutant adsorbed onto M_3-plN_2 column, q_{total} (mg/g or µg/g) and the dynamic adsorption capacity, q_e (mg/g or µg/g) are calculated according to the following equations (Han et al., 2009; Paudyal et al., 2013; Sharma and Singh et al., 2013):

$$q_{total} = \frac{Q}{1000} \int_{t=0}^{t=total} C_{ad} dt \quad (3.2.6.1)$$

$$q_e = \frac{q_{total}}{M} \quad (3.2.6.2)$$

where, t total, Q,M, and Cad are the total time for the column to reach saturation (min), volumetric flow rate (mL/min), the amount of M_3-plN_2 packed in the column (g), and the difference in the pollutant concentration at the initial time and the time t caused by adsorption (mg/L), respectively.

The prediction of the breakthrough curve is essential for designing a continuous adsorption system. The relation between concentration and time provides insights into the adsorbent affinity, adsorbent surface properties, and adsorption pathways (Foo et al., 2013). For that reason, several mathematical models have been developed for this purpose. Four different models were used in this research including Adams–Bohart, Thomas, Yoon–Nelson, and BDST models.

In the Adams–Bohart model, the equilibrium is not instant and the adsorption rate is controlled by external mass transfer (Quintelas et al., 2013). The model was used for analyzing the initial part of the breakthrough curve (C_t/C_o=0-0.5) (Long et al., 2014; Sharma and Singh, 2013). The Adams-Bohart model is expressed as the following equation (Han et al., 2009):

$$\ln \frac{C_t}{C_o} = K_{AB} C_o t - K_{AB} N_0 \frac{Z}{F} \quad (3.2.6.3)$$

where C_o and C_t (mg/L or µg/L) are the influent and effluent pollutant concentration, K_{AB} (L/mg.min or L/µg.min) is the kinetic constant, N_o (mg/L or µg/L) is saturation concentration of the column, Z (cm) is the bed height, F (cm/min) is the linear velocity achieved by dividing the flow rate (cm^3/min) by the column section area (cm^2). The constants K_{AB} and N_o of the Adams–Bohart model can be estimated from the linear plot of $\ln(C_t/C_o)$ against t.

The Thomas model assumes that the adsorption is not restricted by chemical interactions but by mass transfer at the interface and the experimental data follows Langmuir isotherms and second-order kinetics (Foo et al., 2013). Instead of initial part of breakthrough curves as Adams–Bohart model, Thomas model is suitable for depicting the whole breakthrough curve (Bulgariu and Bulgariu, 2013). Thomas model is given as the following equation (Thomas, 1944; Paudyal et al., 2013; Han et al., 2009):

$$\ln\left(\frac{C_o}{C_t} - 1\right) = k_{Th} q_o \frac{m}{Q} - k_{Th} C_o t \qquad (3.2.6.4)$$

where k_{Th} is the Thomas rate constant (mL/min.mg or mL/min.µg), q_o is the adsorption capacity (mg/g or µg/g), C_o is the inlet pollutant concentration (mg/L or µg/L), C_t is the outlet concentration at time t (mg/L or µg/L), m is the mass of adsorbent (g), Q is the feed flow rate (mL/min), and t is the filtration time (min). The values of k_{Th} and q_o were determined from the linear plot of $\ln(C_o/C_t - 1)$ against t.

The Yoon–Nelson model can also predict the whole period of the breakthrough curve. The linear expression of this model is described by the following equation (Yoon and Nelson, 1984; Sharma and Singh, 2013):

$$\ln\left(\frac{C_t}{C_o - C_t}\right) = k_{YN} t - \tau k_{YN} \qquad (3.2.6.5)$$

where k_{YN} stands for the Yoon–Nelson rate constant (min^{-1}), and τ is the time required for 50% pollutant removal breakthrough (min).

The BDST model is used for describing the relationship between bed depth and service time of a column. According to Jain et al. (2013), BDST model can present appropriately the initial part (10–50%) of the breakthrough curve. The BDST model is described as the following equation (Han et al., 2009; Paudyal et al., 2013):

$$t = \frac{ZN_o}{C_o v} - \frac{1}{K_b C_o} \ln\left(\frac{C_o}{C_b} - 1\right) \quad (3.2.6.6)$$

where t is the service time of column (h), Z is the bed depth (cm), C_o is the inlet pollutant concentration (mg/L or µg/L), C_b is the outlet concentration at breakthrough point (mg/L or µg/L), N_o is the column adsorption capacity (mg/L or µg/L), K_b is the rate constant [L/(mg.h) or L/(µg.h)], and v is the linear flow velocity and is calculated by dividing the flowrate by the area of column (cm/min).

From the plots of time versus bed depth, N_o and K_b are calculated as follows (Zach-Maor et al., 2011):

$$m = \text{slope} = \frac{N_o}{C_o v} \rightarrow N_o = mC_o v \quad (3.2.6.7)$$

$$C = \text{intercept} = -\frac{1}{K_b C_o} \ln\left(\frac{C_o}{C_b} - 1\right) \rightarrow K_b = -\frac{1}{C * C_o} \ln\left(\frac{C_o}{C_b} - 1\right) \quad (3.2.6.8)$$

Setting t=0 and solving Eq. 3.2.6.6 for Z produces the following equation (Kumar and Bandyopadhyay, 2006):

$$Z_o = \frac{v}{K_b N_o} \ln\left(\frac{C_o}{C_b} - 1\right) \quad (3.2.6.9)$$

where Z_o (cm) is called the critical bed depth, which is the minimum bed depth required to yield the desired effluent concentration (C_b).

C. A column design for ABs removal by nitrogen plasma modified steel shavings

The affecting factors including flow rate and bed height to ABs removal were studied in the optimal semi-pilot design that was selected in the above section.

Effects of column design parameters

- For studying the effect of flow rate on the removal process of ABs by StS in the system, experiments were carried out at bed height of 35 cm, room temperature (25^0C) and without pH adjustment. Flow rates of the influent were 2500, 5000, 7500 and 10000 L/day (equivalent to 1.74, 3.47, 5.21 and 6.94 L/min). The samples were collected at pre-determined intervals, then the mixtures were filtrated using 0.2 µm paper filters and finally the remaining concentrations of ABs were analyzed by HPLC.
- Effects of bed height were evaluated by experiments with different bed height including 20, 35 and 50 cm (equivalent with certain weights of M_3-plN_2: 6, 10.5 and 15 kg) at the optimal flow rate which was obtained from the effect of flow rate experiments. The samples were collected at pre-determined intervals and then the antibiotics concentrations were defined as in the above procedure.

Calculation of breakthrough curve parameters

Evaluation of experimental data of ABs removal by nitrogen plasma modified steel shavings was conducted using different dynamic models, the same as above including Adams-Bohart, Thomas, Yoon-Nelson, and BDST models.

3.2.7. Heavy metals analysis method

Concentrations of HMs were analyzed using 4100-MP-AES, Agilent Technologies with an auto-sampler at Environmental engineering laboratories, Faculty of Engineering and Information Technology, UTS (Figure 3.13A).

3.2.8. Analytical method of the antibiotic concentrations

For analyzing the concentrations of SMT, TC and CP in water, high performance liquid chromatography (HPLC) with detector UV was utilized (Figure 3.13B).

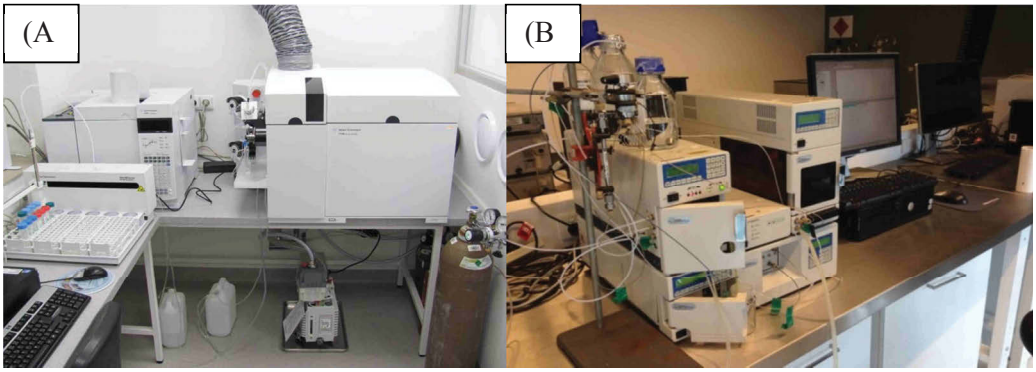

Figure 3.13 MP-AES and HPLC instruments: (A) 4100-MP-AES, Agilent Technologies and (B) Jasco HPLC-UV

The concentrations of SMT, TC and CP were analyzed by HPLC (Jasco) with auto-sampler using a reserve phase Zorbax Bonus RP C-18 column (2.1x1.5 mm, 5 µm particle size, Agilent Technologies). The detection was done utilizing UV absorption at a wavelength of 285nm, by 50 µL injection. Acetonitrile and formic acid were employed as the mobile phase A (v:v = 99.9:0.1) while mobile phase B consisted of Milli-Q water and formic acid (v:v = 99.9:0.1). The applied program of elution is presented in Table 3.5 and the running time of the method was 10 min. The chromatograph of antibiotics by HPLC and the analytical standard lines are depicted in Figure 3.14.

3.2.9. Statistical analysis

All experiments were implemented in triplicate and data represented the average values. The deviations were less than 5%.

Table 3.5 The elution program applied in the antibiotics analysis using HPLC

Time (min)	Flow (mL/min)	%A	%B
Prerun	0.3	40	60
0.1	0.2	15	85
4.0	0.2	15	85
4.1	0.3	40	60

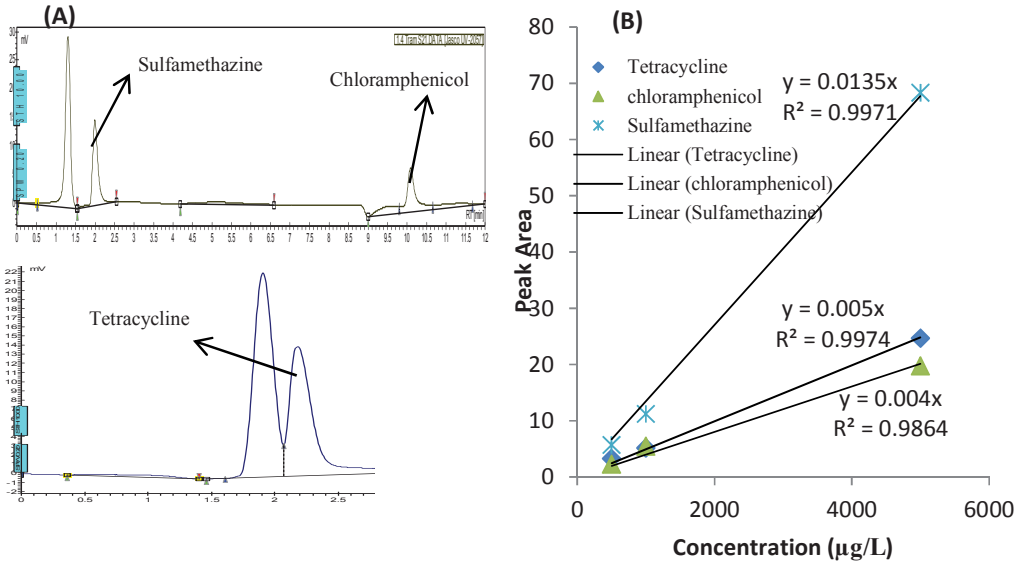

Figure 3.14 (A) Chromatograph of SMT, CP and TC by HPLC- UV and (B) Analytical standard lines of SMT, TC and CP

Faculty of Engineering and Information Technology

CHAPTER 4

DEVELOPMENT OF ADSORBENTS FROM STEEL SHAVINGS FOR HEAVY METALS AND ANTIBIOTICS REMOVAL

4.1. Introduction

In order to develop steel shavings as an adsorbent for water treatment, it is necessary to study its physical and chemical characteristics, adsorption capacity and optimal conditions for modifying the material.

As described in chapter 2 and chapter 3, plasma modification technique was applied for the development of the adsorbents. This chapter focuses on finding the effects of conditions such as particle size of StS and employed gas in plasma modification on the removal of HMs as well as ABs from aqueous solution. From the results, optimal conditions to enhance adsorption capacities of the adsorbents from steel shavings were concluded. The adsorption abilities were also compared with those of commercial iron (III) oxide (Fe_2O_3).

Chapter 4 also describes and analyzes the characterization of the adsorbents obtained from steel shavings. From the experimental outcomes, comparison is made to assess the effects of plasma modification to characteristics of the adsorbents.

Table 4.1 shows adsorption efficiencies between 15 different kinds of adsorbents including 150<StS<425 μm (M_1), M_1-plO_2, M_1-plH_2, M_1-plN_2, M_1-plAr, 75<StS<150 μm (M_2), M_2-plO_2, M_2-plH_2, M_2-plN_2, M_2-plAr, 0<StS<75 μm (M_3), M_3-plO_2, M_3-plH_2, M_3-plN_2, and M_3-plAr for HMs and ABs.

4.2. Effects of particle size, employed gas to adsorptive removal of HMs

Adsorption capacities of different kinds of adsorbents including raw StS (various particle size), Fe (III) oxide, plasma modified StS (H_2, O_2, N_2 and Ar) were investigated to compare and discuss.

4.2.1. Particle size

Particle size wields a very large influence on adsorption efficiency of metal ions on the raw and modified StS. As expected, the finer particles were the ones possessing the highest removal efficiency (Table 4.1). For example, the removal efficiencies of Pb^{2+} on M_1, M_2, M_3 were 73.0, 78.7 and 85.5 %, respectively. The removal efficiencies of HMs on raw and plasma modified StS (at all the three particle sizes) were much higher than those of analytical Fe_2O_3 (Pb^{2+} 31.4, Cu^{2+} 33.2, Cd^{2+} 21.3, Cr^{3+} 19.2 and Zn^{2+} 23.8 %).

Furthermore, plasma modification with gases including H_2, O_2, N_2 and Ar of different particle sizes from 0-75; 75-150; 150-425 μm also achieved the similar outcomes regarding particle size effects on HMs removal. After plasma modification, the finer particle size also led to higher adsorption capacities of HMs on the adsorbents. Percentages of removed metal ions on argon plasma modified StS (at different particle sizes) were Pb^{2+} 73.9, Cu^{2+} 74.3, Cd^{2+} 40.3, Cr^{3+} 33.5, Zn^{2+} 39.9 % by M_1-plAr; Pb^{2+} 80.1, Cu^{2+} 81.1, Cd^{2+} 56.2, Cr^{3+} 46.6, Zn^{2+} 44.7 % by M_2-plAr and Pb^{2+} 94.2, Cu^{2+} 95.6, Cd^{2+} 54.2, Cr^{3+} 55.6, Zn^{2+} 57.0 % by M_3-plAr.

4.2.2. Employed gas in plasma modification

Table 4.1 displays the effects of gas plasma modification on the removal efficiencies of HMs on the adsorbents obtained from steel shavings. Plasma modification significantly affected adsorption efficiencies of heavy metals on steel shavings. Removal efficiencies of HMs on M_3 were Pb^{2+} 85.5, Cu^{2+} 87.4, Cd^{2+} 50.3, Cr^{3+} 49.0 and Zn^{2+} 51.5%. They increased with adsorbents that had been modified with plasma H_2, N_2, Ar, especially those of M_3-plN_2 which were Pb^{2+} 95.8, Cu^{2+}

96.3, Cd^{2+} 58.5, Cr^{3+} 57.3 and Zn^{2+} 59.5 %. In contrast, the removal efficiencies on M_3-plO_2 decreased following plasma modification with O_2, these efficiencies being Pb^{2+} 66.9; Cu^{2+} 72.9; Cd^{2+} 50.6; Cr^{3+} 47.2 and Zn^{2+} 51.0 %. These results demonstrate that O_2-plasma modification has not only cleaned the surface of StS, oxidized carbon to C-N or C-O gases but also oxidized low-oxygen forms of Fe to a rich-oxygen form such as Fe_2O_3. As can be seen from the results, analytical Fe_2O_3 has very low adsorption capacity for heavy metals from water.

The above results indicate that plasma modification with H_2, Ar, N_2 did improve the adsorption capacity of HMs on steel shavings. Especially, plasma modification with N_2 gas has considerably enhanced adsorption efficiencies of the adsorbent. Moreover, N_2 gas is much cheaper and easier to apply than other gases. Hence, raw StS (0-75μm, M_3) and plasma modified StS with nitrogen (0-75μm, M_3-plN_2) were selected for conducting the subsequent experiments.

4.3. Effects of particle size, employed gas to adsorptive removal of ABs

4.3.1. Particle size

The particle size has also great effects on removal efficiencies of SMT, TC and CP by the adsorbents (Table 4.1). The uptake efficiencies of SMT; TC and CP were 54.2, 55.3, 56.7 % by M_1; 58.5, 62.8, 64.6 % by M_2 and 75.2, 78.6, 80.7 % by M_3, respectively. The smaller particle sizes had the better removal efficiencies. The particle size of 0-75 μm best removed the antibiotics from aqueous solution. The removal abilities of antibiotics by the adsorbents were much higher than those of iron (III) oxide (40.8, 41.2 and 43.6 % for SMT, TC and CP, correspondingly). Therefore,

the particle size of 0-75 μm was chosen for removing antibiotics from water in the next experiments.

After plasma modification, the particle sizes also considerably affected the removal efficiencies of ABs. For instance, removal efficiencies of SMT, TC and CP were 55.7, 60.1, 61.2 % on M_1-plAr; 70.2, 74.9, 76.1 % on M_2-plAr; and 91.2, 96.2, 97.5 % on M_3-plAr, respectively.

4.3.2. Employed gas in plasma modification

Table 4.1 exhibits that the plasma modification has influenced the removal efficiencies of SMT, TC and CP by the modified steel shavings. Similar results of plasma modified steel shavings for removing HMs were achieved for removing ABs. Plasma modification in oxygen environment reduced the removal efficiencies of steel shavings. Achieved uptake abilities of SMT, TC and CP by M_1-plO_2 were 50.1, 52.3 and 53.5 % (compared to achieved 54.2, 55.3 and 56.7 % by M_1), respectively.

In contrast, removal efficiencies of ABs by modified adsorbents increased after plasma modification of steel shavings with hydrogen, nitrogen and argon, and this is especially so after steel shavings were plasma modified with nitrogen. Removal efficiencies of ABs by nitrogen plasma modified steel shavings were highest among the adsorbents in the same particle sizes. For instance, the percentages of SMT, CP and TC that removed from water by M_3-plN_2 were 94.8, 97.3 and 99.8 %, respectively.

From the experimental data, M_3 and M_3-plN_2 have been utilized to abate ABs from water in future experiments.

Table 4.1 Removal efficiencies of HMs and ABs on different sizes of raw and plasma modified StS

Adsorbents	Removal efficiencies of HMs (%)					Removal efficiencies of ABs (%)		
	Pb^{2+}	Cu^{2+}	Cd^{2+}	Cr^{3+}	Zn^{2+}	SMT	TC	CP
Fe_2O_3	31.4	33.2	21.3	19.2	23.8	40.8	41.2	43.6
150<StS<425 µm (M_1)	73.0	73.5	43.3	31.0	33.5	54.2	55.3	56.7
M_1-plO_2	68.9	71.2	44.6	29.8	37.7	50.1	52.3	53.5
M_1-plH_2	74.3	76.2	49.5	35.7	40.3	55.4	53.2	54.0
M_1-plN_2	77.4	83.3	53.4	39.5	42.4	60.3	61.5	65.2
M_1-plAr	73.9	74.3	40.3	33.5	39.9	55.7	60.1	61.2
75<StS<150 µm (M_2)	78.7	81.5	47.2	40.1	41.4	58.5	62.8	64.6
M_2-plO_2	67.5	70.8	45.3	38.8	37.9	56.8	61.3	62.7
M_2-plH_2	82.3	85.1	50.7	44.2	41.4	68.9	70.0	75.4
M_2-plN_2	82.8	89.8	56.3	48.8	50.1	72.3	76.8	80.3
M_2-plAr	80.1	81.1	56.2	46.6	44.7	70.2	74.9	76.1
0<StS<75 µm (M_3)	85.5	87.4	50.3	49.0	51.5	75.2	78.6	80.7
M_3-plO_2	66.9	72.9	50.6	47.2	51.0	73.6	75.4	77.5
M_3-plH_2	86.8	88.9	51.2	52.4	53.3	85.9	89.0	92.1
M_3-plN_2	95.8	96.3	58.5	57.3	59.5	94.8	97.3	99.8
M_3-plAr	94.2	95.6	54.2	55.6	57.0	91.2	96.2	97.5

M_1, M_2, M_3: 150<StS<425 µm, 75<StS<150 µm, StS<75 µm; M_x-plO_2, M_x-plH_2, M_x-plN_2, M_x-plAr: M_x was plasma modified with O_2, H_2, N_2, Ar (100 mg/L of metal ions solutions, pH5, 24 hours, room temperature; 1000 µg/L of SMT, TC and CP solutions, pH5, 24 hours, room temperature)

4.4. Characterization of adsorbents

The studied adsorbents were characterized by Zeiss Evo SEM (with attached EDS at 15 kV), SEM-Supra 55VP, Brunauer-Emmett-Teller (BET), Siemens D5000 X-ray Diffractometer (XRD), X-ray photoelectron spectroscopy (XPS) and Fourier transform infrared spectroscopy (FTIR) to obtain the surface morphology, elemental composition, mineral species, surface area, porosity, and appearance of iron oxides and organic groups on the adsorbed materials. Furthermore, Zeta potential and particle size distribution of the adsorbents were also measured.

4.4.1. Surface morphology

The scanning electron microscopy (SEM) micrographs of the surfaces of some kinds of fresh steel shavings particles (raw and modified) as well as after water treatment are shown in Figure 4.1 and Appendix A. The SEM images indicate that the surface of StS has a 'cloud-like' structure with abundant protuberances, which favoured the adsorption of pollutants on its surface (Figures 4.1). As can be seen in these images, the plasma treatment cleans the surface without modifying the particle morphology.

Charging in the surface structure is noticed for most samples, especially after the sorption process which may be due to the pollutants' dispersal on the StS surface.

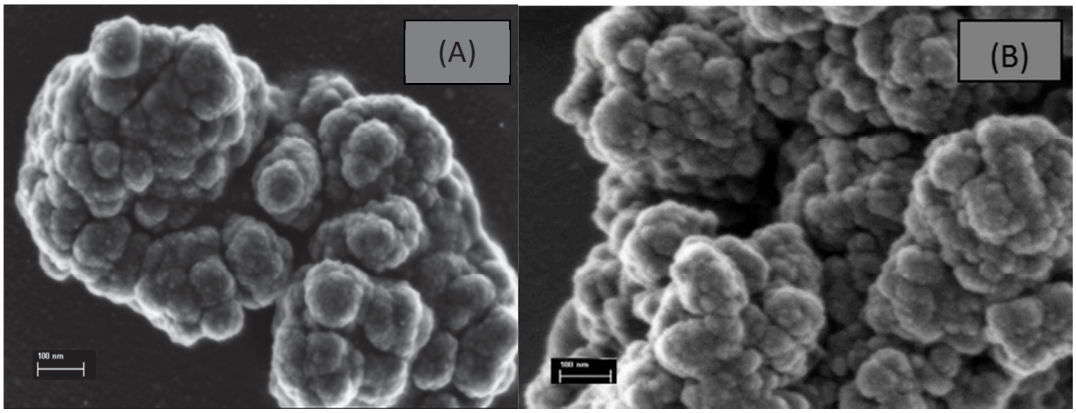

Figure 4.1 SEM results of raw and nitrogen plasma modified adsorbent A: M_3; B: M_3-plN_2 (M_3: StS<75 μm; M_3-plN_2: StS<75 μm was plasma modified with N_2)

4.4.2. Elementary composition

Energy-Dispersive X-ray Spectroscopy (EDS) scans taken at the center of a representative particle from different kinds of adsorbents including Fe_2O_3, M_3, M_3-plO_2, M_3-plAr, M_3-plN_2 were shown in Figure 4.2 and Appendix B with the elemental compositions from the standardless EDS analysis presented in Table 4.2. It was observed that the iron content of raw steel shavings (M_3, 47.7%) was less than

that of analytical iron (III) oxide (62.09%). This result can be explained by the existence of a higher proportion of carbon or other elements resulting from steel manufacturing in steel shavings than that of commercial Fe_2O_3. The iron contents of studied adsorbents in this research were less than those of other studies. In a study conducted by Gheju and Balcu (2011), the fresh scrap iron contained 81.45% of Fe, 15.56% of O, and small amounts of Al, Si, and Mn). Another study reported that the zero-valent iron has particle size ranged from 0.4 to 1.25 mm and Fe^0 content of 98% (Rangsivek and Jekel, 2005).

The results also revealed visible changes in the relative concentration of O, C as well as Fe after plasma modification. The iron content of StS (47.7%) increased after plasma treatment with gases, namely argon (53.4%) and nitrogen (55.2%). In contrast, the iron content of the adsorbent declined after being modified with plasma containing O_2 gas (46.4%). Moreover, the content of carbon and oxygen in samples M_3-plAr and M_3-plN_2 are less than that of M_3. These results can be best explained by the fact that plasma treatment with gases argon and nitrogen will clean the surface of the materials and prevent the formation of oxygen-rich iron oxides (see Figure 3.5). Plasma modified with oxygen gas slightly raised the oxygen content in the adsorbent (32.96% in raw material to 35.76% in M_3-plO_2). These percentages might be due to more formation of oxygen-rich iron oxides such as iron (III) oxide. As oxygen is necessary for the degradation of the organic compounds during plasma cleaning process, it can be referred from the experimental data that steel shavings contains very low content of organic compounds.

The above results suggested the involvement of Fe content as well as the existing form of Fe in the adsorbent to adsorption of HMs and ABs on the

adsorbents, whereas M_3-plN_2 - low oxygen, high iron contents had the highest adsorption capacities for HMs and ABs.

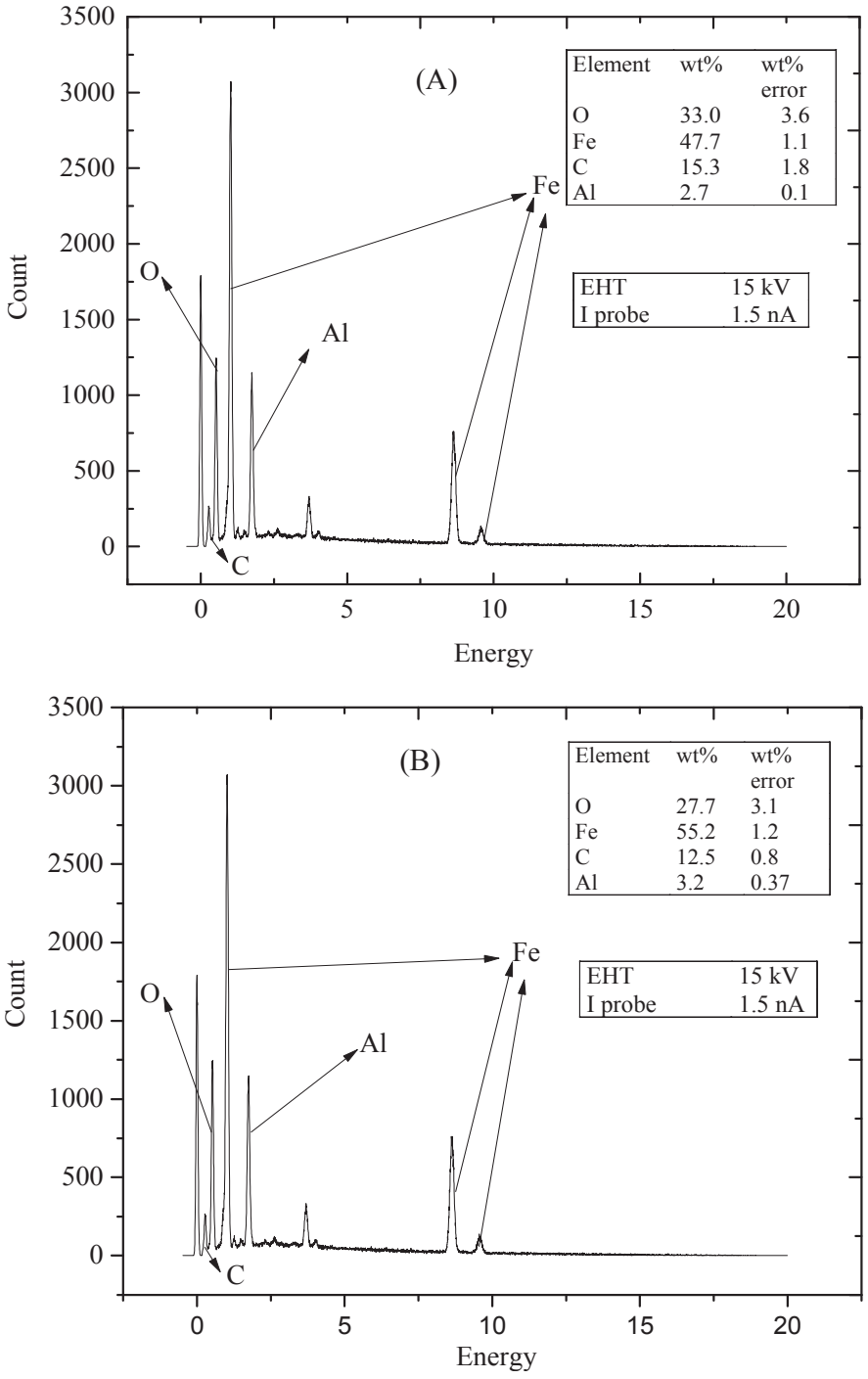

Figure 4.2 EDS results of raw and nitrogen plasma modified adsorbents (A) M_3; (B) M_3-plN_2 (M_3: StS<75 µm; M_3-plN_2: StS<75 µm was plasma modified with N_2)

Table 4.2 Elementary composition of different kinds of adsorbents

Element (%)	Fe_2O_3	M_3	M_3-plO_2	M_3-plAr	M_3-plN_2
O	32.40	32.96	35.76	27.45	27.65
Fe	62.09	47.70	46.40	53.39	55.16
C	4.82	15.31	14.56	12.67	12.52
Al	0.11	2.73	2.08	2.23	3.15
Mg	0.08	0.25	0.00	0.13	0.04
Mo	0.26	0.26	0.00	0.46	0.18
Si	0.06	0.35	0.22	0.98	0.65
Ca	0.09	0.16	0.39	0.11	0.10
Cr	0.07	0.26	0.54	2.57	0.41
K	0.02	0.03	0.15	0.00	0.14

4.4.3. XRD spectrums

The XRD patterns of the StS particles reveals a sharp diffraction peak Fe(110) at $2\theta = 44^{o}$, which is enhanced by the plasma treatments (Figure 4.3). This outcome indicates the surface contaminants were removed by the plasma modification. The strong XRD backgrounds have too many noises which implied that the adsorbents StS particles were not well crystallized or it has an amorphous structure (Fang et al., 2011). The presence of iron was identified in all samples.

The XRD spectra confirmed previous results that the iron content rose after plasma modification using the gases Ar and N_2.

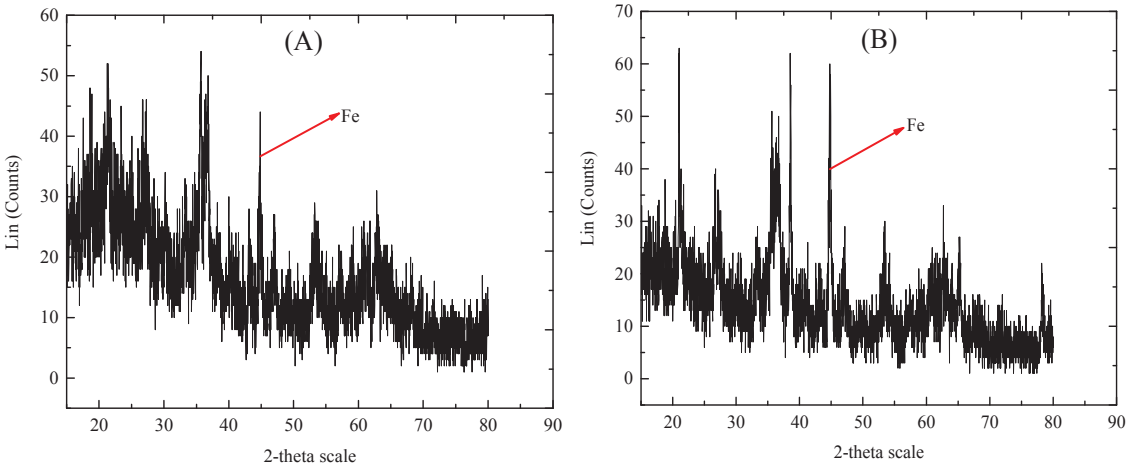

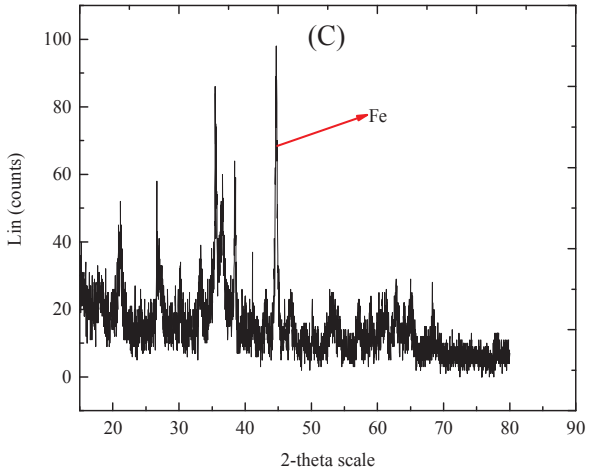

Figure 4.3 XRD patterns of adsorbents: (A) M_3; (B) M_3-plN_2; (C) M_3-plAr (M_3: StS<75 µm; M_3-plN_2, M_3-plAr: StS<75 µm was plasma modified with N_2, Ar)

4.4.4. BET

Table 4.3 summarizes the comparison between before and after nitrogen plasma modification of steel shavings. The experimental results exhibited that the nitrogen plasma modification enhanced the surface area and porosity of the adsorbents. The BET results showed that the surface area of the modified plasma with nitrogen steel shavings (M_3-plN_2) was 1.7-fold larger than that of raw steel shavings (M_3) (Table 4.3). Specific surface area of the adsorbents from the BET analysis of M_3 and M_3-plN_2 were 2.72 and 4.56 m^2/g, respectively. Similarly, the pore volume of the adsorbent slightly enlarged from 0.011319 to 0.01561 cm^3/g (1.4-fold) after modification. This can be explained by plasma modification removing hydrocarbon compounds and contaminants from the materials' surface, thus increasing the surface area and porosity of the adsorbent. Thus, adsorption capacities of adsorbent were improved as shown in the results in 4.3.2.

The surface areas of raw and modified StS were greater than those of zero-valent iron, which was prepared from scrap iron by Rangsivek and Jekel (2005). In

their study, the zero-valent iron has BET surface area of 0.384 m^2/g (Rangsivek and Jekel, 2005). However, the surface areas of the adsorbents were less than that of synthesized nano zero-valent iron, which had a BET surface area of 32.02 m^2/g (Xia et al., 2014).

Table 4.3 Summary comparison in characterisations of raw and plasma modified StS with N_2

Character	**Raw StS (M_3)**	**Gas plasma modified StS (M_3-plN_2)**
Morphology	A special 'cloud-like' structure with abundant protuberances and many pores	There are no visible changes in plasma modified StS compared to raw StS
Composition	• Iron content 47.7% • Oxygen content 33.0% • Carbon content 15.3%	• Iron content 55.2% • Oxygen content 27.7% • Carbon content 12.5%
Surface area		
Single point surface area at p/p° = 0.29	2.6916 m²/g	4.2910 m²/g
BET surface area	2.7179 m²/g	4.5617 m²/g
Langmuir surface area	4.0794 m²/g	9.3362 m²/g
t-Plot Micropore Area	1.4827 m²/g	-
t-Plot External Surface Area	1.2351 m²/g	5.2518 m²/g
Pore volume		
Single point adsorption total pore volume of pores less than 980.2 Å width at p/p° = 0.98	0.011319 cm³/g	0.015610 cm³/g
t-Plot micropore volume	0.000534 cm³/g	-0.001216 cm³/g
BJH adsorption cumulative volume of pores between 10.000 Å and 3,000.000 Å width	0.002454 cm³/g	0.006003 cm³/g
Pore size		
Adsorption average pore diameter (4V/A by BET)	166.5828 Å	136.8825 Å
BJH Adsorption average pore width (4V/A)	33.898 Å	40.857 Å

M_3: raw StS<75 µm; M_3-plN_2: raw StS<75 µm was plasma modified with N_2

4.4.5. XPS

The XPS spectrum determining the binding energy of elements in the top 10 nm of adsorbents was shown in the full survey scans of Figure 4.4A. From the peaks in binding energy regions of the elements in XPS narrow scans, chemical bonds,

states and those elements' environments are determined (Figure 4.4B, C, D). Table 4.4 indicates that the typical chemical states of C in M_3-plN_2 were C-C at ~284.8 eV, C-O-C at ~286 eV and O-C=O at >288.5 eV bonding (Thermo scientific XPS, 2017). Oxygen's chemical states with the adventitious carbon and the metals are displayed in the narrow scans in the O1s region (Table 4.4) (Thermo scientific XPS, 2017).

The Figure 4.4D and Table 4.4 showed the binding energy separation of the Fe2p3/2A and Fe2p3/2B peaks in all spectra. These outcomes implied a mixed oxide of both Fe^{3+} and Fe^{2+} which is Fe_3O_4. It confirmed that the binding energy of an element increases when its valence state also increases. The oxide is the principal oxide existing in the adsorbent M_3-plN_2. As can be seen in all spectra, other components were Fe2p3/2C and Fe2p3/2D which demonstrated the existence of Fe^{2+} and Fe^{3+} in their other separate oxides states of FeO and Fe_2O_3, respectively. It could be assumed that these iron oxides were primarily responsible for the adsorption of HMs and ABs on steel shavings.

Moreover, the spectra of the adsorbents did not show a peak at ~ 706.7eV binding energy, which indicates the chemical state of zero-valent iron (Fe^0) (Thermo scientific XPS, 2017). The XPS technique can only define at 10 nm layer in the top of material. Therefore, it can be presumed that the Fe^0 core of the adsorbent was coated by oxide film that was thicker than 10 nm.

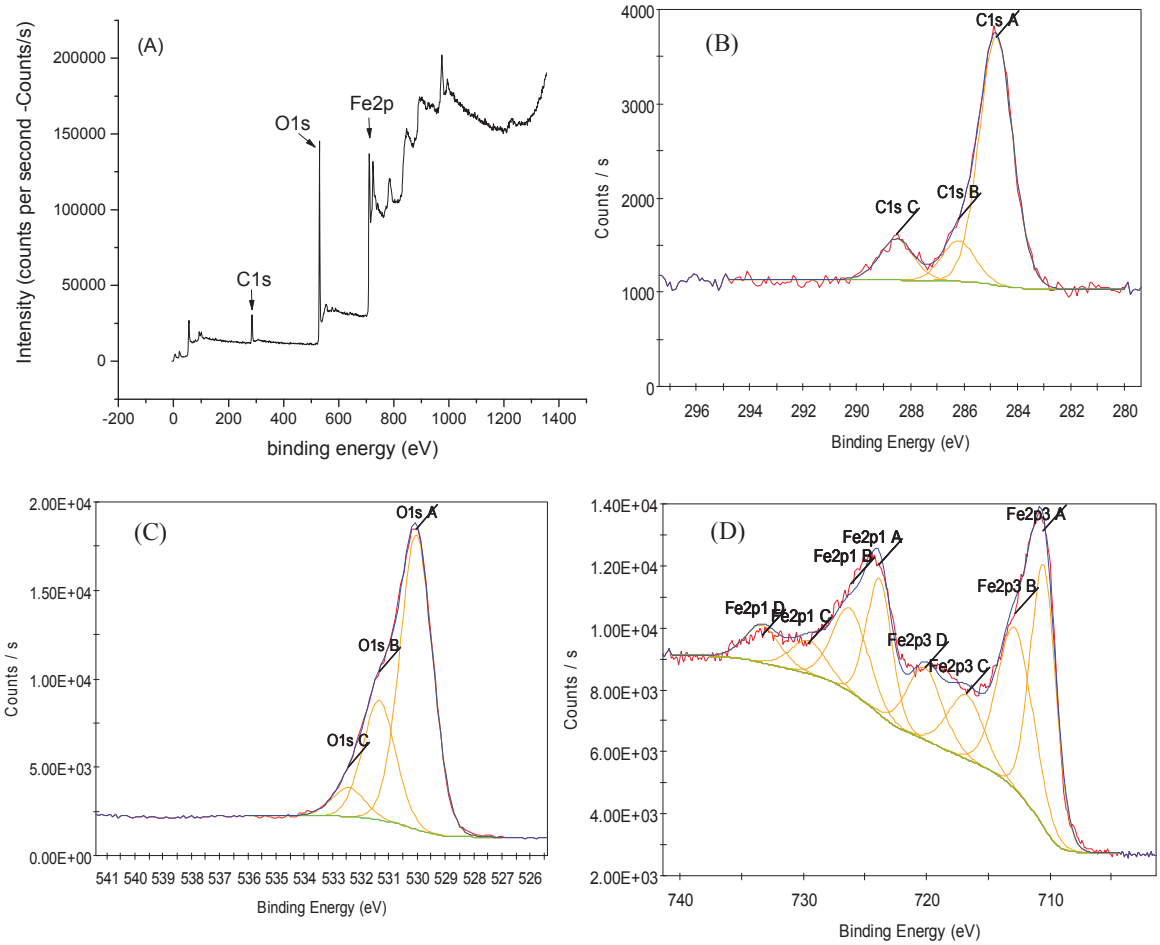

Figure 4.4 The XPS spectra of N_2 plasma modified steel shavings (M_3-plN_2): (A) full survey; (B) narrow scan of C1s region; (C) narrow scan of O1s region; (D) narrow scan of Fe2p region

Table 4.4 Binding energy, chemical state, relative peak area and atomic percentage of peaks in narrow scan of C1s region of M_3-plN_2 scan of O1s region Fe2p3/2 region

Spectrum (Region Peak)	Binding Energy (eV)	Chemical State	Relative Peak Area (CPS.eV)	Atomic %
C1s A	284.79	C-C	4177.22	16.19
C1s B	286.2	C-O-C	687.9	2.67
C1s C	288.51	O-C=O	688.53	2.67
O1s A	530.03	O-metal oxides	24427.48	33.84
O1s B	531.34	C-O	9909.97	13.73
O1s C	532.44	C=O	2407.51	3.34
Fe2p3 A	710.54	Fe_3O_4/Fe^{2+}	21785.43	9.03
Fe2p3 B	712.8	Fe_3O_4/Fe^{3+}	18998.32	7.88
Fe2p3 C	716.79	FeO/Fe^{2+}	7546.61	3.13
Fe2p3 D	720.12	Fe_2O_3/Fe^{3+}	8492.22	3.53

4.4.6. FTIR

The FTIR spectra in Figure 4.5 indicated that an absorption band showing the vibrational properties of Fe-O bond is observed at around 477 cm^{-1} (Gupta et al., 2011). The recorded peaks at 573-588 cm^{-1} showed other iron oxides including Fe_3O_4 and Fe_2O_3 (Dong et al., 2014; Shu and Wang, 2009; Du et al., 2010). The results demonstrated that after nitrogen plasma modification, the content of iron oxide increased with higher peaks at 477 and 573-588 cm^{-1}. These outcomes agreed with the EDS spectra results of M_3 and M_3-plN_2.

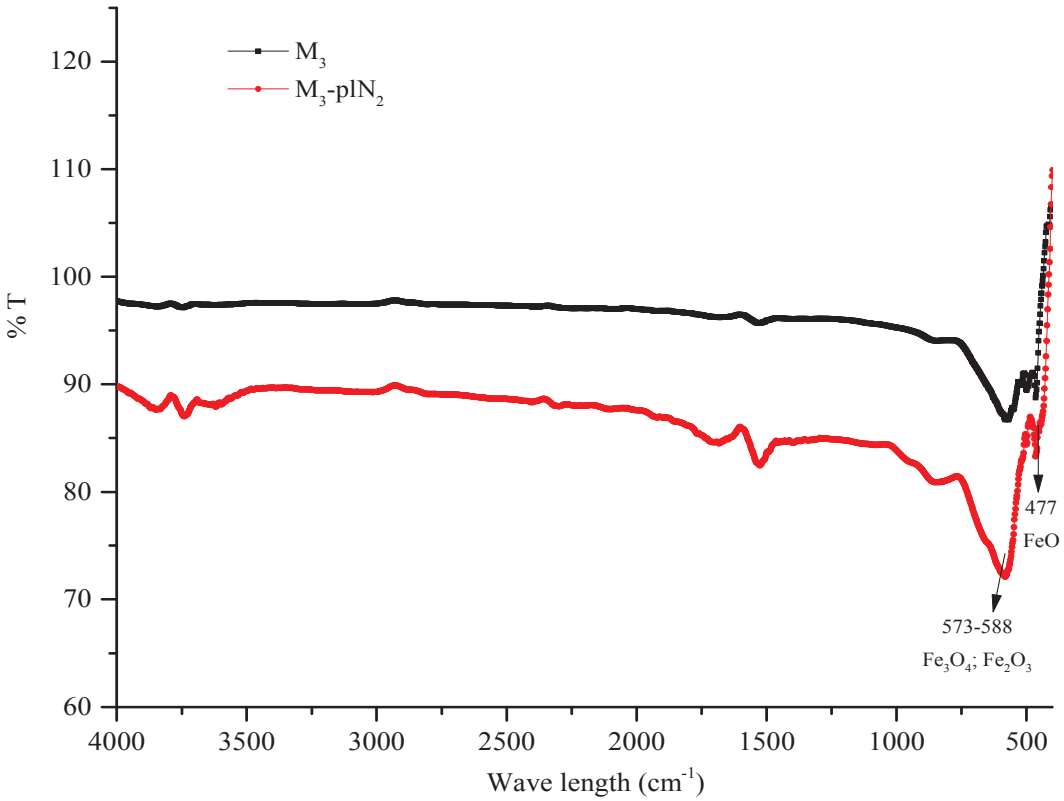

Figure 4.5 FTIR spectra of M_3 and M_3-plN_2

4.4.7. Zeta potential

Surface charge relating zeta potential values of the adsorbents depending on pH of solution were illustrated in Figure 4.6. For M_3 particle, when the initial pH

rose from 3 to 7, the final pH (at equilibrium) of solution tended to increase after the adsorbents were shaken in water for 48 hours; then the final pH reduced from 7 to 8. In the same way, mixing M_3-plN_2 in the solution increased the pH for initial pH from 3.5 to 6, and decreased from 6.5 to 10.5.

The point of zero charge pH values (pH_{pzc}) of M_3 and M_3-plN_2 in water were defined approximately 5.5 and 5, respectively. Below this pH value, surface charge of the adsorbents is positive while pH higher than this value surface charge will become negative. It can be explained for the pH changes of the solution after stirring as the H^+ or OH^- in the solution can interact with the adsorbents' surface. In this case, H^+ can binding on the adsorbents' surface if pH values are less than pH_{pzc} and OH^- can binding on the surface of materials if pH values are higher than pH_{pzc}.

4.4.8. Particle size distribution

In order to assess the applicability of StS to wastewater treatment, the particle size distribution of StS were examined using sieving machine. The Figure 4.7 illustrates the particle size distribution of steel shavings after 3 min grinding with a pug and ring crusher. The results showed that grinded steel shavings had a wide range of particle sizes from 0-1000 μm. The majority of StS was retained on smaller sieves (0-425 μm) containing 88%. These outcomes imply that StS particle size is too small in a fixed-bed column, so a unique design is needed to apply the adsorbent in wastewater treatment. These main particle sizes of steel shavings including 0-75, 75-150 and 150-425 μm (35, 36 and 17%, respectively) were investigated. Besides, the finest particle size (M_3: 0-75 μm) was also achieved after continuous grinding by the pug and ring crusher. Hence, application of M_3 in wastewater treatment has potential.

As described in section 3.2.2E chapter 3, particle size distribution of M_3 was analyzed by the Zeta Potential and sizer. Achieved results of the percentages of particle sizes in M_3 were: 0-0.955 µm (0.162 %), 0.955-1.106 µm (0.422 %), 1.106-1.281 µm (0.572), 1.281-1484 µm (0.494 %), 1.484-1.718 µm (0.162 %), 1.718-1.99 µm (0.186%) and 1.99-75 µm (98%). The experimental outcomes indicated that the majority percentage of M_3 particles existed in the micro size (98% of M_3 particles had size range from 2 to 75 µm).

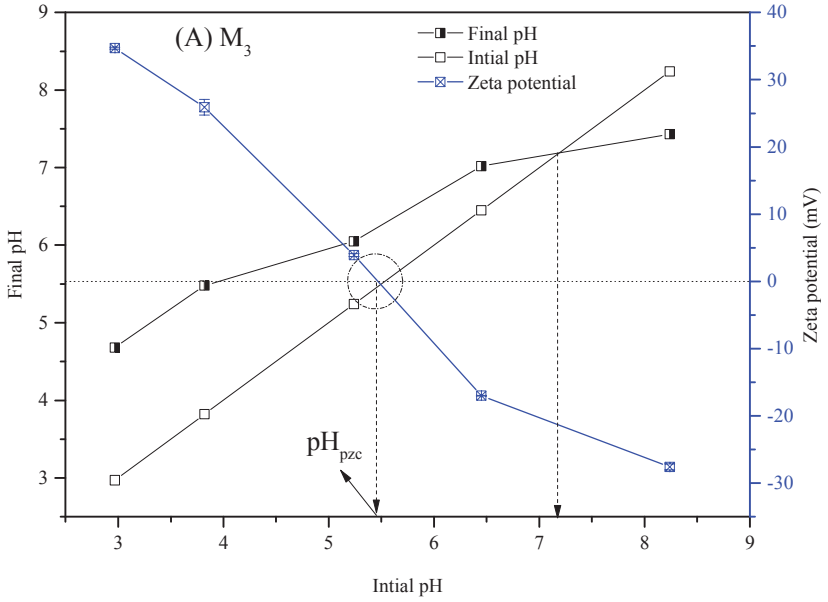

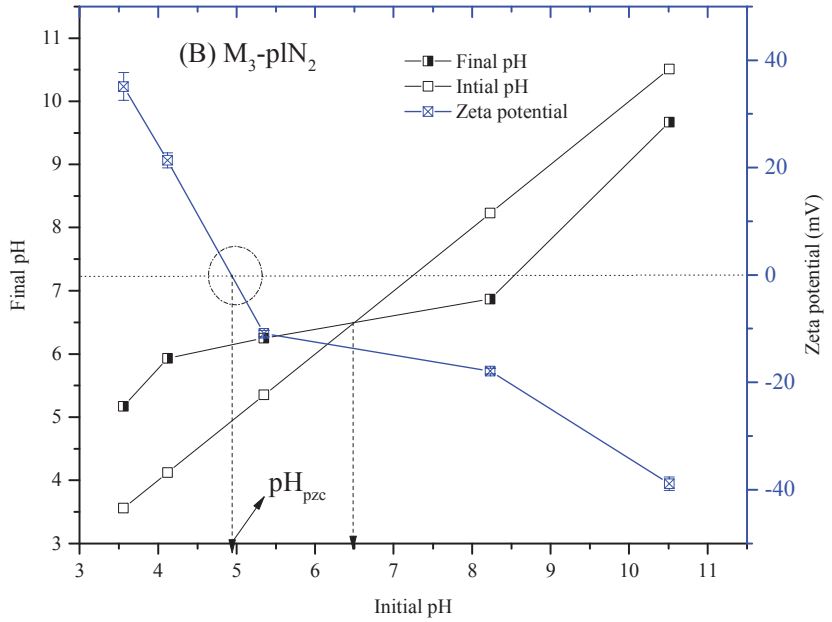

Figure 4.6 Zeta potential as a function of pH solution: (A) M_3: (B) M_3-plN_2

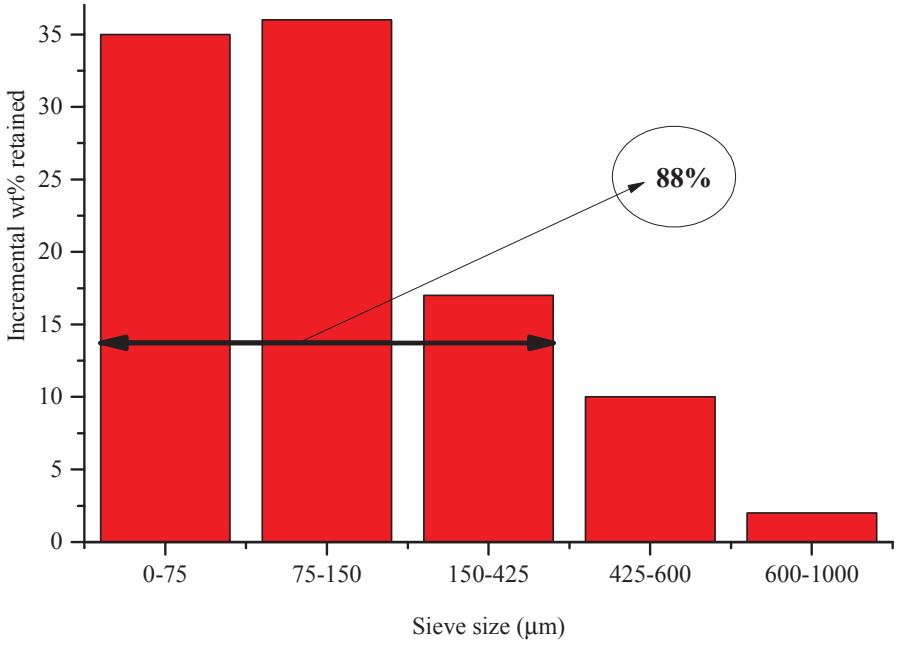

Figure 4.7 Particle size distribution of grinded steel shavings

4.5. Conclusion

The achieved results in this chapter demonstrated that particle sizes and employed gases in plasma cleaning have significant effects on the removal

efficiencies of HMs and ABs from water by raw and modified steel shavings. The finer particle sizes had the higher adsorption capacities of HMs as well as ABs onto both raw and modified StS. Among different studied particle sizes, the finest particle size (0-75 μm) has attained the highest removal efficiencies for HMs and ABs. Plasma modification with H_2, Ar and N_2 improved the adsorption capacities of pollutants onto the adsorbents. However, O_2 plasma modified StS has lower adsorption abilities of the materials. Thus, raw and nitrogen plasma modified of the finest particle size steel shavings (M_3 and M_3-plN_2) will be chosen for next experiments.

Characterizations of the adsorbents were analyzed to better understand the adsorption process and develop the adsorbent for water treatment. SEM images indicated that plasma treatment cleaned the surface without changing the surface morphology of adsorbents. The iron content of StS (47.7%) increased after plasma treatment with gases, namely argon (53.4%) and nitrogen (55.2%), while it decreased with plasma modification containing O_2 gas (46.4%). These outcomes were also confirmed by XRD spectrums. Nitrogen plasma modification has cleaned and improved surface area, pore volume of steel shavings and then increased adsorption capacity of the adsorbent for the antibiotics. The plasma modification with nitrogen gas cleaned and enhanced 1.7-fold the surface area and 1.4-fold the pore volume of steel shavings.

XPS and FTIR results specified that the main components for removing HMs and ABs were Fe_3O_4/Fe^{2+}, Fe_3O_4/Fe^{3+}, FeO/Fe^{2+} and Fe_2O_3/Fe^{3+}. The pH_{pzc} values of M_3 and M_3-plN_2 in aqueous solution were 5.5 and 5, correspondingly. Particle size distribution of grinded steel shavings (after 3 min of grinding) showed that

application of steel shavings as an adsorbent for removing HMs and ABs from water has a high potential.

Faculty of Engineering and Information Technology

CHAPTER 5

RAW AND PLASMA MODIFIED STEEL SHAVINGS FOR REMOVING HEAVY METALS FROM AQUEOUS SOLUTION: A BATCH STUDY

5.1. Introduction

The pollution in aquatic environment caused by heavy metals (HMs) in wastewater such as lead, copper, cadmium, chromium and zinc can endanger public health and the natural environment due to their toxicity, persistence and steady accumulation (Ali et al., 2013; Fu and Wang, 2011). Exposure to HMs can cause damage to internal organs and many diseases, even at very low dosages. The United States Environmental Protection Agency (USEPA) has established maximum contamination levels of some typical HMs for surface or groundwater to be used in the drinking supply (Nguyen et al., 2013). For instance, the safe levels of lead, copper, cadmium, chromium and zinc were, respectively, 0.006, 0.25, 0.01, 0.05 and 0.80 mg/L.

Several common methods have been used for removal of HMs from aqueous solution such as chemical precipitation, ion exchange, adsorption, membrane filtration, coagulation-flocculation, flotation, electrochemical, electrodialysis and photocatalysis (Fu and Wang, 2011; Nguyen et al., 2013). Adsorption has distinct advantages over other methods for removing HMs at low concentration because it is environmentally friendly, economical and highly efficient (Tran et al., 2015; Wang and Chen, 2009). Hence, the adsorption technique is at the forefront among the major processes for removing heavy metal from water (Hua et al., 2012).

Iron, particularly in the zero-valent (Fe^0) state has garnered interest and studies as an adsorbent because of its adsorption ability, abundance and its known role in the environment as a cycler of heavy metal contaminants (Cundy et al., 2008). Moreover, some types of iron-based adsorbents are magnetic and offer advantages in the separation process from aqueous solutions under a magnetic field for recycling or

regeneration (Hua et al., 2012). Several types of magnetic materials have been employed in HMs abatement, for instance, magnetic iron, nanoparticles, magnetite, iron coated sand, blast furnace slag, green rust and iron oxides (Bhatnagar and Mika, 2010; Haider, 2011; Üzüm et al., 2008; Sikder et al., 2014; Gheju and Balcu, 2011). The use of adsorbents obtained from wastes and by-products can diminish the great quantity of solid waste as well as add more value to the materials. Steel shavings are a magnetic waste generated from industrial steel processing in very large amounts. There were only a few studies which focus on HMs removal by using steel shavings (Gheju and Balcu, 2011; Rangsivek and Jekel, 2005). Furthermore, in those studies, steel shavings in millimetre particle size were used only. Additionally, exploring a novel modification method to improve adsorption capacity of the adsorbent is very helpful for its practical application.

The results in chapter 4 showed that raw and nitrogen plasma modified steel shavings at particle size of 0-75 μm (M_3 and M_3-plN_2) have good adsorption capacities for HMs from water. Thus, this chapter aims to study HMs adsorption in batch experiments onto the adsorbents. Firstly, factors influencing the removal process of HMs (pH, dose, temperature) were studied. Secondly, this chapter focuses on single and competitive adsorption isotherm and kinetics investigations. Finally, desorption and regeneration of the adsorbents were tested. From the experimental results, mechanisms for HMs uptake were proposed.

5.2. Affecting factors to removal efficiencies

5.2.1. Solution pH

The pH of the solution plays an important role in HMs adsorption due to its influence on the solubility of metal ions and the interaction of metal-adsorbents

(Hossain et al., 2014). It has been theoretically and experimentally proved that the Pb^{2+}, Cu^{2+}, Cd^{2+}, Cr^{3+} and Zn^{2+} precipitate into $Pb(OH)_2$, $Cu(OH)_2$, $Cd(OH)_2$, $Cr(OH)_3$ and $Zn(OH)_2$ in aqueous solution at the pH levels of 7.18, 7.36, 9.08, 7-9 and 10.1, respectively (Hossain, 2013; Wu et al., 2008; Kusvuran et al., 2012; Sampaio et al., 2009). Experiments on the adsorption process of a pH range of 2-8 were carried out in this study (Figure 5.1A, 5.1C).

In general, the removal efficiencies of all five HMs (Pb^{2+}, Cu^{2+}, Cd^{2+}, Cr^{3+} and Zn^{2+}) rose when the pH increased under some limited conditions such as constant temperature and out of range metal precipitate pH with hydroxide anion. As can be seen in Figure 5.1A and 5.1C, the amount of Pb^{2+} adsorbed on M_3, M_3-plN_2 rose from 15.9% to 57.6% and 17.1% to 62.0%, correspondingly by increasing the pH from 2 to 5. These results agreed with previous studies on the sorption of copper and chromium on chitosan–caboxymethyl-β-cyclodextrin entrapped nanozero-valent iron composite and the removal of aqueous Co^{2+} ions by zero-valent iron nanoparticles (Üzüm et al., 2008; Sikder et al., 2014). When pH rose from 5 to 6, there was a slight decrease in the efficiency in removing Pb^{2+}, while with pH from 7 to 8 it increased considerably. This outcome may have been caused by a formation of $Pb(OH)_2$. To avoid the precipitation of lead hydroxide during the sorption process, the pH values of the solution were kept below 7 in further experiments. Moreover, pH 5 value is often obtained at normal $Pb(NO_3)_2$ solution. Thus, pH 5 was chosen as the optimum level for the adsorption of Pb^{2+} by M_3 and M_3-plN_2.

The poor removal efficiency at low pH is apparently due to the presence of a higher concentration of H^+ in the solution, which competes with Pb^{2+} ion for the adsorption sites on the adsorbents. When pH increases, the H^+ concentration

decreases leading to increased Pb^{2+} uptake. These results can also be explained by ion-exchange occurring between Fe on the adsorbent's surface and the metal ions. During the ion-exchange process the adsorbed cation (M^{n+}) exchanges for a proton (H^+) according to the following simplified equation (Okochi, 2013):

$$(Surface)OH + M^{n+} \rightarrow (Surface)OM^{n-1} + H^+$$

According to Okochi (2013), as pH increases, the uptake of metals on Fe sorption sites becomes more important, with certain metals displaying a greater affinity for those Fe sorption sites. At low pH, adsorption was targeted at the non-specific ion exchange sites. A similar outcome was achieved in the adsorption of Cu^{2+}, Cd^{2+}, Cr^{3+} and Zn^{2+}. Adsorption capacities of metal ions by M_3 and M_3-plN_2 are poor at low pH value but increased when the level of pH was raised. The removal efficiency of Cu(II) increased dramatically from pH 2-5, then slightly decreased from 5-6 before increasing again because of precipitation of $Cu(OH)_2$. Hence, pH 5 was chosen as the optimum pH value for adsorption of Cu^{2+} onto raw and modified StS. Meanwhile the removal efficiencies of Cd^{2+}, Cr^{3+} and Zn^{2+} were achieved at approximately pH 6 but did not significantly increase from pH 6-8. However, precipitate could not be excluded at a higher pH (Wu et al., 2008). To make sure the maximum adsorption capacities were attained and to avoid precipitation of metal ions, for further experiments, pH 5 was chosen as the optimum pH value. As the pH of the prepared medium with distilled water was very close to that pH value, few or no practical pH adjustments were required for the experiments. Therefore the experimental processes were both economic and environmentally friendly.

Quite similar outcomes were recorded such as Cr^{3+} removal on lignin, Cu^{2+} and Ni^{2+} removal on Fe_3O_4 nanoparticles and Zn^{2+} removal on nanoscale zero-valent

iron (Wu et al., 2008; Hu, 2005; Kržišnik et al. 2014). Conversely, the effect of pH on Cr^{3+} removal by M_3 and M_3-plN_2 differed to that of Cr^{6+} being removed by iron nanoparticles where the optimum pH was 2.5 (Hu, 2005).

5.2.2. Adsorbent dosage

The effect of adsorbent dose (g adsorbent/L solution) on the removal efficiency of HMs on M_3 and M_3-plN_2 was tested, and the results are shown in Figure 5.1B and 5.1D. Similar trends of adsorption are found for all five metal ions on both raw and plasma modified materials.

The results indicated that the removal percentage of Pb^{2+}, Cu^{2+}, Cd^{2+}, Cr^{3+} and Zn^{2+} dramatically increased when the dose was increased from 0.5 to 5 g/L; after that any observed changes were negligible. Removal efficiencies of Pb^{2+}, Cu^{2+}, Cd^{2+}, Cr^{3+}, Zn^{2+} were 93.5, 88.6, 77.9, 69.8, 70.5% on M_3 and 99.6, 90.6, 85.7, 71.6, 72.7 % on M_3-plN_2, respectively. Consequently, a dose of 5g of adsorbent with 1 litre of the adsorption solution was chosen for the following experiments.

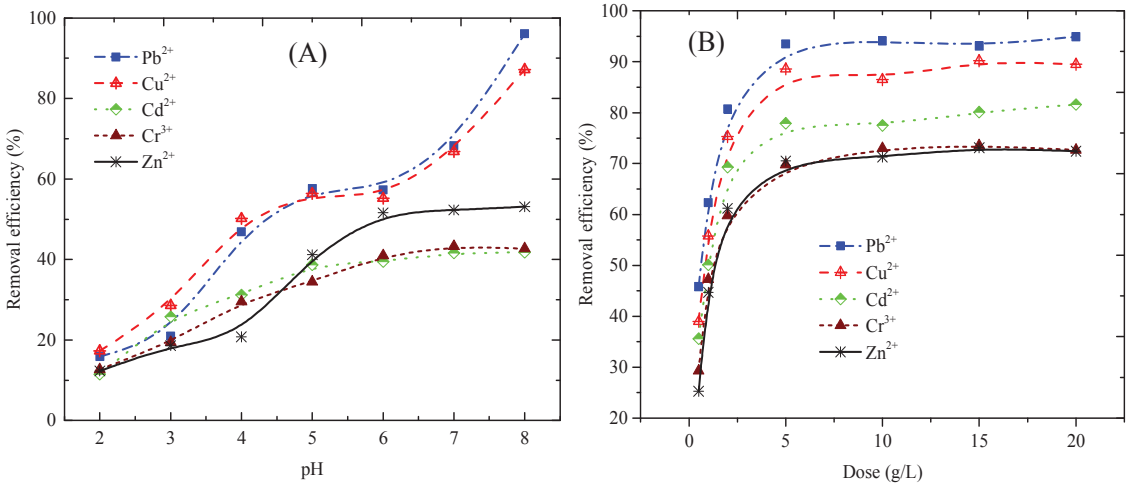

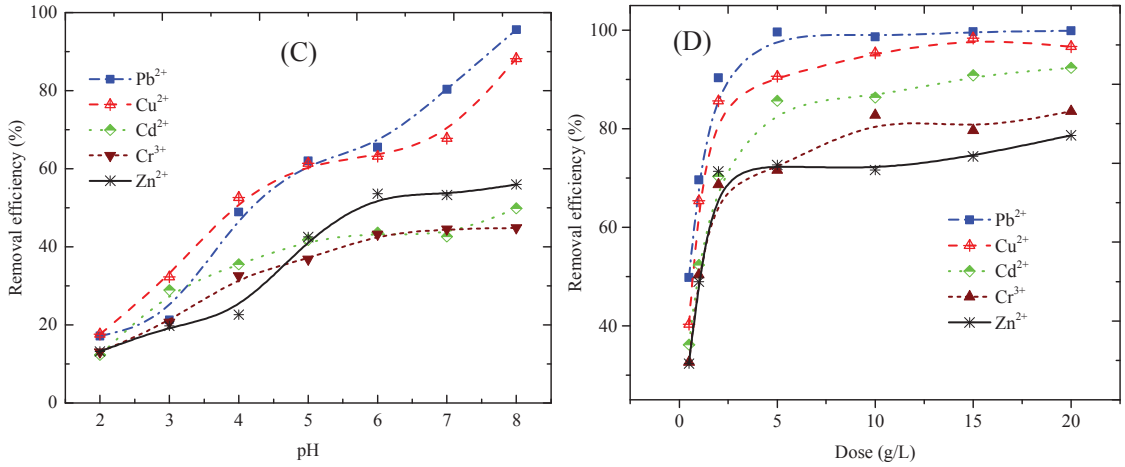

Figure 5.1 Effect of factors to removal efficiency of metal ions: (A) pH-M_3; (B) dose-M_3; (C) pH-M_3-plN_2; (D) dose-M_3-plN_2

5.2.3. Temperature/thermodynamic

The thermodynamic parameters for the adsorption of HMs onto M_3 and M_3-N_3 were calculated from experimental data, using Van't Hoff and Arrhenius equations (Boparai et al., 2011):

$$\Delta G^o = -RT\ln K_d \qquad (5.2.3.1)$$

$$\ln K_d = \frac{-\Delta H}{RT} + \frac{\Delta S}{R} \qquad (5.2.3.2)$$

where K_d is the distribution coefficient of the adsorption process; $\Delta G°$, $\Delta H°$, and $\Delta S°$ are the changes in Gibbs free energy (J/mol), enthalpy (J/mol) and entropy (J/mol/K), respectively; T is the absolute temperature (K); and R is the gas constant (8.314 J/mol/K).

K_d at a specific temperature was defined by plotting ln(qe/Ce) versus qe, using linear regression type. The value of K_d was represented by the intercept of the plot (Boparai et al., 2011; Benyoucef and Amrani, 2011). Then, $\Delta G°$ was obtained

by the Equation 5.2.3.1. Finally, lnK_d was plotted against 1/T to calculate ΔH° and ΔS° from the slope and intercept of the plot respectively, using Equation 5.2.3.2.

Generally, adsorption capacity of HMs on M_3 and M_3-plN_2 increased with an increase of temperature from 20 to 30°C. Table 5.1 shows thermodynamic parameters for Pb^{2+}, Cu^{2+}, Cd^{2+}, Cr^{3+}, Zn^{2+} at 20, 25 and 30°C (293, 298, 303°K, respectively). The negative values of ΔG° indicated that the adsorption of metal ions on M_3 and M_3-plN_2 are spontaneous in nature. ΔG° values reduced with the rise of temperature from 20 to 30°C, demonstrating an improvement in HMs uptake at higher temperature. This can be attributed to the degree of spontaneity of the reaction increases with increasing temperature (Boparai et al., 2011); activation of StS's surface by the temperature (Benyoucef and Amrani, 2011).

A positive ΔH° specified endothermic nature of the adsorption process (Nguyen et al., 2015). The positive values of ΔS° revealed high affinity of adsorbents for metal ions and an increased randomness between solid-solution interfaces during the sorption process (Hossain, 2013; Sengil and Özacar, 2008).

Table 5.1 Thermodynamic parameters for HMs adsorption on M_3 and M_3-plN_2

Metals	Temperature (°C)	Qmax exp. (mg/g)	Kd	ΔG° (J/mol)	ΔH° (J/mol)	ΔS° (J/mol/K)	r^2
M_3							
Pb^{2+}	20	20.21	5.101	-3969	3898	27	0.943
	25	24.67	5.298	-4131			
	30	25.23	5.377	-4237			
Cu^{2+}	20	14.94	4.489	-3658	19293	78	0.937
	25	17.09	5.434	-4194			
	30	18.46	5.826	-4439			
Cd^{2+}	20	10.16	2.982	-2662	41253	149	0.774
	25	13.47	3.055	-2767			

Metals	Temperature (^oC)	Qmax exp. (mg/g)	Kd	ΔG^o (J/mol)	ΔH^o (J/mol)	ΔS^o (J/mol/K)	r^2
	30	14.40	5.230	-4168			
	20	9.75	2.266	-1993			
Cr^{3+}	25	12.83	3.833	-3329	43633	156	0.837
	30	14.27	4.083	-3544			
	20	12.5	3.351	-2946			
Zn^{2+}	25	15.68	3.916	-3382	29932	112	0.980
	30	17.47	5.030	-4070			
M_3-plN_2							
	20	21.68	6.138	-4420			
Pb^{2+}	25	27.87	7.225	-4899	36410	139	0.959
	30	30.16	10.062	-5816			
	20	16.95	3.192	-2827			
Cu^{2+}	25	21.09	6.154	-4502	58058	209	0.875
	30	22.75	6.989	-4898			
	20	13.94	2.835	-2538			
Cd^{2+}	25	16.87	5.503	-4225	62249	222	0.906
	30	18.43	6.571	-4743			
	20	10.42	2.967	-2649			
Cr^{3+}	25	14.72	4.249	-3584	56733	203	0.998
	30	16.16	6.400	-4676			
	20	15.72	3.524	-3069			
Zn^{2+}	25	18.99	5.459	-4205	38520	142	0.872
	30	20.86	5.928	-4483			

M_3: raw StS<75 µm; M_3-plN_2: raw StS<75 µm was plasma modified with N_2

5.3. Modeling of adsorption isotherm and kinetics

5.3.1. Adsorption isotherm

Langmuir and Freundlich equations and their linear forms are illustrated in Table 3.3, 5.3 and Figure 5.2. Adsorption was better described by the Langmuir isotherm than the Freundlich model due to the correlation coefficient (r^2) of the

Langmuir is higher than that of the Freundlich isotherm. Maximum Langmuir adsorption capacities (Q_{max}) in mg/g of lead, copper, cadmium, chromium and zinc on M_3, M_3-plN_2 were 24.34, 16.79, 13.31, 12.83, 14.97 mg/g, respectively and 27.04, 20.64, 16.87, 14.89, 18.47 mg/g, respectively. The adsorption capacity of the adsorbent increased from 11.1 to 26.7% after nitrogen plasma modification. The order of the HMs sorption affinity on M_3 and M_3-plN_2 in mg/g can be shown as follows: Pb^{2+}>Cu^{2+}>Zn^{2+}>Cd^{2+}>Cr^{3+}.

The maximum adsorption capacities of HMs on raw and N_2 plasma treated StS were less than those of Fe_3O_4 nanoparticles. It has been documented in a previous study that Q_{max} values of Cr^{6+}, Cu^{2+} and Ni^{2+} onto the magnetic nanoparticles were 19.4, 27.0 and 25.4 mg/g (Hu et al., 2005). However, in this study, the iron particles were used in micro size instead of nanoparticles. The Q_{max} values (in mmol/g) of single metal ions on the two adsorbents followed the order of Cu^{2+} > Cr^{3+} > Zn^{2+} > Cd^{2+} > Pb^{2+}. The Q_{max} value of copper (in mmol/g) is the highest adsorption capacity among the five metal ions.

Following the Freundlich isotherm, maximum adsorption constant (K_F) values with smaller r^2 values for Pb^{2+}, Cu^{2+}, Cd^{2+}, Cr^{3+}, Zn^{2+} were: 9.40, 7.31, 4.86, 4.81, 4.90 $(mg/g)(L/mg)^{1/n}$, respectively on M_3 and 13.50, 9.26, 6.79, 5.53, 7.39 $(mg/g)(L/mg)^{1/n}$, respectively on M_3-plN_2.

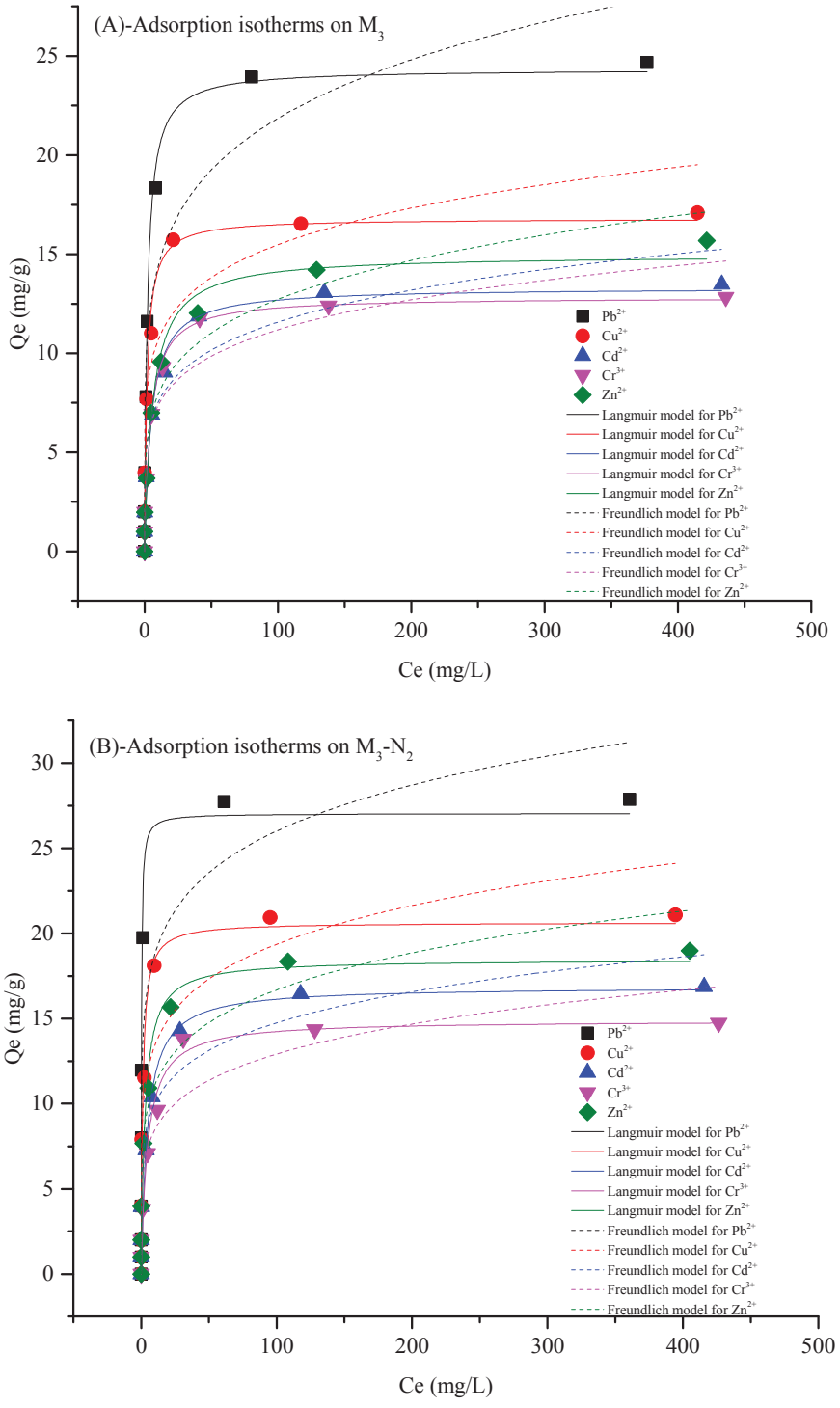

Figure 5.2 Adsorption isotherm of HMs on (A) M_3 and (B) M_3-plN_2 (initial concentration 0-500 mg/L single metal ion; pH 5, dose 5g/L; at 130 rpm; at 25^0C; for 24 hours)

5.3.2. Adsorption kinetics

Adsorption kinetics of HMs on M_3 and M_3-plN_2 are depicted in Figure 5.3 and Table 5.2. The kinetics sorption of Pb^{2+}, Cu^{2+}, Cd^{2+}, Cr^{3+} and Zn^{2+} on M_3 and M_3-plN_2 were fitted to pseudo-first-order (PFO), pseudo-second-order (PSO) and intra-particle diffusion model (IDM) as given in Table 3.3 and 5.3. The results of the correlation coefficient (r^2) and Q_e cal values indicated that the sorption kinetics were well fitted with PFO and PSO kinetic models with high r^2 values. In contrast, the kinetic data was not fitted with the IDM model due to low r^2 values. The order of PFO rate constant k_{1p} and PSO rate constant k_{2p} for the removal of HMs by M_3-plN_2 declined as $Cr^{3+}>Pb^{2+}>Cu^{2+}>Zn^{2+}>Cd^{2+}$ and $Cr^{3+}>Zn^{2+}>Cd^{2+}>Cu^{2+}>Pb^{2+}$, respectively.

The adsorption speed of HMs on M_3 and M_3-plN_2 increased dramatically during the first 4 hours and reached equilibrium at 8 hours. The adsorbents gave an average equilibrium time compared to the other adsorbents. As reported earlier, the equilibrium time of Cr^{6+} adsorption on Fe_3O_4 nanoparticles, activated carbons were 30 minutes, 10-50 hours (Hu et al., 2005; Lalvani et al., 2000). In another study on Cr^{3+} removal by lignin, the adsorption equilibrium was reached at around 24 hours (Wu et al., 2008).

Maximum PFO sorption constants (Qe cal) of Pb^{2+}, Cu^{2+}, Cd^{2+}, Cr^{3+}, Zn^{2+} were 18.45, 14.36, 8.33, 8.36, 11.00 mg/g on M_3 and 19.42, 16.39, 12.70, 10.19, 12.06 mg/g on M_3-plN_2, correspondingly. Following PSO kinetic model, the adsorption capacities (Qe cal) were 20.38, 15.80, 9.18, 9.20, 12.08 mg/g on M_3 and 21.41, 18.05, 14.00, 11.24, 13.31 mg/g on M_3-plN_2, correspondingly.

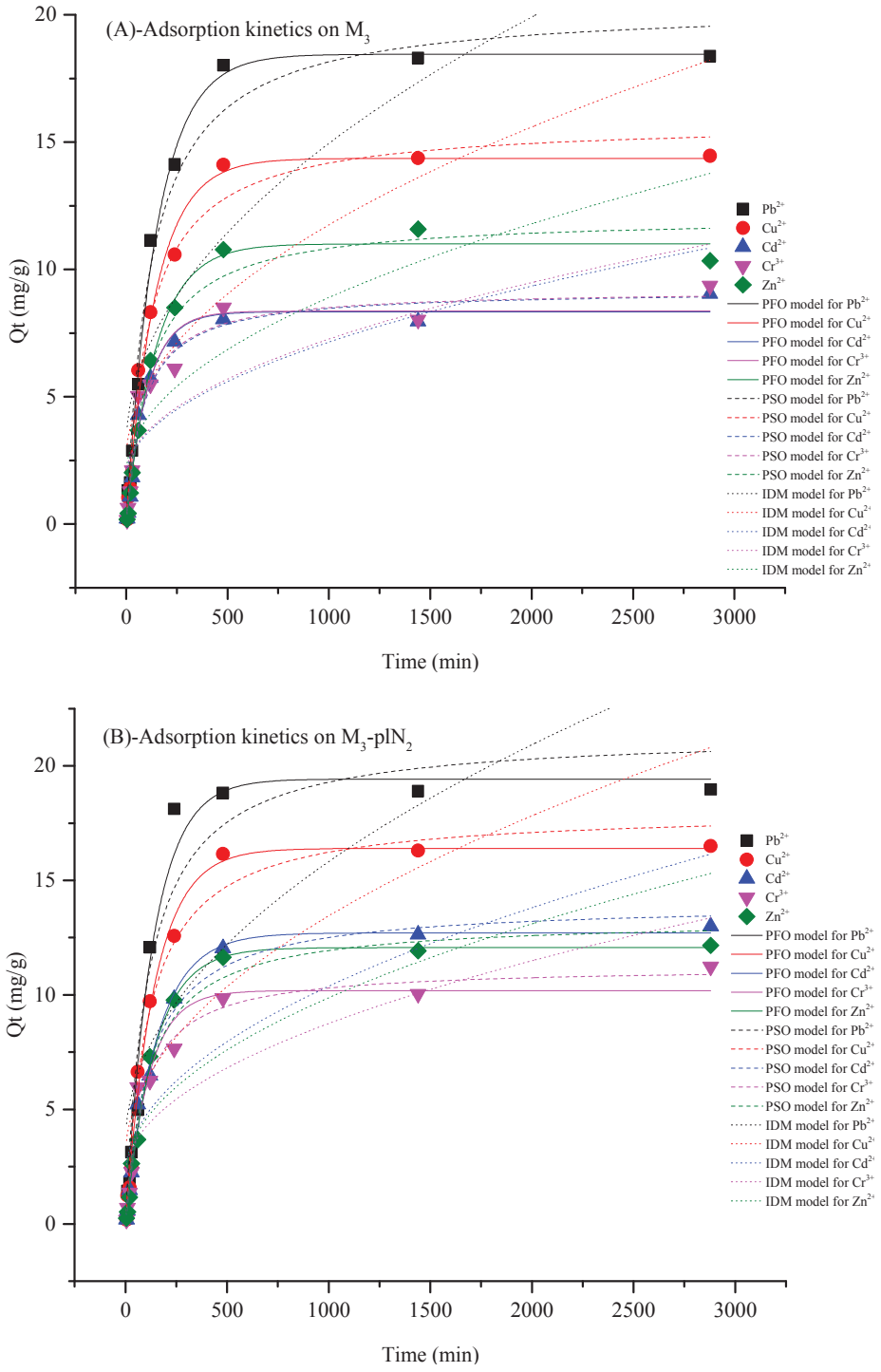

Figure 5.3 Adsorption kinetic models of HMs on (A) M_3 and (B) M_3-plN_2 (initial concentration: 100 mg/L single metal ion; no pH adjustment; dose 5g/L; at 130 rpm shaking speed; at room temperature)

Table 5.2 Isotherm and kinetic parameters using the non-linear regression method for HMs adsorption onto raw and N_2 treated plasma M_3 particles

Parameters	**Pb^{2+}**		**Cu^{2+}**		**Cd^{2+}**		**Cr^{3+}**		**Zn^{2+}**	
	M_3	M_3-plN_2	M_3	M_3-plN_2	M_3	M_3-plN_2	M_3	M_3-plN_2	M_3	M_3-plN_2
Langmuir isotherm model										
Qmax exp. (mg/g)	24.67	27.87	17.09	21.09	13.47	16.87	12.83	14.72	15.68	18.99
Qmax cal. (mg/g)	24.34	27.04	16.79	20.64	13.31	16.87	12.83	14.89	14.97	18.47
Qmax cal. (mmol/g)	0.1175	0.1305	0.2642	0.3248	0.1184	0.1501	0.2467	0.2864	0.2290	0.2825
r^2	0.979	0.982	0.960	0.957	0.969	0.954	0.978	0.969	0.973	0.959
K_L (L/mg)	0.4707	3.6746	0.5370	0.8519	0.2006	0.2185	0.2248	0.2161	0.1638	0.3564
Freundlich isotherm model										
K_F $(mg/g)(L/mg)^{1/n}$	9.40	13.50	7.31	9.26	4.86	6.79	4.81	5.53	4.90	7.39
N	5.4595	7.0207	6.1369	6.2402	5.3091	5.9349	5.4529	5.4324	4.8320	5.6540
r^2	0.914	0.893	0.906	0.899	0.933	0.949	0.909	0.905	0.953	0.939
Kinetic Pseudo−first-order (PFO)										
Qe exp (mg/g)	18.37	18.97	14.46	16.50	9.04	13.00	9.36	11.24	11.58	12.16
Qe cal (mg/g)	18.45	19.42	14.36	16.39	8.33	12.70	8.36	10.19	11.00	12.06
K_1p (min^{-1})	0.0066	0.0074	0.0068	0.0071	0.0096	0.0066	0.0096	0.0087	0.0067	0.007
r^2	0.995	0.981	0.988	0.992	0.984	0.992	0.945	0.954	0.993	0.996
Kinetic Pseudo−second-order (PSO)										
Qe cal (mg/g)	20.38	21.41	15.80	18.05	9.18	14.00	9.20	11.24	12.08	13.31
K_2p (min^{-1})	3.9945×10^{-4}	4.2259×10^{-4}	5.4973×10^{-4}	4.9344×10^{-4}	0.0013	5.9466×10^{-4}	0.0013	9.7879×10^{-4}	7.1265×10^{-4}	6.5667×10^{-4}
r^2	0.977	0.946	0.980	0.980	0.977	0.987	0.962	0.970	0.975	0.980
Intra-particle diffusion model (IDM)										
Kp ($mg.g^{-1}.min^{-1}$)	0.3786	0.3897	0.2933	0.3337	0.1676	0.2616	0.1695	0.2092	0.2209	0.2462
C	2.9776	3.4974	2.4764	2.8954	1.8479	2.1060	1.9025	2.1363	1.9117	2.0912
r^2	0.680	0.604	0.687	0.676	0.649	0.713	0.680	0.700	0.650	0.674

M_3: raw StS<75 µm; M_3-plN_2: raw StS<75 µm was plasma modified with N_2

From the results of adsorption isotherm and kinetics of HMs on the adsorbents, M_3-plN_2 was the most effective adsorbent for removing Pb^{2+}, Cu^{2+}, Cd^{2+},

Cr^{3+} and Zn^{2+} from aqueous solution. Thus, M_3-plN_2 was chosen for the next experiments for regeneration of the material.

5.4. Competitive adsorption of multi-metals solutions on the adsorbents

The isotherms and kinetics studies of competitive adsorption of multi-metal solutions were carried out as in 3.2.4C, chapter 3.

5.4.1. Competitive adsorption isotherms

Isotherms plots and parameters of HMs competitive adsorption on M_3 and M_3-plN_2 are shown in Figure 5.4 and Table 5.3. Adsorption data were better fitted with Langmuir than Freundlich through higher r^2 constants. These results showed that sorption of HMs on StS's surface were of monolayer coverage in nature.

Maximum Langmuir competitive adsorption capacities (Q_{max}) in mg/g of lead, copper, cadmium, chromium and zinc were 13.39, 9.78, 7.92, 7.31, 8.79 on M_3, respectively and 16.62, 14.00, 9.73, 8.69, 12.28 on M_3-plN_2, respectively. Each competitive solute adsorption capacities of multi-metals were approximately 2-fold less than the single adsorption capacities. The Equations (3.2.4.3 to 3.2.4.6) were used to calculate the total sorption capacities of the competitive solutes by adding individual contributions to the overall sorption for both Langmuir and Freundlich models.

The total of competitive adsorption capacities onto M_3 and M_3-plN_2 was higher than those of single solute sorption. These results can be explained by sorption of HMs on adsorbents through two uptake mechanisms, adsorption and co-precipitation. Furthermore, different metals have different molecular sizes. The results indicated that the adsorbents worked well with single and multi-metal ions.

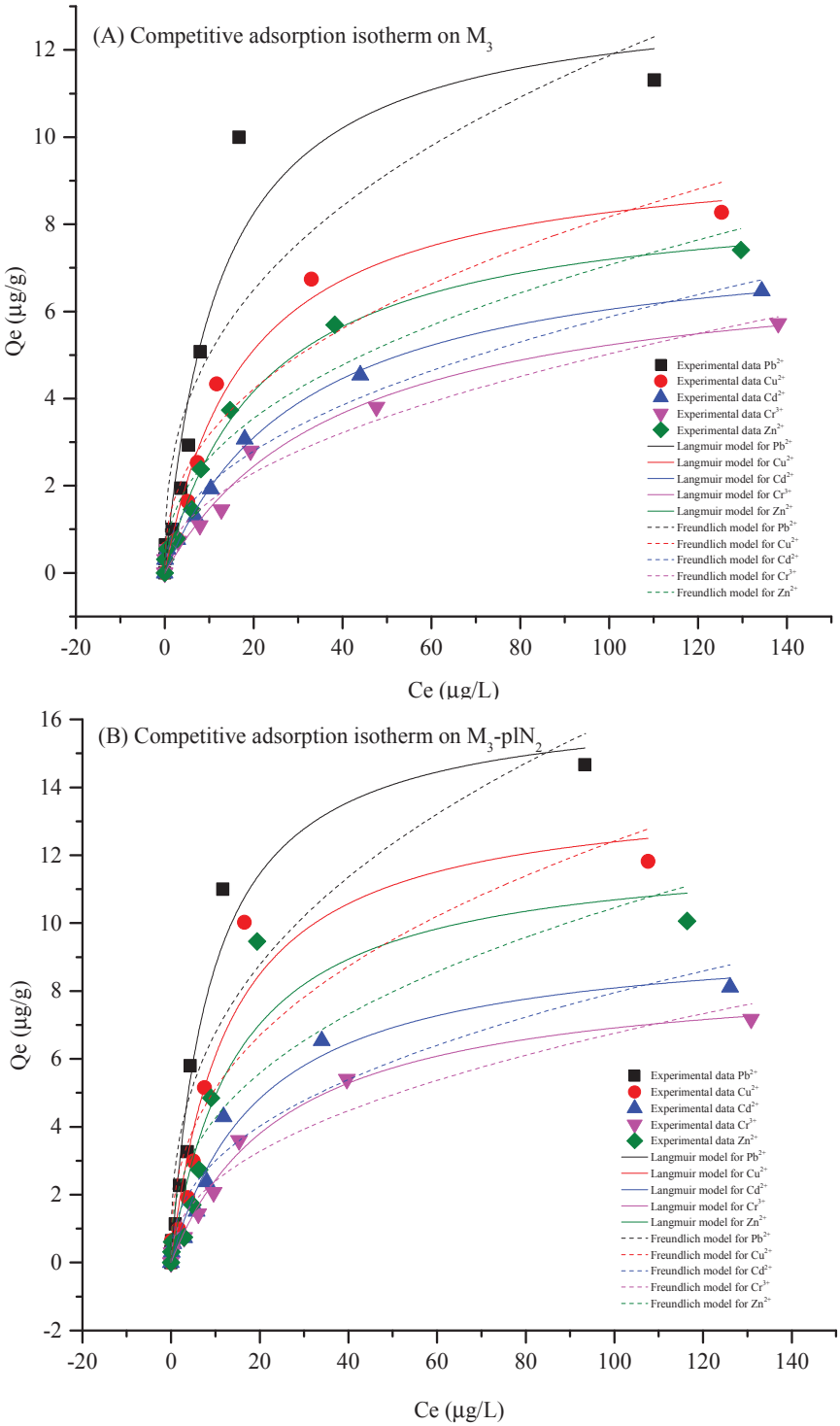

Figure 5.4 Competitive adsorption isotherms of HMs on (A) M_3 and (B) M_3-plN$_2$ (total initial concentration 0-500 mg/L; 0-166.67 mg/L single metal ion; pH 5; dose 5g/L; at 130 rpm; at 25^0C; for 24 hours)

5.4.2. Competitive adsorption kinetics

Competitive adsorption kinetics of HMs on M_3 and M_3-plN_2 are described in Figure 5.5 and Table 5.3. The PFO and PSO kinetic well described the experimental adsorption data of Pb^{2+}, Cu^{2+}, Cd^{2+}, Cr^{3+}, Zn^{2+} on M_3 and M_3-plN_2. The adsorption data were best fitted with PFO kinetic isotherm model through high correlation coefficient (r^2) constants.

Conversely, the IDM kinetic model did not successfully describe the experimental adsorption data of HMs on raw and modified StS. Equilibrium of adsorption process was also achieved at 8 hours of contact time. The order of PFO rate constant k_{1p} for HMs removal by raw and modified StS decreased as $Cr^{3+}>Pb^{2+}>Cu^{2+}>Zn^{2+}>Cd^{2+}$, correspondingly.

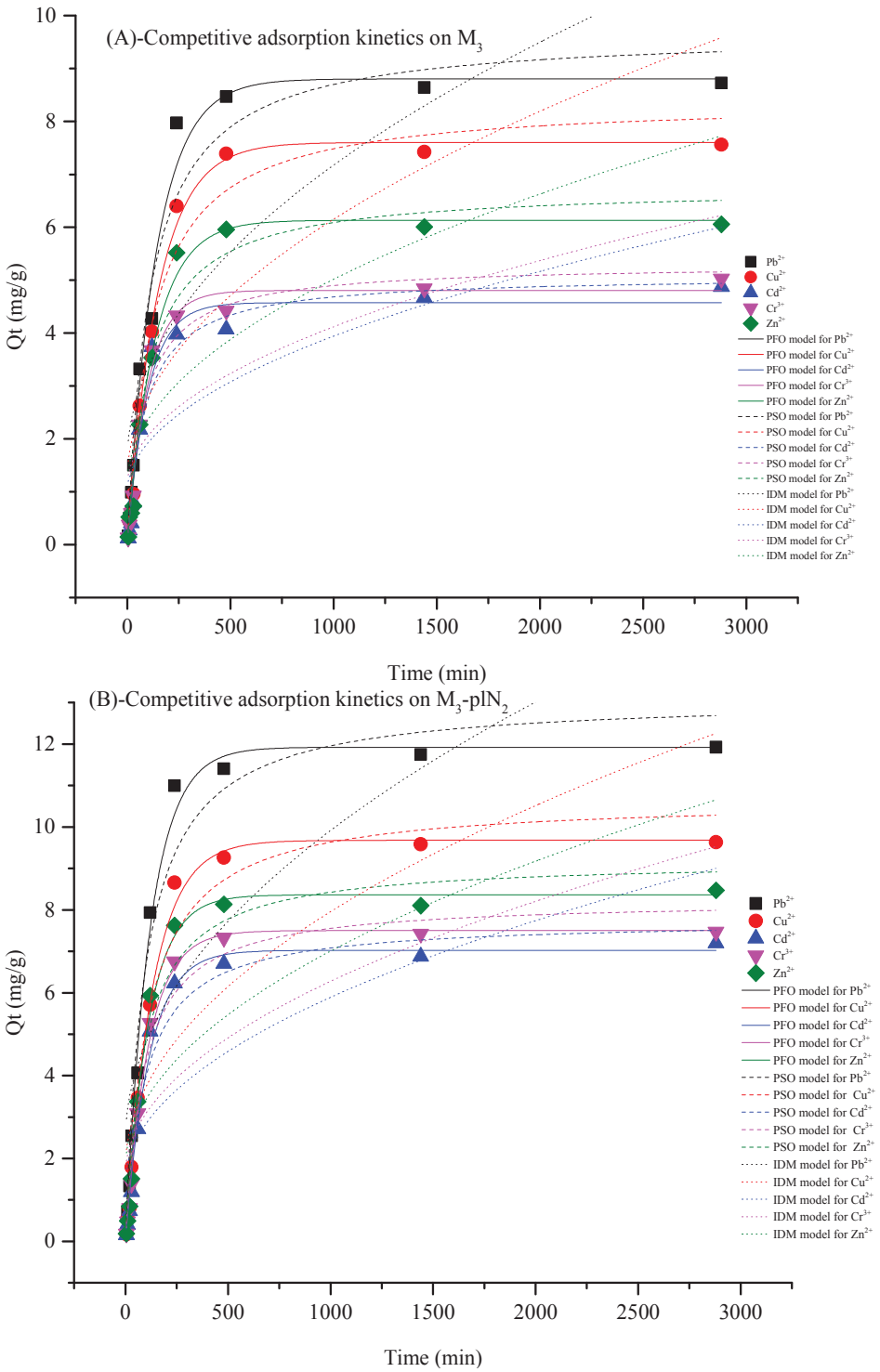

Figure 5.5 Competitive adsorption kinetics of HMs on (A) M_3 and (B) M_3-plN_2 (total initial concentration: 100 mg/L, 20mg/L single metal ion; no pH adjustment; dose 5g/L; at 130 rpm shaking speed; at room temperature)

Table 5.3 Isotherm and kinetic parameters using the non-linear regression method for competitive HMs adsorption onto raw and N_2 treated plasma M_3 particles

Parameters	**Pb^{2+}**		**Cu^{2+}**		**Cd^{2+}**		**Cr^{3+}**		**Zn^{2+}**	
	M_3	M_3-plN_2	M_3	M_3-plN_2	M_3	M_3-plN_2	M_3	M_3-plN_2	M_3	M_3-plN_2
Langmuir isotherm model										
Qmax exp. (mg/g)	11.31	14.67	8.27	11.82	6.47	8.11	5.72	7.17	7.41	10.06
Q max cal. (mg/g)	13.39	16.62	9.78	14.00	7.92	9.73	7.31	8.69	8.79	12.28
Q max cal. (mmol/g)	0.0646	0.0802	0.1539	0.2203	0.0705	0.0866	0.1409	0.1671	0.1344	0.1878
r^2	0.929	0.967	0.980	0.938	0.991	0.971	0.976	0.990	0.990	0.894
K_L (L/mg)	0.0802	0.1106	0.0548	0.0770	0.0323	0.0493	0.0252	0.0388	0.045	0.0668
Freundlich isotherm model										
K_F $(mg/g)(L/mg)^{1/n}$	2.11	2.86	1.23	2.11	0.70	1.13	0.53	0.85	0.98	1.73
n	2.6692	2.6782	2.4319	2.6001	2.1703	2.3598	2.0542	2.2230	2.3355	2.5638
r^2	0.822	0.877	0.908	0.837	0.975	0.902	0.970	0.947	0.943	0.776
Kinetic Pseudo−first-order (PFO)										
Qe exp (mg/g)	8.73	11.93	7.56	9.63	4.88	7.20	5.02	7.49	6.06	8.47
Qe cal (mg/g)	8.80	11.92	7.60	9.68	4.58	7.02	4.81	7.50	6.13	8.36
K_1p (min^{-1})	0.007	0.0083	0.0066	0.0075	0.01	0.0087	0.01	0.0089	0.0074	0.0089
r^2	0.987	0.992	0.994	0.994	0.967	0.989	0.985	0.993	0.990	0.991
Kinetic Pseudo−second-order (PSO)										
Qe cal (mg/g)	9.69	13.11	8.40	10.67	5.09	7.75	5.31	8.24	6.75	9.20
K_2p (min^{-1})	9.0965 $x10^{-4}$	7.8801 $x10^{-4}$	9.7285 $x10^{-4}$	8.7484 $x10^{-4}$	0.0023	0.0014	0.0023	0.0013	0.0014	0.0012
r^2	0.963	0.966	0.970	0.970	0.954	0.966	0.969	0.967	0.962	0.963
Intra-particle diffusion model (IDM)										
Kp ($mg.g^{-1}.min^{-1}$)	0.1774	0.2367	0.1559	0.1954	0.0935	0.1412	0.0955	0.1475	0.1230	0.1657
C	1.5644	2.4293	1.2228	1.7789	0.9876	1.4260	1.1004	1.6125	1.1287	1.7665
r^2	0.648	0.614	0.664	0.638	0.622	0.619	0.617	0.598	0.628	0.599

M_3: raw StS<75 μm; M_3-plN_2: raw StS<75 μm was plasma modified with N_2

5.5. Uptake mechanisms of heavy metals by steel shavings

The proposed mechanisms of HMs removal by iron materials was described in Figure 5.6. O'Carroll et al. (2013) have proposed 4 mechanisms for heavy metals removal by iron including: reduction for HMs such as Cr, As, Cu, U, Pb, Ni, Se, Co, Pd, Pt, Hg, Ag; adsorption for HMs such as Cr, As, U, Pb, Ni, Se, Co, Cd, Zn, Ba; oxidation/Re-oxidation such as As, U, Se, Pb; co-precipitation such as Cr, As, Ni, Se; and precipitation such as Cu, Pb, Cd, Co, Zn.

From the theoretical and experimental results, the mechanisms of HMs removal from water using steel shavings which could be proposed are adsorption and co-precipitation.

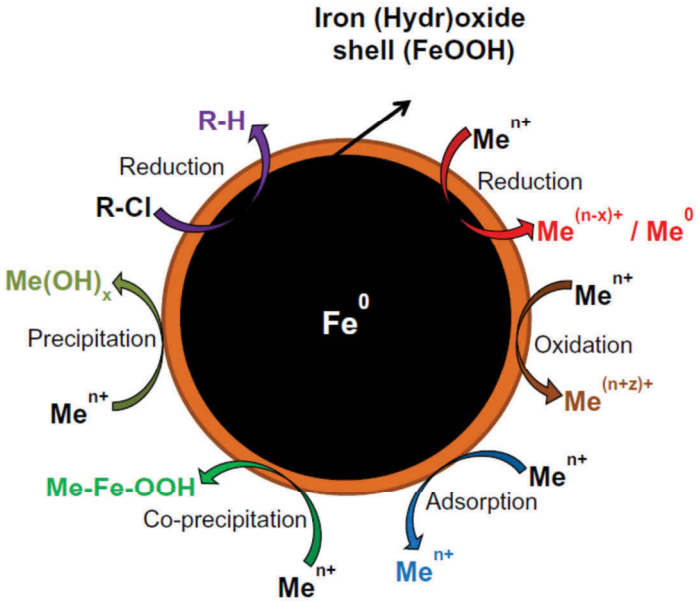

Figure 5.6 Removal mechanisms of metals and chlorinated compounds with Fe^0 (O'Carroll et al. 2013)

5.6. Desorption and regeneration of the HMs loaded adsorbents

5.6.1. Selecting desorption reagent

After HMs adsorption, modified StS (M_3-plN_2) was tested for its ability to regenerate and the results are showed in Figure 5.7. Percentages of recovery metals were very different for various kinds of regeneration agents including tap water, HCl 0.1N, H_2SO_4 0.1N, HNO_3 0.1N, CH_3COOH 0.1N and NaOH 0.1N. The H_2SO_4 solution demonstrated that, of all the researched reagents, it was the best candidate to regenerate the adsorbent. The results revealed that 98.9% of Pb^{2+}, 93.4% of Cu^{2+}, 77.2% of Cd^{2+}, 53.8% of Cr^{3+} and 54.9% of Zn^{2+} were recovered with H_2SO_4 0.1N from metals-loaded M_3-plN_2. The three other acids indicated similar and quite high efficiencies – these being HCl, HNO_3 and CH_3COOH. Sodium hydroxide solution 0.1N achieved slightly less efficiency in the recovery of metals. Tap water showed the lowest efficiency in adsorbent regeneration (<30% for all the five HMs).

According to the above results, acid solutions are better for desorption of HMs from metals-loaded adsorbent than sodium hydroxide solution. These results can be explained as follows: the removal efficiencies of HMs on M_3-plN_2 increased when pH increased, so low pH or acidic environment was good for desorption of metal ions from adsorbed M_3-plN_2 (Hu, 2005).

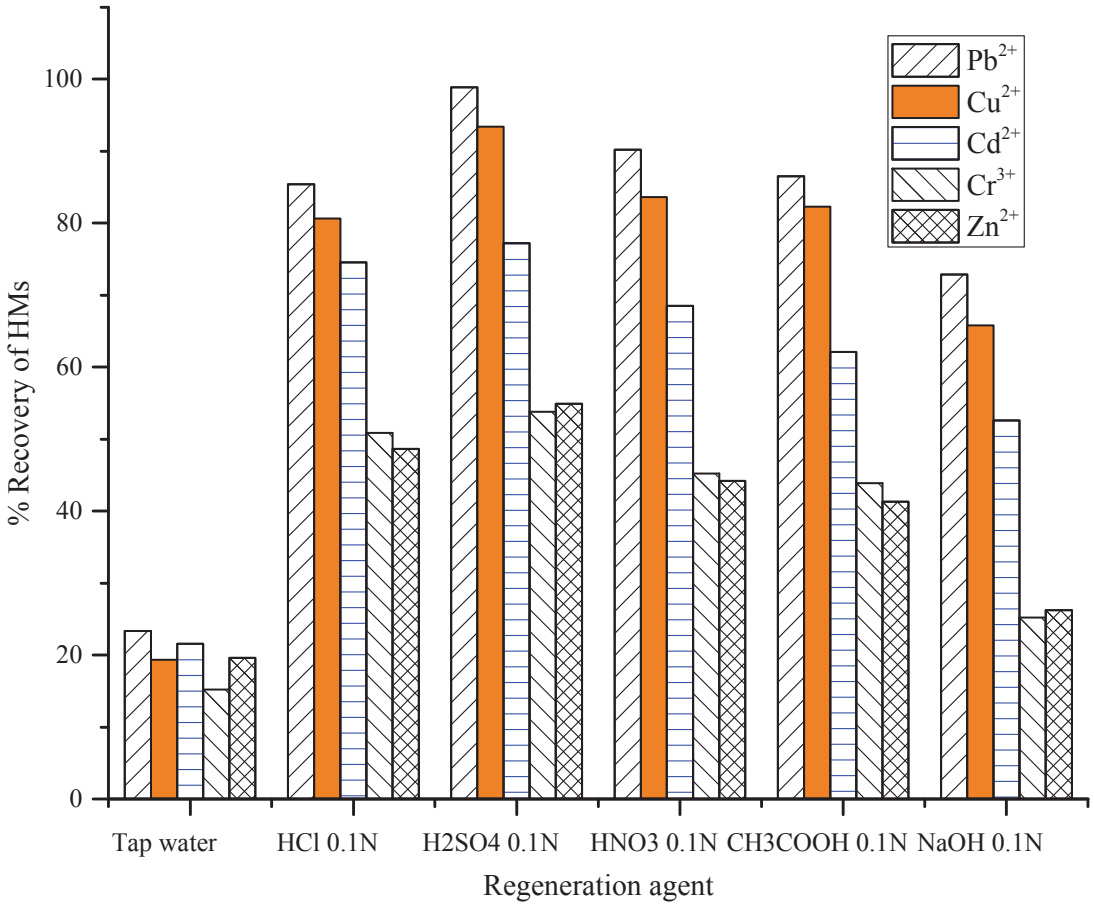

Figure 5.7 Regeneration of M_3-plN_2 after adsorption of Pb^{2+}, Cu^{2+}, Cd^{2+}, Cr^{3+} and Zn^{2+}

5.6.2. Adsorption-desorption cycles

For assessment of the reusability of steel shavings in removing heavy metals from water, the metals-loaded adsorbents were regenerated repeatedly using 5 cycles of adsorption-desorption by the best regeneration reagent (0.1N H_2SO_4). The Figure 5.8 shows five cycles of adsorption and desorption of heavy metals onto the adsorbents. The results indicated the adsorbents can be successfully regenerated and after 5 times the adsorption efficiencies were stable. In some cases, especially after 1-2 times of regeneration, even removal efficiencies for heavy metals of the

adsorbent increased. It can be explained that the low concentration acid solution (0.1N H_2SO_4) played a role as a modification agent to clean and enhance adsorption capacities of the materials.

These results demonstrated that plasma modified steel shavings with N_2 is a very promising adsorbent for removing heavy metal from aqueous solutions. A previous study on metal ions adsorption on Fe_3O_4 nanoparticles by Hu (2005) also achieved the same result that the magnetic material can efficiently work after 5 cycles of adsorption – desorption (Hu, 2005).

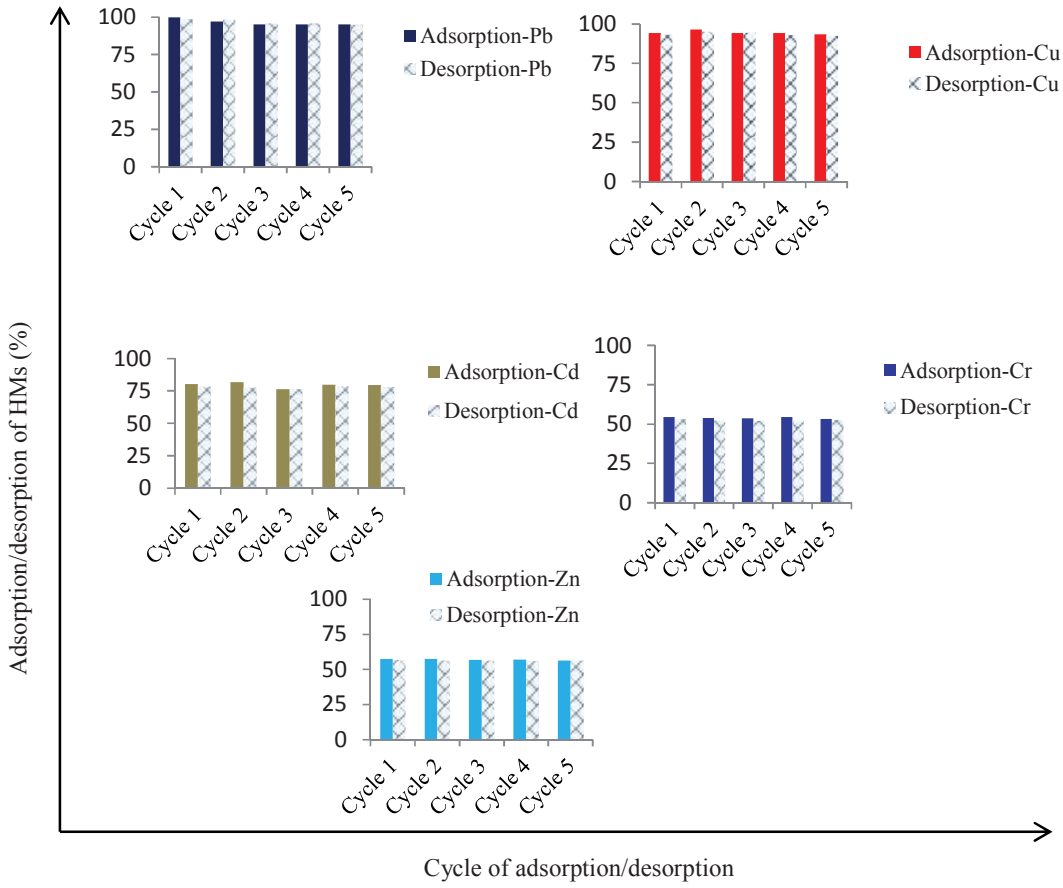

Figure 5.8 Adsorption and desorption cycles for HMs on M_3-plN_2

5.7. Conclusion

From experimental results achieved in this chapter, it could be concluded that both raw and nitrogen plasma steel shavings (M_3 and M_3-plN_2) can be used as an adsorbent for the removal of heavy metals Pb^{2+}, Cu^{2+}, Cd^{2+}, Cr^{3+} and Zn^{2+} from water. However, the Langmuir adsorption capacities of the adsorbent increased from 11.1 to 26.7% after nitrogen plasma modification. Effects of operating conditions such as pH, adsorbent dose and temperature on the HMs adsorption were significant. Optimum conditions for the removal process were pH 5-6, 5 g/L dose of adsorbent and at 25^{o}C. Thermodynamic study revealed that adsorption of HMs onto the adsorbents was a spontaneous, endothermic and highly feasible process.

The experimental data of HMs adsorption onto the adsorbents was better fitted with the Langmuir rather than the Freundlich isotherm model. The Q_{max} values (in mmol/g) of single metal ions on the M_3 and M_3-plN_2 reduced in the order of Cu^{2+} > Cr^{3+} > Zn^{2+} > Cd^{2+} > Pb^{2+}. Maximum single adsorption capacities of HMs onto M_3-plN_2 following Langmuir isotherm were: Pb^{2+} 27.04, Cu^{2+} 20.64, Cd^{2+} 16.87, Cr^{3+} 14.89 and Zn^{2+}18.47 mg/g, respectively. The sorption kinetic data was well fitted with PFO and PSO kinetic models, while the IDM model inappropriately described the kinetic adsorption.

Chapter 5 also revealed that M_3 and M_3-plN_2 can also remove HMs in competitive solutions of the five HMs. Maximum Langmuir competitive adsorption volumes (Q_{max}) of Pb^{2+}, Cu^{2+}, Cd^{2+}, Cr^{3+} and Zn^{2+} were 13.39, 9.78, 7.92, 7.31, 8.79 mg/g on M_3, respectively and 16.62, 14.00, 9.73, 8.69, 12.28 mg/g on M_3-plN_2, respectively. The HMs removal onto M_3 and M_3-plN_2 can result from adsorption and co-precipitation mechanisms.

Due to its highest adsorption capacities, nitrogen plasma modification steel shavings, M_3-plN_2 was chosen for the next experiments on desorption and regeneration. Of the agents analyzed for their ability to regenerate used adsorbents, sulfuric acid (H_2SO_4) 0.1N was the most suitable solution. Further study on the surface modification methods for better adsorption capacity and more cost effective adsorbents from StS is necessary. After 5 cycles of adsorption and desorption, M_3-plN_2 was still stable and demonstrated good adsorption capacities for heavy metals. To apply M_3-plN_2 in wastewater treatment, more studies such as HMs removal in a semi-pilot scale should be implemented.

Faculty of Engineering and Information Technology

CHAPTER 6

RAW AND PLASMA MODIFIED STEEL SHAVINGS FOR REMOVING ANTIBIOTICS FROM AQUEOUS SOLUTION: A BATCH STUDY

6.1. Introduction

Antibiotics (ABs) are expansively used in human and veterinary medicine for inhibiting illness (Lu et al., 2016). Water pollution by the chemicals has become a widespread environmental problem (Rajapaksha et al., 2015). Recent studies have shown that a number of antibiotics are detected in surface and groundwater (Adams et al., 2002). Most antibiotics enter the environment, notably in the aquatic matrix, through discharge or disposal from medical, municipal, and agricultural sources (Adams et al., 2002, Pouran et al., 2014). ABs can pose serious problems to the ecosystem such as their potential risks of environmental toxicity and promotion of microbial resistance (Chen et al., 2011; Qiang et al., 2013; Fan et al., 2010; Lu et al., 2016).

Three typical antibiotics were selected in this study including sulfamethazine (SMT), tetracycline (TC) and chloramphenicol (CP). Sulfamethazine (SMT) is a compound belonging to the sulphonamide group. SMT is usually used in human therapy as well as veterinary medicine or livestock feeds for cattle and swine, and can be detected at high concentration in aqueous solution due to the poor ability of soil to adsorb it (Rajapaksha et al., 2015; Ahmed et al. 2017). Tetracycline (TC), which belongs to the tetracyclines group of antibiotics, is also applied to livestock as additives to combat diseases (Chen et al., 2011). Chloramphenicol (CP) is an antibiotic commonly utilized in veterinary clinics. The appearance of the compounds in water results in several side effects such as aplastic anemia (Nie et al., 2015). While being banned from application to food-producing animals in developed countries, these chemicals are still used in many developing nations due to their low cost, effectiveness and availability (Nie et al., 2015). Thus, developments in efficient

and cost-effective techniques for the removal of such compounds from water are necessary (Chen et al., 2011).

Recently, a variety of methods to remove antibiotics and other pharmaceuticals from the aquatic matrix such as advanced oxidation processes, combined chemical/biological treatment, aerobic digestion integrated with activated carbon, ion exchange, coagulation, flocculation, sedimentation, ultraviolet irradiation, have been attempted (Adams et al., 2002; Homem and Santos, 2011; Qiang et al., 2013; Nie et al., 2015). In comparison with other methods, adsorption using cost-effective adsorbents is considered an effective process that removes antibiotics from aqueous solution (Homem and Santos, 2011). The advantage of adsorption is removing ABs instead of producing potentially more dangerous metabolites (Putra et al., 2009; Homem and Santos, 2011). The technique also effectively eliminates contaminants at very low concentration (less than 1 mg/L) (Putra et al., 2009).

Among the various kinds of adsorbents, iron, particularly in the zero-valent (Fe^0) form, does function as a good candidate due to its adsorption ability and abundance (Cundy et al., 2008, Aredes et al., 2012, Pouran et al., 2014). Some iron-based adsorbents have been used for removing antibiotics from water; for example, persulfate activated by Fe^{2+} and zero-valent iron, microscale zero-valent iron, nanoscale zero-valent iron, (Ghauch et al., 2009; Xia et al., 2014; Nie et al., 2015). Also, iron-based adsorbents often have a magnetic characteristic and consequently, they offer advantages in solid-liquid separation processes under a magnetic field (Hua et al., 2012). Using adsorbents from wastes or by-products of agricultural, municipal and industrial sectors can reduce the quantity of solid waste, coupling with

an increase in the value of the materials. Steel shavings (StS), a magnetic waste generated in very large amounts from the steel processing industry, contain large amounts of zero-valent iron. Hence, studies on the utilization of steel shavings to abate antibiotics from aqueous solution are urgently required. Applying a novel modification technique to produce a superior adsorbent is undoubtedly useful for wastewater treatment. One of the most promising modification methods for Fe^0 is plasma cleaning (see 2.5, chapter 2).

When exposing the iron to a plasma generated in a vacuum, the surface of the adsorbent is bombarded. It leads to adventitious hydrocarbons being removed from the iron surface and enhances the iron surface available for adsorption processes. The selection of gas to produce the plasma is important. Oxygen is effective in removing hydrocarbons both physically and chemically on the surfaces of oxidation-resistant metals such as aluminum and stainless steel. However, when using a material prone to oxidation as iron, inert gases, for instance argon and nitrogen, can serve to generate the plasma with the purpose of achieving the same result without further oxidizing the sample. Moreover, the cost of nitrogen is considerably cheaper than that of argon; therefore, the application of nitrogen plasma is more feasible.

From the outcomes in chapter 4, nitrogen plasma modified steel shavings (M_3-plN_2) have the highest adsorption capacities for SMT, TC and CP. Thus, this chapter aimed to study adsorption of ABs onto M_3 and M_3-plN_2 in batch experiments. Similar to chapter 5 regarding HMs adsorption, this chapter begins with studying factors influencing the removal efficiencies of ABs such as pH, adsorbent dose and temperature. In the next step, adsorption isotherms and kinetics were evaluated in cases of single and competitive solutions. Then, desorption and

regeneration abilities of M_3-plN_2 were examined. Finally, adsorption mechanisms were proposed by analyzing the adsorbent before and after working with ABs solutions.

6.2. Affecting factors to removal efficiencies

6.2.1. pH

The effects of pH on antibiotics removal by raw steel shavings (M_3) and plasma modified steel shavings (M_3-plN_2) are shown in Figure 6.1A and 6.1B. Generally, pH value of the reaction solution exerts a great impact on the raw and modified steel shavings' capacity to remove antibiotics. Plasma modification has improved the absorbents' ability to remove the antibiotics.

The removal efficiency of SMT by M_3 was very high in acidic solution, pH 2.5 to 2.9 (89.3 to 93.6%) but this fell significantly when pH increased from 3.8 to 9.2 (from 32.2% to 4.4%). These changes could be attributed to the effect of pH on the speciation of SMT and the surface electrical properties of the adsorbent. The cationic, neutral and anionic species of SMT were dominant at pH<3, neutral pH and alkaline pH, respectively (Qiang et al., 2013). During the ion-exchange process, the adsorbed cation (M^{n+}) exchanges for a proton (H^+) on the surface of the adsorbents as in the following equation:

$$(Surface)OH + M^{n+} \rightarrow (Surface)OM^{n-1} + H^+$$

These results partly agreed with the study by Ahmed et al. (2017) on the removal of sulphonamide antibiotics by functionalized biochar which achieved maximum adsorption at pH from 3.25 to 4.5. In contrast, the removal efficiency of SMT by MCM-48 modified magnetic nanocomposite (positive surface charge) was

low at acidic pH, rose when the pH increased and reached a maximum at pH 6.3 (Qiang et al., 2013). The maximum removal efficiency of SMT by M_3 reached 93.6% at pH 2.9. The same trend was observed for the plasma modified steel shavings efficiency in removing SMT (Figure 6.1B). The adsorbents' ability to remove SMT declined when the pH level increased. The sorption process reached a maximum at pH 3.01 with a removal efficiency of 95.3%.

The adsorption of TC on M_3 and M_3-plN_2 were also pH-dependent processes. The removal efficiency of TC by M_3 improved when pH increased from 2.4 to 5.1, then fell away with a decrease in pH from 6.8 to 8.3. The adsorption maximum reached a value of 68.1% of TC at pH 5.1. The removal efficiency of TC by M_3-plN_2 was higher than that by M_3 with the maximum adsorption efficiency of 82.1% at pH 4.7. The experimental results displayed that adsorptions of TC on the adsorbents were effective in both acidic and neutral pH. These findings could be due to the fact that smimilar to SMT, TC exists in cationic, zwitterionic and anionic forms under acidic, moderately acidic to neutral and alkaline conditions (Chen et al., 2011). When pH>7 or an alkaline condition creates repulsion at the surface of the adsorbate and the adsorbent; this results in poor removal efficiency.

Compared to the sorptions of SMT and TC, the sorption of CP on M_3 and M_3-plN_2 was more stable regarding pH changes (Figure 6.1). Variation in pH values did not significantly change the efficiency of CP degradation. However, the results indicated that CP was also most effectively removed by the adsorbent at low pH values. From pH 3-3.8, CP in the solution was completely removed by the adsorbents and maximum removal efficiencies were obtained (100%). The adsorption of CP

slightly reduced at neutral and alkaline pH values and reached its lowest at pH 7.9 with M_3 (86.4%) and pH 6.3 with M_3-plN_2 (87.1%). These outcomes were similar to a previous report using persulfate activated by Fe^{2+} and zero-valent iron for removing CP from aqueous solution (Nie et al., 2015).

Of the three antibiotics, most CP was removed by M_3 and M_3-plN_2 and removal efficiency remained moderately stable with observed changes in pH while the process of removing SMT and TC were less efficient and largely depended on pH value. The adsorbents best removed SMT and TC when ABs exist in their neutral species. These outcomes were verified by the pH values of solution at which SMT and CP were most efficiently abated, at pH 3, while the highest adsorption of TC was achieved at pH 5 (Figure 6.1).

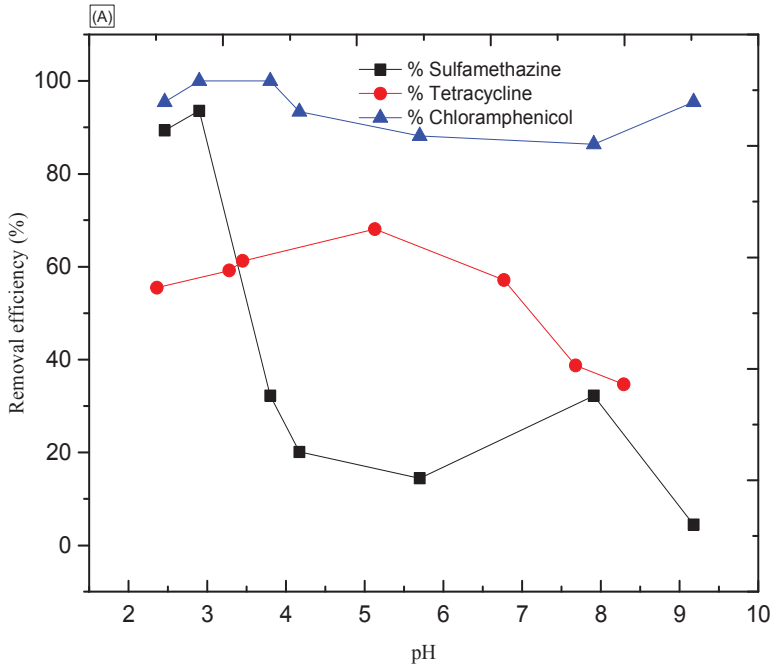

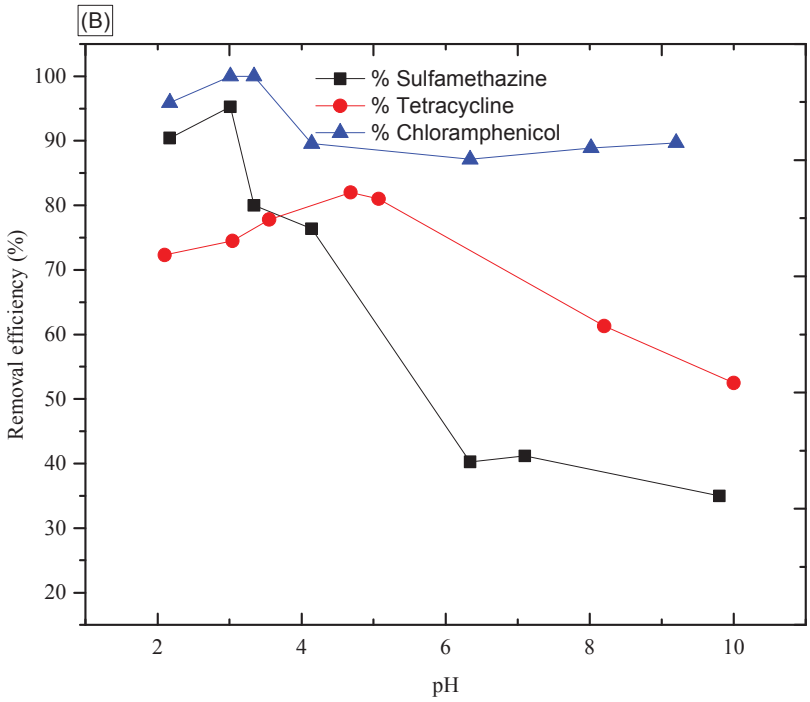

Figure 6.1 Effect of pH on adsorption of the antibiotics on (A) M_3; (B) M_3-plN_2

6.2.2. Adsorbent dosage

For the selection of adsorbent dose, different doses of adsorbent used were 0.1, 0.2, 0.5, 1, 2, 5, 10 and 20 g/L in order to compare removal efficiencies of antibiotics by M_3 and M_3-plN_2. The results in Figure 6.2 reveal that the removal efficiency of the antibiotics improved with an increase in doses. This improvement was a result of the catalytic reduction happening on the surface of the materials for adsorption and reaction sites (Xia et al., 2014). The maximum adsorption processes of antibiotics on both M_3 and M_3-plN_2 were reached at a dose of 2 g/L. Using a dose of 2 g/L, the removal efficiencies of SMT, TC and CP by M_3 and M_3-plN_2 were 40.6, 67.8, 91.4% and 48.9, 68.4, 95.5% respectively. In the study by Xia et al. (2014), at the dose of 1.06 g/L of adsorbent, initial pH 6.8 and air presence, CP (100 mg/L) was totally removed by nano zero-valent iron within 5 min.

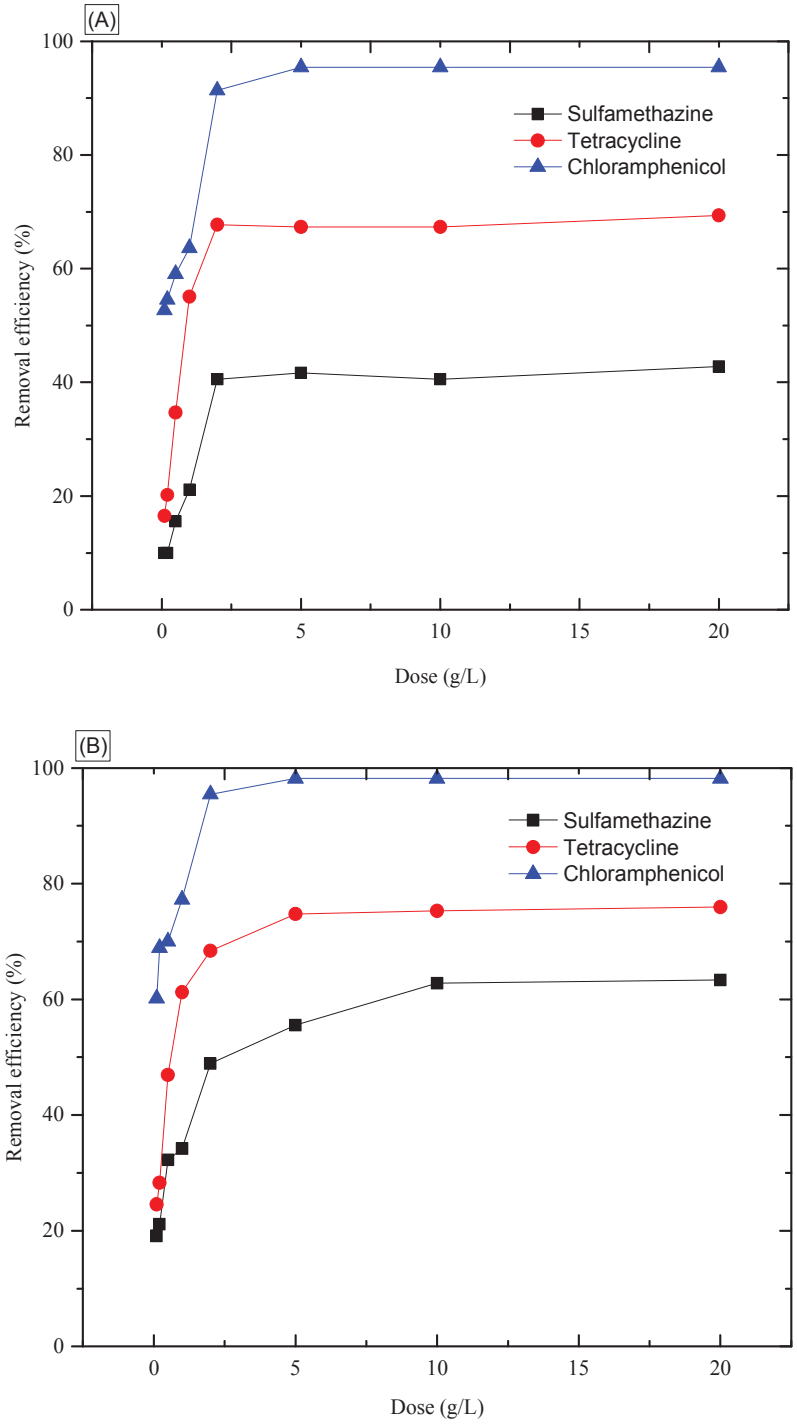

Figure 6.2 Effect of dose on antibiotics adsorption efficiency using (A) M_3; (B) M_3-plN_2

6.2.3. Temperature/thermodynamic

The thermodynamic parameters for the adsorptive removal of ABs onto M_3 and M_3-N_3 were determined from experimental data, using Van't Hoff and Arrhenius equations (see equations 5.2.3.1 and 5.2.3.2, section 5.2.3, chapter 5).

From the results, the adsorption of SMT, TC and CP were best at 25^{o}C among the studied temperature range from 20 to 30^{o}C. Adsorption capacities rose significantly from 20 to 25^{o}C. A further increase of temperature from 25 to 30^{o}C decreased the adsorption capacity. Table 6.1 illustrates the thermodynamic parameters for ABs removal by M_3 and M_3-plN_2. The negative values of $\Delta G°$ indicated that the adsorption of SMT, TC and CP on M_3 and M_3-plN_2 are spontaneous in nature. The $\Delta G°$ values reduced with the rise of temperature from 20 to 25^{o}C and increased from 25 to 30^{o}C, demonstrating at 25^{o}C the adsorption process most effectively occurred.

The similar results were achieved with changes of the adsorption capacities at different temperatures and can be ascribed to the activation of adsorbents by the temperature. In detail, temperature rise from 21 to 25^{o}C is needed to overcome activation energy, but further rise above 25^{o}C triggered a reduction of adsorption which releases heat. That is probably explained by the complex relation between chemical activation energy and exothermic reaction nature of adsorption (Ahmed et al., 2017).

The $\Delta H°$ values of SMT and TC adsorption were positive, while a negative $\Delta H°$ of the CP adsorption was achieved. These results specified that the adsorption of SMT and TC was endothermic in nature whereas exothermic was the nature of CP adsorption (Nguyen et al., 2015). The outcomes in Table 6.1 showed that the values

of ΔS° in most cases of antibiotics elimination by the adsorbents were positive. According to Sengil and Özacar (2008), the results discovered high affinity of adsorbents for most cases of antibiotics adsorption on M_3 and M_3-plN_2 and an increased randomness between solid-solution interfaces during the removal process.

Table 6.1 Thermodynamic parameters for ABs adsorption on M_3 and M_3-plN_2

ABs	Temperature (°C)	Qmax exp. (µg/g)	Kd	ΔG (J/mol)	ΔH^o (J/mol)	ΔS^o (J/mol/K)	r^2
M_3							
SMT	20	1512	8.715	-5274	1436	23	0.394
	25	2590	8.987	-5440			
	30	1555	8.884	-5503			
TC	20	988	4.143	-3463	3565	25	0.014
	25	1549	6.003	-4440			
	30	1084	4.331	-3693			
CP	20	1874	8.876	-5319	-7494	-7	0.607
	25	2920	9.043	-5456			
	30	2009	8.012	-5242			
M_3-plN_2							
SMT	20	1972	5.765	-4263	8302	44	0.053
	25	2747	9.209	-5501			
	30	2065	6.421	-4685			
TC	20	1015	4.654	-3746	9924	48	0.078
	25	1988	7.422	-4966			
	30	1281	5.300	-4201			
CP	20	2336	8.904	-5326	-667	16	0.058
	25	4018	9.147	-5484			
	30	2801	8.821	-5485			

6.3. Modeling of adsorption isotherms and kinetics

6.3.1. Adsorption isotherms

Sorption isotherm plots and isotherm parameters of Langmuir and Freundlich isotherm models are presented and summarized in Figure 6.3, Table 3.4 and Table 6.2. Adsorption capacities of antibiotics increased when the initial concentrations rose. Table 6.2 shows that the sorption data for the antibiotics favored both the

Langmuir and Freundlich isotherm models. Yet they slightly better fitted with the Langmuir model where good regressions ($0.923 \leq r^2 \leq 0.985$) were observed.

Maximum Langmuir adsorption capacities (Q_{max}) of SMT, TC, CP were: 2519.98, 1720.20, 2772.81 µg/g on M_3; 2702.55, 2158.36, 2920.11 µg/g on M_3-plN_2, respectively. The order of the antibiotics' sorption affinity on the adsorbents can be shown as follows: CP>SMT>TC. On the other hand, maximum adsorption constant (K_F) values following Freundlich isotherm with smaller r^2 values were: 741.81, 101.58, 920.30 $\mu g^{1-n}L^n g^{-1}$; and 851.17, 183.67, 944.14 $\mu g^{1-n}L^n g^{-1}$, respectively for SMT, TC, CP on M_3 and M_3-plN_2.

The observed K_F values were higher than reported values in other studies using different adsorbents for removing SMT, TC and CP. For instance, nano zero-valent iron was found to indicate maximum Freundlich SMT adsorption capacities of 8.08; 7.03; 6.11 $\mu g^{1-n}L^n g^{-1}$, respectively, at 288; 298; 308 K (Qiang et al., 2013). Additionally, bamboo charcoal prepared by Liao et al. (2013) exhibited the K_F constants of 0.76; 0.04 $mg^{1-n}L^n g^{-1}$ in the removal of TC and CP, respectively.

6.3.2. Adsorption kinetics

The kinetics of SMT, TC, and CP sorption on M_3 and M_3-plN_2 were fitted to pseudo-first-order (PFO), pseudo-second-order (PSO) and intra-particle diffusion model (IDM) as presented in Figure 6.4, Table 3.4 and Table 6.2. Depending on the correlation coefficient (r^2) and Q_e cal (adsorption capacity at equilibrium was calculated following kinetic equation) values, the sorption kinetics of the antibiotics on the adsorbents were well fitted with both PFO and PSO (high r^2) while the data was not fitted to the IDM model (at very low r^2). The values of PFO rate constant k_{1p} and PSO rate constant k_{2p} decreased as SMT-M_3>SMT-M_3-plN_2>TC-M_3-plN_2>TC-

M_3>CP-M_3>CP-M_3-plN_2 and SMT-M_3>SMT-M_3-plN_2>TC-M_3>TC-M_3-plN_2>CP-M_3>CP-M_3-plN_2, respectively.

The antibiotics were adsorbed significantly in the first 30 min then reduced and reached equilibrium at 60 min. This equilibrium time is the same as that in another study using polyvinylpyrrolidone modified nanoscale zero-valent iron to remove TC (1 hour) (Chen et al., 2011). It is also quicker than the time documented in one report utilizing MCM-48 modified magnetic mesoporous nanocomposite (24 hours) (Qiang et al., 2013).

Maximum sorption constants (Qe cal) of SMT, TC, CP on M_3 and M_3-plN_2 following the PFO model of 212.81, 369.74, 370.16 µg/g on M_3; and 290.38; 417.01, 445.09 µg/g on M_3-plN_2 correspondingly, while the PSO adsorption capacities (Qe cal) were 218.16, 384.15, 391.81 µg/g; and 299.95; 434.97; 470.1 µg/g, correspondingly.

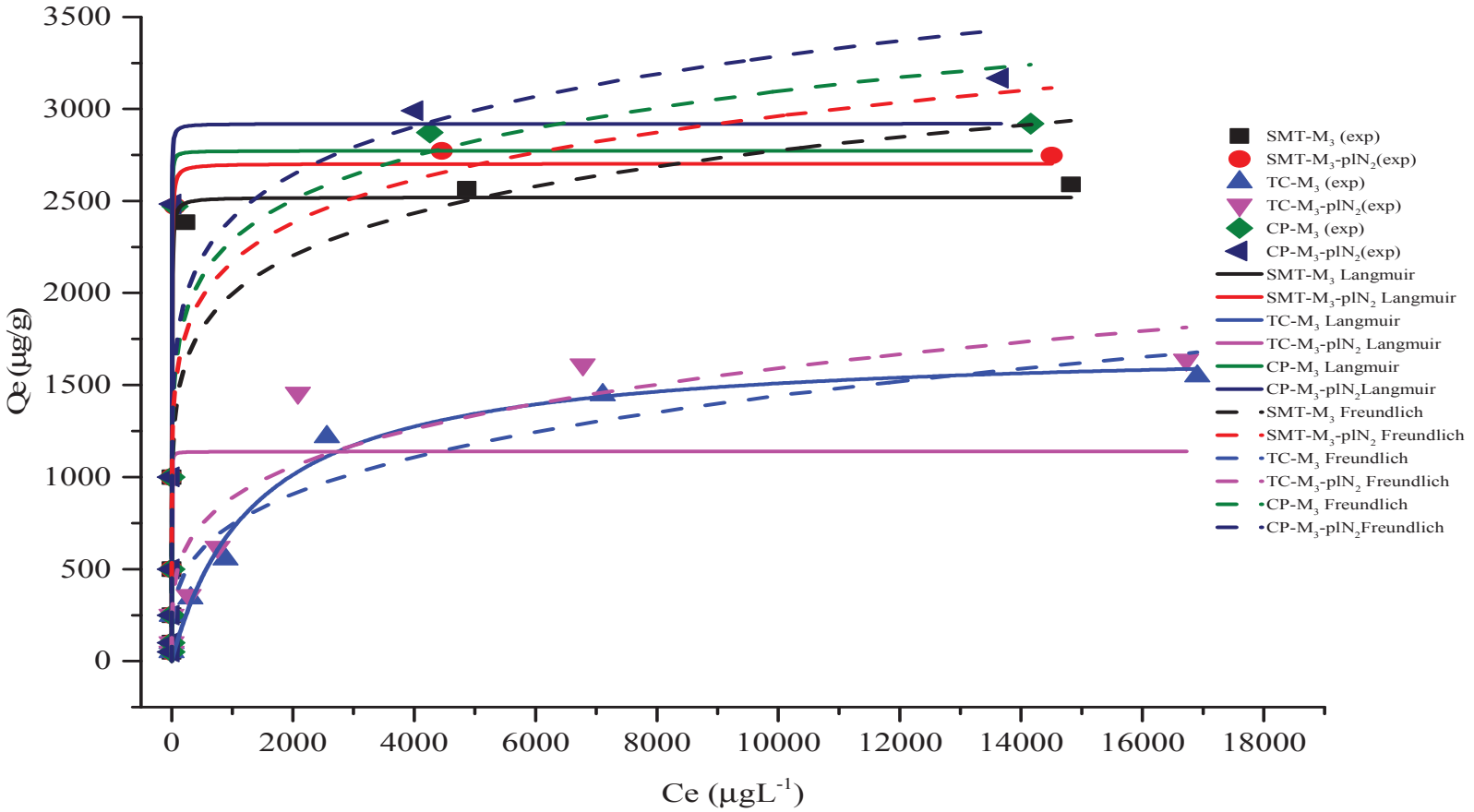

Figure 6.3 Langmuir and Freundlich adsorption of SMT, TC, CP on M_3 and M_3-plN_2 (initial concentration: 100 - 20000 µg/L; pH 3 was adjusted for SMT, CP; pH 5 for TC; adsorbent dose of 2g/L; at 25^0C)

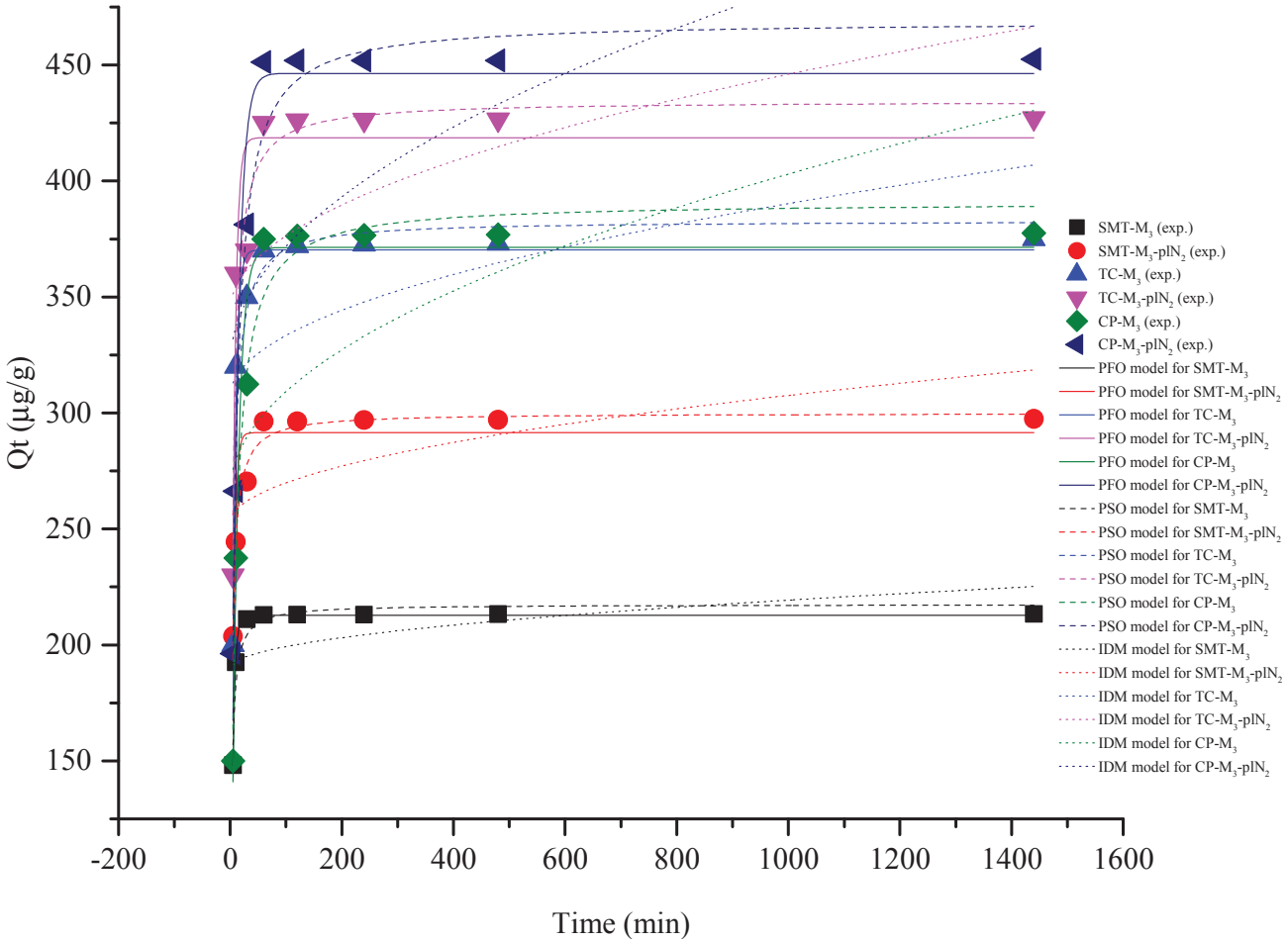

Figure 6.4 Sorption kinetics of SMT, TC and CP on M_3 and M_3-plN_2 (initial concentration: 1000 µg/L; no pH adjustment; adsorbent dose of 2g/L; at room temperature)

Table 6.2 Isotherm and kinetic parameters using the non-linear regression method for antibiotics adsorption onto M_3 and M_3-plN_2

Isotherm parameters	**Antibiotic/adsorbent**						**Kinetic parameters**	**Antibiotic/adsorbent**					
	SMT-M_3	SMT-M_3-plN_2	TC-M_3	TC-M_3-plN_2	CP-M_3	CP-M_3-plN_2		SMT-M_3	SMT-M_3-plN_2	TC-M_3	TC-M_3-plN_2	CP-M_3	CP-M_3-plN_2
1. Langmuir							1. Pseudo−first-order						
Qmax exp. (µg/g)	2590.1	2746.5	1548.5	1987.5	2920.1	3167.5	Qe exp (µg/g)	213.3	297.4	375.1	427.2	377.5	452.5
Qmax cal. (µg/g)	2519.98	2702.55	1720.20	2158.36	2772.81	2920.11	Qe cal (µg/g)	212.81	290.38	369.74	417.01	370.16	445.09
K_L	0.340	0.374	7.1441 x10^{-4}	0.001	1.1103	0.86	K_1p (min^{-1})	0.2374	0.2206	0.1714	0.1725	0.0962	0.0947
r^2	0.985	0.982	0.958	0.952	0.981	0.923	r^2	0.999	0.872	0.960	0.895	0.958	0.956
2. Freundlich							2. Pseudo−second-order						
K_F	741.81	851.17	101.58	183.67	920.30	944.14	Qe cal (µg/g)	218.16	299.95	384.15	434.97	391.81	470.1
n	6.9821	7.3873	3.4716	3.9235	7.5920	7.3824	K_2p (min^{-1})	0.0023	0.0014	7.6671 x10^{-4}	6.5598 x10^{-4}	3.6496 x10^{-4}	3.0641 x10^{-4}
r^2	0.864	0.820	0.926	0.910	0.843	0.833	r^2	0.913	0.980	0.894	0.895	0.972	0.974
							3. IDM						
							Kp (µg.g^{-1}.min^{-1})	0.90	1.69	2.56	3.14	4.22	5.00
							C	189.16	250.58	304.41	340.59	261.21	314.86
							r^2	0.075	0.238	0.125	0.175	0.242	0.247

6.4. Competitive adsorption of multi-antibiotics solution on the adsorbents

6.4.1. Competitive adsorption isotherms

Isotherm plots and parameters of competitive adsorption of ABs on M_3 and M_3-plN_2 are shown in Figure 6.5 and Table 6.3. The high values of correlation coefficients (r^2) showed that experimental competitive adsorption data fitted both Langmuir and Freundlich isotherm models. However, Langmuir isotherm slightly better describes the adsorption data.

Maximum Langmuir adsorption capacities (μg/g) of competitive solutes of SMT, TC and CP on the adsorbents were 809.06, 495.69, 920.27 on M_3 and 958.97, 616.89, 1075.83 on M_3-plN_2, respectively. Competitive adsorption capacities were nearly 2-fold less than individual adsorption capacities. The total competitive adsorption of ABs was calculated in Equations 3.2.5.3 to 3.2.5.6 and achieved same values as individual solute adsorption.

The K_F values (μg/g) following the Freundlich isotherm of SMT, TC, CP were 224.51, 139.14, 275.86 on M_3 and 257.55, 174.19, 357.34 on M_3-plN_2. These results indicated that the adsorbents can work in both single and competitive solutes of ABs and the adsorption of ABs on raw and modified StS is monolayer adsorption in nature.

6.4.2. Competitive adsorption kinetics

Competitive adsorption kinetics of SMT, TC, CP on M_3 and M_3-plN_2 were shown in Figure 6.6 and Table 6.3. Adsorption data fitted both PFO and PSO kinetic models with high r^2 constants while low r^2 values showed that the data was not fitted

with IDM. Same as adsorption of single solute of ABs, the adsorption process for competitive solutes also reached equilibrium at 60 min. The order of PFO rate constant k_{1p} for ABs removal by M_3 and M_3-plN_2 increased as SMT-M_3<TC-M_3<CP-M_3<SMT-M_3-plN_2<TC-M_3-plN_2<CP-M_3-plN_2, respectively.

Maximum PFO competitive adsorption capacities (μg/g) of SMT, TC, CP were 111.88, 179.25, 188.18 on M_3 and 142.61, 209.25, 222.62 on M_3-plN_2, respectively. Following the PSO kinetic model, the order of k_{2p} constant decreased as SMT-M_3-plN_2>SMT-M_3>CP-M_3-plN_2>TC-M_3-plN_2>TC-M_3-plN_2>TC-M_3>CP-M_3. Maximum PSO competitive adsorption capacities (μg/g) of SMT, TC, CP were 119.29, 190.22, 199.37 on M_3 and 151.02, 221.17, 235.18 on M_3-plN_2, respectively.

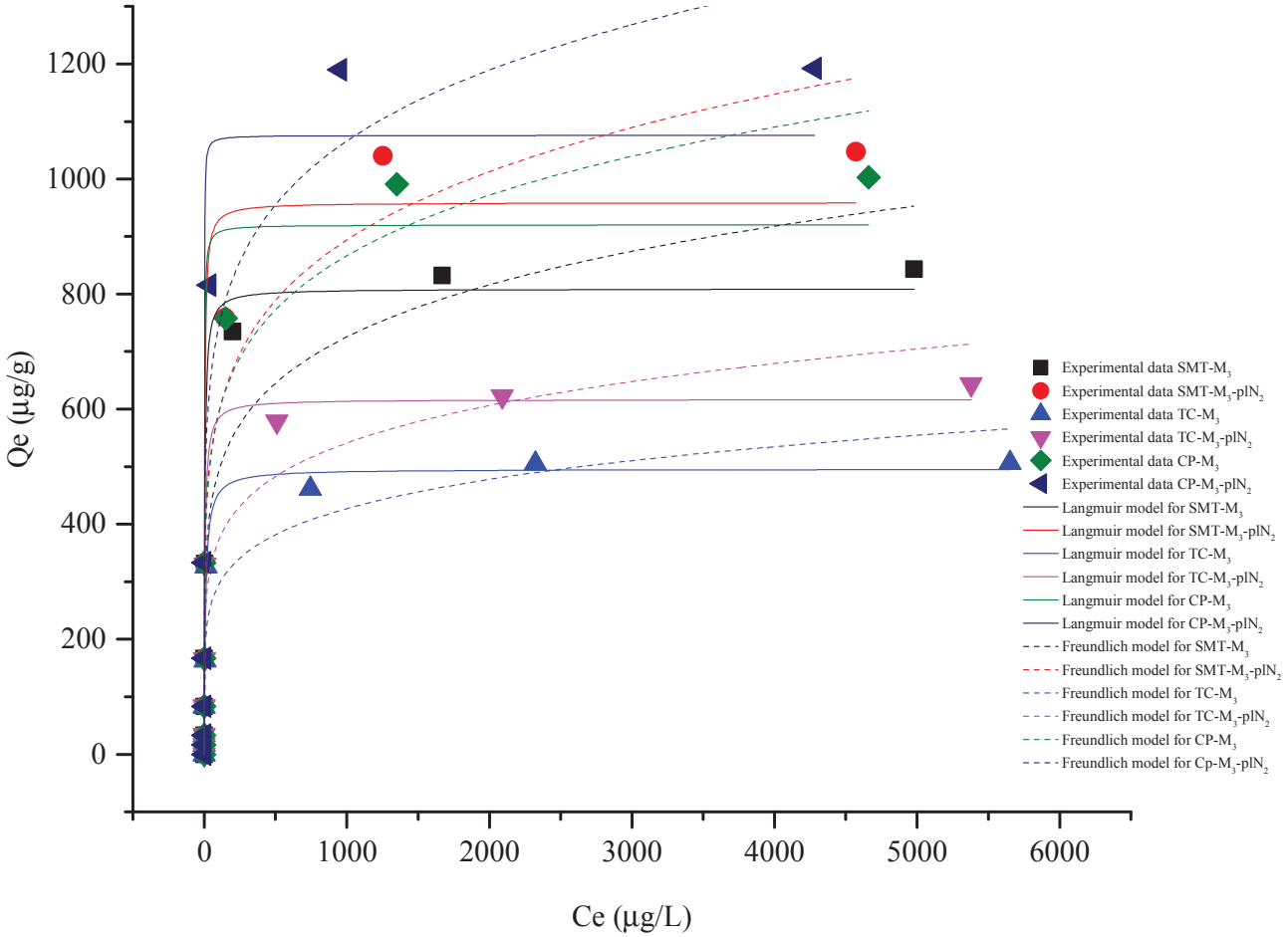

Figure 6.5 Competitive adsorption isotherm of ABs on M_3 and M_3-plN_2 (total multi-antibiotics initial concentration: 0 - 20000 µg/L, each solute concentration: 0-6666.67 µg/L; pH 3; adsorbent dose of 2g/L; at 25^0C)

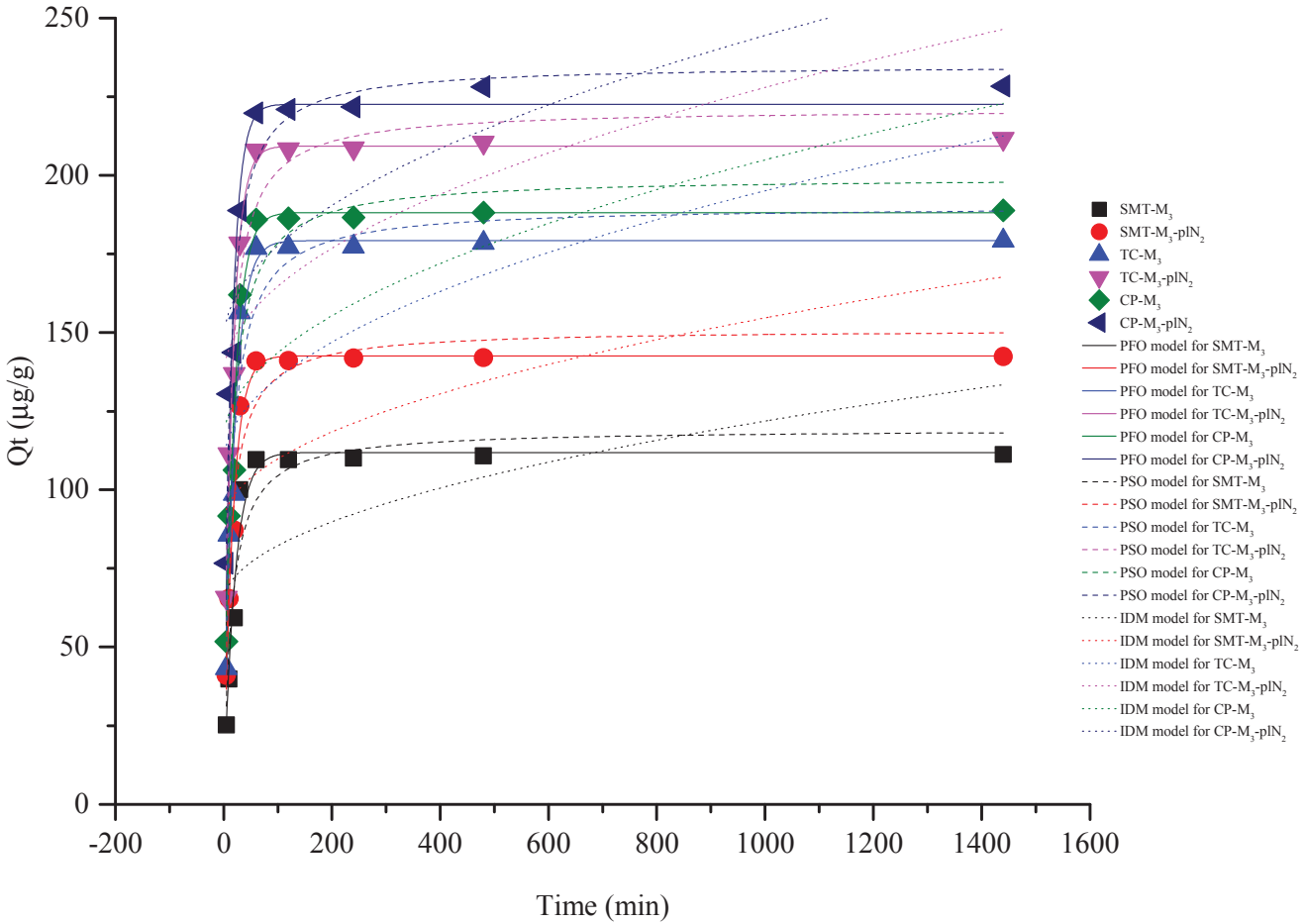

Figure 6.6 Competitive adsorption kinetics of ABs on M_3 and M_3-plN_2 (total competitive initial concentration: 1000 µg/L, each solute concentration is 333.33 µg/L; no pH adjustment; adsorbent dose of 2g/L; at room temperature)

Table 6.3 Isotherm and kinetic parameters using the non-linear regression method for competitive adsorption kinetics and isotherms of ABs on M_3 and M_3-plN_2

Isotherm parameters	**Antibiotic/adsorbent**						**Kinetic parameters**	**Antibiotic/adsorbent**					
	SMT-M_3	SMT-M_3-plN_2	TC-M_3	TC-M_3-plN_2	CP-M_3	CP-M_3-plN_2		SMT-M_3	SMT-M_3-plN_2	TC-M_3	TC-M_3-plN_2	CP-M_3	CP-M_3-plN_2
1. Langmuir							1. Pseudo−first-order						
Qmax exp. (μg/g)	843.02	1047.35	506.59	643.30	1002.87	1192.39	Qe exp. (μg/g)	111.23	142.36	179.25	211.59	188.83	228.36
Qmax cal. (μg/g)	809.06	958.97	495.69	616.89	920.27	1075.83	Qe cal. (μg/g)	111.88	142.61	179.25	209.25	188.18	222.62
K_L	0.2230	0.2935	0.1046	0.1749	0.6894	1.4690	K_1p (min^{-1})	0.0495	0.0592	0.0547	0.0651	0.0564	0.0692
r^2	0.987	0.957	0.980	0.989	0.957	0.936	r^2	0.960	0.978	0.963	0.978	0.965	0.946
2. Freundlich							2. Pseudo−second-order						
K_F	224.51	257.55	139.14	174.19	275.86	357.34	Qe cal (μg/g)	119.29	151.02	190.22	221.17	199.37	235.18
n	5.8894	5.5515	6.1602	6.0951	6.0356	6.3207	K_2p (min^{-1})	5.9336 $x10^{-4}$	5.9434 $x10^{-4}$	4.2992 $x10^{-4}$	4.5742 $x10^{-4}$	4.2954 $x10^{-4}$	4.6356 $x10^{-4}$
r^2	0.921	0.948	0.914	0.937	0.949	0.928	r^2	0.899	0.933	0.920	0.961	0.932	0.962
							3. IDM						
							Kp ($\mu g.g^{-1}.min^{-1}$)	1.8321	2.0731	2.7548	2.9243	2.8351	3.0907
							C	63.91	89.09	107.98	135.46	115.26	146.71
							r^2	0.283	0.283	0.292	0.309	0.306	0.346

6.5. Desorption and regeneration of the ABs loaded adsorbents

6.5.1. Selecting desorption reagent

Several reagents including tap water, H_2SO_4 0.1N; NaOH 0.1N, methanol 0.1N and ethanol 0.1N were utilized for desorbing antibiotics loaded adsorbents (see 3.2.5D, chapter 3). The Figure 6.7 indicates the desorption efficiencies of ABs from antibiotic-loaded M_3-plN_2. As illustrated in Figure 6.7, reagents with organic solvents such as methanol, ethanol better desorbed the adsorbent after adsorption. The percentages of ABs were recovered as SMT 89.3, TC 90.2 and CP 92.5 % with methanol 0.1N and SMT 66.3, TC 70.3 and CP 71.7 % with ethanol 0.1N. However, the desorption efficiencies were very low with the inorganic reagents including tap water, sulfuric acid 0.1N and sodium hydroxide 0.1N solutions. The percentages of recovery ABs ranged from SMT 15.1 to 25.3; TC 16.3 to 26.1 and CP 17.5 to 27.6 % with the three inorganic reagents.

From the experimental data, the solution of methanol 0.1N was the best solution to desorb the ABs-loaded M_3-plN_2 and was chosen for experiments of adsorption-desorption cycles. Similar results were reported by Hu et al. (2012) who concluded that methanol solution was also the best reagent for desorbing Ofloxacin, norfloxacin, ciprofloxacin, enrofloxacin and sulfamethazine from longitudinally packing molecularly imprinted fibers.

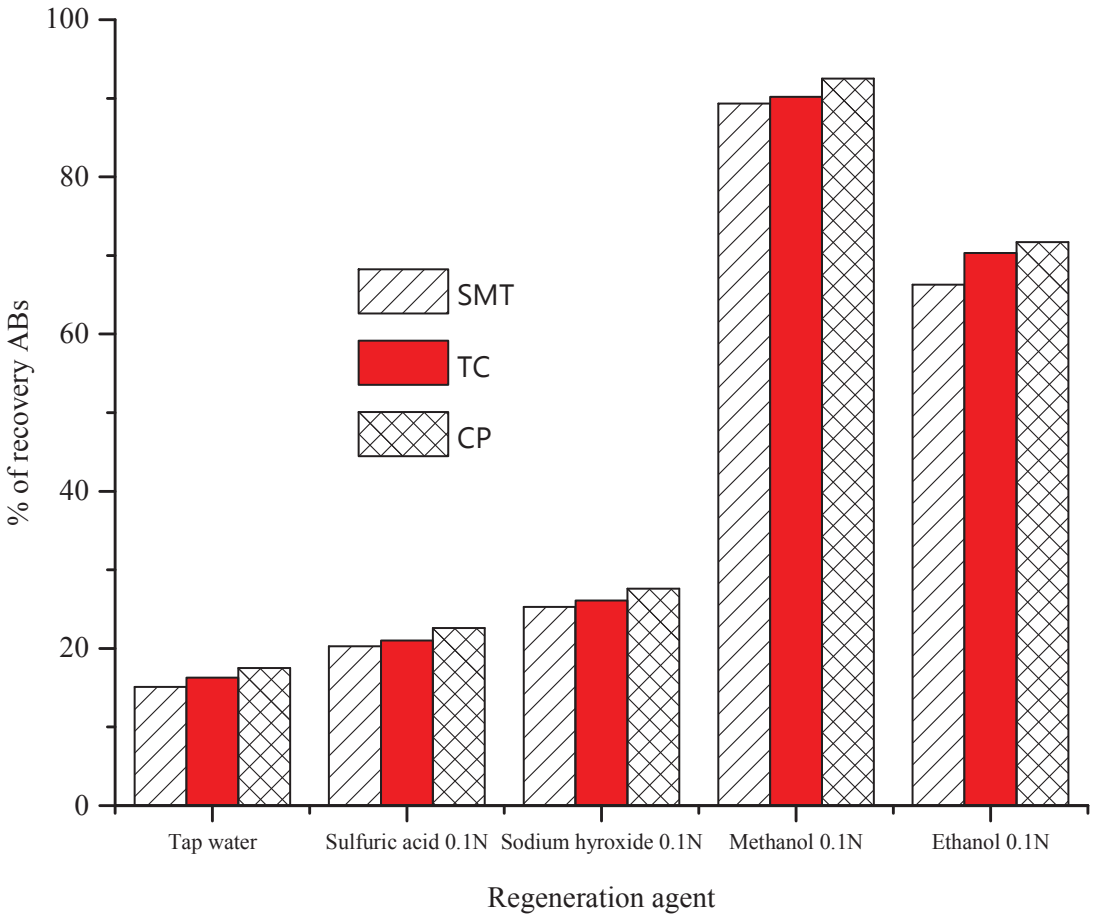

Figure 6.7 Regeneration of M_3-plN_2 after adsorption of ABs

6.5.2. Adsorption-desorption cycles

Figure 6.8 shows the adsorption-desorption cycles for ABs on M_3-plN_2 using the reagent methanol 0.1N solution. The outcomes revealed that M_3-plN_2 was effectively regenerated. In the first three cycles, the adsorption and desorption capacities of M_3-plN_2 were slightly reduced. Adsorption efficiencies of ABs at the first, second and third cycle were SMT 95.1, 90.2, 86.5 %; TC 98.3, 94.6, 88.7 % and CP 99.8, 96.2, 90.2 %. From the fourth to the fifth cycle, adsorption and desorption

abilities of the adsorbent were lower. At the fifth cycle, removal efficiencies of the regenerated M_3-plN_2 were SMT 75.5; TC 76.3 and CP 77.2 %.

Experimental results clarified that M_3-plN_2 can be effectively regenerated by methanol and this makes the adsorbent has more potential in applicability for wastewater treatment. In another study conducted by Li et al. (2014), a mixture of $CaCl_2$ 0.01 M and NaN_3 200 mg/L solution was used for regeneration of carbon nanotubes. However, the adsorption-desorption was only successful after 2-3 cycles.

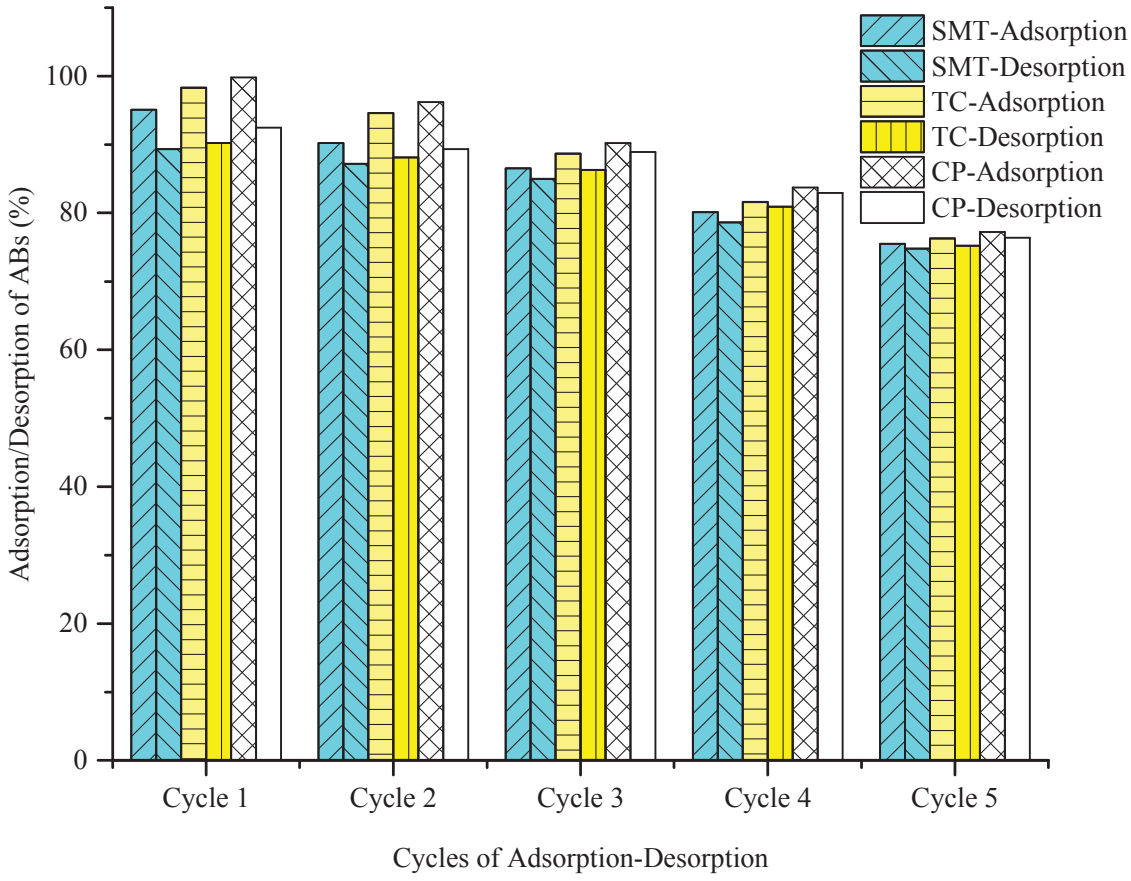

Figure 6.8 Adsorption and desorption cycles for ABs on M_3-plN_2 using methanol 0.1N

6.6. Proposed mechanisms of ABs removal by steel shavings

To generate insights into the adsorption of antibiotics from aqueous solution by the adsorbents, FTIR and XPS were employed. FTIR spectra of the adsorbents before and after adsorption including M_3, M_3-plN_2, SMT loaded M_3-plN_2, TC loaded M_3-plN_2, CP loaded M_3-plN_2 and mixed antibiotics (SMT, TC and CP) loaded M_3-plN_2 are indicated in Figure 6.9. An absorption band showing the vibrational properties of Fe-O bond is observed at around 477 cm^{-1} (Gupta et al., 2011). Other iron oxides namely Fe_3O_4 and Fe_2O_3 were also recorded as peaks at 573-588 cm^{-1} (Dong et al., 2014; Shu and Wang, 2009; Du et al., 2010).

The spectra also indicated the existence of organic groups of antibiotics after adsorption on M_3-plN_2. The peaks in the range of 3800-3900 cm^{-1} correspond to –OH groups in TC-M_3-plN_2, CP-M_3-plN_2 and mixed antibiotics loaded-M_3-plN_2, indicating the existence of hydroxyl groups on the surface of loaded adsorbents, originated from TC and CP (Ahmed et al., 2017). Those at 1550-1540 cm^{-1} are the N-H and C-N stretching mode of groups of the three antibiotics (Parikh and Chorover, 2006). The peaks at 2920 cm^{-1} shows the C-H stretch vibration and peaks at 1520 cm^{-1} correspond to C=O, originated from TC and CP (Ahmed et al., 2017).

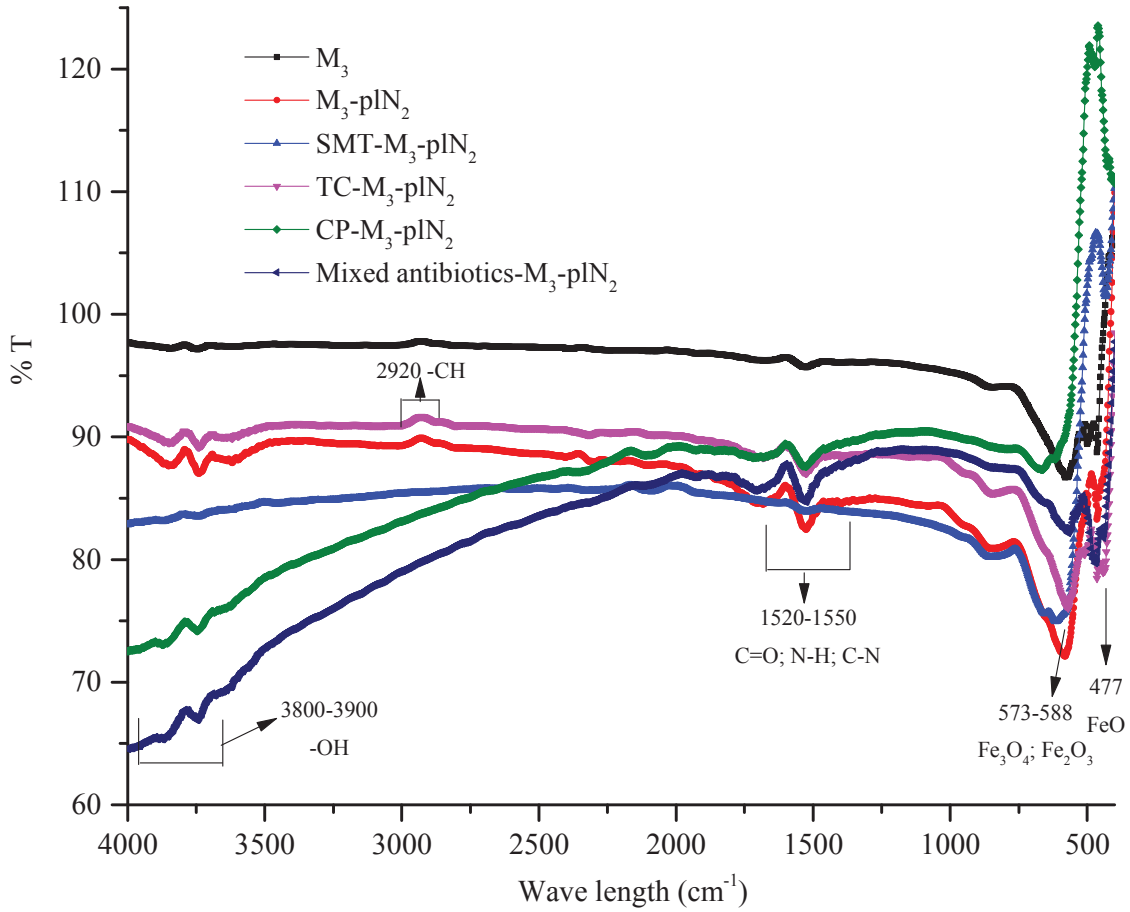

Figure 6.9 FTIR spectrums for M_3, M_3-plN_2 and antibiotics loaded M_3-plN_2

XPS is a surface sensitive method which can determine the binding energy of elements in the top 10 nm of a sample as shown in the full survey scans of Figure 6.10.

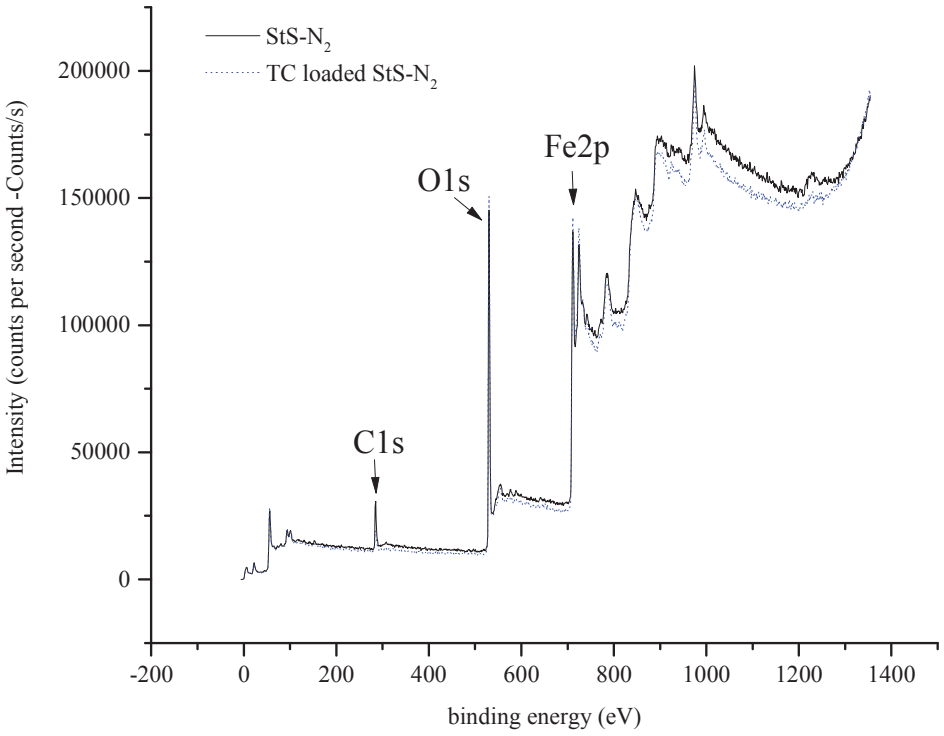

Figure 6.10 Full survey of N_2 plasma modified steel shavings before and after adsorption

By executing narrow scans in the binding energy regions of the elements, it is possible to relate the peaks in binding energy to chemical bonds, states and those elements' environments.

Starting with the two narrow scans in the C1s region (Figure 6.11), displayed here are peaks that are characteristic of adventitious carbon contamination of the adsorbent surface (layer thickness 1-2nm). The typical chemical states of C were C-C at ~284.8 eV, C-O-C at ~286 eV and O-C=O at >288.5 eV bonding (Table 6.4; Thermo scientific XPS, 2017).

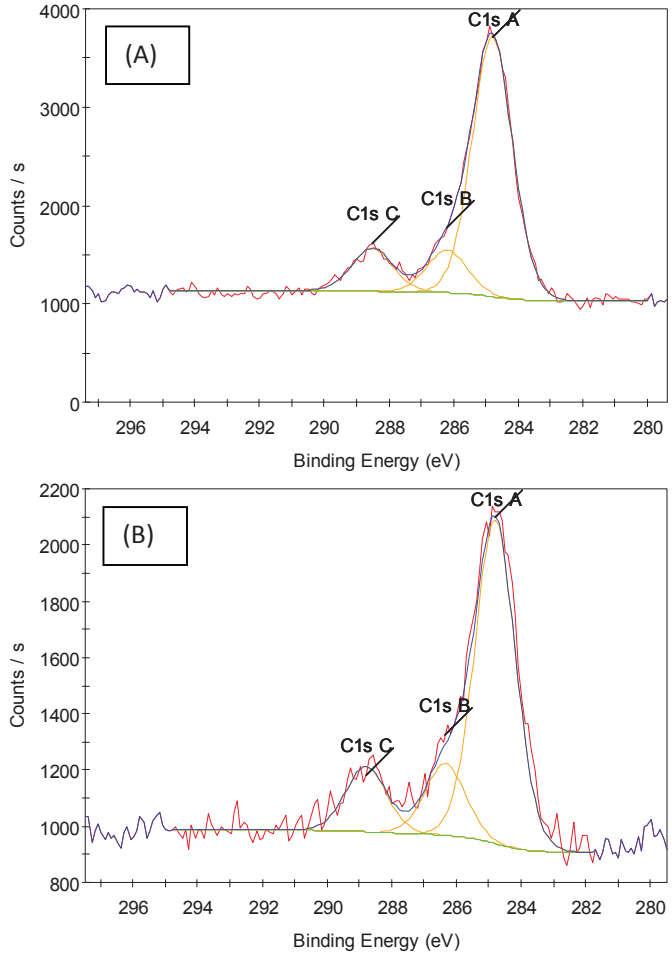

Figure 6.11 XPS narrow scan of C1s region for M_3-plN_2 (A) before adsorption and (B) after adsorption

Table 6.4 Binding energy, chemical state, relative peak area and atomic percentage of peaks in narrow scan of C1s region of the adsorbent before and after adsorption

Name	**Spectrum (Region Peak)**	**Binding Energy (eV)**	**Chemical State**	**Relative Peak Area (CPS.eV)**	**Atomic %**
M_3-plN_2	C1s A	284.79	C-C	4177.22	16.19
	C1s B	286.2	C-O-C	687.9	2.67
	C1s C	288.51	O-C=O	688.53	2.67
TC loaded	C1s A	284.8	C-C	1827.1	7.7
M_3-plN_2	C1s B	286.34	C-O-C	403.7	1.7
	C1s C	288.79	O-C=O	368.94	1.56

Figure 6.12 shows that oxygen chemical states with the adventitious carbon and the metals are presented in the narrow scans in the O1s region. The O1sA peaks (~529-530 eV) in each spectrum are characteristic of metal oxides (Fe_2O_3, Fe_3O_4, FeO) while the O1sB and O1sC are characteristic of adventitious carbon C-O (~531.5-532 eV) and C=O (~533 eV) bonding, respectively (Table 6.5; Thermo scientific XPS, 2017).

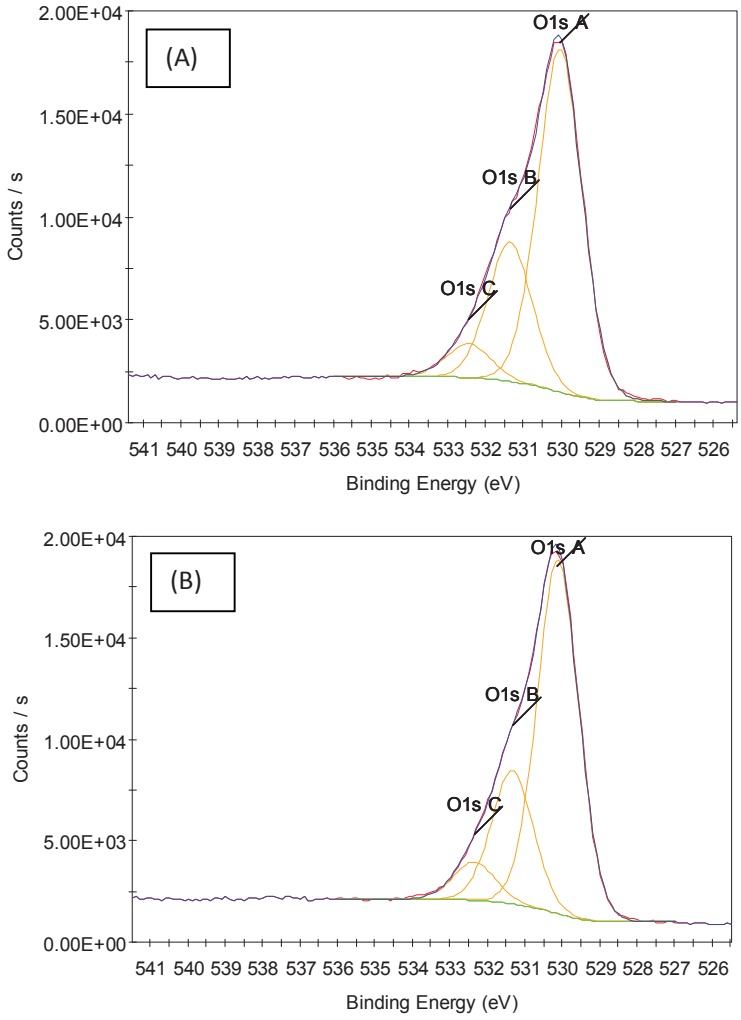

Figure 6.12 XPS narrow scan of O1s region for M_3-plN_2 (A) before adsorption and (B) after adsorption

Table 6.5 Binding energy, chemical state, relative peak area and atomic percentage of peaks in narrow scan of O1s region of the adsorbent before and after adsorption

Name	Spectrum (Region Peak)	Binding Energy (eV)	Chemical State	Relative Peak Area (CPS.eV)	Atomic %
M_3-plN_2	O1s A	530.03	O-metal oxides	24427.48	33.84
	O1s B	531.34	C-O	9909.97	13.73
	O1s C	532.44	C=O	2407.51	3.34
TC loaded	O1s A	530.12	O-metal oxides	24518.67	36.92
M_3-plN_2	O1s B	531.33	C-O	9242.38	13.92
	O1s C	532.34	C=O	2650.33	3.99

The binding energy of an element increases when its valence state also increases. This was demonstrated by the binding energy separation of the Fe2p3/2A and Fe2p3/2B peaks in all spectra in Figure 6.13, suggesting a mixed oxide of both Fe^{3+} and Fe^{2+} which is Fe_3O_4. This oxide is the dominant oxide present for both before and after adsorption processes (Table 6.6). The other two constituents - Fe2p3/2C and Fe2p3/2D in all spectra - are representative of Fe^{2+} and Fe^{3+} in their other separate oxides states of FeO and Fe_2O_3, respectively. These oxides are mainly responsible for the adsorption of SMT, TC and CP on raw and modified steel shavings. Figure 13 does not show the spectrum peak at ~ 706.7eV binding energy, which indicates the chemical state of zero-valent iron (Fe^0) (Thermo scientific XPS, 2017). Since the detected limitation of XPS technique is 10 nm in the top surface of the material, it can be assumed that the Fe^0 core of the adsorbent was covered by an iron oxide film that was thicker than 10 nm.

Based on the XPS results and what previous studies have found, the mechanisms that could be proposed for the removal of antibiotics are: SMT: hydrogen bonding; TC: electrostatic and non- electrostatic interaction; and CP removal: redox reaction (Qiang et al., 2013; Chen et al., 2011; Nie et al., 2015; Xia et

al., 2014). Qiang et al. (2013) proposed three kinds of hydrogen bonding between the nitrogen of the aniline, sulfinol or pyrimidine group of SMT and the surface hydroxyl group of FeM48 being the major driving force for adsorption. Additionally, the л-л electron-donor acceptor interaction between SMT (л-electroneacceptor) and the adsorbent (л-electronedonor) also promoted adsorption (Qiang et al., 2013). Chen et al. (2011) confirmed that the adsorption pathway of TC on PVP-nano zero-valent iron included electrostatic interactions and Fe-TC complexation reactions. Meanwhile the removal of CP as reported by Nie et al. (2015) and Xia et al. (2014) was a redox reaction.

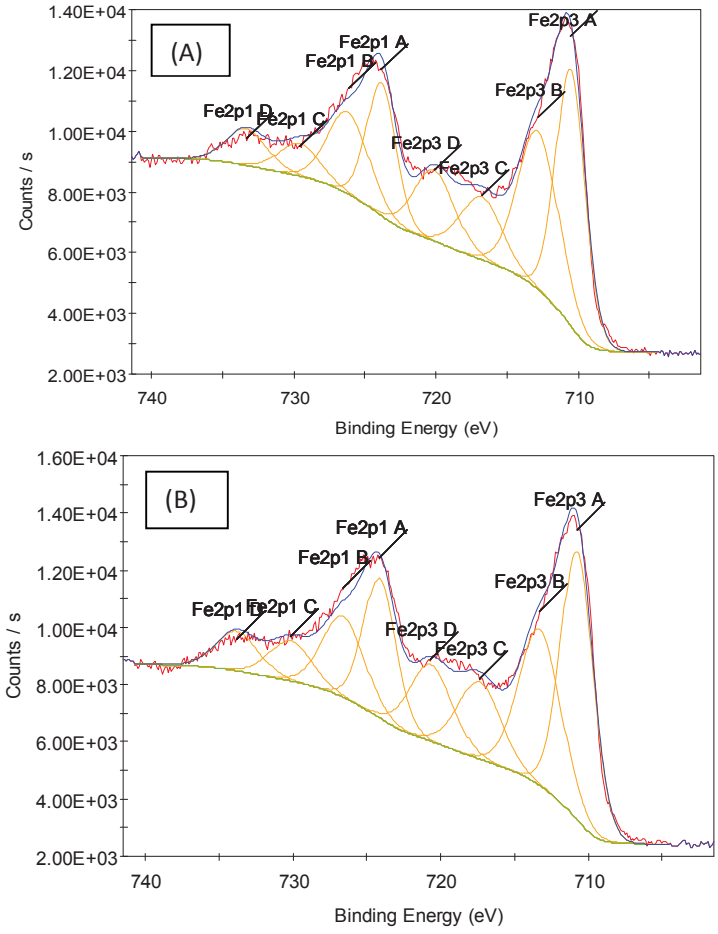

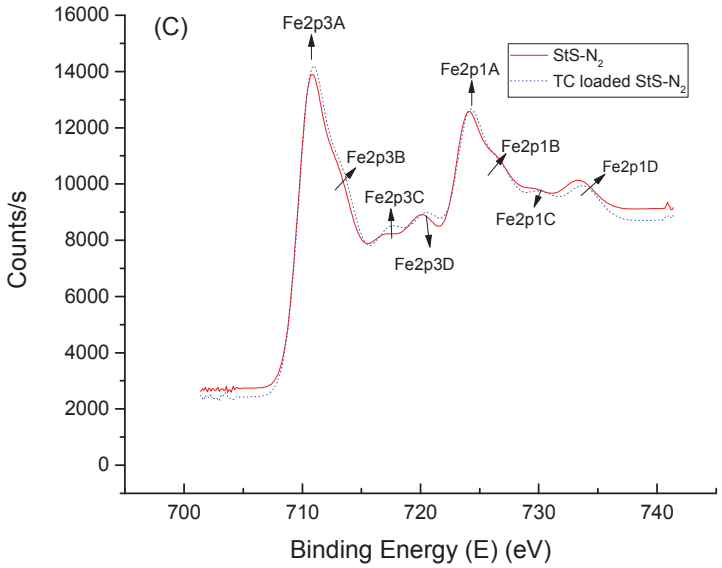

Figure 6.13 XPS narrow scan of Fe2p region for M_3-plN_2 (A) before adsorption; (B) after adsorption; (C) combined spectrums of before and after adsorption

Table 6.6 Binding energy, chemical state, relative peak area and atomic percentage of peaks in narrow scan of Fe2p3/2 region of the adsorbent before and after adsorption

Name	Spectrum (Region Peak)	Binding Energy (eV)	Chemical State	Relative Peak Area (CPS.eV)	Atomic %
M_3-plN_2	Fe2p3 A	710.54	Fe_3O_4/Fe^{2+}	21785.43	9.03
	Fe2p3 B	712.8	Fe_3O_4/Fe^{3+}	18998.32	7.88
	Fe2p3 C	716.79	FeO/Fe^{2+}	7546.61	3.13
	Fe2p3 D	720.12	Fe_2O_3/Fe^{3+}	8492.22	3.53
TC loaded	Fe2p3 A	710.77	Fe_3O_4/Fe^{2+}	26057.06	11.74
M_3-plN_2	Fe2p3 B	713.26	Fe_3O_4/Fe^{3+}	19896.5	8.97
	Fe2p3 C	717.35	FeO/Fe^{2+}	9810.93	4.43
	Fe2p3 D	720.65	Fe_2O_3/Fe^{3+}	9747.22	4.4

6.7. Conclusions

This study demonstrated that the raw and modified steel shavings did effectively remove the antibiotics SMT, TC and CP from aqueous solution. Nitrogen plasma modification has cleaned and improved the surface area of steel shavings and then increased adsorption capacity of the adsorbent for the antibiotics.

The adsorbents can work well in both single and competitive solutions of antibiotics. The adsorption data fitted better to the Langmuir isotherm model than the Freundlich model. The antibiotics' maximum Langmuir sorption capacity declined in the following order: CP>SMT>TC on both M_3 and M_3-plN_2. In single adsorption of ABs, maximum Langmuir adsorption capacities following the Langmuir isotherm (Q_{max}) of SMT, TC, CP were: 2519.98, 1720.20, and 2772.81 µg/g on M_3; 2702.55, 2158.36, and 2920.11 µg/g on M_3-plN_2, respectively. The competitive adsorption capacities were nearly 2-fold less than individual adsorption capacities.

The sorption of SMT, TC and CP on the adsorbents reached equilibrium within an hour and both PFO and PSO models could be used to simulate the kinetic data. The solution pH remarkably affected the efficiency of M_3 and M_3-plN_2 in removing the pollutants. The optimum pH value for removing SMT and CP was 3 while a level of pH 5 was the most suitable for abating TC from the water. The adsorbent dose of 2 g/L best degraded SMT, TC and CP. Furthermore, the adsorption of SMT, TC and CP were best at 25^{o}C. The nature of adsorption process was feasible, endothermic and spontaneous. The ABs-loaded M_3-plN_2 was best desorb by using the solution of methanol 0.1N and the adsorbent was only successful after 2-3 adsorption-desorption cycles.

Finally, the proposed mechanisms for removing SMT, TC and CP by raw and nitrogen plasma modified steel shavings were hydrogen bonding, electrostatic and non- electrostatic interactions and redox reaction. In order to apply steel shavings as an adsorbent in wastewater treatment, it is necessary to study ABs removal in a semi-pilot scale.

Faculty of Engineering and Information Technology

CHAPTER 7

DEVELOPMENT OF A SEMI-PILOT TREATMENT DESIGN FOR REMOVING HMs AND ABs USING NITROGEN PLASMA MODIFIED STEEL SHAVINGS

7.1. Introduction

Water pollution caused by toxic heavy metals (HMs) and antibiotics (ABs) has been the subject of many studies due to the destructive effects of the pollutants on the ecosystem and human health (Badruddoza et al. 2013; Rajapaksha et al., 2015).

Metal ions such as lead (Pb^{2+}), copper (Cu^{2+}), cadmium (Cd^{2+}), chromium (Cr^{3+}) and zinc (Zn^{2+}) are toxic and they endanger communities, whole societies and the environment even at very low dosages. They are allergens or highly toxic carcinogenic mutagens, and ions can easily accumulate in the bodies of animals and aquatic organisms. Furthermore the human body can be impacted through bio-accumulation, bio-concentration and biomagnification when potential poisons are transported through the food chain (Hossain et al., 2014). Industries generate and discharge wastes containing different heavy metals into the environment, such as mining and smelting, surface-finishing, energy and fuel production, fertilizer and pesticides, metallurgy, iron and steel production, electroplating, electrolysis, electro-osmosis, leather tanning, photography, electric appliance manufacturing, metal surface treating, painting, etc. (Wang and Chen, 2009; Badruddoza et al., 2013).

ABs are used to abate illnesses suffered by humans and animals, and numerous ABs are being detected in surface and groundwater (Adams et al., 2002; Lu et al., 2016) supplies. Most of the chemicals originate from medical, municipal, and agricultural sources (Adams et al., 2002; Pouran et al., 2014). ABs can caused problems to the ecosystem in terms of dangerous toxicity and promote microbial resistance (Chen et al., 2011; Qiang et al., 2013; Fan et al., 2010; Lu et al., 2016). Some typical antibiotics analyzed in this research include sulfamethazine (SMT),

tetracycline (TC) and chloramphenicol (CP). For this reason it is critical to develop efficient and cost-effective techniques for removing HMs and ABs from water.

Different treatment techniques available for abating toxic metals exist, such as adsorption, chemical precipitation, ion exchange, coagulation, reverse osmosis, electrolysis and membrane processes (Fu and Wang, 2011; Nguyen et al., 2013). Additionally, a variety of methods to remove antibiotics and other pharmaceuticals from the aquatic matrix such as advanced oxidation processes, combined chemical/biological treatment, aerobic digestion integrated with activated carbon, ion exchange, coagulation, flocculation, sedimentation, ultraviolet irradiation, have been attempted (Adams et al., 2002; Homem and Santos, 2011; Qiang et al., 2013; Nie et al., 2015).

Of these techniques, however, the most efficient, economic and environmentally friendly is adsorption using cost-effective adsorbents to remove HMs and ABs from water (Hua et al., 2012; Tran et al., 2015; Qiang et al., 2013). Referring to the kinds of adsorbents, iron, particularly in its zero-valent (Fe^0) and oxides form, does function as a good candidate due to its adsorption ability and abundance (Cundy et al., 2008; Aredes et al., 2012, Pouran et al., 2014). Several kinds of iron-based adsorbents are magnetic in character, hence leading to good outcomes in the solid-liquid separation process under a magnetic field (Hua et al., 2012). Many types of magnetic adsorbents have been utilised for the removal of HMs and ABs from aqueous solution. These include, for instance, scrap iron, iron nanoparticles, magnetite, magnetic montmorillonite, iron oxides, persulfate activated by Fe^{2+} and zero-valent iron, microscale zero-valent iron, nanoscale zero-valent iron

(Oliveira et al., 2004a; Liu et al., 2008; Gupta et al., 2011; Gheju and Balcu, 2011; Hua et al., 2012; Ghauch et al., 2009; Xia et al., 2014; Nie et al., 2015).

Since magnetic waste is generated from industrial steel processing in large amounts, steel shavings have been studied for their ability to remove HMs and ABs (Rangsivek and Jekel, 2005; Gheju and Balcu, 2011; Tran et al., 2017). However, the number of studies on this process is very limited. Subsequently, more research is needed to understand more and confirm whether the application of steel shavings in removing HMs and ABs from water is warranted. One of the most promising modification methods for Fe^0 is plasma cleaning.

From the previous results in batch studies (chapter 5 and chapter 6), nitrogen plasma modified steel shavings (M_3-plN_2) have successfully removed HMs as well as ABs from water. As the next step, adsorption research has been conducted at semi-pilot scale for synthesized wastewater. This chapter aims to design an effective wastewater treatment unit at semi-pilot scale (up to $5m^3$/day) and discover the best or optimum operating conditions for removing HMs and ABs.

7.2. Selecting treatment unit

When selecting a potentially well-designed treatment unit utilising the StS for removing HMs from water, different designs have been assessed (see 3.2.6A in chapter 3). The semi-pilot experiments were conducted with synthesized wastewater using the three designs.

7.2.1. Removal of HMs by different treatment designs

As described above (3.2.6, chapter 3), concentrations of HMs in the wastewater were added before using them for semi-pilot tests and measured by MP-AES as Pb^{2+} 5.94, Cu^{2+} 4.74, Cd^{2+} 6.48, Cr^{3+} 6.44 and Zn^{2+} 5.18 mg/L. Figure 7.1

shows the remaining concentrations of the HMs by StS using the four treatment units.

Based on the experimental results, design 1 and design 2 (see 3.2.6A in chapter 3) did not successfully remove metal ions from water. With design 1, the remaining concentrations of Pb^{2+}, Cu^{2+}, Cd^{2+}, Cr^{3+}, Zn^{2+} after treatment with the design did reach 2.65, 2.86, 4.02, 3.15, and 2.98 mg/L, respectively. Similar outcomes were recorded with the removal of metal ions in design 2. The remaining concentrations of Pb^{2+}, Cu^{2+}, Cd^{2+}, Cr^{3+}, and Zn^{2+} in the outlet flow with design 2 reached 3.97, 3.1, 5.03, 4.78, and 3.58 mg/L, also respectively. Thus, the removal process using the two designs proved to be ineffective. These outcomes can be explained by the contact between M_3-plN_2 and the aqueous solution. The materials were stored inside the bags as well as the high density of the StS, so the water flow pressure was not enough for water to establish good contact with the materials, especially the particles inside the bulk of the M_3-plN_2.

In contrast, the removal efficiency had much better potential when referring to the column design. With design 3 when the flow rate was $5m^3$/day, Pb^{2+}, Cu^{2+}, Cd^{2+}, Cr^{3+} and Zn^{2+} in water were completely removed during most of the running time. The levels of Pb^{2+}, Cu^{2+}, Cd^{2+}, Cr^{3+} and Zn^{2+} in the effluent were less than 0.007, 0.16, 0.008, 0.096 and 0.16 mg/L, respectively. Furthermore they were lower than limited standards as advised in the US-EPA guideline (Nguyen et al., 2013). The above outcomes confirmed that design 3 was the most effective treatment unit for removing HMs from wastewater. For this reason the column design served for the subsequent experiments on removing HMs by M_3-plN_2 in the semi-pilot scale context.

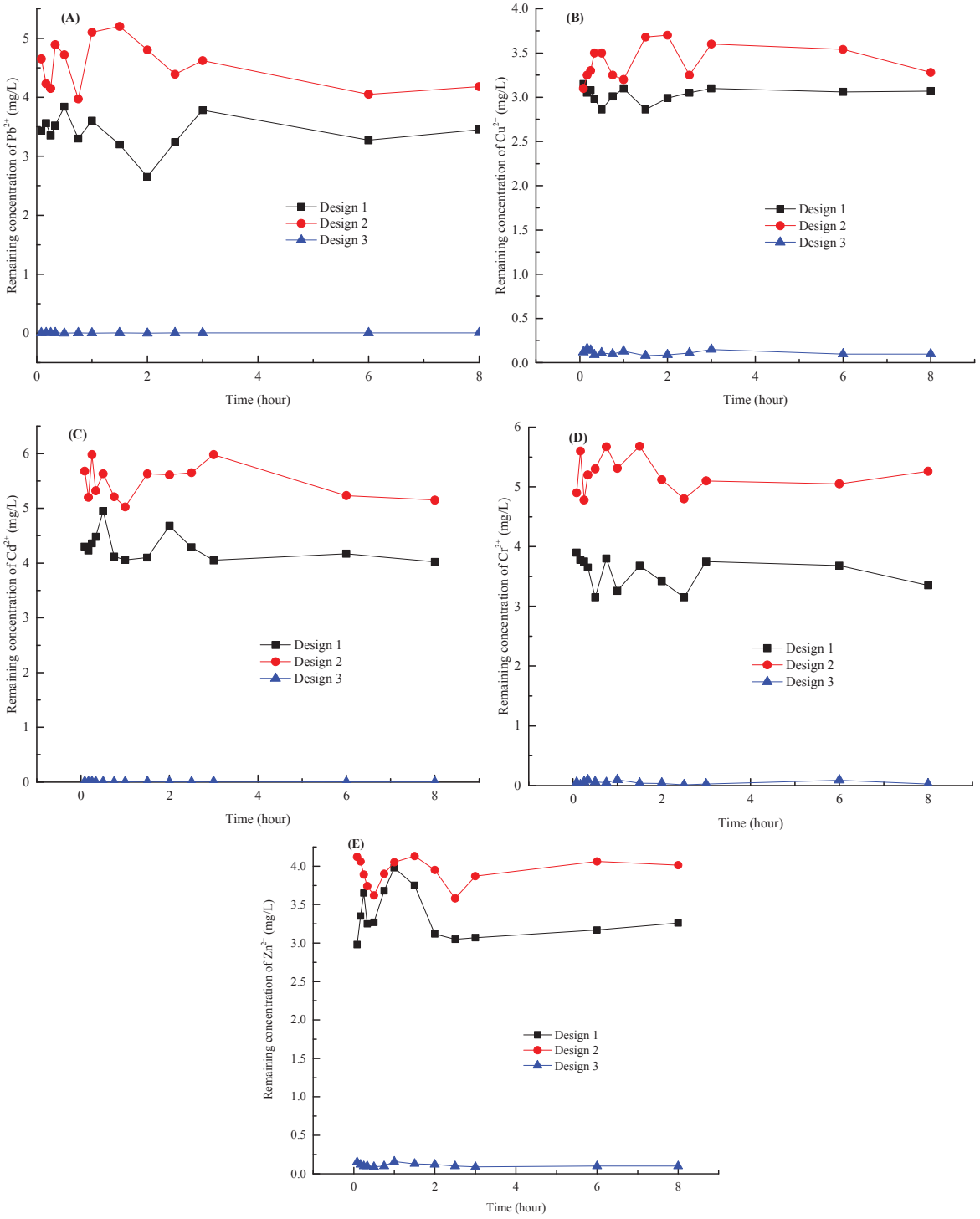

Figure 7.1 Remaining concentrations of HMs in the outlet flow after treatment using nitrogen plasma modified StS (M_3-plN_2) with different designs: (A) Pb^{2+}; (B) Cu^{2+}; (C) Cd^{2+}; (D) Cr^{3+} and (E) Zn^{2+}

7.2.2. Removal of ABs by different treatment designs

The same procedure for removing HMs was applied to study ABs (combined SMT, TC and CP solutions) uptake from synthesized wastewater using column design. Experiments were executed with specific initial concentrations of ABs, these being SMT 100.1, TC 97.3 and CP 99.5 µg/L, at room temperature and the natural pH value. Figure 7.2 illustrates the remaining concentrations of ABs in water after treatment using M_3-plN_2.

Similar results involving HMs removal experiments in semi-pilot scale were achieved in the ABs removal study. Design 1 and design 2 failed to remove the ABs from the synthesized wastewater. At contact time lasting 8 hours the remaining concentrations of SMT, TC and CP in the outlet flow were: firstly, 81.6, 72.1, and 64.6 µg/L with design 1; and secondly, 95.8, 91.57, and 85.7 µg/L with design 2. Conversely, design 3 did effectively abate the ABs from wastewater. The remaining concentrations of SMT, TC and CP in the effluent at 8 hours of treating time were 1.93, 1.62 and 1.1 µg/L. Therefore design 3 was selected for the following experiments in semi-pilot scale study on removing ABs via M_3-plN_2.

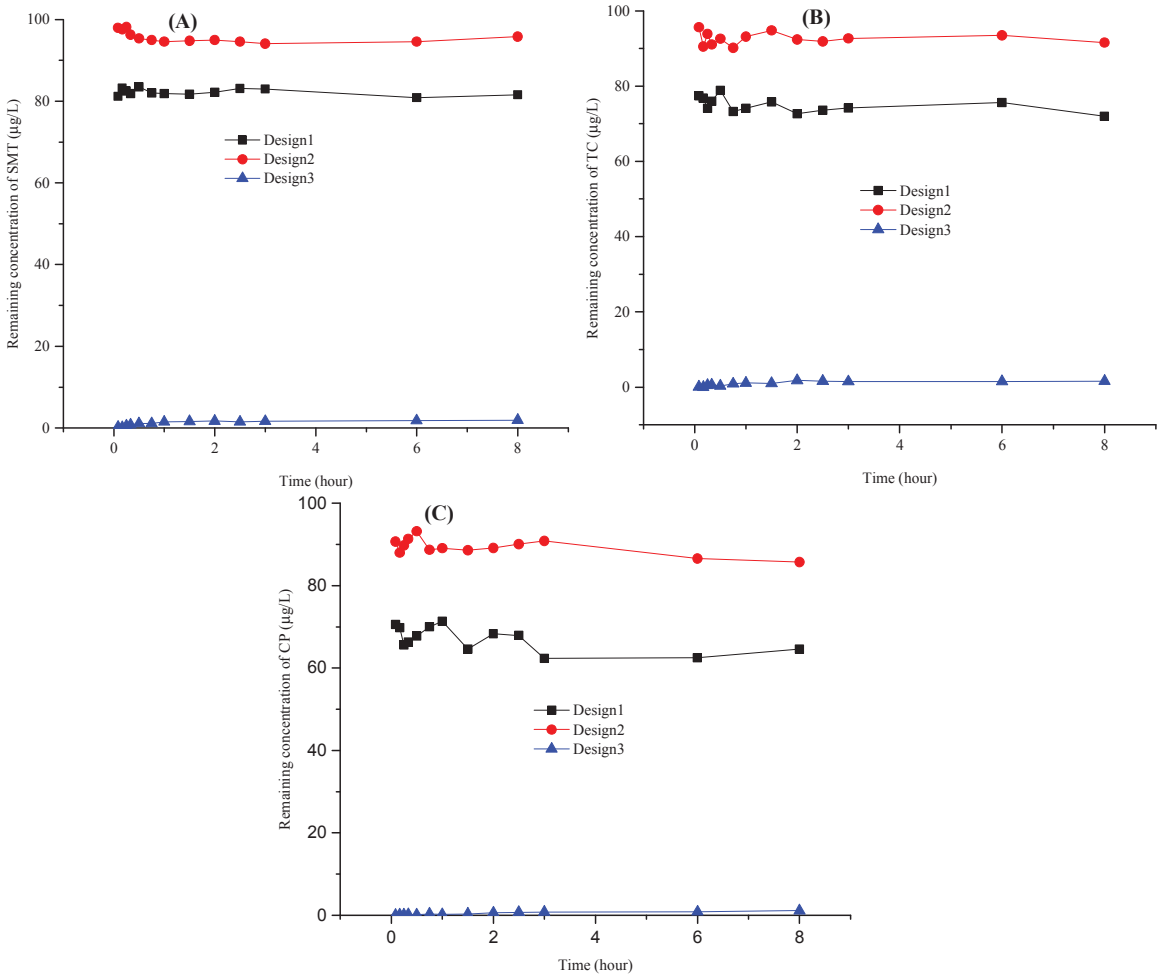

Figure 7.2 Remaining concentrations of ABs in the outlet flow after semi-pilot scale treatment units using M_3-plN_2: (A) SMT; (B) TC and (C) CP

7.3. HMs removal in the column design

7.3.1. Affecting factors

A. Flow rate

The effects of influent flow rate (m^3/day or L/min) on the efficiency in removing HMs by nitrogen plasma modified StS are shown in Figure 7.3. Various flow rates (2500, 5000, 7500 and 10000 L/day or equivalent to 1.74, 3.47, 5.21, and 6.94 L/min, respectively) were chosen to examine the effects of metal ions' adsorption ability on M_3-plN_2. Judging by the results, the flow rate had a great impact on removing HMs from water by M_3-plN_2 in the fixed-bed column design.

The breakthrough curves for the adsorption in the column are determined by plotting the C_t/C_o (C_t is the concentration of metal ions at time t and C_o is the initial concentration of HMs) against the time (t) and displayed in Figure 7.3 and Table 7.1.

The effects indicated that the shorter breakthrough time occurred at higher flow rate, which is explained by the fact that the higher the flow rate, then more water passed through the column. As a result, more metal ions became attached to the binding sites of M_3-plN_2 and caused the adsorbent to be saturated more rapidly. These results agreed with previous studies which concluded that higher flow rate brought about a lower residence time and vice versa (Acheampong et al., 2013). Thus, the high flow rate decreased the service time of the fixed-bed column as shown in Figure 7.3 (Hossain, 2013).

Table 7.1 shows that with the high flow rates of 6.94 and 5.21 L/min, the metal ions were not removed effectively. In case of Pb^{2+} ion, the breakthrough times (t_b) at the two flow rates were undefined as outlet concentrations were higher than 10% of the initial concentration of HMs. For Cu^{2+}, Cd^{2+}, Cr^{3+} and Zn^{2+}, the t_b was undefined at a flow rate of 6.94 L/min. However, the breakthrough times at the flow rate of 5.21 L/min were also short and achieved at 120, 298, 220 and 298 min for Cu^{2+}, Cd^{2+}, Cr^{3+} and Zn^{2+}, respectively.

In contrast, flow rates of 1.74 and 3.47 L/min are suitable for removing HMs by M_3-plN_2. The breakthrough time (t_b) and exhaustion/service time (t_s) ranged from 440 to 1920 min and 3360 to 12350 min, respectively. The achieved breakthrough time, service time and adsorption capacities demonstrated that 3.47 L/min was the optimal flow rate for removing HMs (Pb^{2+}, Cu^{2+}, Cd^{2+}, Cr^{3+} and Zn^{2+}) by M_3-plN_2 in the column design (Figure 7.3 and Table 7.1). Consequently, this value of flow rate was chosen for the following experiments.

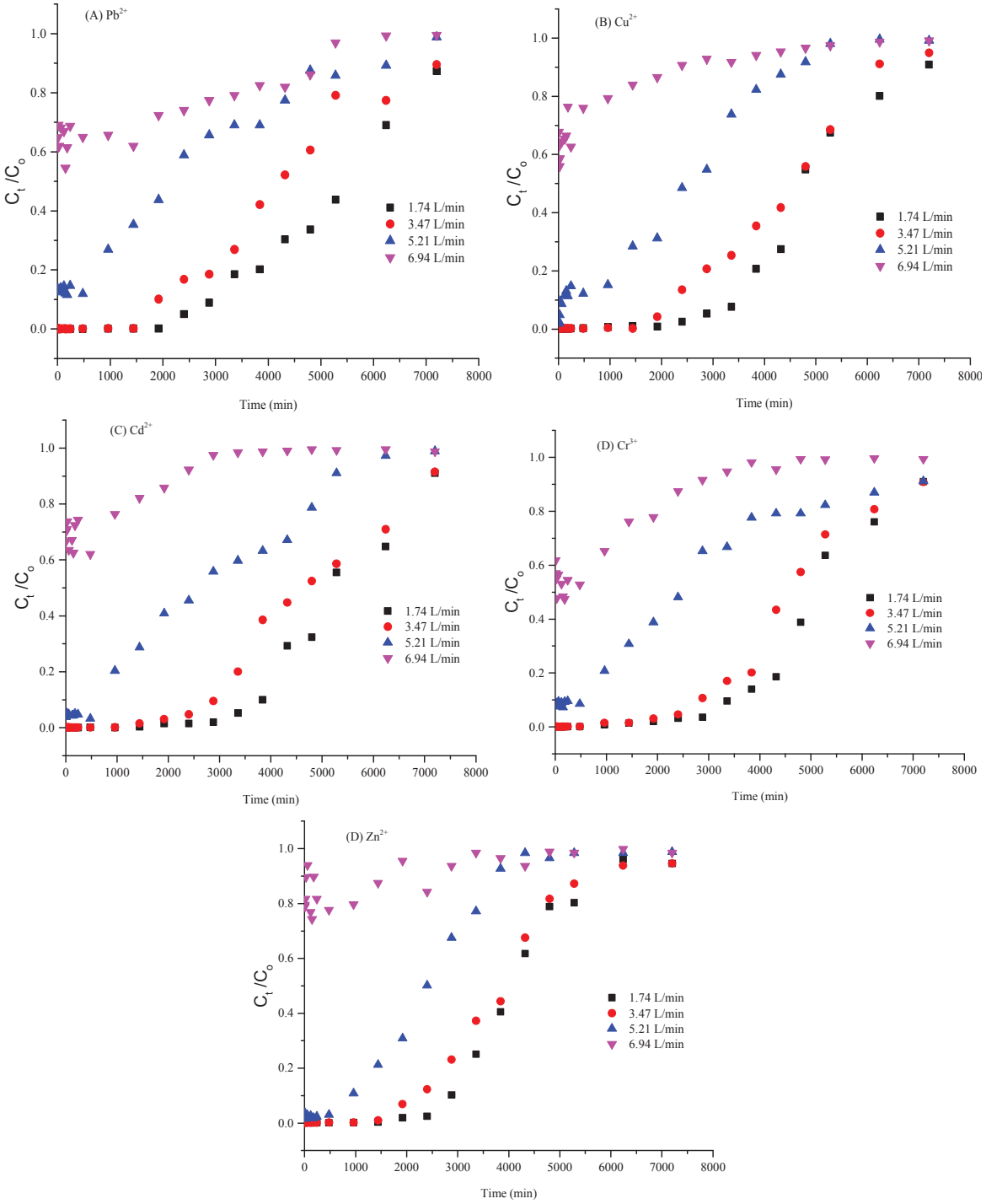

Figure 7.3 Effects of flow rate on the breakthrough curve of HMs adsorption on M_3-plN_2: (A) Pb^{2+}; (B) Cu^{2+}; (C) Cd^{2+}; (D) Cr^{3+} and (E) Zn^{2+} (natural pH, bed height = 35 cm; initial concentrations (C_o) of HMs: Pb^{2+} 5.94; Cu^{2+} 4.74; Cd^{2+} 6.48; Cr^{3+} 6.44 and Zn^{2+} 5.18 mg/L)

B. Bed height

The breakthrough curves for varying bed heights (20, 35 and 50cm), given the flow rate of 3.47 L/min are illustrated in Figure 7.4 and Table 7.1. The results revealed that the lower bed height the shorter breakthrough curves occurred. For instance, the breakthrough time (at C_t/C_o 10%) of Pb^{2+} adsorption was 480, 960 and 1920 min when the bed height was 20, 35, and 50 cm, respectively. Similarly, the service time (at C_t/C_o 90%) of the adsorptive removal of lead increased from 3698 to 10560 min when the bed height rose from 20 to 50 cm.

As listed in Table 7.1, the adsorption capacities of HMs on M_3-plN_2 at exhaustion points with different bed heights of 20, 35 and 50 cm were as follows: Pb^{2+} 12.7, 14.06 and 14.51 mg/g; Cu^{2+} 9.1, 11.16 and 11.05 mg/g; Cd^{2+} 8.36, 8.95 and 9.2 mg/g; Cr^{3+} 7, 7.15 and 7.35 mg/g; and Zn^{2+} 9.35, 10.25 and 10.39 mg/g, respectively. The results were in agreement with competitive adsorption data in batch experiments where the order of HMs adsorption capacities (in mg/g) reduced as: $Pb^{2+}>Cu^{2+}>Zn^{2+}>Cd^{2+}>Cr^{3+}$. Moreover, the column adsorption capacities of HMs at exhaustion points were approximately 80 - 85% of the Langmuir maximum competitive adsorption capacities in batch experiments.

These outcomes suggested that an increase in bed height from 20 to 50 cm resulted in more HMs uptake. Based on these outcomes, it seems that when the bed height rose, the diffusion of metallic ions into the adsorbent increased (Malkoc and Nuhoglu, 2006; Taty-costodes et al., 2005). However, when the bed height increased from 35 to 50 cm, the adsorption capacities did slightly increase or remained the same, thus demonstrating that the optimal condition state was virtually reached at the bed height of 35 cm. Moreover, according to Sousa et al. (2010) it is evident at a high bed height (50 cm) the M_3-plN_2 was not dispersed properly in the used flow rate of 3.47 L/min. Therefore this caused the uptake capacities remain or to decline.

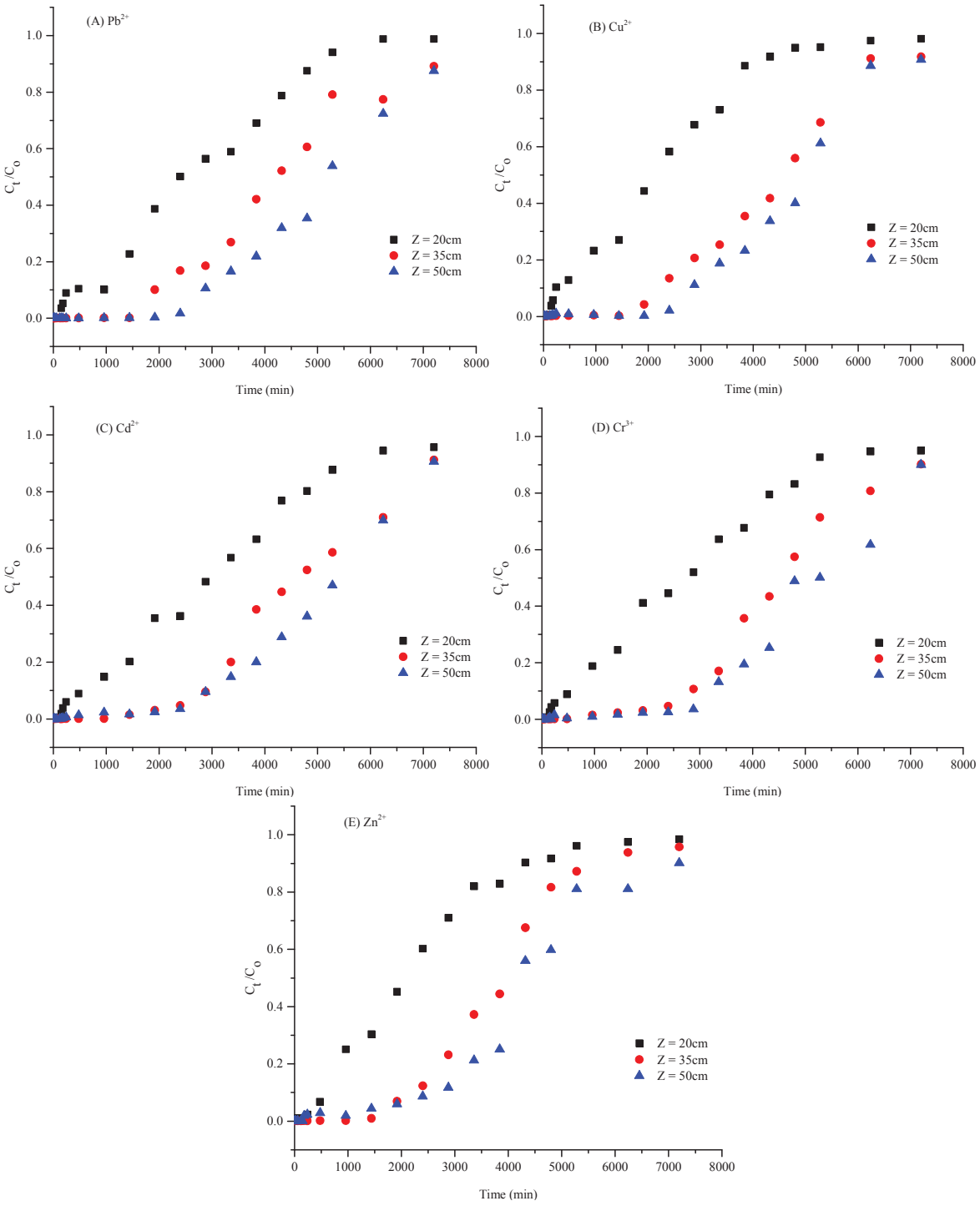

Figure 7.4 Effects of bed height (Z) on the breakthrough curve of HMs adsorption on M_3-plN_2: (A) Pb^{2+}; (B) Cu^{2+}; (C) Cd^{2+}; (D) Cr^{3+} and (E) Zn^{2+} (natural pH, flow rate = 3.47 L/min; initial concentrations (C_o) of HMs: Pb^{2+} 5.94; Cu^{2+} 4.74; Cd^{2+} 6.48; Cr^{3+} 6.44 and Zn^{2+} 5.18 mg/L)

Table 7.1 Breakthrough curve parameters for HMs adsorption onto M_3-plN_2 at different operating conditions

HMs	Flow rate, Q (L/min)	Bed height, Z (cm)	t_b (min)	V_b (L)	q_b (mg/g)	R_b (%)	t_s (min)	V_s (L)	q_s (mg/g)	R_s (%)
Pb^{2+}	1.74	35	1920	3340.8	1.89	94.9	12350	21489	12.16	12.6
	3.47	35	960	3331	1.88	99.8	7160	24845	14.06	17.5
	5.21	35	-	-	-	-	4320	22507	12.73	12.5
	6.94	35	-	-	-	-	3360	23318	13.19	13.8
	3.47	20	480	1666	1.65	96.5	3698	12832	12.7	31
	3.47	50	1920	6662	2.64	99.7	10560	36643	14.51	22.6
Cu^{2+}	1.74	35	1750	3045	1.37	92.4	12320	21437	9.68	19.8
	3.47	35	925	3209.8	1.45	95.8	7124	24720	11.16	31.4
	5.21	35	120	625.2	0.28	88.4	4452	23195	10.47	18.4
	6.94	35	-	-	-	-	2400	16656	7.52	16
	3.47	20	462	1603	1.27	94.3	3320	11520	9.1	27
	3.47	50	1880	6524	2.06	97.9	10090	35012	11.06	38.8
Cd^{2+}	1.74	35	1025	1783.5	1.1	94.8	8960	15590	9.62	35.2
	3.47	35	496	1721.1	1.06	95.2	4180	14505	8.95	29
	5.21	35	298	1552.6	0.96	91.4	2480	12921	7.97	38
	6.94	35	-	-	-	-	1980	13741	8.48	23.6
	3.47	20	260	902.2	0.97	94	2230	7738	8.36	43.2
	3.47	50	860	2984	1.29	96.5	6136	21292	9.2	30.1
Cr^{3+}	1.74	35	1160	2018.4	1.24	94.7	7200	12528	7.68	23.9
	3.47	35	440	1526.8	0.94	95.3	3360	11659	7.15	28.6
	5.21	35	220	1146.2	0.7	79.5	1940	10107	6.2	33.2
	6.94	35	-	-	-	-	1440	9994	6.13	22.2
	3.47	20	252	874.4	0.94	95.7	1880	6524	7.0	32.3
	3.47	50	810	2811	1.21	97.7	4930	17107	7.35	38.2
Zn^{2+}	1.74	35	1360	2366.4	1.17	89.8	12260	21332	10.52	21.1
	3.47	35	560	1943.2	0.96	93.1	5988	20778	10.25	32.4
	5.21	35	298	1552.6	0.77	89.2	3840	20006	9.87	7.3
	6.94	35	-	-	-	-	1920	13325	6.57	4.4
	3.47	20	298	1034	0.89	93.2	3120	10826	9.35	29
	3.47	50	1106	3838	1.33	95.6	8670	30085	10.39	40.2

Notation: Q - volumetric flow rate (L/min); Z - bed height (cm); t_b, V_b – the service time and treated volume at 10% breakthrough point (L); t_s, V_s – the service time and treated volume at 90% saturation point; q_b, q_s – the amount of metal ions loaded per unit of dry weight of M_3-plN_2 at 10% breakthrough point and 90% saturation points, respectively; R_b, R_s – the removal percentage of metal ions at 10% breakthrough point and 90% saturation points, respectively; -: undefined values.

7.3.2. Breakthrough curves modeling

The results following the calculation of the breakthrough curves modeling for experimental data on HMs removal by M_3-plN_2 column are shown in Table 7.2.

A. Adams–Bohart model

As can be seen in Table 7.2, the adsorption capacities of Pb^{2+} and Cu^{2+} onto the M_3-plN_2 bed (N_o) increased when the flow rate rose from 1.74 to 6.94 L/min. The adsorption capacities ($x10^3$) at flow rates of 1.74, 3.47, 5.21 and 6.94 L/min were, respectively, 5.47, 10.25, 17.80 and 24.82 mg/L for Pb^{2+} ion; and 4.31, 8.13, 10.97, and 16.73 mg/L for Cu^{2+} ion, also respectively. However, changes in the flow rate insignificantly affected the N_o values in the cases of Cd^{2+}, Cr^{3+} and Zn^{2+}. These results were due to the higher flow rate leading to larger amounts of HMs passing through the bed and then more ions becoming attached to the adsorbent's surface. The kinetic constant (k_{AB}) decreased when - in all the metal ions - the flow rate increased.

In contrast, N_o values fell when the bed height increased from 20 to 50 cm. Furthermore, the growing bed height from 20 to 50 cm resulted in an increase in the K_{AB} constant. The outcomes specified a good arrangement between the experimental data and predicted values, suggesting that Adams–Bohart may be valid for modeling adsorption processes of HMs onto M_3-plN_2 (Han et al., 2009). This conclusion was also confirmed by the obtained correlation coefficients which proved to be quite high. While Adams–Bohart is a simple and comprehensive model for evaluating the fixed-bed column adsorption, its validity depends on the conditions being employed (Kundu and Gupta, 2005).

B. Thomas model

Table 7.2 shows that the Thomas rate constant (k_{Th}) of HMs adsorption onto M_3-plN_2 tended to decrease when the flow rate increased from 1.74 to 6.94 L/min. Adsorption capacities of metal ions were negative at 6.94 L/min, suggesting the flow rate was too high for good adsorption performance. Referring to the remaining flow rates (1.74, 3.47 and 5.21 L/min), achieved q_o values at a flow rate of 3.47 L/min were the highest for all five HMs. These outcomes agreed with effects of flow rate on the HMs removal process, thus demonstrating that the flow rate of 3.47 L/min was the best one for removing HMs from the synthesized wastewater by M_3-plN_2 in the fixed-bed column. Apart from this, an increase in the bed height (20 to 50 cm) caused the Thomas rate constant to: slightly increase in the cases of Pb^{2+} and Cd^{2+}; an increase (from 20 to 35 cm) and a decrease (from 35 to 50 cm) in the case of Cr^{3+}; and almost no changes in the Cu^{2+} and Zn^{2+}.

The correlation cofficients of the Thomas model were mostly higher than those of the Adams–Bohart model, indicating that the Thomas model could appropriately be applied to HMs adsorption onto M_3-plN_2 column. In comparison with the other adsorbents, the adsorption capacities of M_3-plN_2 were equal and relatively poorer, but the adsorbents were cost-effective when treating water (Han et al., 2009; Han et al., 2006b).

C. Yoon–Nelson model

The Yoon–Nelson model parameters (k_{YN} and τ) are presented in Table 7.2. The k_{YN} and τ values relatively reduced when the flow rate increased from 1.74 to 6.94 L/min. It can be explained by the faster saturation of the column at higher flow rate (Sharma and Singh, 2013). These results disagreed with those documented by

Hossain (2013) for the removal of Pb^{2+}, Cu^{2+}, Cd^{2+} and Zn^{2+} onto cabbage powder. The outcomes also illustrated that the HMs removal process was not successful at a flow rate of 6.94 L/min or 10000 L/day. This very high flow rate led to not enough time for HMs to become attached to the M_3-plN_2'surface and when the outlet concentrations of HMs were too high, the τ values in Yoon-Nelson model proved to be negative.

Table 7.2 confirms that at higher bed heights, τ values were extended. A similar trend was reported by Hossain (2013) and Nguyen (2015). The correlation coefficients (R^2) of the Yoon–Nelson model in most cases are the same as those of the Thomas model but higher than the Adams–Bohart model. This proves that the Thomas and Yoon–Nelson models fitted better to the adsorption of HMs onto M_3-plN_2 bed than the Adams–Bohart model.

Table 7.2 Adams–Bohart, Thomas and Yoon-Nelson model constants for HMs adsorption onto M_3-plN_2 column

HMs	Conditions		Adams–Bohart			Thomas			Yoon-Nelson		
	Q (L/min)	Z (cm)	k_{AB}	N_o	R^2	k_{Th}	q_o	R^2	k_{YN}	τ	R^2
Pb^{2+}	1.74	35	2.19	5.47	0.901	2.53	5.07	0.941	1.5	5147.8	0.941
	3.47	35	2.19	10.25	0.860	2.69	8.9	0.921	1.6	4534.25	0.921
	5.21	35	0.51	17.80	0.868	1.35	7.11	0.968	0.8	2411.25	0.968
	6.94	35	0.12	24.82	0.881	0.84	-1.96	0.788	0.5	-499	0.788
	3.47	20	1.85	17.43	0.705	2.53	11.59	0.806	1.5	3374.67	0.806
	3.47	50	2.53	7.31	0.931	2.69	7.22	0.967	1.6	5236.13	0.968
Cu^{2+}	1.74	35	2.32	4.31	0.965	2.74	3.94	0.990	1.3	5015.77	0.990
	3.47	35	2.32	8.13	0.895	2.95	6.93	0.961	1.4	4424.36	0.961
	5.21	35	1.05	10.97	0.769	2.32	6.04	0.955	1.1	2447.64	0.955
	6.94	35	0.15	16.73	0.761	1.27	-3.45	0.978	0.6	-1049.8	0.978
	3.47	20	1.9	12.21	0.593	2.95	8.51	0.824	1.4	3103.57	0.824
	3.47	50	2.32	6.36	0.832	2.95	5.37	0.894	1.4	4901.79	0.894
Cd^{2+}	1.74	35	1.85	12.23	0.957	2.01	6.06	0.980	1.3	5643.62	0.980
	3.47	35	1.85	11.55	0.897	2.16	10.6	0.951	1.4	4950.14	0.951
	5.21	35	0.77	11.61	0.832	1.54	9.77	0.971	1.0	3038.6	0.971

HMs	Conditions		Adams–Bohart			Thomas			Yoon-Nelson		
	Q (L/min)	Z (cm)	k_{AB}	N_o	R^2	k_{Th}	q_o	R^2	k_{YN}	τ	R^2
	6.94	35	0.11	10.34	0.781	1.23	-4.16	0.892	0.8	-970.63	0.892
	3.47	20	1.39	17.86	0.626	2.01	13.38	0.808	1.3	3570.15	0.808
	3.47	50	1.85	8.25	0.804	2.16	7.56	0.872	1.4	5043.36	0.872
Cr^{3+}	1.74	35	1.71	12.47	0.950	2.02	5.68	0.984	1.3	5321.54	0.984
	3.47	35	1.71	11.73	0.927	2.17	9.92	0.977	1.4	4658.93	0.977
	5.21	35	0.62	11.53	0.853	1.09	10.25	0.951	0.7	3207.14	0.951
	6.94	35	0.16	11.84	0.814	1.24	-0.12	0.952	0.8	-27.13	0.952
	3.47	20	1.4	17.45	0.606	2.02	13.01	0.794	1.3	3493.38	0.794
	3.47	50	1.71	8.75	0.827	2.02	7.7	0.896	1.2	5321.33	0.932
Zn^{2+}	1.74	35	2.32	9.04	0.929	3.09	3.7	0.976	1.6	4307.5	0.976
	3.47	35	2.32	8.51	0.892	2.9	7.39	0.965	1.5	4318.93	0.965
	5.21	35	1.35	7.95	0.822	2.7	6.68	0.953	1.4	2597.93	0.953
	6.94	35	0.06	10.61	0.594	0.97	-10.18	0.732	0. 5	-2974	0.732
	3.47	20	1.74	13.79	0.687	2.9	8.99	0.884	1.5	3001.4	0.884
	3.47	50	2.12	6.34	0.754	2.7	5.36	0.848	1.4	4471.71	0.848

Notation: Q - volumetric flow rate (L/min); Z - bed height (cm); k_{AB} - Adams–Bohart model rate constant (L/mg min)x10^{-4}; N_o – saturation concentration (mg/L)x10^3; k_{Th} – Thomas model rate constant (mL/mg min)x10^{-4}; q_o – equilibrium HMs adsorption capacity (mg/g); k_{YN} - Yoon-Nelson model rate constant (1/min)x10^{-3}; τ – the time required for 50% breakthrough (min); R^2 values - the correlation coefficients.

D. BDST model

BDST parameters (N_o and K_b) and bed depth (Z_o) for breakthrough points (10%) and exhaustion point (90%) (constant concentration of HMs: Pb^{2+} 5.94; Cu^{2+} 4.74; Cd^{2+} 6.48; Cr^{3+} 6.44 and Zn^{2+} 5.18 mg/L; flow rate of 3.47 L/min) are listed in Figure 7.5 and Table 7.3. The quite high correlation coefficients confirmed that the BDST model fitted relatively well to the HMs-M_3-plN_2 dynamic adsorption system. However, negative Z_o values at exhaustion point in Table 7.3 confirmed that the BDST can suitably describe the initial part (10-50%) of the breakthrough curve only (Jain et al., 2013). The column adsorption capacities N_o of HMs at breakthrough 10% were as follows: Pb^{2+} 70.03; Cu^{2+} 76.84; Cd^{2+} 95.49; Cr^{3+} 94.9; and Zn^{2+} 61.07 mg/L.

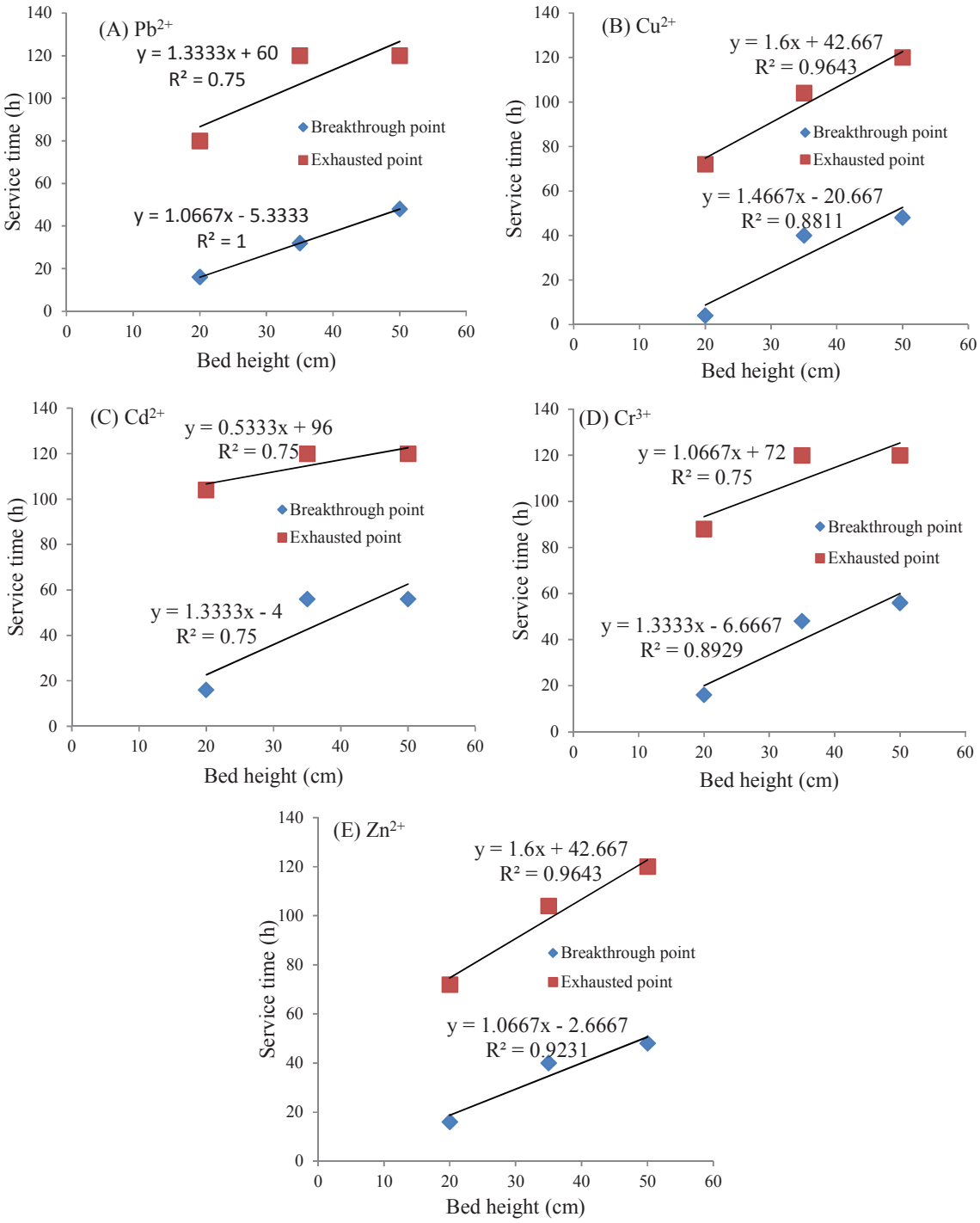

Figure 7.5 BDST model plots for 10% and 90% breakthrough of Pb^{2+}, Cu^{2+}, Cd^{2+}, Cr^{3+}, Zn^{2+} adsorption onto M_3-plN_2 column at different bed heights (natural pH, flow rate = 3.47 L/min; initial concentrations (C_o) of HMs: Pb^{2+} 5.94; Cu^{2+} 4.74; Cd^{2+} 6.48; Cr^{3+} 6.44 and Zn^{2+} 5.18 mg/L)

Table 7.3 BDST model constants for HMs adsorption onto M_3-plN_2

Metal ion	Breakpoint (%)	N_o (mg/L)	K_b (L/mg h)	Z_o (cm)	R^2
Pb^{2+}	10	70.03	0.0694	5	1
	90	87.53	0.0062	-45	0.75
Cu^{2+}	10	76.84	0.0224	14.1	0.881
	90	83.82	0.0109	-26.7	0.964
Cd^{2+}	10	95.49	0.0848	3	0.75
	90	38.19	0.0035	-80	0.75
Cr^{3+}	10	94.90	0.0512	5	0.893
	90	75.93	0.0047	-67.5	0.75
Zn^{2+}	10	61.07	0.1591	2.5	0.923
	90	91.60	0.0099	-26.7	0.964

7.4. ABs removal in the column design

7.4.1. Affecting factors

A. Flow rate

The effects of flow rates (1.74; 3.47; 5.21 and 6.94 L/min) on the adsorption breakthrough of ABs by M_3-plN_2 column are shown in Figure 7.6. The results illustrate that flow rate significantly affected the ABs adsorption onto the adsorbent. The breakthrough time decreased when the flow rate increased. In their research, Kim et al. (2010) achieved the same outcome regarding the removal of the antibiotic known as trimethoprim by powdered and granular activated carbon. A similar explanation for HMs adsorption can be proposed whereby at a high flow rate more ABs binding on the M_3-plN_2's surface and this makes the adsorption process reach saturation more quickly (Acheampong et al., 2013).

The listed parameters in Table 7.4 indicate that the M_3-plN_2 bed ineffectively removed ABs from wastewater at high flow rates, specifically 5.21 and 6.94 L/min. For all three ABs, the breakthrough times (t_b) at the flow rates were undefined due to the outlet concentrations being higher than 10% of the initial concentration of ABs. Nevertheless, ABs adsorption onto the M_3-plN_2 column was effective at flow rates of

1.74 and 3.47 L/min. At the flow rate of 3.47 L/min, the highest adsorption capacities of ABs onto the adsorbent at exhaustion time were achieved: SMT 470.74, TC 363.61 and CP 514.61 µg/g. These column adsorption capacities of ABs onto the M_3-plN_2 column were about 48 – 59 % of the competitive adsorption capacities which observed from batch experiments. Hence, 3.47 L/min was chosen as the optimal flow rate for evaluating the applicability of M_3-plN_2 fixed-bed column to abate ABs from wastewater for the next experiments.

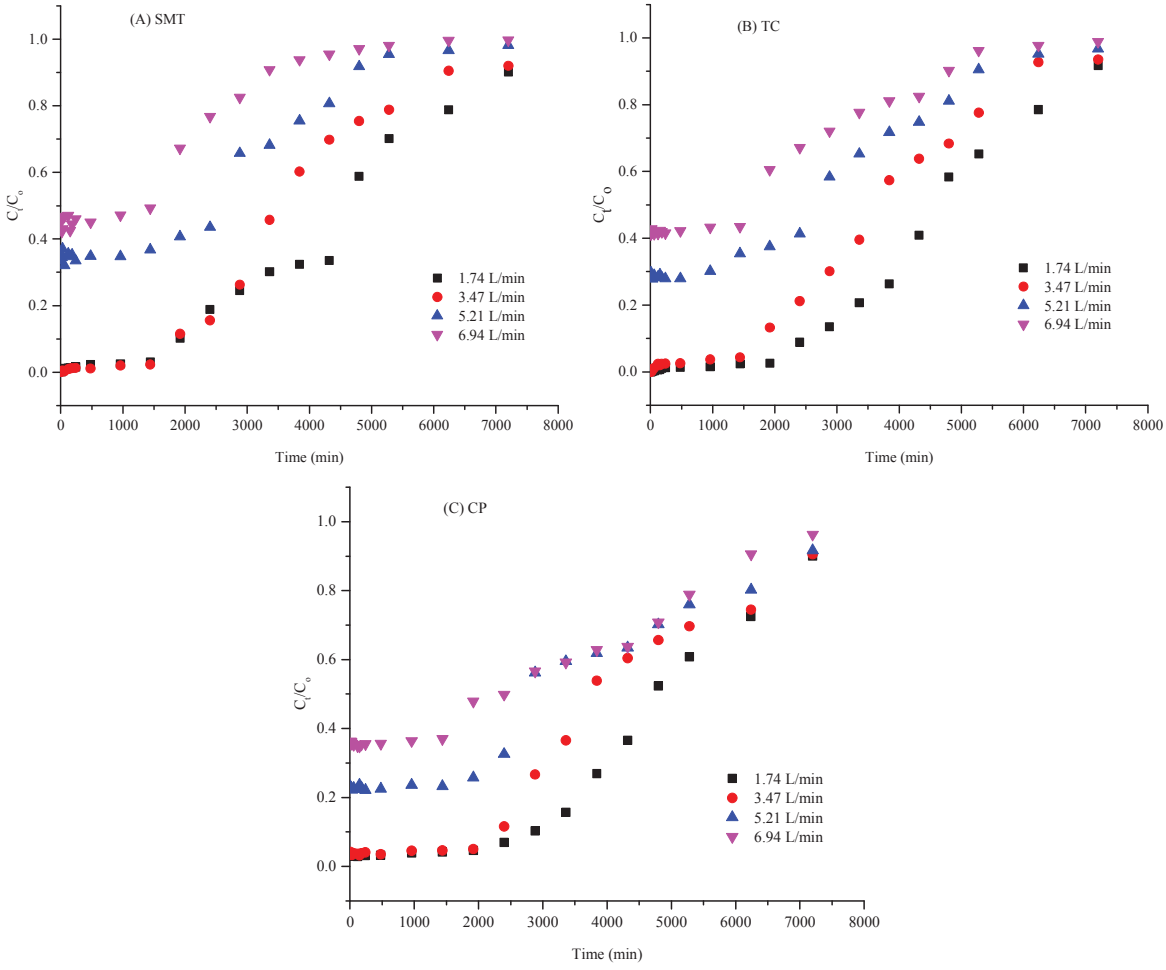

Figure 7.6 Effects of flow rate on the breakthrough curve of ABs adsorption on M_3-plN_2: (A) SMT; (B) TC and (C) CP (natural pH, bed height = 35 cm; initial concentrations (C_o) of ABs: SMT 100.1; TC 97.3 and CP 99.5 µg/L)

B. Bed height

Figure 7.7 and Table 7.4 depict the influences of bed heights from 20 to 50 cm on the breakthrough curves of ABs adsorption onto M_3-plN_2. Generally, an increase in the bed height led to the growth of breakthrough and exhaustion times. Specifically, when bed height increased from 20 to 50 cm, t_b of SMT, TC and CP rose from 690 to 2230, 586 to 2030 and 1030 to 2750 min, respectively. This finding can be explained by the higher the bed height the longer the contact time of ABs with adsorbent in the column (Kim et al., 2010). Furthermore, the column adsorption capacities of ABs on the M_3-plN_2 bed at exhaustion point significantly rose with an increase of bed height from 20 to 35 cm. However, when the bed height rose from 35 to 50 cm this virtually had no effect on the adsorption capacities. These data confirmed that the best operating condition was achieved when the bed height was 35 cm.

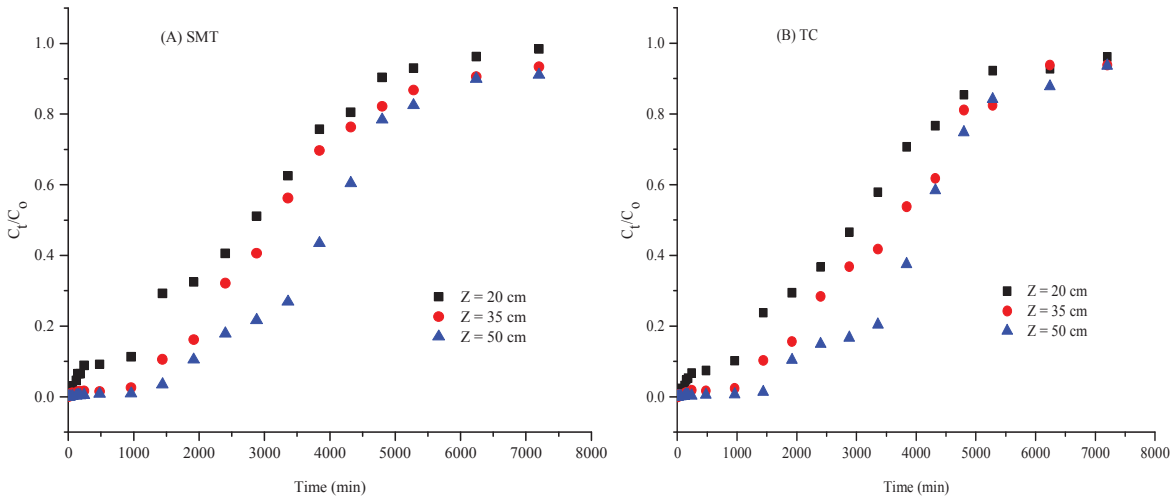

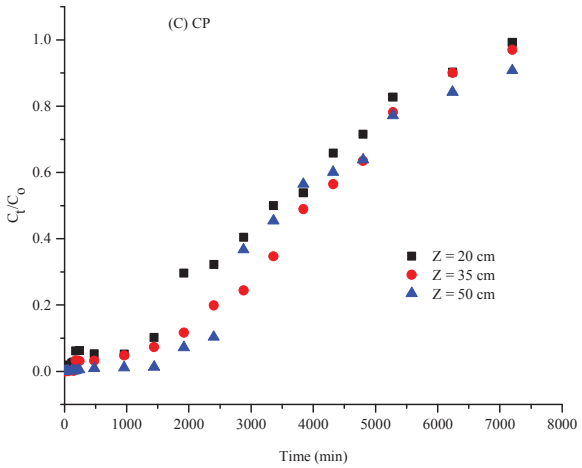

Figure 7.7 Effects of bed height (Z) on the breakthrough curve of ABs adsorption on M_3-plN_2: (A) SMT; (B) TC and (C) CP (natural pH, flow rate = 3.47 L/min; initial concentrations (C_o) of ABs: SMT 100.1; TC 97.3 and CP 99.5 µg/L)

Table 7.4 Breakthrough curve parameters for ABs adsorption onto M_3-plN_2 at different operating conditions

ABs	Q (L/min)	Z (cm)	t_b (min)	V_b (L)	q_b (µg/g)	R_b (%)	t_s (min)	V_s (L)	q_s (µg/g)	R_s (%)
SMT	1.74	35	2920	5081	48.4	89.8	23652	41154	392.34	21.2
	3.47	35	1440	4997	47.6	91.7	14230	49378	470.74	17.8
	5.21	35	-	-	-	-	8623	44926	428.29	19.3
	6.94	35	-	-	-	-	5320	36921	351.98	17.5
	3.47	20	690	2394.3	39.94	90.8	7160	24845.2	414.5	19.5
	3.47	50	2230	7738.1	51.6	92.6	20632	71593	477.76	17.5
TC	1.74	35	2880	5011	46.44	86.5	22305	38811	358.54	21.5
	3.47	35	1360	4719	43.73	90.8	11308	39239	363.61	17.6
	5.21	35	-	-	-	-	7035	36652	338.6	18.9
	6.94	35	-	-	-	-	4800	33312	307.74	17.6
	3.47	20	586	2033	32.98	91.4	6030	20924.1	339.32	14.6
	3.47	50	2030	7044	45.69	91.1	16650	57775.5	374.77	12.2
CP	1.74	35	3960	6890	64.97	87.9	26893	46794	443.43	27.5
	3.47	35	1920	6662	63.13	88.3	15650	54306	514.61	21.8
	5.21	35	-	-	-	-	9635	50198	475.69	19.8
	6.94	35	-	-	-	-	6240	43306	410.37	21.1
	3.47	20	1030	3574	59.27	92	7895	27395.7	454.31	17.3
	3.47	50	2750	9543	63.3	89.6	22305	77398.4	513.41	15.8

Notation: Q - volumetric flow rate (L/min); Z - bed height (cm); t_b, V_b – the service time and treated volume at 10% breakthrough point (L); t_s, V_s – the service time and treated volume at

90% saturation point; q_b, q_s – the amount of ABs loaded per unit of dry weight of M_3-plN_2 at 10% breakthrough point and 90% saturation points, respectively; R_b, R_s – the removal percentage of ABs at 10% breakthrough point and 90% saturation points, respectively; -: undefined values.

7.4.2. Breakthrough curves modeling

The experimental data of ABs adsorption onto M_3-plN_2 was calculated through different models and the outcomes are summarized in Table 7.5.

A. Adams–Bohart model

Table 7.5 indicates that an increase in the flow rate resulted in growing adsorption capacities for all three ABs. However, as mentioned in section 4.1A, the effects of flow rate on the adsorption process indicated that at high flow rates, outlet concentrations of ABs were too high (more than 10% of inlet concentrations). High adsorption capacities of ABs at high flow rates were possibly caused by more ABs running through the bed and then more compounds did bind on the M_3-plN_2's surface. In contrast, a decrease in the kinetic constant (k_{AB}) was recorded when the flow rate increased from 1.74 to 6.94 L/min in most cases for the three ABs.

The bed height's increase led to a contrasting trend for N_o and k_{AB} values. While N_o values fell when bed height increased from 20 to 50 cm, the k_{AB} constants rose for all ABs including SMT, TC and CP. At a flow rate of 3.47 L/min and bed height of 35 cm, N_o values of ABs adsorption were achieved as SMT 177, TC 169.61 and CP 176.83 µg/L(x10^3). As a consequence, a lower bed height and higher flow rate led to the column having higher adsorption capacities. Similar outcomes were reported elsewhere recently: firstly, by Nazari et al. (2016) on adsorption of cephalexin by walnut shell-based activated carbon; and secondly, Liao et al. (2013) on tetracycline and chloramphenicol adsorption onto bamboo charcoal.

B. Thomas model

As offered in Table 7.5, Thomas rate constants (k_{Th}) of ABs uptake by M_3-plN_2 tended to reduce when the flow rate increased. This result disagreed with another study regarding the removal of amoxicillin by NH_4Cl-activated carbon (Yaghmaeian et al., 2014). Among the four flow rates, adsorption capacities of SMT, TC and CP were the highest at 3.47 L/min. At that flow rate value, the column ABs adsorption capacities (q_o) on the adsorbent were SMT 132.63, TC 127.86 and CP 143.26 μg/g. These results confirmed the optimal flow rate for ABs adsorption reported in section 7.4.1A.

Apart from that, k_{Th} values of SMT and TC removal increased when the bed height grew (20 to 50 cm). Conversely, the k_{Th} constant declined when the bed height increased in the case of CP. The lower bed height caused higher adsorption capacity which was confirmed by Nazari et al. (2016) who successfully removed cephalexin using walnut shell-based activated carbon. The highest attained q_o values of SMT, TC and CP at 20 cm were 175.15, 181.52 and 197.38 μg/g, respectively. The Thomas model fitted better to the experimental data than the Adams-Bohart model due to higher correlation cofficients.

C. Yoon–Nelson model

The Yoon–Nelson constant (k_{YN}) decreased when the flow rate rose from 3.47 to 6.94 L/min (Table 7.5). From 1.74 to 3.47 L/min of flow rate, k_{YN} values stayed the same or slightly increased. When the flow rate grew from 1.74 to 6.94 L/min the τ values promptly reduced for SMT, TC and CP. A similar finding was noted by Nazari et al. (2016). These effects demonstrated that at higher flow rate the adsorption became saturation more quickly (Sharma and Singh, 2013).

As expected, the outcomes validated that τ values went up when the bed height was raised. Similar to the Thomas model, the Yoon-Nelson model's correlation coefficients (R^2) were higher than those of the Adams-Bohart model. This means that the Yoon-Nelson model better fitted the adsorption data of ABs.

Table 7.5 Adams–Bohart, Thomas and Yoon-Nelson model constants for ABs adsorption onto M_3-plN_2 column

ABs	Conditions		Adams–Bohart			Thomas			Yoon-Nelson		
	Q (L/min)	Z (cm)	k_{AB}	N_o	R^2	k_{Th}	q_o	R^2	k_{YN}	τ	R^2
SMT	1.74	35	0.08	92.97	0.848	0.11	73.09	0.929	1.1	4406	0.929
	3.47	35	0.09	177	0.854	0.13	132.63	0.942	1.3	4009.39	0.942
	5.21	35	0.02	260.26	0.932	0.06	77.19	0.930	0.6	1554	0.930
	6.94	35	0.01	497.54	0.889	0.09	38.39	0.972	0.9	552.56	0.972
	3.47	20	0.06	288.84	0.757	0.11	175.15	0.948	1.1	3025.46	0.948
	3.47	50	0.12	113.26	0.802	0.15	97.7	0.898	1.5	4218.93	0.898
TC	1.74	35	0.10	90.51	0.773	0.13	75.15	0.863	1.3	4660.46	0.863
	3.47	35	0.09	169.61	0.646	0.11	127.86	0.734	1.3	3960.31	0.797
	5.21	35	0.02	295.01	0.958	0.06	92.8	0.957	0.6	1922.17	0.957
	6.94	35	0.01	537.45	0.937	0.06	61.75	0.951	0.6	960.17	0.951
	3.47	20	0.07	261.16	0.760	0.11	181.52	0.925	1.1	3225.82	0.925
	3.47	50	0.12	115.79	0.811	0.15	100.02	0.904	1.5	4443.53	0.904
CP	1.74	35	0.05	113.02	0.963	0.07	87.68	0.956	0.7	5317.57	0.956
	3.47	35	0.06	176.83	0.925	0.08	143.26	0.959	0.8	4356.63	0.959
	5.21	35	0.02	359.72	0.929	0.05	137.71	0.950	0.5	2789.2	0.950
	6.94	35	0.01	667.56	0.978	0.04	126.71	0.930	0.4	1926.75	0.930
	3.47	20	0.07	304.53	0.740	0.12	197.38	0.906	1.2	3430.08	0.906
	3.47	50	0.12	119.59	0.782	0.07	122.4	0.956	1.5	4452	0.869

Notation: Q - volumetric flow rate (L/min); Z - bed height (cm); k_{AB} - Adams–Bohart model rate constant (L/μg min)x10^{-4}; N_o – saturation concentration (μg/L)x10^3; k_{Th} – Thomas model rate constant (mL/μg min)x10^{-4}; q_o – equilibrium ABs adsorption capacity (μg/g); k_{YN} - Yoon-Nelson model rate constant (1/min)x10^{-3}; τ – the time required for 50% breakthrough (min); R^2 values - the correlation coefficients.

D. BDST model

Figure 7.8 and Table 7.6 indicate the BDST parameters for breakthrough points (10%) and exhaustion point (90%) of ABs adsorption onto the M_3-plN_2 column. As can be seen from Table 7.6, correlation coefficients of ABs adsorption were higher than those of HMs adsorption by the adsorbent, therefore demonstrating that the data concerning adsorptive removal of ABs fitted better to the BDST model. The adsorption capacities of ABs were: SMT 590.01; TC 573.51; CP 586.48 µg/L at breakthrough point and SMT 885.08; TC 1147.13; and CP 586.48 µg/L. Nevertheless, the Z_o values in all three ABs for breakthrough and exhaustion points were negative.

Table 7.6 BDST model constants for ABs adsorption onto M_3-plN_2

ABs	Breakpoint (%)	N_o (µg/L)	K_b (L/µg h)	Z_o (cm)	R^2
SMT	10	590.01	-0.0041	-10	1
	90	885.08	0.0003	-97.69	0.75
TC	10	573.51	-0.0042	-10	1
	90	1147.13	0.0003	-62.5	1
CP	10	586.48	-0.0017	-25	1
	90	586.48	0.0002	-170	0.75

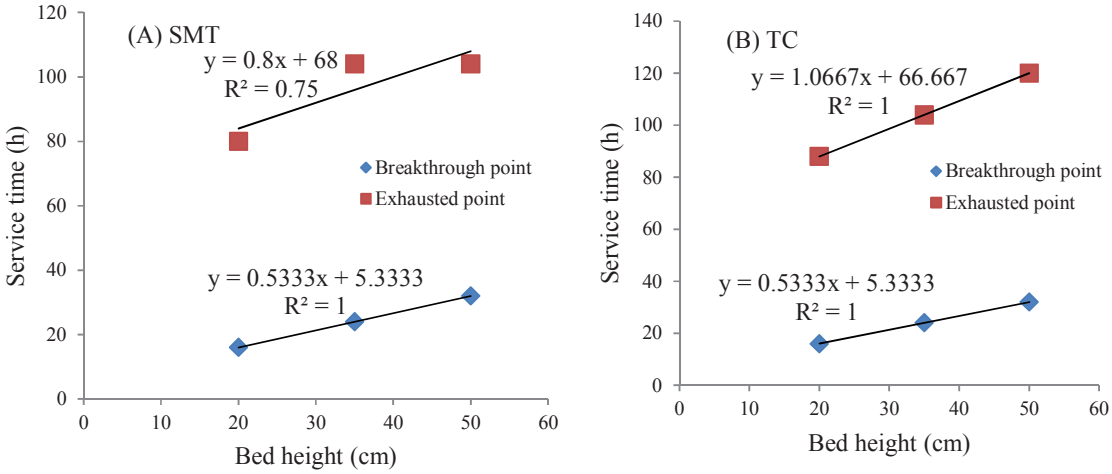

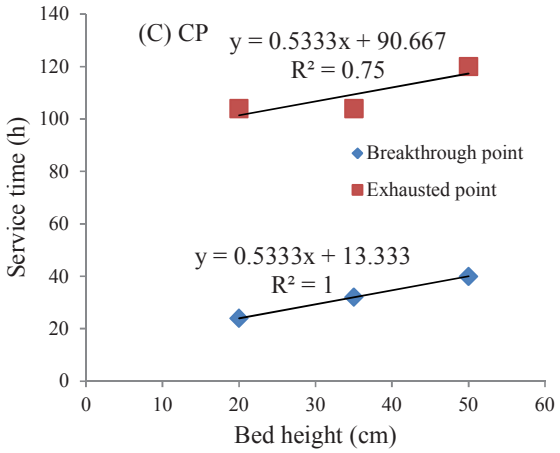

Figure 7.8 BDST model plots for 10% and 90% breakthrough of SMT, TC and CP adsorption onto M_3-plN_2 column at different bed heights (natural pH, flow rate = 3.47 L/min; initial concentrations (C_o) of ABs: SMT 100.1; TC 97.3 and CP 99.5 µg/L)

7.5. Conclusion

Chapter 7 investigated the application of nitrogen plasma modified steel shavings (M_3-plN_2) to the removal of HMs and ABs at a semi-pilot scale. The study found that design 1 and design 2 ineffectively abated HMs and ABs from aqueous solution. However, design 3 (M_3-plN_2 fixed-bed column) did effectively remove HMs (Pb^{2+}, Cu^{2+}, Cd^{2+}, Cr^{3+} and Zn^{2+}) as well as ABs (SMT, TC and CP) from synthesized wastewater at semi-pilot scale (flow rate of 5 m^3/day). The outlet concentrations of pollutants meet the standards established by US-EPA.

The column's adsorption performance was significantly influenced by the bed height of the column and influent's flow rate. Based on the experimental data, optimal conditions for the removal of HMs were similar to ABs at a flow rate of 3.47 L/min and bed height of 35 cm. At these conditions, adsorption capacities were 14.06, 11.16, 8.95, 7.15 and 10.25 mg/g in cases of Pb^{2+}, Cu^{2+}, Cd^{2+}, Cr^{3+} and Zn^{2+}, respectively; and 470.74, 363.61 and 514.61 µg/g in cases of SMT, TC and CP,

respectively. In comparison with other conventional adsorbents, the adsorption capacities of M_3-plN_2 are relative high. For example, adsorption capacities of lead and copper on chaff were 6.72 and 1.98 mg/g, respectively (Han et al., 2006a). In another study, total hexavalent chromium uptake by short-chain polyaniline synthesized on jute fiber were from 4.14 to 4.66 (Kumar and Chakraborty, 2009). In their study, Monser and Adhoum concluded that adsorption capacities of copper, zinc and chromium on modified activated carbon were 38, 9.9 and 6.84 mg/g, respectively.

Experimental data of HMs adsorption and ABs adsorption in the dynamic column system were evaluated by different models, namely the Adams–Bohart, Thomas, Yoon-Nelson and BDST variants. The Thomas and Yoon-Nelson models better described the adsorption of both HMs and ABs uptake by the column system than the Adams–Bohart model. Furthermore, the BDST model also fitted well with the experimental data regarding HMs and ABs. While this model was suitable applied in breakthrough points 10%, it is not reliable described the adsorption data at exhaustion point.

Faculty of Engineering and Information Technology

CHAPTER 8

CONCLUSIONS AND RECOMMENDATIONS

8.1. Overall conclusion

In the previous chapters, different aspects of adsorptive removal of heavy metals (Pb^{2+}, Cu^{2+}, Cd^{2+}, Cr^{3+} and Zn^{2+}) and antibiotics (sulfamethazine, tetracycline and chloramphenicol) from aqueous solution onto raw and modified steel shavings were evaluated. The specific outcomes and contributions for the fields of this study are presented as follows:

8.1.1. Major findings

- The study "Plasma modified steel processing by-product for removing heavy metals and antibiotics from water" demonstrated that steel shavings can be used as an efficient and cost-effective means for removing pollutants such as HMs and ABs from water. Particle size has significantly effects on the removal efficiency. The finest particle sizes M_3 (0-75 μm) provided optimal performance of pollutant removal. The plasma cleaning processes with H_2, N_2 and Ar improved adsorption capacities of HMs and ABs onto the adsorbents. Among different kinds of adsorbents, nitrogen plasma modified material (M_3-plN_3) provided the highest adsorption capacities for both HMs and ABs. The plasma modification in the nitrogen gas environment enhanced 1.7-fold the surface area and 1.4-fold the pore volume of steel shavings. The iron content of steel shavings (47.7%) improved after plasma treatment with argon and nitrogen (53.4 and 55.2%, respectively) whereas it declined with plasma modification containing O_2 gas (46.4%). In addition, characterization of M_3-plN_2 showed that the main components on the adsorbent surface were Fe_3O_4/Fe^{2+}, Fe_3O_4/Fe^{3+}, FeO/Fe^{2+} and Fe_2O_3/Fe^{3+} which can be responsible

for removing HMs and ABs from water. The pH_{pzc} values of raw and nitrogen plasma modified M_3 in water were 5.5 and 5, respectively.

- Metal ions adsorption batch experiments indicated that raw and nitrogen plasma modified steel shavings (M_3 and M_3-plN_2) can effectively remove heavy metals: Pb^{2+}, Cu^{2+}, Cd^{2+}, Cr^{3+} and Zn^{2+} from water. Plasma modification with nitrogen improved adsorption capacities of HMs on the adsorbents from 11.1 to 26.7%. At the conditions: pH 5-6, 5 g/L adsorbent dose and at 25^{o}C, the highest removal efficiency was observed. Thermodynamic data discovered that adsorption of HMs onto the adsorbents was a spontaneous, endothermic and highly feasible process. The Langmuir isotherm model better described the adsorption data of HMs onto the adsorbents than Freundlich isotherm model. The Langmuir adsorption capacities Q_{max} values (in mmol/g) of single metal ions on both M_3 and M_3-plN_2 reduced in the order of $Cu^{2+} > Cr^{3+} > Zn^{2+} > Cd^{2+} > Pb^{2+}$. Maximum single adsorption capacities of HMs onto M_3-plN_2 following Langmuir isotherm were: Pb^{2+} 27.04, Cu^{2+} 20.64, Cd^{2+} 16.87, Cr^{3+} 14.89 and Zn^{2+}18.47 mg/g, respectively. The PFO and PSO kinetic models provided a good agreement with the adsorption kinetic data. In competitive solutions of the five HMs, maximum Langmuir competitive adsorption volumes (Q_{max}) of Pb^{2+}, Cu^{2+}, Cd^{2+}, Cr^{3+} and Zn^{2+} were 13.39, 9.78, 7.92, 7.31, 8.79 mg/g on M_3, respectively and 16.62, 14.00, 9.73, 8.69, 12.28 mg/g on M_3-plN_2, respectively. Adsorption and co-precipitation were proposed as the main driving forces for HMs removal by the adsorbents. The sulfuric acid (H_2SO_4) 0.1N solution was the most suitable reagent for desorbing metal-loaded

adsorbents. The adsorption and desorption capacities on M_3-plN_2 were high and stable after 5 cycles, demonstrating that the adsorbent has a high potential in the application for HMs removal from water.

- This research showed that M_3 and M_3-plN_2 could also remove antibiotics (SMT, TC and CP) from the aqueous solution. Single adsorption capacities of SMT, TC and CP onto M_3-plN_2 (2702.55, 2158.36 and 2920.11 µg/g, respectively) were higher than those of M_3 (2519.98, 1720.20 and 2772.81 µg/g, respectively). The competitive adsorption capacities of ABs onto the adsorbents were nearly 2-fold less than individual adsorption capacities. The adsorption process reached equilibrium within an hour and was well simulated by PFO and PSO models. pH 3 was the optimal condition for eliminating SMT and CP while TC was most effectively removed at pH 5. The adsorption mechanisms of ABs onto the adsorbents stated were hydrogen bonding, electrostatic and non- electrostatic interactions and redox reaction. The most suitable adsorbent dose and temperature for the removal were 2 g/L and 25^{o}C, respectively. The nature of adsorption process confirmed by thermodynamic study was feasible, endothermic and spontaneous. The most effective reagent to regenerate the adsorbent was methanol 0.1N solution and adsorption-desorption of the adsorbents was successful after 2-3 cycles.
- The semi-pilot scale experiments confirmed that fixed-bed column using M_3-plN_2 could efficiently abate both HMs and ABs from water flow rate of 5 m^3/day. After treating with the column, the concentrations of Pb^{2+}, Cu^{2+}, Cd^{2+}, Cr^{3+} and Zn^{2+} in the effluent met the discharge standards as advised in the US-EPA guideline. In cases of mixed solution of ABs, the remaining

levels of SMT, TC and CP in the effluent at 8 hours were 1.93, 1.62 and 1.1 µg/L, respectively. The highest obtained removal efficiencies of HMs were similar to ABs at a flow rate of 3.47 L/min and bed height of 35 cm. Column adsorption capacities were 14.06, 11.16, 8.95, 7.15 and 10.25 mg/g in cases of Pb^{2+}, Cu^{2+}, Cd^{2+}, Cr^{3+}, Zn^{2+}, respectively; and 470.74, 363.61 and 514.61 µg/g in cases of SMT, TC, CP, respectively at the above optimal parameters. The Thomas, Yoon-Nelson and BDST models better described the column adsorption data for HMs and ABs rather than the Adams-Bohart model.

8.1.2. Contributions to the field

- The successful use of a novel adsorbent from industrial waste (steel shavings) for removing metal ions and antibiotics from aqueous solution can reduce volume of solid waste and add more value to the material. Moreover, the adsorbents studied in this research were used in micro-scale particle size which can have good adsorption capacities whilst avoiding disadvantages of nano-scale iron materials such as risks to human health, generating a new by-product in the aquatic environment.
- Development of an efficient method for modifying surface of steel shavings (nitrogen plasma technique) helps to improve adsorption capacities of the adsorbents.
- Adsorption batch experiments and characterization of adsorbents improve the understandings on adsorption mechanisms of HMs and ABs onto the adsorbents.
- Low concentration sulfuric acid solution is the most suitable reagent to desorb the post-HMs adsorption M_3-plN_2 and the ABs-loaded adsorbent can

be regenerated using methanol solution, consequently, the reduced cost of the adsorbent.

8.2. Recommendations for future works

To apply nitrogen plasma modified steel shavings for the practical application for the treatment of real wastewater containing HMs and ABs, further studies can be made as the following recommendations:

- Further studies on the surface modification for producing better adsorption capacity and more cost-effective adsorbents from steel shavings are necessary, such as scaling up nitrogen plasma system;
- A pilot-scale column using M_3-plN_2 can be conducted to remove HMs and ABs from real wastewater;
- Influences of other pollutants in real wastewater to removal efficiencies of HMs and ABs by the adsorbents can be further evaluated. Thus, a combination of treatment system including several methods such as filtration, biological treatment and adsorption (using M_3-plN_2) can be proposed and investigated;
- Research on other semi-pilot/pilot scale water treatment designs to utilize magnetic character of M_3-plN_2 for continuous water treatment; and
- Studies on the recovery of HMs and antibiotics from desorption solutions (in adsorbents regeneration experiments) can be implemented. Thus, the recovery HMs and ABs can be separated and used for other purposes.

Faculty of Engineering and Information Technology

REFERENCES

Abdolali, A., Guo, W.S., Ngo, H.H., Chen, S.S., Nguyen, N.C., Tung, K.L. 2014. Typical lignocellulosic wastes and by-products for biosorption process in water and wastewater treatment: a critical review. *Bioresource technology*, 160, 57-66.

Acar, F.N., Eren, Z. 2006. Removal of Cu(II) ions by activated poplar sawdust (Samsun Clone) from aqueous solutions. *Journal of hazardous materials,* 137(2), 909-914.

Acero, J.L., Benitez, F.J., Real, F.J., Roldan, G. 2010. Kinetics of aqueous chlorination of some pharmaceuticals and their elimination from water matrices. *Water Research*, 44, 4158-4170.

Acheampong, M.A., Pakshirajan, K., Annachhatre, A.P., Lens, P.N.L. 2013. Removal of Cu(II) by biosorption onto coconut shell in fixed-bed column systems. *Journal of Industrial and Engineering Chemistry*, 19(3), 841-848.

Adams, C., Wang, Y., Loftin, K., Meyer, M. 2002. Removal of antibiotics from surface and distilled water in conventional water treatment processes. *Journal of environmental engineering*, 128(3), 253-260.

Ahmad, A., Rafatullah, M., Sulaiman, O., Ibrahim, M.H., Chii, Y.Y., Siddique, B.M. 2009. Removal of Cu(II) and Pb(II) ions from aqueous solutions by adsorption on sawdust of Meranti wood. *Desalination,* 247(1-3), 636-646.

Ahmady-Asbchin, S., Andres, Y., Gerente, C., Cloirec, P.L. 2009. Natural seaweed waste as sorbent for heavy metal removal from solution. *Environmental Technology*, 30(7), 755-762.

Ahmed, M.B., Zhou, J.L., Ngo, H.H., Guo, W. 2015. Adsorptive removal of antibiotics from water and wastewater: progress and challenges. *Science of The Total Environment*, 532, 112-126.

Ahmed, M.B., Zhou, J.L., Ngo, H.H., Guo, W., Johir, M.A.H., Sornalingam, K. 2017. Single and competitive sorption properties and mechanism of functionalized biochar for removing sulfonamide antibiotics from water. *Chemical Engineering,* 311, 348-358.

Ahmed, M.J., Theydan, S.K. 2014. Fluoroquinolones antibiotics adsorption onto microporous activated carbon from lignocellulosic biomass by microwave pyrolysis. *Journal of the Taiwan Institute of Chemical Engineers*, 45(1), 219-226.

Akar, S.T., Yetimoglu, Y., Gedikbey, T. 2009. Removal of chromium (VI) ions from aqueous solutions by using Turkish montmorillonite clay: effect of activation and modification. *Desalination,* 244(1-3), 97-108.

Aksu, Z., Tunç, Ö. 2005. Application of biosorption for penicillin G removal: comparison with activated carbon. *Process biochemistry*, 40(2), 831-847.

Ali, H., Khan, E., Sajad, M.A. 2013. Phytoremediation of heavy metals-concepts and applications. *Chemosphere*, 91(7), 869-881.

Altundoğan, H.S., Altundoğan, S., TuÈmen, F., Bildik, M. 2000. Arsenic removal from aqueous solutions by adsorption on red mud. *Waste Management*, 20(8), 761-767.

An, H.K., Park, B.Y., Kim, D.S. 2001. Crab shell for the removal of heavy metals from aqueous solution. *Water research,* 35(15), 3551-3556.

Ansari, R., Fahim, N.K. 2007. Application of polypyrrole coated on wood sawdust for removal of Cr (VI) ion from aqueous solutions. *Reactive and Functional Polymers*, 67(4), 367-374.

Apak, R., Tütem, E., Hügül, M., Hizal, J. 1998. Heavy metal cation retention by unconventional sorbents (red muds and fly ashes). *Water research,* 32(2), 430-440.

Arain, M.B., Kazi, T.G., Jamali, M.K., Jalbani, N., Afridi, H.I., Baig, J.A. 2008. Speciation of heavy metals in sediment by conventional, ultrasound and microwave assisted single extraction methods: a comparison with modified sequential extraction procedure. *Journal of Hazardous Materials*, 154(1), 998-1006.

Aredes, S., Klein, B., Pawlik, M. 2012. The removal of arsenic from water using natural iron oxide minerals. *Journal of Cleaner Production*, 29, 208-213.

Aroguz, A.Z. 2006. Kinetics and thermodynamics of adsorption of azinphosmethyl from aqueous solution onto pyrolyzed (at 600^{o}C) ocean peat moss (Sphagnum sp.). *Journal of hazardous materials*, 135(1), 100-105.

Ata, A., Nalcaci, O.O., Ovez, B. 2012. Macro algae Gracilaria verrucosa as a biosorbent: A study of sorption mechanisms. *Algal Research*, 1(2), 194-204.

Atta, A.M., Al-Lohedan, H.A., ALOthman, Z.A., Abdel-Khalek, A.A., Tawfeek, A.M. 2015. Characterization of reactive amphiphilic montmorillonite nanogels and its application for removal of toxic cationic dye and heavy metals water pollutants. *Journal of Industrial and Engineering Chemistry*, 31, 374-384.

Ayala, J., Blanco, F., García, P., Rodriguez, P., Sancho, J. 1998. Asturian fly ash as a heavy metals removal material. *Fuel,* 77 (11), 1147-1154.

Badruddoza, A.Z.M., Shawon, Z.B.Z., Tay, W.J.D., Hidajat, K., Uddin, M.S. 2013. Fe_3O_4/cyclodextrin polymer nanocomposites for selective heavy metals removal from industrial wastewater. *Carbohydrate polymers*, 91(1), 322-332.

Bailey, S.E., Olin, T.J., Bricka, R.M., Adrian, D.D. 1999. A review of potentially low-cost sorbents for heavy metals. *Water research,* 33(11), 2469-2479.

Baker H.M., Massadeh A.M., Younes H.A. 2009. Natural Jordanian zeolite: removal of heavy metal ions from water samples using column and batch methods. *Environmental Monitoring and Assessment*, 157(1-4), 319-330.

Balarak, D., Mostafapour, F.K. 2016. Canola Residual as a Biosorbent for Antibiotic Metronidazole Removal. *The Pharmaceutical and Chemical Journal*, 3(2), 12-17.

Barakat, M.A., Kumar, R. 2015. Synthesis and characterization of porous magnetic silica composite for the removal of heavy metals from aqueous solution. *Journal of Industrial and Engineering Chemistry*, 23, 93-99.

Barakat, M.A. 2011. New trends in removing heavy metals from industrial wastewater. *Arabian Journal of Chemistry*, 4(4), 361-377.

Baral, S.S., Das, S.N., Rath, P. 2006. Hexavalent chromium removal from aqueous solution by adsorption on treated sawdust. *Biochemical Engineering Journal*, 31(3), 216-222.

Barceloux, D.G., Barceloux, D. 1999. Chromium. *Journal of Toxicology: Clinical Toxicology*, 37(2), 173-194.

Basha, S., Murthy Z.V.P., Jha B. 2009. Removal of Cu(II) and Ni(II) from Industrial Effluents by Brown Seaweed, Cystoseira indica. *Industrial and Engineering Chemistry Research*, 48(2), 961-975.

Basha, S., Murthy, Z.V.P., Jha, B. 2011. Kinetics, isotherms, and thermodynamics of Hg (II) biosorption onto Carica papaya. *Bioremediation Journal*, 15(1), 26-34.

Bautitz, I.R., Nogueira, R.F.P. 2007. Degradation of tetracycline by photo-Fenton process-Solar irradiation and matrix effects. *Journal of Photochemistry and Photobiology A: Chemistry*, 187(1), 33-39.

Belkind, A., Gershman, S. 2008. Plasma cleaning of surfaces. *Vacuum Coating and Technology*, November, 46-57.

Benyoucef, S., Amrani, M., 2011. Removal of phosphorus from aqueous solutions using chemically modified sawdust of Aleppo pine (*Pinus halepensis Miller*): Kinetics and isotherm studies. *Environmentalist*, 31, 200-207.

Bertocchi, A.F., Ghiani, M., Peretti, R., Zucca, A. 2006. Red mud and fly ash for remediation of mine sites contaminated with As, Cd, Cu, Pb and Zn. *Journal of hazardous materials,* 134(1-3), 112-119.

Bhatnagar, A., Sillanpää, M. 2010. Utilization of agro-industrial and municipal waste materials as potential adsorbents for water treatment - a review. *Chemical Engineering Journal*, 157(2), 277-296.

Bhattacharyya, K.G., Gupta, S.S. 2008. Adsorption of a few heavy metals on natural and modified kaolinite and montmorillonite: A review. *Advances in Colloid and Interface Science,* 140(2), 114-131.

Bhowmik, M., Bajpai, S.K. 2012. Sorptive removal of gatifloxacin from synthetic wastewater using chitin: an equilibrium study. *Environmental Engineering and Management Journal (EEMJ), 11*(8).

Blasioli, S., Martucci, A., Paul, G., Gigli, L., Cossi, M., Johnston, C.T., Marchese, L., Braschi, I. 2014. Removal of sulfamethoxazole sulfonamide antibiotic from water by high silica zeolites: a study of the involved host - guest interactions by a combined structural, spectroscopic, and computational approach. *Journal of colloid and interface science*, 419, 148-159.

Boddu, V.M., Abburi, K., Talbott, J.L., Smith, E.D., Haasch, R. 2008. Removal of arsenic (III) and arsenic (V) from aqueous medium using chitosan-coated biosorbent. *Water research*, 42(3), 633-642.

Boparai, H.K., Joseph, M., O'Carroll, D.M. 2011. Kinetics and thermodynamics of cadmium ion removal by adsorption onto nano zerovalent iron particles. *Journal of hazardous materials*, 186(1), 458-465.

Brown, P.A., Gill, S.A., Allen, S.J. 2000. Metal removal from wastewater using peat. *Water research,* 34 (16), 3907-3916.

Bulgariu, D., Bulgariu, L. 2013. Sorption of Pb(II) onto a mixture of algae waste biomass and anion exchanger resin in a packed bed column. *Bioresource Technology*, 129, 374-380.

Carabineiro, S.A.C., Thavorn-Amornsri, T., Pereira, M.F.R., Figueiredo, J.L. 2011. Adsorption of ciprofloxacin on surface-modified carbon materials. *Water research*, 45(15), 4583-4591.

Chang, C., Chang, C., Chen, K., Tsai, W., Shie, J., Chen, Y. 2004. Adsorption of naphthalene on zeolite from aqueous solution. *Journal of colloid and interface science,* 277(1), 29-34.

Chen, H., Li, J., Shao, D., Ren, X., Wang, X. 2012. Poly (acrylic acid) grafted multiwall carbon nanotubes by plasma techniques for Co (II) removal from aqueous solution. *Chemical engineering journal*, 210, 475-481.

Chen, H., Luo, H., Lan, Y., Dong, T., Hu, B., Wang, Y. 2011. Removal of tetracycline from aqueous solutions using polyvinylpyrrolidone (PVP-K30) modified nanoscale zero valent iron. *Journal of hazardous materials*, 192(1), 44-53.

Choi, K.J., Kim, S.G., Kim, S.H. 2008. Removal of antibiotics by coagulation and granular activated carbon filtration. *Journal of hazardous materials*, 151(1), 38-43.

Choi, K.J., Son, H.J., Kim, S.H. 2007. Ionic treatment for removal of sulfonamide and tetracycline classes of antibiotic. *Science of the total environment*, 387(1), 247-256.

Couillard, D. 1994.'The use of peat in wastewater treatment. *Water research,* 28(6), 1261-1274.

Coupal, B., Lalancette, J. 1976. The treatment of waste waters with peat moss. *Water research,* 10(12), 1071-1076.

Cundy, A.B., Hopkinson, L., Whitby, R.L. 2008. Use of iron-based technologies in contaminated land and groundwater remediation: a review. *Science of the total environment*, 400(1), 42-51.

Dal Bosco, S.M., Jimenez, R.S., Carvalho, W.A. 2005. Removal of toxic metals from wastewater by Brazilian natural scolecite. *Journal of colloid and interface science,* 281(2), 424-431.

Dayan, A.D., Paine, A.J. 2001. Mechanisms of chromium toxicity, carcinogenicity and allergenicity: review of the literature from 1985 to 2000. *Human and experimental toxicology*, 20(9), 439-451.

Deborde, M., Von Gunten, U.R.S. 2008. Reactions of chlorine with inorganic and organic compounds during water treatment - kinetics and mechanisms: a critical review. *Water research*, 42(1), 13-51.

Demirbas, A. 2004. Adsorption of lead and cadmium ions in aqueous solutions onto modified lignin from alkali glycerol delignication. *Journal of hazardous materials,* 109(1-3), 221-226.

Dickert, C. 2000. Ion exchange. *Kirk-Othmer Encyclopedia of Chemical Technology*.

Dong, L., Peng, H., Wang, S., Zhang, Z., Li, J., Ai, F., Zhao, Q., Luo, M., Xiong, H., Chen, L. 2014. Thermally and magnetically dual-responsive mesoporous silica nanospheres: preparation, characterization, and properties for the controlled release of sophoridine. *Journal of Applied Polymer Science*, 131(40477), 1-8.

Dong, L., Zhu, Z., Qiu, Y., Zhao, J. 2010. Removal of lead from aqueous solution by hydroxyapatite/magnetite composite adsorbent. *Chemical Engineering Journal*, 165(3), 827-834.

Dreamstime. 2017. Metal shavings. https://www.dreamstime.com/stock-image-metal-shavings-image17852401. (accessed 16.05.2017).

Eckenfelder, W. 2006. Wastewater treatment. *John Wiley & Sons, Inc.*

El Samrani, A.G., Lartiges, B.S., Villiéras, F. 2008. Chemical coagulation of combined sewer overflow: Heavy metal removal and treatment optimization. *Water research*, 42(4), 951-960.

Electronic diener. 2017. Plasma surface technology. https://www.plasma.com/en/plasmatechnik/low-pressure-plasma/. (accessed 12.05.2017).

Erdem, E., Karapinar, N., Donat, R. 2004. The removal of heavy metal cations by natural zeolites. *Journal of colloid and interface science,* 280 (2), 309-314.

European Commission, 2002. DG ENV. E3, Project ENV.E3/ETU/2000/0058, Heavy Metals in Waste, Final Report.

European Union. 1990. COUNCIL REGULATION (EEC) No 2377/90 of 26 June 1990 laying down a Community procedure for the establishment of maximum residue limits of veterinary medicinal products in foodstuffs of animal origin. Official Journal L, 224(18/08), pp.0001-0008.

Fan, Y., Wang, B., Yuan, S., Wu, X., Chen, J., Wang, L. 2010. Adsorptive removal of chloramphenicol from wastewater by NaOH modified bamboo charcoal. *Bioresource Technology*. 101, 7661-7664.

Fang, Z., Chen, J., Qiu, X., Qiu, X., Cheng, W., Zhu, L. 2011. Effective removal of antibiotic metronidazole from water by nanoscale zero-valent iron particles. *Desalination*, 268(1), 60-67.

Feng, D., Aldrich, C., Tan, H. 2000. Removal of heavy metal ions by carrier magnetic separation of adsorptive particulates. *Hydrometallurgy*, 56(3), 359-368.

Foo, K.Y., Lee, L.K., Hameed, B.H. 2013. Preparation of tamarind fruit seed activated carbon by microwave heating for the adsorptive treatment of landfill leachate: A laboratory column evaluation. *Bioresource Technology*, 133, 599-605.

Fouodjouo, M., Fotouo-Nkaffo, H., Laminsi, S., Cassini, F.A., de Brito-Benetoli, L.O., Debacher, N.A. 2017. Adsorption of copper (II) onto cameroonian clay modified by non-thermal plasma: Characterization, chemical equilibrium and thermodynamic studies. *Applied Clay Science*, 142, 136-144.

Fu, F., Wang, Q. 2011. Removal of heavy metal ions from wastewaters: a review. *Journal of environmental management*, 92(3), 407-418.

Fukahori, S., Fujiwara, T. 2014. Modeling of sulfonamide antibiotic removal by TiO_2/high-silica zeolite HSZ-385 composite. *Journal of hazardous materials*, 272, 1-9.

Fukahori, S., Fujiwara, T., Funamizu, N., Matsukawa, K., Ito, R. 2012. Adsorptive removal of sulfonamide antibiotics in livestock urine using the high-silica zeolite HSZ-385. *Water Science and Technology*, 67(2), 319-325.

Fukahori, S., Fujiwara, T., Ito, R., Funamizu, N. 2011. pH-dependent adsorption of sulfa drugs on high silica zeolite: modeling and kinetic study. *Desalination*, 275(1), 237-242.

Gan, S., Lau, E.V., Ng, H.K. 2009. Remediation of soils contaminated with polycyclic aromatic hydrocarbons (PAHs). *Journal of Hazardous Materials*, 172(2), 532-549.

Genç, N., Dogan, E.C. 2015. Adsorption kinetics of the antibiotic ciprofloxacin on bentonite, activated carbon, zeolite, and pumice. *Desalination and Water Treatment*, 53(3), 785-793.

Genç, N., Dogan, E.C., Yurtsever, M. 2013. Bentonite for ciprofloxacin removal from aqueous solution. *Water Science and Technology*, 68(4), 848-855.

Genç-Fuhrman, H., Bregnhøj, H., McConchie, D. 2005. Arsenate removal from water using sand–red mud columns. *Water research,* 39(13), 2944-2954.

Ghauch, A., Tuqan, A., Assi, H.A. 2009. Antibiotic removal from water: elimination of amoxicillin and ampicillin by microscale and nanoscale iron particles. *Environmental pollution*, 157(5), 1626-1635.

Gheju, M., Balcu, I. 2011. Removal of chromium from Cr (VI) polluted wastewaters by reduction with scrap iron and subsequent precipitation of resulted cations. *Journal of hazardous materials*, 196, 131-138.

Girginova, P.I., Daniel-da-Silva, A.L., Lopes, C.B., Figueira, P., Otero, M., Amaral, V.S., Pereira, E., Trindade, T. 2010. Silica coated magnetite particles for magnetic

removal of Hg^{2+} from water. *Journal of Colloid and Interface Science*, 345(2), 234-240.

Gosset, T., Trancart, J., Thévenot, D.R. 1986. Batch metal removal by peat. Kinetics and thermodynamics. *Water research,* 20(1), 21-26.

Gray, W.G., Schrefler, B.A. 2001. Thermodynamic approach to effective stress in partially saturated porous media. *European Journal of Mechanics-A/Solids*, 20(4), 521-538.

Güçlü, K., Apak, R. 2000. Modeling of Copper(II), Cadmium(II), and Lead(II) Adsorption on Red Mud from Metal-EDTA Mixture Solutions. *Journal of colloid and interface science,* 228(2), 238-252.

Guo, H., Stüben, D., Berner, Z. 2007. Removal of arsenic from aqueous solution by natural siderite and hematite. *Applied Geochemistry*, 22(5), 1039-1051.

Guo, X., Zhang, S., Shan, X. 2008. Adsorption of metal ions on lignin. *Journal of hazardous materials,* 151(1), 134-142.

Gupta, S., Babu, B.V. 2009. Removal of toxic metal Cr(VI) from aqueous solutions using sawdust as adsorbent: Equilibrium, kinetics and regeneration studies. *Chemical Engineering Journal,* 150(2-3), 352-365.

Gupta, S.S., Bhattacharyya, K.G. 2006. Removal of Cd(II) from aqueous solution by kaolinite, montmorillonite and their poly(oxo zirconium) and tetrabutylammonium derivatives. *Journal of hazardous materials,* 128(2-3), 247-257.

Gupta, V. K., Sharma, S. 2002. Removal of Cadmium and Zinc from Aqueous Solutions Using Red Mud. *Environmental Science and Technology,* 36(16), 3612-3617.

Gupta, V.K., Ali, I. 2004. Removal of lead and chromium from wastewater using bagasse fly ash - a sugar industry waste. *Journal of colloid and interface science,* 271(2), 321-328.

Gupta, V.K., Agarwal, S., Saleh, T.A. 2011. Chromium removal by combining the magnetic properties of iron oxide with adsorption properties of carbon nanotubes. *Water research*, *45*(6), 2207-2212.

Gupta, V.K., Gupta, M., Sharma, S. 2001. Process development for the removal of lead and chromium from aqueous solutions using red mud - an aluminium industry waste. *Water research,* 35(5), 1125-1134.

Haider, M.I. 2011. Electrochemical synthesis of green rust, its characterization and performance study for removal of arsenic and nitrate. *Doctoral thesis*. *Lamar University-Beaumont, Texas*.

Han S.W., Kim D.K., Hwang I.G., Bae J.H. 2002. Development of pellet-type adsorbents for removal of heavy metal ions from aqueous solutions using red mud. *Industrial and Engineering Chemistry,* 8(2), 120-125.

Han, R., Zhang, J., Zou, W., Xiao, H., Shi, J., Liu, H. 2006a. Biosorption of copper (II) and lead (II) from aqueous solution by chaff in a fixed-bed column. *Journal of Hazardous materials,* 133(1), 262-268.

Han, R., Zou, L., Zhao, X., Xu, Y., Xu, F., Li, Y., Wang, Y. 2009. Characterization and properties of iron oxide-coated zeolite as adsorbent for removal of copper (II) from solution in fixed bed column. *Chemical Engineering Journal*, 149(1), 123-131.

Han, R., Zou, W., Li, H., Li, Y., Shi, J. 2006b. Copper (II) and lead (II) removal from aqueous solution in fixed-bed columns by manganese oxide coated zeolite. *Journal of hazardous materials*, 137(2), 934-942.

Harrick plasma. 2017. Harrick plasma. http://harrickplasma.com/applications/plasma-cleaning.(accessed 16.05.2017).

Hernando, M.D., Mezcua, M., Fernández-Alba, A.R., Barceló, D. 2006. Environmental risk assessment of pharmaceutical residues in wastewater effluents, surface waters and sediments. *Talanta*, 69(2), 334-342.

Homem, V., Santos, L. 2011. Degradation and removal methods of antibiotics from aqueous matrices–a review. *Journal of environmental management*, 92(10), 2304-2347.

Hossain, M.A. 2013. Development of Novel Biosorbents in Removing Heavy Metals from Aqueous Solution. *Doctoral thesis, University of Technology Sydney, Sydney*.

Hossain, M.A., Ngo, H.H., Guo, W.S., Nghiem, L.D., Hai, F.I., Vigneswaran, S., Nguyen, T.V. 2014. Competitive adsorption of metals on cabbage waste from multi-metal solutions. *Bioresource technology*, 160, 79-88.

Hu, J., Chen, G., Lo, I.M.C. 2005. Removal and recovery of Cr(VI) from wastewater by maghemite nanoparticles. *Water research,* 39(18), 4528-4536.

Hu, Y., Song, C., Li, G. 2012. Fiber-in-tube solid-phase microextraction with molecularly imprinted coating for sensitive analysis of antibiotic drugs by high performance liquid chromatography. *Journal of Chromatography A*, 1263, 21-27.

Hua, M., Zhang, S., Pan, B., Zhang, W., Lv, L., Zhang, Q. 2012. Heavy metal removal from water/wastewater by nanosized metal oxides: a review. *Journal of Hazardous Materials*, 211, 317-331.

Huguenot, D., Bois, P., Jézéquel, K., Cornu, J.Y., Lebeau, T. 2010. Selection of low cost materials for the sorption of copper and herbicides as single or mixed compounds in increasing complexity matrices. *Journal of hazardous materials*, 182(1), 18-26.

Huo, P., Lu, Z., Liu, X., Wu, D., Liu, X., Pan, J., Gao, X., Guo, W., Li, H., Yan, Y. 2012. Preparation photocatalyst of selected photodegradation antibiotics by molecular imprinting technology onto TiO_2/fly-ash cenospheres. *Chemical engineering journal*, 189, 75-83.

Igwe, J.C., Abia, A.A. 2007. Equilibrium sorption isotherm studies of Cd(II), Pb(II) and Zn(II) ions detoxification from waste water using unmodified and EDTA modified maize husk. *Electronic Journal of Biotechnology*, 10(4), 536-548.

Ijagbemi, C.O., Baek, M., Kim, D. 2009. Montmorillonite surface properties and sorption characteristics for heavy metal removal from aqueous solutions. *Journal of hazardous materials,* 166(1), 538-46.

Ikehata, K., Jodeiri Naghashkar, N., Gamal El-Din, M. 2006. Degradation of aqueous pharmaceuticals by ozonation and advanced oxidation processes: a review. *Ozone: Science and Engineering*, 28(6), 353-414.

Ilhan, Z.E., Ong, S.K., Moorman, T.B. 2012. Herbicide and antibiotic removal by woodchip denitrification filters: Sorption processes. *Water, Air and Soil Pollution*, 223(5), 2651-2662.

Imamoglu, M., Tekir, O. 2008. Removal of copper (II) and lead (II) ions from aqueous solutions by adsorption on activated carbon from a new precursor hazelnut husks. *Desalination,* 228(1-3), 108-113.

Jain, M., Garg, V.K., Kadirvelu, K. 2013. Cadmium(II) sorption and desorption in a fixed bed column using sunflower waste carbon calcium-alginate beads. *Bioresource Technology*, 129, 242-248.

Jara, C.C., Fino, D., Specchia, V., Saracco, G., Spinelli, P. 2007. Electrochemical removal of antibiotics from wastewaters. *Applied Catalysis B: Environmental*, 70(1), 479-487.

Jia, S., Yang, Z., Ren, K., Tian, Z., Dong, C., Ma, R., Yu, G., Yang, W. 2016. Removal of antibiotics from water in the coexistence of suspended particles and natural organic matters using amino-acid-modified-chitosan flocculants: A combined experimental and theoretical study. *Journal of Hazardous Materials*, 317, 593-601.

Jiang, B., Zheng, J., Qiu, S., Wu, M., Zhang, Q., Yan, Z., Xue, Q. 2014. Review on electrical discharge plasma technology for wastewater remediation. *Chemical Engineering Journal*, 236, 348-368.

Johari, K., Saman, N., Song, S.T., Heng, J.Y.Y., Mat, H. 2014. Study of Hg (II) removal from aqueous solution using lignocellulosic coconut fiber biosorbents: equilibrium and kinetic evaluation. *Chemical Engineering Communications*, 201(9), 1198-1220.

Jorgensen, H., Kristensen, J.B., Felby, C. 2007. Enzymatic conversion of lignocellulose into fermentable sugars: challenges and opportunities. *Biofuels, Bioproducts and Biorefining,* 1(2), 119-134.

Kadirvelu, K., Namasivayam, C. 2003. Activated carbon from coconut coirpith as metal adsorbent: adsorption of Cd(II) from aqueous solution. *Advances in Environmental Research,* 7(2), 471-478.

Kamala, C.T., Chu, K.H., Chary, N.S., Pandey, P.K., Ramesh, S.L., Sastry, A.R.K., Sekhar, K.C. 2005. Removal of arsenic (III) from aqueous solutions using fresh and immobilized plant biomass. *Water Research*, 39(13), 2815-2826.

Karvelas, M., Katsoyiannis, A., Samara, C. 2003. Occurrence and fate of heavy metals in the wastewater treatment process. *Chemosphere*, 53(10), 1201-1210.

Kemper, N. 2008. Veterinary antibiotics in the aquatic and terrestrial environment. *Ecological indicators*, 8(1), 1-13.

Khaloo, S.S., Matin, A.H., Sharifi, S., Fadaeinia, M., Kazempour, N., Mirzadeh, S. 2012. Equilibrium, kinetic and thermodynamic studies of mercury adsorption on almond shell. *Water Science and Technology*, 65(8), 1341-1349.

Khoramzadeh, E., Nasernejad, B., Halladj, R. 2013. Mercury biosorption from aqueous solutions by sugarcane bagasse. *Journal of the Taiwan Institute of Chemical Engineers*, 44(2), 266-269.

Kim, S.H., Shon, H.K., Ngo, H.H., 2010. Adsorption characteristics of antibiotics trimethoprim on powdered and granular activated carbon. *Journal of Industrial and Engineering Chemistry*, 16(3), 344-349.

Kobya, M. 2004. Removal of Cr(VI) from aqueous solutions by adsorption onto hazelnut shell activated carbon: kinetic and equilibrium studies. *Bioresource technology,* 91(3), 317-321.

Krishnani, K.K., Meng, X., Christodoulatos, C., Boddu, V.M. 2008. Biosorption mechanism of nine different heavy metals onto biomatrix from rice husk. *Journal of Hazardous Materials*, 153(3), 1222-1234.

Kržišnik, N., Mladenovič, A., Škapin, A.S., Škrlep, L., Ščančar, J., Milačič, R. 2014. Nanoscale zero-valent iron for the removal of Zn^{2+}, Zn (II)–EDTA and Zn (II)–citrate from aqueous solutions. *Science of the Total Environment*, 476, 20-28.

Kuleyin, A. 2007. Removal of phenol and 4-chlorophenol by surfactant-modified natural zeolite. *Journal of hazardous materials,*144(1-2), 307-315.

Kumar, P.A., Chakraborty, S. 2009. Fixed-bed column study for hexavalent chromium removal and recovery by short-chain polyaniline synthesized on jute fiber. *Journal of hazardous materials,* 162(2), 1086-1098.

Kumar, U., Bandyopadhyay, M. 2006. Fixed bed column study for Cd (II) removal from wastewater using treated rice husk. *Journal of hazardous materials*, 129(1), 253-259.

Kumari, P., Sharma, P., Srivastava, S., Srivastava, M.M. 2006. Biosorption studies on shelled Moringa oleifera Lamarck seed powder: removal and recovery of arsenic from aqueous system. *International Journal of Mineral Processing*, 78(3), 131-139.

Kümmerer, K. 2009. Antibiotics in the aquatic environment - a review: part I. *Chemosphere*, 75(4), 417-434.

Kundu, S., Gupta, A.K. 2005. Analysis and modeling of fixed bed column operations on As (V) removal by adsorption onto iron oxide-coated cement (IOCC). *Journal of colloid and interface science*, 290(1), 52-60.

Kurniawan, T.A., Chan, G., Lo, W. H., Babel, S. 2006. Physico–chemical treatment techniques for wastewater laden with heavy metals. *Chemical Engineering Journal*, 118(1), 83-98.

Kusvuran, E., Yildirim, D., Samil, A., Gulnaz, O. 2012. A study: Removal of Cu (II), Cd (II), and Pb (II) ions from real industrial water and contaminated water using activated sludge biomass. *Clean - Soil, Air, Water*, 40(11), 1273-1283.

Lalvani, S.B., Hubner, A., Wiltowski, T.S. 2000. Chromium adsorption by lignin. *Energy sources*, 22 (1), pp.45-56.

Larous, S., Meniai, A.H., Lehocine, M.B. 2005. Experimental study of the removal of copper from aqueous solutions by adsorption using sawdust. *Desalination*, 185(1-3), 483-490.

Lee, T., Lim, H., Lee, Y., Park, J.W. 2003. Use of waste iron metal for removal of Cr (VI) from water. *Chemosphere*, 53(5), 479-485.

Li, H., Zhang, D., Han, X., Xing, B. 2014. Adsorption of antibiotic ciprofloxacin on carbon nanotubes: pH dependence and thermodynamics. *Chemosphere*, 95, 150-155.

Li, J., Chen, C., Zhao, Y., Hu, J., Shao, D., Wang, X. 2013. Synthesis of water-dispersible Fe_3O_4@β-cyclodextrin by plasma-induced grafting technique for pollutant treatment. *Chemical engineering journal*, 229, 296-303.

Li, Z., Burt, T., Bowman R.S. 2000. Sorption of ionizable organic solutes by surfactant-modified zeolite. *Environmental Science and Technology*, 34(17), 3756-3760.

Liao, P., Zhan, Z., Dai, J., Wu, X., Zhang, W., Wang, K., Yuan, S. 2013. Adsorption of tetracycline and chloramphenicol in aqueous solutions by bamboo charcoal: a batch and fixed-bed column study. *Chemical engineering journal*, 228, 496-505.

Liu, H., Zhang, G., Liu, C.Q., Li, L., Xiang, M. 2009. The occurrence of chloramphenicol and tetracyclines in municipal sewage and the Nanming River, Guiyang City, China. *Journal of Environmental Monitoring*, 11(6), 1199-1205.

Liu, J.F., Zhao, Z.S., Jiang, G.B. 2008. Coating Fe_3O_4 magnetic nanoparticles with humic acid for high efficient removal of heavy metals in water. *Environmental science and technology*, 42(18), 6949-6954.

Liu, M., Hou, L.A., Yu, S., Xi, B., Zhao, Y., Xia, X. 2013. MCM-41 impregnated with a zeolite precursor: synthesis, characterization and tetracycline antibiotics removal from aqueous solution. *Chemical engineering journal*, 223, 678-687.

Liu, P., Liu, W.J., Jiang, H., Chen, J.J., Li, W.W., Yu, H.Q. 2012. Modification of bio-char derived from fast pyrolysis of biomass and its application in removal of tetracycline from aqueous solution. *Bioresource technology*, 121, 235-240.

Long, Y., Lei, D., Ni, J., Ren, Z., Chen, C., Xu, H. 2014. Packed bed column studies on lead (II) removal from industrial wastewater by modified Agaricusbisporus. *Bioresource Technology*, 152, 457-463.

López, E., Soto, B., Arias, M., Núñez, A., Rubinos, D., Barral, M.T. 1998. Adsorbent properties of red mud and its use for wastewater treatment. *Water research,* 32 (4), 1314-1322.

Lu, H., Zou, W., Chai, P., Wang, J., Bazinet, L. 2016. Feasibility of antibiotic and sulfate ions separation from wastewater using electrodialysis with ultrafiltration membrane. *Journal of Cleaner Production*, 112, 3097-3105.

Lu, Z., Huo, P., Luo, Y., Liu, X., Wu, D., Gao, X., Li, C., Yan, Y. 2013. Performance of molecularly imprinted photocatalysts based on fly-ash cenospheres

for selective photodegradation of single and ternary antibiotics solution. *Journal of Molecular Catalysis A: Chemical*, 378, 91-98.

Maheshwari, M., Vyas, R.K., Sharma, M. 2013. Kinetics, equilibrium and thermodynamics of ciprofloxacin hydrochloride removal by adsorption on coal fly ash and activated alumina. *Desalination and Water Treatment*, 51(37-39), 7241-7254.

Maldonado, P.S.D.V., Hernández-Montoya, V., Concheso, A., Montes-Morán, M.A. 2016. Formation of cerussite and hydrocerussite during adsorption of lead from aqueous solution on oxidized carbons by cold oxygen plasma. *Applied Surface Science*, 386, 381-388.

Malkoc, E., Nuhoglu, Y. 2006. Fixed bed studies for the sorption of chromium (VI) onto tea factory waste. *Chemical Engineering Science*, 61(13), 4363-4372.

Martucci, A., Pasti, L., Marchetti, N., Cavazzini, A., Dondi, F., Alberti, A. 2012. Adsorption of pharmaceuticals from aqueous solutions on synthetic zeolites. *Microporous and Mesoporous Materials*, 148(1), 174-183.

McKenzie, R.M. 1980. The adsorption of lead and other heavy metals on oxides of manganese and iron. *Soil Research*, 18(1), 61-73.

Memon, S.Q., Memon, N., Shah, S.W., Khuhawar, M.Y., Bhanger, M.I. 2007. Sawdust - A green and economical sorbent for the removal of cadmium (II) ions. *Journal of hazardous materials,* 139(1), 116-21.

Mohan, D., Singh, K.P., Singh, V.K. 2006. Trivalent chromium removal from wastewater using low cost activated carbon derived from agricultural waste material and activated carbon fabric cloth. *Journal of hazardous materials,* 135 (1-3), 280-95.

Mohan, S., Gandhimathi, R. 2009. Removal of heavy metal ions from municipal solid waste leachate using coal fly ash as an adsorbent. *Journal of hazardous materials,* 169 (1-3), 351-359.

Monser, L., Adhoum, N. 2002. Modified activated carbon for the removal of copper, zinc, chromium and cyanide from wastewater. *Separation and purification technology,* 26(2), 137-146.

Nadaroglu, H., Kalkan, E., Demir, N. 2010. Removal of copper from aqueous solution using red mud. *Desalination,* 251(1-3), 90-95.

Nagajyoti, P.C., Lee, K.D., Sreekanth, T.V.M. 2010. Heavy metals, occurrence and toxicity for plants: a review. *Environmental Chemistry Letters*, 8(3), 199-216.

Naiya, T.K., Chowdhury, P., Bhattacharya, A.K., Das, S.K. 2009. Saw dust and neem bark as low-cost natural biosorbent for adsorptive removal of Zn(II) and Cd(II) ions from aqueous solutions. *Chemical Engineering Journal,* 148 (1), 68-79.

Nascimento, M., Soares, P.S.M., de Souza, V.P. 2009. Adsorption of heavy metal cations using coal fly ash modified by hydrothermal method. *Fuel*, 88(9), 1714-1719.

Nasernejad, B., Zadeh, T.E., Pour, B.B., Bygi, M.E., Zamani, A. 2005. Camparison for biosorption modeling of heavy metals (Cr (III), Cu (II), Zn (II)) adsorption from wastewater by carrot residues. *Process Biochemistry,* 40 (3-4), 1319-1322.

Nazari, G., Abolghasemi, H., Esmaieli, M., Pouya, E.S. 2016. Aqueous phase adsorption of cephalexin by walnut shell-based activated carbon: A fixed-bed column study. *Applied Surface Science*, *375*, 144-153.

Nguyen, T.A.H., Ngo, H.H., Guo, W.S., Pham, T.Q., Li, F.M., Nguyen, T.V., Bui, X.T. 2015. Adsorption of phosphate from aqueous solutions and sewage using zirconium loaded okara (ZLO): fixed-bed column study. *Science of the Total Environment*, 523, 40-49.

Nguyen, T.A.H., Ngo, H.H., Guo, W.S., Zhang, J., Liang, S., Yue, Q.Y., Li, Q., Nguyen, T.V. 2013. Applicability of agricultural waste and by-products for adsorptive removal of heavy metals from wastewater. *Bioresource technology*, 148, 574-585.

Nie, M., Yan, C., Li, M., Wang, X., Bi, W., Dong, W. 2015. Degradation of chloramphenicol by persulfate activated by Fe^{2+} and zerovalent iron. *Chemical Engineering Journal*, 279, 507-515.

O'Carroll, D., Sleep, B., Krol, M., Boparai, H., Kocur, C. 2013. Nanoscale zero valent iron and bimetallic particles for contaminated site remediation. *Advances in Water Resources*, 51, 104-122.

Okochi, N.C. 2013. Phosphorus removal from stormwater using electric ARC furnace steel slag. *Doctoral dissertation, Faculty of Graduate Studies and Research, University of Regina*.

Oliveira, L.C., Petkowicz, D.I., Smaniotto, A., Pergher, S.B. 2004a. Magnetic zeolites: a new adsorbent for removal of metallic contaminants from water. *Water Research*, 38(17), 3699-3704.

Oliveira, L.C., Rios, R.V., Fabris, J.D., Lago, R.M., Sapag, K. 2004b. Magnetic particle technology. A simple preparation of magnetic composites for the adsorption of water contaminants. *Journal of chemical education*, 81(2), 248-250.

Ötker, H.M., Akmehmet-Balcıoğlu, I. 2005. Adsorption and degradation of enrofloxacin, a veterinary antibiotic on natural zeolite. *Journal of Hazardous Materials*, 122(3), 251-258.

Ou, H., Chen, Q., Pan, J., Zhang, Y., Huang, Y., Qi, X. 2015. Selective removal of erythromycin by magnetic imprinted polymers synthesized from chitosan-stabilized Pickering emulsion. *Journal of hazardous materials*, 289, 28-37.

Padmapriya, G., Murugesan, A.G. 2013. Biosorption of Hg (II) Ions From Aqueous Solution Using the Aquatic Weed Water Hyacinth With Equilibrium and Kinetic Modeling. *Remediation Journal*, 23(2), 127-139.

Panday, K.K., Prasad, G., Singh, V.N. 1985. Copper(II) removal from aqueous solutions by fly ash. *Water research,* 19(7), 869-73.

Panizza, M., Cerisola, G. 2009. Direct and mediated anodic oxidation of organic pollutants. *Chemical reviews*, 109(12), 6541-6569.

Paudyal, H., Pangeni, B., Inoue, K., Kawakita, H., Ohto, K., Alam, S. 2013. Adsorptive removal of fluoride from aqueous medium using a fixed bed column packed with Zr(IV) loaded dried orange juice residue. *Bioresource Technology*, 146, 713-720.

Perić, J., Trgo, M., Vukojević Medvidović, N. 2004. Removal of zinc, copper and lead by natural zeolite - a comparison of adsorption isotherms. *Water research,* 38(7), 1893-1899.

Pino, G.H., Souza de Mesquita, L.M., Torem, M.L., Saavedra Pinto, G.A. 2006. Biosorption of cadmium by green coconut shell powder. *Minerals Engineering,* 19(5), 380-387.

Pinterest. 2017. Aplastic anemia. https://uk.pinterest.com/explore/aplastic-anemia/.(accessed 10.03.2017).

Plasma electronic. 2017. Changing surfaces. http://www.plasma-electronics.com/plasma.html. (accessed 10.05.2017).

Plasma etch. 2017. Plasma cleaning. http://www.plasmaetch.com/plasma-cleaning.php. (accessed 16.05.2017).

Pouran, S.R., Raman, A.A.A., Daud, W.M.A.W. 2014. Review on the application of modified iron oxides as heterogeneous catalysts in Fenton reactions. *Journal of Cleaner Production*, 64, 24-35.

Pradhan, J., Das, S.N., Thakur, R.S. 1999. Adsorption of hexavalent chromium from aqueous solution by using activated red mud. *Journal of colloid and interface science,* 217(1), 137-41.

Priya, B., Raizada, P., Singh, N., Thakur, P., Singh, P. 2016a. Adsorptional photocatalytic mineralization of oxytetracycline and ampicillin antibiotics using Bi 2 O 3/BiOCl supported on graphene sand composite and chitosan. *Journal of Colloid and Interface Science*, 479, 271-283.

Priya, B., Shandilya, P., Raizada, P., Thakur, P., Singh, N., Singh, P. 2016b. Photocatalytic mineralization and degradation kinetics of ampicillin and oxytetracycline antibiotics using graphene sand composite and chitosan supported BiOCl. *Journal of Molecular Catalysis A: Chemical*, 423, 400-413.

Pubchem. 2017. Open chemistry database. https://pubchem.ncbi.nlm.nih.gov/compound/5959#section=Top (accessed 01.03.17).

Putra, E.K., Pranowo, R., Sunarso, J., Indraswati, N., Ismadji, S. 2009. Performance of activated carbon and bentonite for adsorption of amoxicillin from wastewater: Mechanisms, isotherms and kinetics. *Water research*, 43(9), 2419-2430.

Qiang, Z., Bao, X., Ben, W. 2013. MCM-48 modified magnetic mesoporous nanocomposite as an attractive adsorbent for the removal of sulfamethazine from water. *Water research*, 47(12), 4107-4114.

Querol, X., Moreno, N., Umaña, J.C., Alastuey, A., Hernández, E., López-Soler, A., Plana, F. 2002. Synthesis of zeolites from coal fly ash: an overview. *International Journal of Coal Geology,* 50(1-4), 413-423.

Quintelas, C., Pereira, R., Kaplan, E., Tavares, T. 2013. Removal of Ni(II) from aqueous solutions by an Arthrobacterviscosus biofilm supported on zeolite: from laboratory to pilot scale. *Bioresource Technology*, 142, 368-374.

Radjenović, J., Petrović, M., Ventura, F., Barceló, D. 2008. Rejection of pharmaceuticals in nanofiltration and reverse osmosis membrane drinking water treatment. *Water Research*, 42(14), 3601-3610.

Rafatullah, M., Sulaiman, O., Hashim, R., Ahmad, A. 2010. Adsorption of methylene blue on low-cost adsorbents: A review. *Journal of hazardous materials,* 177(1-3), 70-80.

Rahimi, S., Moattari, R.M., Rajabi, L., Derakhshan, A.A., Keyhani, M. 2015. Iron oxide/hydroxide (α, γ-FeOOH) nanoparticles as high potential adsorbents for lead removal from polluted aquatic media. *Journal of Industrial and Engineering Chemistry*, 23, 33-43.

Rajapaksha, A.U., Vithanage, M., Ahmad, M., Seo, D.C., Cho, J.S., Lee, S.E., Lee, S.S., Ok, Y.S. 2015. Enhanced sulfamethazine removal by steam-activated invasive plant-derived biochar. *Journal of hazardous materials*, 290, 43-50.

Raji, C., Anirudhan, T.S. 1998. Batch Cr (VI) removal by polyacrylamide-grafted sawdust: kinetics and thermodynamics. *Water Research*, 32(12), 3772-3780.

Rangsivek, R., Jekel, M.R. 2005. Removal of dissolved metals by zero-valent iron (ZVI): Kinetics, equilibria, processes and implications for stormwater runoff treatment. *Water Research*, 39(17), 4153-4163.

Ranjan, D., Talat, M., Hasan, S.H. 2009. Biosorption of arsenic from aqueous solution using agricultural residue 'rice polish'. *Journal of Hazardous Materials*, 166(2), 1050-1059.

Raskin, I., Smith, R.D., Salt, D.E. 1997. Phytoremediation of metals: using plants to remove pollutants from the environment. *Current opinion in biotechnology*, 8(2), 221-226.

Ravi Kumar, M.N.V. 2000. A review of chitin and chitosan applications. *Reactive and Functional Polymers,* 46(1), 1-27.

Rinaudo, M. 2006. Chitin and chitosan: Properties and applications. *Progress in Polymer Science,* 31(7), 603-632.

Ruthven, D. 2008. Fundamentals of adsorption equilibrium and kinetics in microporous solids. *Adsorption and Diffusion*, 1-43.

Şahin, Ö., Kaya, M., Saka, C. 2015. Plasma-surface modification on bentonite clay to improve the performance of adsorption of methylene blue. *Applied Clay Science*, 116, 46-53.

Sampaio, R.M.M., Timmers, R.A., Xu, Y., Keesman, K.J., Lens, P.N.L. 2009. Selective precipitation of Cu from Zn in a pS controlled continuously stirred tank reactor. *Journal of Hazardous Materials*, 165(1), 256-265.

Santona, L., Castaldi, P., Melis, P. 2006. Evaluation of the interaction mechanisms between red muds and heavy metals. *Journal of hazardous materials,* 136(2), 324-329.

Sapkota, A., Sapkota, A.R., Kucharski, M., Burke, J., McKenzie, S., Walker, P., Lawrence, R. 2008. Aquaculture practices and potential human health risks: current knowledge and future priorities. *Environment international*, 34(8), 1215-1226.

Šćiban, M., Klašnja, M., Škrbić, B. 2006. Modified hardwood sawdust as adsorbent of heavy metal ions from water. *Journal of Wood Science Technology,*40(3), 217-27.

Segura, Y., Martínez, F., Melero, J.A. 2013. Effective pharmaceutical wastewater degradation by Fenton oxidation with zero-valent iron. *Applied Catalysis B: Environmental*, 136, 64-69.

Selvi, K., Pattabhi, S., Kadirvelu, K. 2001. Removal of Cr(VI) from aqueous solution by adsorption onto activated carbon. *Bioresource technology,* 80(1), 87-89.

Sen, T.K., Azman, A.F., Maitra, S., Dutta, B.K. 2010. Removal of Hg (II) and Cd (II) metal ions by leaves of rambai tree ('Baccaurea motleyana'). *Chemeca 2010: Engineering at the Edge; 26-29 September 2010, Hilton Adelaide, South Australia*, 2067-2077.

Sengil, I.A., Özacar, M. 2008. Biosorption of Cu(II) from aqueous solutions by mimosa tannin gel. *Journal of Hazardous Materials*, 157(2-3), 277-285.

Shao, D., Hu, J., Chen, C., Sheng, G., Ren, X. and Wang, X. 2010. Polyaniline multiwalled carbon nanotube magnetic composite prepared by plasma-induced graft technique and its application for removal of aniline and phenol. *The Journal of Physical Chemistry C*, 114(49), 21524-21530.

Sharma, R., Singh, B. 2013. Removal of Ni (II) ions from aqueous solutions using modified rice straw in a fixed bed column. *Bioresource technology*, 146, 519-524.

Sikder, M.T., Mihara, Y., Islam, M.S., Saito, T., Tanaka, S., Kurasaki, M. 2014. Preparation and characterization of chitosan–caboxymethyl-β-cyclodextrin entrapped nanozero-valent iron composite for Cu (II) and Cr (IV) removal from wastewater. *Chemical Engineering Journal*, 236, 378-387.

Simate, G.S., Ndlovu, S. 2015. The removal of heavy metals in a packed bed column using immobilized cassava peel waste biomass. *Journal of Industrial and Engineering Chemistry*, 21, 635-643.

Singh, D.B., Rupainwar, D.C., Prasad, G., Jayaprakas, K.C. 1998. Studies on the Cd(II) removal from water by adsorption. *Journal of Hazardous Materials*, 60(1), 29-40.

Song, S.T., Saman, N., Johari, K., Mat, H. 2013. Removal of Hg (II) from aqueous solution by adsorption using raw and chemically modified rice straw as novel adsorbents. *Industrial & Engineering Chemistry Research*, 52(36), 13092-13101.

Sousa, F.W., Oliveira, A.G., Ribeiro, J.P., Rosa, M.F., Keukeleire, D., Nascimento, R.F. 2010. Green coconut shells applied as adsorbent for removal of toxic metal ions using fixed-bed column technology. *Journal of environmental management*, 91(8), 1634-1640.

Srivastava, N., Majumder, C. 2008. Novel biofiltration methods for the treatment of heavy metals from industrial wastewater. *Journal of Hazardous Materials*, 151(1), 1-8.

Srivastava, S.K., Tyagi, R., Pant, N. and Pal, N. 1989. Studies on the removal of some toxic metal ions. Part II (removal of lead and cadmium by montmorillonite and kaolinite). *Environmental Technology*, 10(3), 275-282.

Taty-Costodes, V.C., Fauduet, H., Porte, C., Delacroix, A. 2003. Removal of Cd(II) and Pb(II) ions, from aqueous solutions, by adsorption onto sawdust of Pinus sylvestris. *Journal of hazardous materials,* 105(1-3), 121-42.

Taty-Costodes, V.C., Fauduet, H., Porte, C., Ho, Y. 2005. Removal of lead (II) ions from synthetic and real effluents using immobilized Pinus sylvestris sawdust: Adsorption on a fixed-bed column. *Journal of hazardous materials,* 123(1-3), 135-144.

Tchounwou, P.B., Yedjou, C.G., Patlolla, A.K., Sutton, D.J. 2012. Heavy metal toxicity and the environment. *Molecular, clinical and environmental toxicology, Springer Basel*, 133-164.

Tekin, H., Bilkay, O., Ataberk, S.S., Balta, T.H., Ceribasi, I.H., Sanin, F.D., Dilek, F.B., Yetis, U. 2006. Use of Fenton oxidation to improve the biodegradability of a pharmaceutical wastewater. *Journal of Hazardous Materials*, 136(2), 258-265.

Thermo scientific XPS. 2017. XPS reference. http://xpssimplified.com/periodictable.php (accessed 28.02.17).

Thomas, H.C. 1944. Heterogeneous ion exchange in a flowing system. *Journal of the American Chemical Society*, 66(10), 1664-1666.

Torres-Pérez, J., Gérente, C., Andrès, Y. 2012. Sustainable activated carbons from agricultural residues dedicated to antibiotic removal by adsorption. *Chinese Journal of Chemical Engineering*, 20(3), 524-529.

Tran, V.S., Ngo, H.H., Guo, W., Ton-That, C., Li, J., Li, J., Liu, Y. 2017. Removal of antibiotics (sulfamethazine, tetracycline and chloramphenicol) from aqueous solution by raw and nitrogen plasma modified steel shavings. *Science of The Total Environment*, 601, 845-856.

Tran, V.S., Ngo, H.H., Guo, W., Zhang, J., Liang, S., Ton-That, C., Zhang, X. 2015. Typical low cost biosorbents for adsorptive removal of specific organic pollutants from water. *Bioresource Technology*, 182, 353-363.

Trovó, A.G., Nogueira, R.F., Agüera, A., Sirtori, C., Fernández-Alba, A.R. 2009. Photodegradation of sulfamethoxazole in various aqueous media: persistence, toxicity and photoproducts assessment. *Chemosphere*, 77(10), 1292-1298.

Urik, M., Littera, P., Kolen, M. 2009. Removal of arsenic (V) from aqueous solutions using chemically modified sawdust of spruce (Picea abies): Kinetics and isotherm studies. *International Journal of Environmental Science and Technology*, 6(3), 451-456.

USEPA. 2002. Lead and Copper Monitoring and Reporting Guidance for Public Water Systems, Ground Water and Drinking Water Division, *US Environmental Protection Agency*, 245-789.

Üstün, G.E., Solmaz, S.K.A., Birgül, A. 2007. Regeneration of industrial district wastewater using a combination of Fenton process and ion exchange - A case study. *Resources, Conservation and Recycling*, 52(2), 425-440.

Üzüm, Ç., Shahwan, T., Eroğlu, A.E., Lieberwirth, I., Scott, T.B., Hallam, K.R. 2008. Application of zero-valent iron nanoparticles for the removal of aqueous Co^{2+} ions under various experimental conditions. *Chemical Engineering Journal*, 144(2), 213-220.

Visa, M., Bogatu, C., Duta, A. 2010. Simultaneous adsorption of dyes and heavy metals from multicomponent solutions using fly ash. *Applied Surface Science*, 256(17), 5486-5491.

Wan Ngah, W.S., Teong, L.C., Hanafiah, M.A.K.M. 2011. Adsorption of dyes and heavy metal ions by chitosan composites: A review. *Carbohydrate Polymers*, 83(4), 1446-1456.

Wang, J. and Chen, C., 2009. Biosorbents for heavy metals removal and their future. *Biotechnology advances*, 27(2), 195-226.

Wang, L.K., Hung, Y.T., Shammas, N.K. eds. 2007. *Advanced physicochemical treatment technologies*. Humana Press.

World Health Organization (WHO), 2011. Pharmaceuticals in drinking-water.

Wiltowski, S.B., Lalvani, A., Hubner, T.S. 2000. Chromium Adsorption by Lignin. *Energy Sources,* 22(1), 45-56.

Wong, K.K., Lee, C.K., Low, K.S., Haron, M.J. 2003. Removal of Cu and Pb by tartaric acid modified rice husk from aqueous solutions. *Chemosphere,* 50(1), 23-28.

Wu, G.Q., Zhang, X., Hui, H., Yan, J., Zhang, Q.S., Wan, J.L., Dai, Y. 2012. Adsorptive removal of aniline from aqueous solution by oxygen plasma irradiated bamboo based activated carbon. *Chemical Engineering Journal*, 185, 201-210.

Wu, P., Wu, W., Li, S., Xing, N., Zhu, N., Li, P., Wu, J., Yang, C., Dang, Z. 2009. Removal of Cd^{2+} from aqueous solution by adsorption using Fe-montmorillonite. *Journal of hazardous materials,* 169 (1-3), 824-830.

Wu, Y., Zhang, S., Guo, X., Huang, H. 2008. Adsorption of chromium (III) on lignin. *Bioresource technology*, 99(16), 7709-7715.

Xia, S., Gu, Z., Zhang, Z., Zhang, J., Hermanowicz, S.W. 2014. Removal of chloramphenicol from aqueous solution by nanoscale zero-valent iron particles. *Chemical Engineering Journal*, 257, 98-104.

Xiao, J., Chen, Y., Xu, J. 2014. Plasma grafting montmorillonite/iron oxide composite with β-cyclodextrin and its application for high-efficient decontamination of U (VI). *Journal of Industrial and Engineering Chemistry*, 20(5), 2830-2839.

Yaghmaeian, K., Moussavi, G., Alahabadi, A. 2014. Removal of amoxicillin from contaminated water using NH_4Cl-activated carbon: continuous flow fixed-bed adsorption and catalytic ozonation regeneration. *Chemical Engineering Journal*, 236, 538-544.

Yoon, Y.H., Nelson, J.H. 1984. Application of Gas Adsorption Kinetics I. A Theoretical Model for Respirator Cartridge Service Life. *American Industrial Hygiene Association Journal*, 45(8), 509-516.

Yu, Y., Wang, W., Shi, J., Zhu, S., Yan, Y. 2017. Enhanced levofloxacin removal from water using zirconium (IV) loaded corn bracts. *Environmental Science and Pollution Research*, 24(11), 10685-10694.

Zach-Maor, A., Semiat, R., Shemer, H. 2011. Fixed bed phosphate adsorption by immobilized nano-magnetite matrix: experimental and a new modeling approach. *Adsorption*, 17(6), 929-936.

Zafar, M.N., Parveen, A., Nadeem, R. 2013. A pretreated green biosorbent based on Neem leaves biomass for the removal of lead from wastewater. *Desalination and Water Treatment*, 51(22-24), 4459-4466.

Zamzow, M.J., Eichbaum, B.R., Sandgren, K.R., Shanks, D.E. 1990. Removal of Heavy Metals and Other Cations from Wastewater Using Zeolites. *Separation Science and Technology,* 25(13-15), 1555-69.

Zhang, J.X., Zhou, Q.X., Li, W. 2013a. Adsorption of enrofloxacin from aqueous solution by bentonite. *Clay Minerals*, 48(4), 627-637.

Zhang, T., Li, Q., Xiao, H., Mei, Z., Lu, H., Zhou, Y. 2013b. Enhanced fluoride removal from water by non-thermal plasma modified CeO_2/Mg–Fe layered double hydroxides. *Applied Clay Science*, 72, 117-123.

Zhou, Y., Zhang, J., Luo, X., Lin, X. 2014. Adsorption of Hg (II) in aqueous solutions using mercapto-functionalized alkali lignin. *Journal of Applied Polymer Science*, 131(40749), 1-9.

Faculty of Engineering and Information Technology

APPENDICES

Appendix A - SEM images

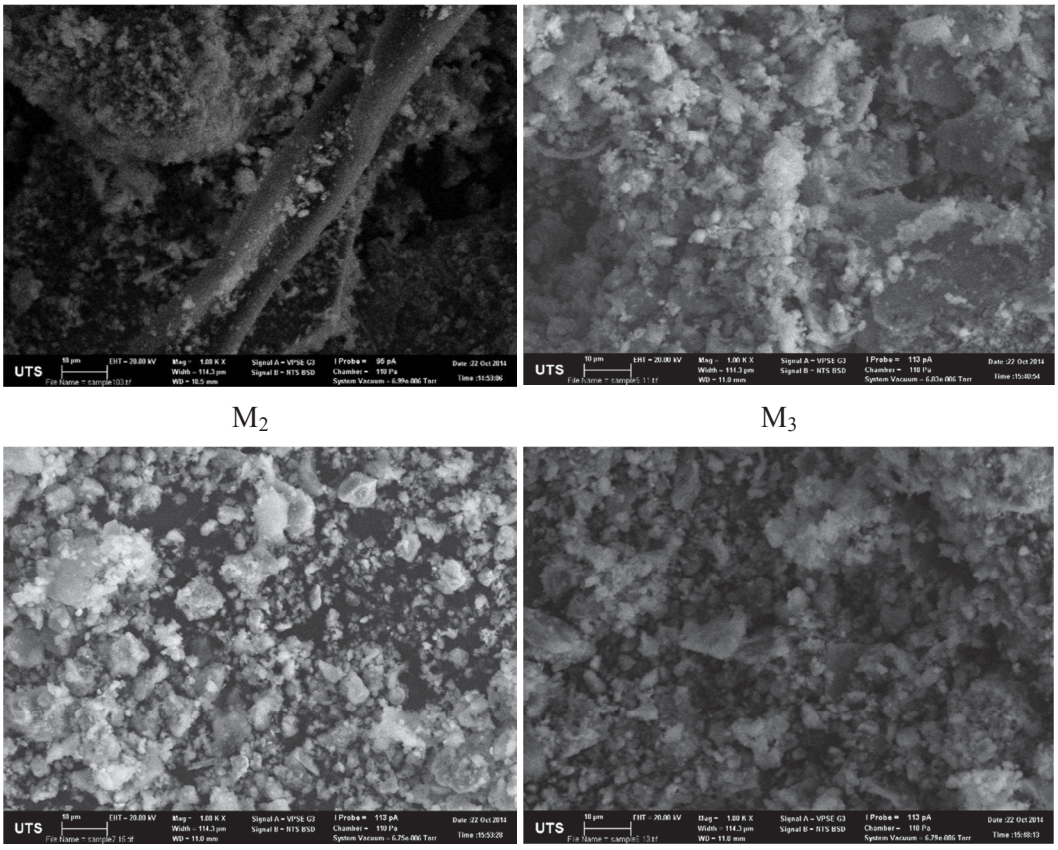

M_2 M_3

M_3-plAr M_3-plN_2

Figure A1 SEM images of adsorbents at magnification (x1000)

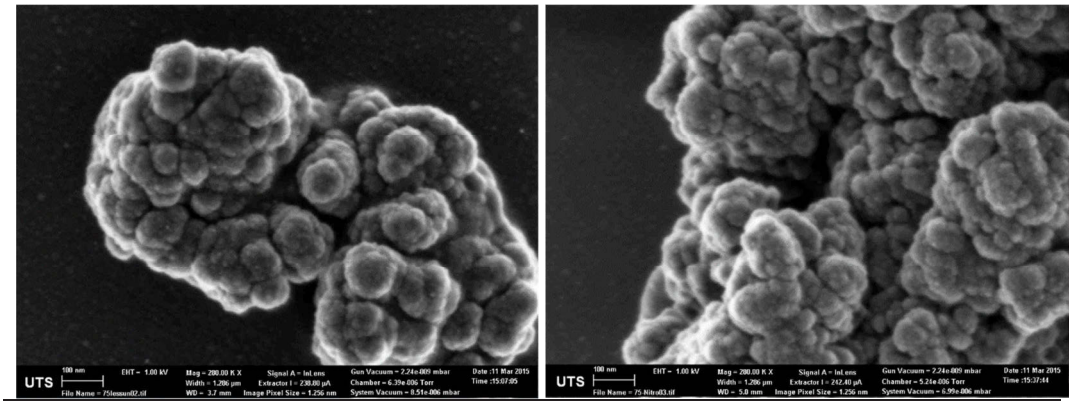

M_3 M_3-plN_2

Figure A2 SEM images of adsorbents at magnification (x200,000)

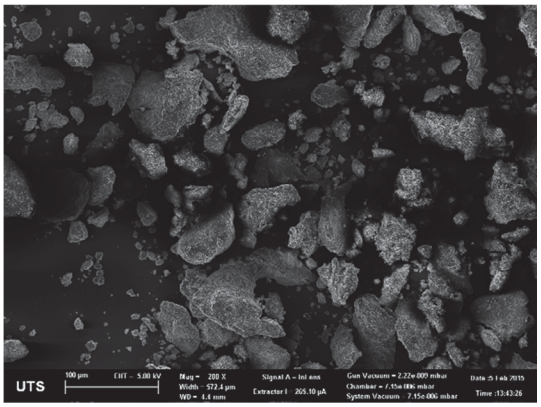

(x200)

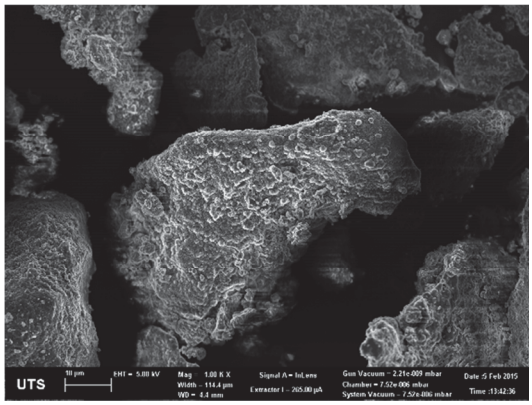

(x1000)

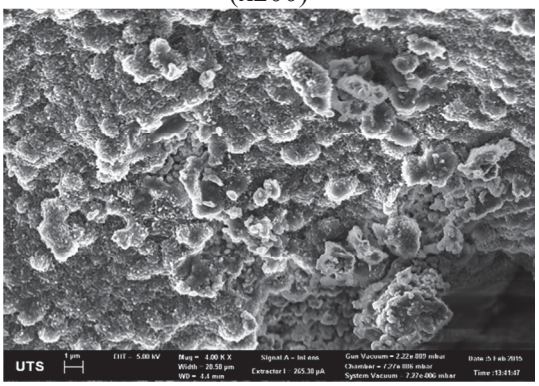

(x4000)

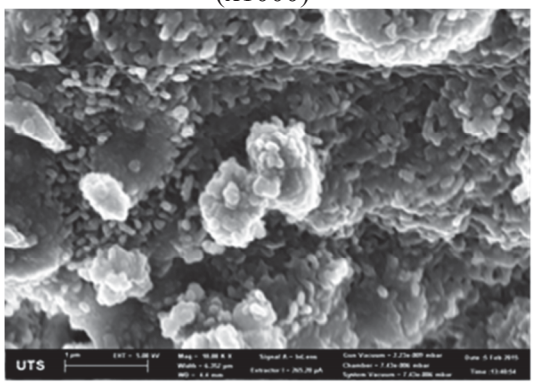

(x18000)

Figure A3 SEM images of M_3-plN_2 (after adsorption)

Appendix B - EDS spectrums

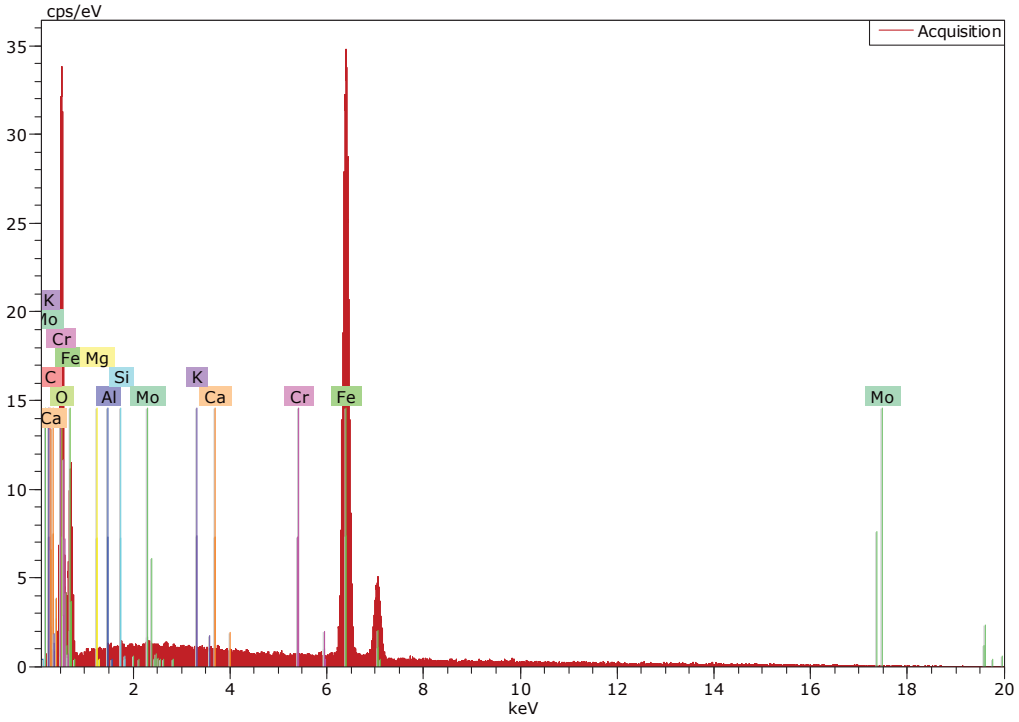

Figure B1 Spectrum of Fe_2O_3

El	AN	Series	unn. C [wt.%]	norm. C [wt.%]	Atom. C [at.%]	Error (1 Sigma) [wt.%]
O	8	K-series	29.64	32.40	56.98	4.56
Fe	26	K-series	56.78	62.09	31.28	1.63
C	6	K-series	4.41	4.82	11.28	1.56
Al	13	K-series	0.10	0.11	0.11	0.04
Mg	12	K-series	0.07	0.08	0.09	0.04
Mo	42	L-series	0.24	0.26	0.08	0.05
Si	14	K-series	0.06	0.06	0.06	0.04
Ca	20	K-series	0.08	0.09	0.06	0.04
Cr	24	K-series	0.06	0.07	0.04	0.04
K	19	K-series	0.02	0.02	0.02	0.03
Total:			91.46	100.00	100.00	

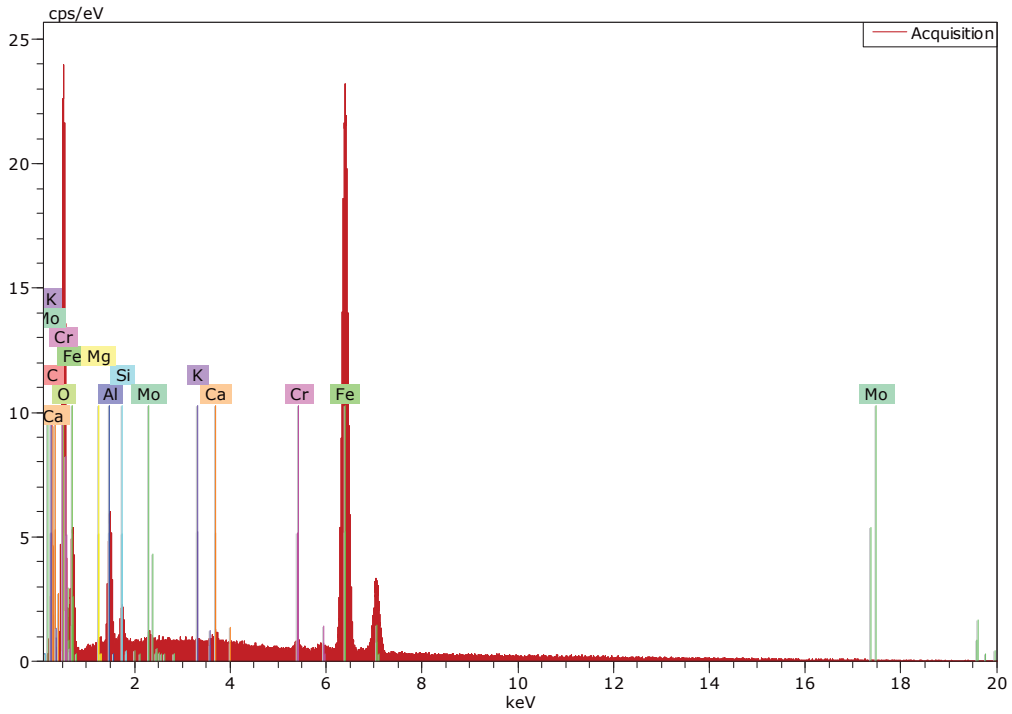

Figure B2 Spectrum of M_3

El	AN	Series	unn. C [wt.%]	norm. C [wt.%]	Atom. C [at.%]	Error (1 Sigma) [wt.%]
O	8	K-series	31.83	32.96	47.63	4.64
C	6	K-series	14.79	15.31	29.47	3.03
Fe	26	K-series	46.07	47.70	19.75	1.31
Al	13	K-series	2.64	2.73	2.34	0.18
Si	14	K-series	0.34	0.35	0.29	0.05
Mg	12	K-series	0.24	0.25	0.23	0.05
Cr	24	K-series	0.25	0.26	0.11	0.05
Ca	20	K-series	0.16	0.16	0.09	0.04
Mo	42	L-series	0.25	0.26	0.06	0.05
K	19	K-series	0.03	0.03	0.02	0.03
Total:			96.58	100.00	100.00	

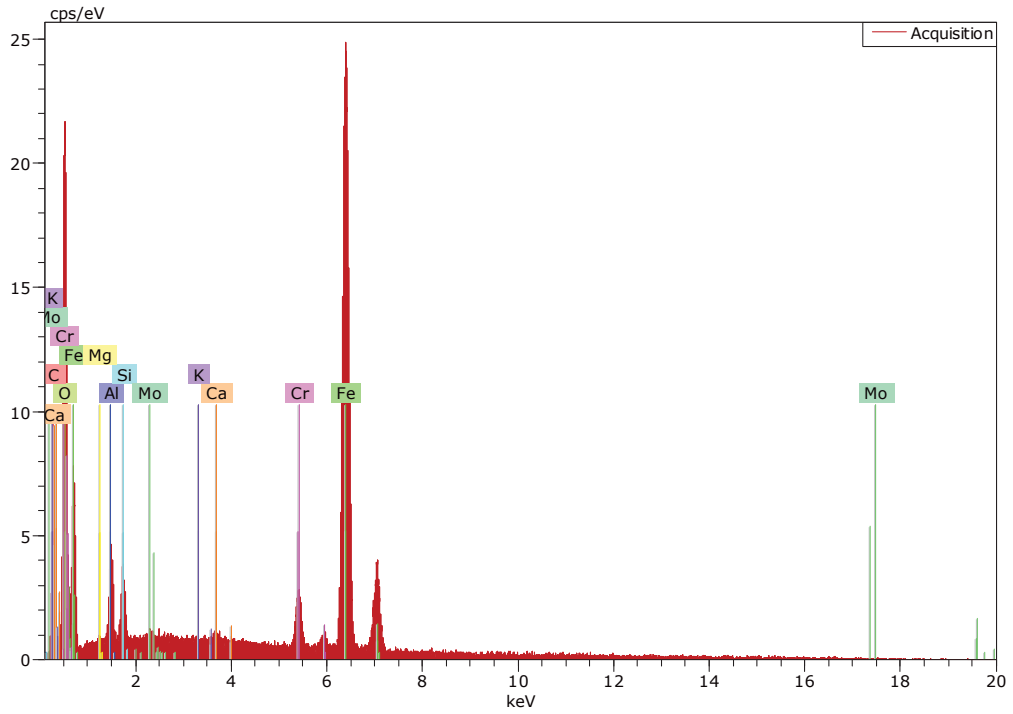

Figure B3 Spectrum of M_3-plAr

El	AN	Series	unn. C [wt.%]	norm. C [wt.%]	Atom. C [at.%]	Error (1 Sigma) [wt.%]
O	8	K-series	27.06	27.45	43.92	4.51
C	6	K-series	12.49	12.67	27.00	3.25
Fe	26	K-series	52.62	53.39	24.47	1.53
Al	13	K-series	2.20	2.23	2.12	0.17
Cr	24	K-series	2.54	2.57	1.27	0.14
Si	14	K-series	0.97	0.98	0.89	0.09
Mg	12	K-series	0.13	0.13	0.14	0.05
Mo	42	L-series	0.45	0.46	0.12	0.07
Ca	20	K-series	0.11	0.11	0.07	0.04
K	19	K-series	0.00	0.00	0.00	0.00
Total:			98.56	100.00	100.00	

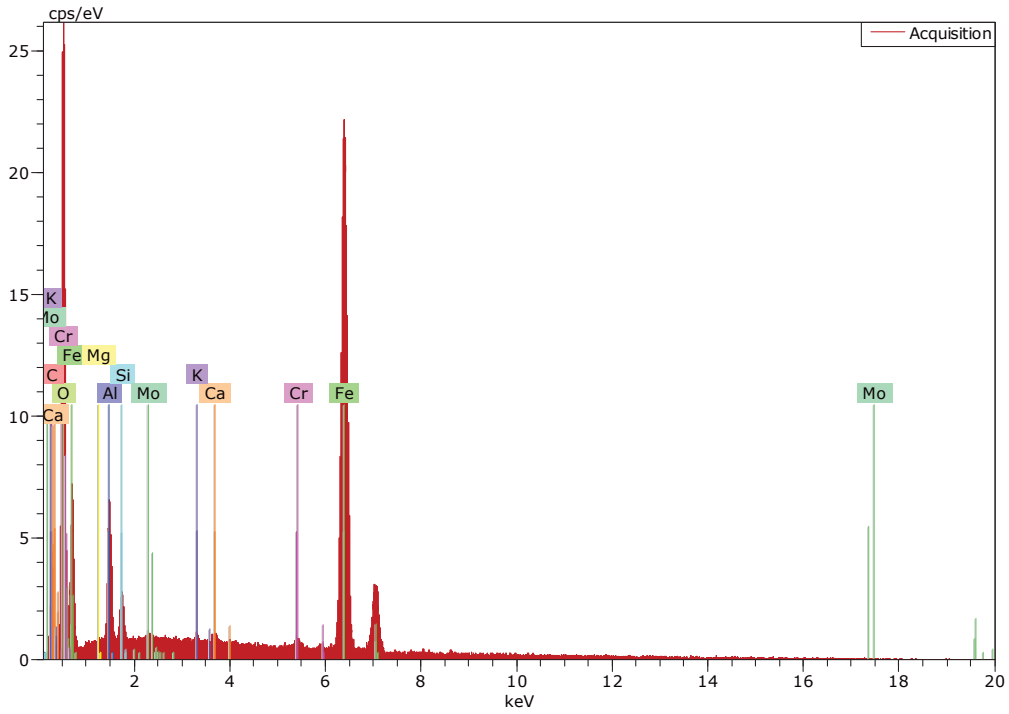

Figure B4 Spectrum of M_3-plN_2

El	AN	Series	unn. C [wt.%]	norm. C [wt.%]	Atom. C [at.%]	Error (1 Sigma) [wt.%]
O	8	K-series	33.56	27.65	52.16	4.49
C	6	K-series	11.78	12.52	24.39	2.28
Fe	26	K-series	44.39	55.16	19.77	1.24
Al	13	K-series	2.96	3.15	2.73	0.18
Si	14	K-series	0.61	0.65	0.54	0.06
Cr	24	K-series	0.39	0.41	0.19	0.05
K	19	K-series	0.13	0.14	0.08	0.04
Ca	20	K-series	0.09	0.10	0.06	0.03
Mo	42	L-series	0.17	0.18	0.04	0.04
Mg	12	K-series	0.03	0.04	0.03	0.03
Total:			94.12	100.00	100.00	

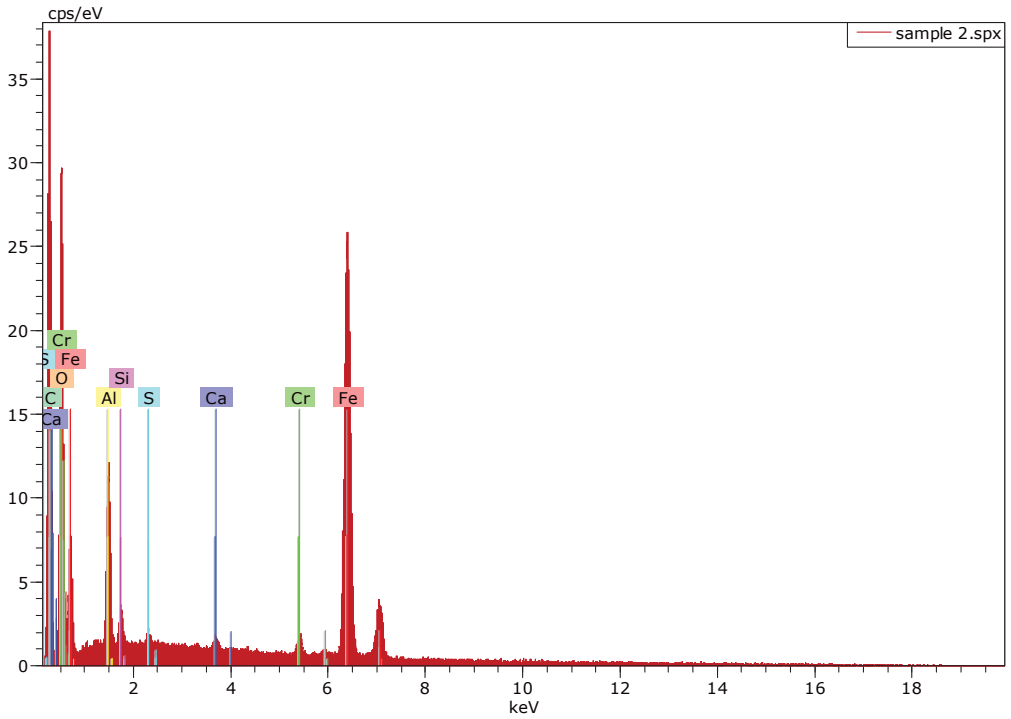

Figure B5 Spectrum of M_3-plO_2

El	AN	Series	unn. C [wt.%]	norm. C [wt.%]	Atom. C [at.%]	Error (1 Sigma) [wt.%]
C	6	K-series	49.79	14.56	58.93	6.10
O	8	K-series	35.76	35.76	31.77	4.47
Fe	26	K-series	30.03	46.40	7.64	0.83
Al	13	K-series	2.47	2.08	1.30	0.15
Cr	24	K-series	0.59	0.54	0.16	0.05
Si	14	K-series	0.26	0.22	0.13	0.04
Ca	20	K-series	0.13	0.11	0.05	0.03
S	16	K-series	0.02	0.02	0.01	0.03
Total:			119.06	100.00	100.00	